Impact of small-scale transverse bed slope effects on large-scale morphology

Experimental and modelling studies

Invloed van lokale dwarshellingseffecten op de grootschalige morfologie

Experimenten en modelstudies

(met een samenvatting in het Nederlands)

P R O E F S C H R I F T

ter verkrijging van de graad van doctor aan de Universiteit Utrecht
op gezag van de rector magnificus, prof. dr. H.R.B.M. Kummeling,
ingevolge het besluit van het college voor promoties in het openbaar te verdedigen
op vrijdag 22 maart 2019 des middags te 2.30 uur

door

Anne Wilhelmina Baar
geboren op 18 november 1989 te Hilversum

Promotor:
Prof. dr. M. G. Kleinhans

This work was financially supported by the Dutch Technology Foundation (TTW) of the Netherlands Organization for Scientific Research (NWO) (grant Vici 016.140.316/13710)

Impact of small-scale transverse bed slope effects on large-scale morphology

Promotor:
Prof. dr. M. G. Kleinhans

Examination committee:
Prof. dr. J.L. Best
University of Illinois, USA

Prof. dr. W.S.J. Uijttewaal
Delft University of Technology, The Netherlands

Prof. dr. H.J. de Vriend
Delft University of Technology, The Netherlands

Prof. dr. L.C. van Rijn
Utrecht University, The Netherlands

Dr. C.J. Sloff
Deltares, The Netherlands

Prof. dr. H.E. de Swart
Utrecht University, The Netherlands

ISBN 978-90-6266-528-0

Published by Faculty of Geosciences, Universiteit Utrecht, The Netherlands, in:
Utrecht Studies in Earth Sciences (USES), ISSN 2211-4335

Typeset using XeLaTeX

Cover: Lena Delta, Russia. Landsat 8 top-of-atmosphere reflection (RGB: band 6, band 5, band 4): 2016-2017 composite of highest thermal-infrared reflection (band 10)

Printed by Ridderprint BV, Ridderkerk, The Netherlands

Correspondence to: Anne Baar, annebaar@gmail.com

Utrecht Studies in Earth Sciences 174

Impact of small-scale transverse bed slope effects on large-scale morphology

Experimental and modelling studies

Anne Baar

Utrecht 2019

Faculty of Geosciences, Utrecht University

Contents

Summary 1

Samenvatting 5

1 Introduction 11

1.1 Problem definition and project aims . . . 11
1.2 Sediment transport processes on transverse bed slopes . . . 14
1.3 Past research on predicting transverse sediment transport . . . 16
1.4 Transverse bed slope effect in morphodynamic models . . . 18
1.5 Specific research questions and thesis outline . . . 22

2 Sediment transport of fine sand to fine gravel on transverse bed slopes in rotating annular flume experiments 27

2.1 Introduction . . . 28
2.2 Existing transverse slope predictors . . . 30
2.3 Methods . . . 36
2.4 Results . . . 41
2.5 Discussion . . . 50
2.6 Conclusions . . . 59

3 Influence of grain size-dependent bedform morphology on flow and transverse slope in river bends 63

3.1 Introduction . . . 64
3.2 Methods . . . 66
3.3 Results . . . 69
3.4 Discussion . . . 74
3.5 Conclusions . . . 78

4 Interaction between lateral sorting in river bends and vertical sorting in dunes 81

4.1 Introduction . . . 82
4.2 Methods . . . 84
4.3 Results . . . 90
4.4 Discussion . . . 96
4.5 Conclusion . . . 101

5 Critical dependence of morphological models of fluvial and tidal systems on empirical downslope sediment transport **103**

5.1 Introduction 104
5.2 Results 106
5.3 Discussion 118
5.4 Methods 122

6 Improving large-scale morphodynamic models starts at small-scale bed slope effects: a discussion **127**

6.1 Introduction 127
6.2 Transverse slope effect: a non-linear relation with sediment mobility 128
6.3 Imbalance between incision and transverse slope effect in morphodynamic models 131
6.4 Transverse slope effect controls channel dynamics 132
6.5 Recommendations for further research 135
6.6 Implications for calibration practices of large-scale morphodynamic models 138

Appendix A Analytical estimation of near-bed flow velocities in the rotating annular flume **143**

Appendix B Sediment transport and slope effect in Delft3D **147**

Appendix C Theoretical balance between incision and transverse sediment transport **151**

Appendix D Slope effect in previous morphodynamic model studies **155**

Appendix E Experimental data: uniform sediment **159**

Appendix F Experimental data: sorting experiments **167**

References **171**

Acknowledgements **183**

About the author **185**

Summary

Morphodynamic models are essential tools to predict the development of fluvial and tidal systems in scientific and engineering studies. These models are increasingly used to optimize e.g. engineering interventions, flood protection, sand mining and shipping fairway maintenance, and to predict the system evolution under the influence of pressures such as sea level rise and human interference. However, many existing morphodynamic models predict unrealistically deep and narrow channels, suggesting a lack of understanding of local sediment transport dynamics at the scale of bars and channels.

Channel formation is initially the result of the balance of two processes: channel erosion, and gravity-driven downslope sediment transport on the side slopes of the channel. The latter is called the transverse bed slope effect, since these side slopes are transverse to the main flow direction. Furthermore, transverse sediment transport is essential in balancing secondary flows induced by bars and bends when channel patterns evolve. Secondary flows in bends are inward-directed near the river bed and therefore drag sediment upslope towards the inner bend, but this is balanced by sediment traveling downslope due to gravity. When the riverbed consists of a sediment mixture, sediment is sorted along the slope, since gravity pulls the heavier grains further downslope and the secondary flow drags the finer grains further upslope. These processes show that the transverse bed slope effect strongly determines the equilibrium channel dimensions and their dynamics. However, the magnitude and direction of the transverse sediment transport is poorly understood and therefore oversimplified in morphodynamic models.

Transverse bed slope predictors in morphodynamic models are based on previous studies that isolated a specific transport mechanism or bed state, and study its separate effect on the transverse bed slope effect. Consequently, existing transverse slope predictors were validated against a small set of experiments with a limited range in near-bed flow conditions and sediment sizes, depending on the process that was studied. However, these predictors are now used to predict large-scale morphology where all sediment transport processes act in combination. Therefore, the unrealistic channel erosion in morphodynamic models is often counteracted by artificially increasing the transverse bed slope parameter, which linearly increases the transverse sediment transport and is therefore an effective calibration parameter. However, previous model studies reported transverse slope parameters up to a hundred times the default value to get realistic morphology, meaning an increase of two orders of magnitude in downslope sediment transport. This raises the question whether the default value that was based on literature is physically correct, or if other sediment transport processes are missing in the model.

The objective of this thesis is to experimentally quantify the physical processes that influence sediment transport on transverse bed slopes for a large range of flow velocities, secondary flow intensities and sediment sizes to obtain transverse slope parameters for morphological modelling that cover all sediment transport modes and bed state regimes. Additionally, the cause of the severe incision in morphodynamic models is identified, and why

there are extremely large differences in transverse slope parameter needed to get realistic large-scale morphology.

Experiments were conducted in a rotating annular flume, which allows control of secondary flow intensity separately from the main flow velocity, and therefore varying bend radii can be simulated. Sediment characteristics were varied in three ways: using 1) uniform sediment ranging from fine sand to fine gravel (0.17–4mm), 2) low-density sediment, and 3) a sediment mixture to quantify sediment sorting processes. In total, 252 experiments were conducted. To identify possible explanations for the severe incision in morphodynamic models and to study the effect on large-scale morphology, five sets of model simulations were conducted for various scales and environments.

Results with uniform sediment showed that the balance between the transverse slope effect and secondary flow is not a linear function with sediment mobility, as suggested in previous literature, but severely depends on several sediment transport processes that act together (Chapter 2). This balance was grain size-dependent since this determined the mobility of the sediment, bed state and the dominant mode of sediment transport. Sediment mobility limited the development of transverse slopes just above the beginning of motion and mainly influenced the transverse slope by determining the bed state. The balance between secondary flow and transverse slope differed between experiments with fine and coarse sand, due to the distinct bedform types that developed (Chapter 3). Coarse sediment ($D_{50} > 0.7$ mm) showed a direct relation between grain size-dependent dune lee-side angle and transverse slope, since sufficiently high lee-side angles theoretically result in permanent flow separation that enhances secondary flow in the dune troughs. In experiments with fine sediments ($D_{50} < 0.7\ mm$), different bedforms developed, ranging from ripples, dunes with superimposed ripples, dunes, to an upper stage plane bed. These bedforms showed no direct interaction with the secondary flow, and lee-side angles mainly depended on bedform type instead of grain size and bedform dimension.

The experiments with a sediment mixture showed the same balance between secondary flow intensity and transverse slope as the uniform sediment experiments, which indicates that there was no feedback between sorting and the magnitude of the slope itself (Chapter 4). To quantify bend sorting, sediment samples were taken over the cross-section of 13 experiments with varying transverse slope. Results showed that all mobile sediment fractions were efficiently sorted along the transverse slope, where the volume change over the cross-section of specific fractions increases with grain size and magnitude of the slope. Furthermore, bulk samples that were taken over the entire height of a dune showed minor effects of vertical sorting along the lee side of dunes, since the difference with surface sample were small. This implies that lateral sorting can be modelled independently of dunes, which allows application of the active layer concept in morphodynamic models.

Even though the experimental results showed a new relation between bend flow and transverse sediment transport, resulting transverse slope parameters were still in the same order of the default values in morphodynamic models in case of the fine sediment experiments, or even lower for most of the coarse sediment experiments. This implies that the need to artificially increase the transverse slope parameter in models to counteract severe incision is not

caused by the oversimplified implementation of the transverse slope effect, but is necessary to compensate for other model weaknesses.

Model results demonstrated that the rate of channel incision with the default slope parameter depends on grid size and the relative amount of sediment in suspension (Chapter 5). With a physically realistic transverse bed slope effect, the flow seems to prefer flowing through as few grid cells as possible, which resulted in more incision with a finer grid. The initial response determines whether a system tends to incise or goes towards an equilibrium channel by eroding the banks. The magnitude of the slope parameter that was needed to overcome grid size-dependent incision was determined by the bed load transport rate that was available for deflection downslope. The transport predictor of Van Rijn makes a distinction between bedload and suspended load, and therefore the rate of incision depends on the amount of sediment in suspension. On the other hand, the total load predictor of Engelund-Hansen overdampened perturbations by predicting a much higher sediment transport rate, which is all subjected to bed slope effects. These models therefore needed significantly lower transverse slope parameters to balance unrealistic incision.

The large-scale environment that is modelled influences how likely models are to incise and how sensitive they are to changes in bed slope effect. To model a dynamic system, the model has to overcome the grid size-dependent incision at the channel scale by increasing slope effects. Only when this is balanced by downslope sediment transport, the channel can migrate sideways. Therefore, results showed that channels in models with Van Rijn were static once they were formed, while channels in models with Engelund Hansen could migrate and avulse. Furthermore, models with Van Rijn showed unnaturally sharp angular bends that clearly followed the rectangular grid. Environments that depend on a large-scale balance between erosion and deposition, such as estuaries and rivers, need a high slope parameter to be dynamic, especially when modelled with the transport predictor of Van Rijn. Increasing the bed slope effect results in longer and wider bars and increased active channel width, and therefore in weaker braiding and fewer bifurcations. Erosional environments, e.g. tidal basins, only need increased slope effects when the objective of a model study requires the channels to migrate. Here, increasing the slope effect will mainly set channel dimensions but not necessarily the number of channels. Depositional models where lateral dynamics are initially less important, e.g. delta's and fans, will show more natural looking bars with default slope parameters. However, channels that form on the deposits will incise during the model run and will also show the unnaturally sharp angular bends. It is difficult to use the predictor of Engelund-Hansen to model depositional environments due to the diffusive nature of this predictor.

If models are designed to represent existing morphology e.g. for decision making or case studies, results critically depend on the choice of slope predictor in combination with the sediment transport predictor. The two different methods to calculate transverse sediment transport that are implemented in Delft3D, i.e. Ikeda or Koch Flokstra, result in different sediment transport magnitudes and directions on the same slope, due to the different methods of calculating the transverse transport vector. This will lead to different local channel dynamics, such as bank erosion rates and location of erosion and deposition. On a larger scale, this will result in different bar dimensions and channel network. Practically, this means that

when a model is calibrated on morphology but is used to make an estimate of erosion or sediment migration rates, these estimates will depend on the choice of slope predictor. On the other hand, when models are calibrated to sediment transport rates, morphology and bed slopes will differ between predictors. These are for example models that focus on the migration rate of dumped sediment, the sediment distribution at bifurcations, or the rate of bank erosion. Therefore, when models are calibrated by increasing downslope sediment transport, either sediment transport magnitude or bed slopes match to measured data, while both are not possible.

To conclude, results from this thesis show that the balance between secondary flow intensity and the transverse slope is a non-linear relation with sediment mobility, which is grain size dependent due to differences in bedform morphology. Even though this is in contrast with the linear relations described in literature, the experimental results are still in the same order as the default value for the transverse slope parameter in morphodynamic models. The increase of the transverse slope parameter up to two orders of magnitude that is needed to obtain realistic morphology therefore implies an imbalance between the incision and downslope sediment transport in the models due to another cause. The rate of incision depends on grid size and the suspended sediment transport rate, and future research should focus on the role of slope effects and diffusion on suspended sediment transport. An arbitrary bed slope calibration to counteract extreme incision may cause an order of magnitude error in rate of morphological change, channel depth, the degree of braiding and bar dimensions. Furthermore, it is impossible to calibrate a model on both sediment transport magnitude and morphology, which has major implications for calibrated models that are used to make decisions for e.g. navigation or engineering.

Samenvatting

Morfologische modellen zijn essentieel in het voorspellen van de ontwikkeling van rivieren en getijsystemen. Deze modellen worden in toenemende mate gebruikt voor het optimaliseren van bijvoorbeeld technische ingrepen, hoogwaterveiligheid, zandwinning en baggerstrategieën voor de scheepvaart, en om de lange termijn ontwikkeling van het systeem te voorspellen onder invloed van bijvoorbeeld zeespiegelstijging en menselijke ingrepen. Veel bestaande morfologische modellen voorspellen echter onrealistisch diepe en smalle geulen, wat wijst op een gebrek aan inzicht in de dynamiek van geulen en zandbanken.

De vorming van geulen en zandbanken hangt af van de balans tussen twee processen: erosie van de geul doordat sediment wordt meegenomen door de stroming, en neerwaarts sedimenttransport aan de zijkant van de geul als gevolg van de erosie. Dit laatste wordt het dwarshellingseffect genoemd, omdat de hellingen aan de zijkant van de geul dwars op de stroming staan. Dit sedimenttransport naar het midden van de geul is ook essentieel in het balanceren van spiraalstroming. Spiraalstroming wordt veroorzaakt door bochten en zandbanken, die ontstaan wanneer geulpatronen zich ontwikkelen. Als een gevolg van de spiraalstroming is de stroming dicht bij de bodem naar binnen gericht en neemt het sediment mee hellingopwaarts. Dit wordt gecompenseerd door het neerwaartse sedimenttransport door de zwaartekracht, waardoor er een evenwichtshelling ontstaat richting de binnenbocht. Dit evenwicht hangt af van de sterkte van de spiraalstroming en de eigenschappen van het sediment. Wanneer de rivierbedding uit een mengsel bestaat van verschillende korrelgroottes, wordt het sediment langs de helling uitgesorteerd, omdat de zwaartekracht de zwaardere korrels verder naar beneden trekt en de spiraalstroming de fijnere korrels verder omhoog mee kan nemen. Door het balanceren van erosie en spiraalstroming, heeft het dwarshellingseffect een grote invloed op de dynamiek van banken en geulen. Echter, de invloed van de sedimenteigenschappen en de sterkte van de spiraalstroming op de grootte en richting van het sedimenttransport op dwarshellingen is nog niet systematisch onderzocht, waardoor dit proces erg is versimpeld in morfologische modellen.

Dwarshellingsvoorspellers in morfologische modellen zijn gebaseerd op eerdere studies die het effect van een specifiek transportmechanisme of beddingvorm op sedimenttransport op dwarshellingen bestudeerden. Als gevolg werden deze dwarshellingsvoorspellers gevalideerd met een kleine reeks experimenten met een beperkt bereik in stromingscondities en korrelgrootte, afhankelijk van het proces dat werd bestudeerd. Deze voorspellers worden nu echter gebruikt voor het voorspellen van grootschalige morfologie waarbij meerdere sedimenttransportprocessen elkaar beïnvloeden. De vorming van onrealistisch diepe geulen in morfologische modellen wordt daarom vaak tegengegaan door de dwarshellingsparameter kunstmatig te verhogen, waardoor het sedimenttransport in de dwarsrichting lineair toeneemt. Hierdoor is de dwarshellingsparameter een effectieve kalibratieparameter, en wordt dit schijnbaar willekeurig verhoogd tot honderd keer de standaardwaarde om een realistische morfologie te krijgen. Dit betekent echter ook een toename van mogelijk twee ordegroottes in zijwaarts sedimenttransport. Dit roept hierdoor de vraag op of de standaardwaarde die op de literatuur gebaseerd is niet klopt, of dat er andere processen in het model ontbreken.

Het doel van dit proefschrift is om processen die sedimenttransport op dwarshellingen beïnvloeden te kwantificeren voor een groot bereik in stroomsnelheid, spiraalstroming en korrelgrootte. Door dit grote bereik wordt het mogelijk om dwarshellingsparameters te definiëren voor morfologische modellen die het effect van alle sedimenttransportprocessen beschrijven, zoals verschillende beddingvormen en sedimenttransportmechanismes. Daarnaast is het doel om de oorzaak van de extreme insnijding van geulen in morfologische modellen te identificeren en te onderzoeken waarom de grootte van de dwarshellingsparameter, die nodig is om een realistische morfologie te verkrijgen, sterk varieert tussen verschillende modellen.

Om sedimenttransportprocessen op dwarshellingen te kwantificeren zijn er experimenten uitgevoerd in een carrousel stroomgoot. Deze stroomgoot maakt het mogelijk om spiraalstroming te variëren onafhankelijk van de gemiddelde stroming in de richting van de geul, waardoor verschillende bochtstralen gesimuleerd kunnen worden. De eigenschappen van het sediment zijn op drie manieren gevarieerd, door het gebruik van uniform sediment van fijn zand tot fijn grind (0.17–4mm), lichtgewicht sediment en een sedimentmengsel om bochtsortering te kwantificeren. In totaal zijn er 252 experimenten uitgevoerd. Hiernaast zijn er vijf morfologische modellen opgezet van verschillende systemen en ruimtelijke schalen, ten eerste om mogelijke verklaringen te identificeren voor de extreme insnijding, en ten tweede om het effect van het verhogen van de dwarshellingsparameter op de grootschalige morfologie te bestuderen.

Resultaten van de experimenten met uniform sediment toonden aan dat het evenwicht tussen het dwarshellingseffect en de spiraalstroming geen lineaire functie is met sedimentmobiliteit, zoals toegepast in de modellen, maar sterk afhankelijk is van verschillende processen die elkaar beïnvloeden, zoals transportmodus en beddingvormen (Hoofdstuk 2). Dit evenwicht was afhankelijk van de korrelgrootte, omdat dit de mobiliteit van het sediment, het type beddingvorm dat ontstaat en het sedimenttransportmechanisme bepaalt. De mobiliteit van het sediment beperkte de ontwikkeling van dwarshellingen vlak boven het begin van beweging en beïnvloedde daarnaast de dwarshelling bij een hogere mobiliteit door te bepalen welke beddingvormen ontwikkelden bij een bepaalde stroomsnelheid. Het evenwicht tussen de dwarshelling en de spiraalstroming verschilden tussen experimenten met fijn en grof sediment door de verschillende beddingvormen die ontwikkelden (Hoofdstuk 3). Grof sediment ($D_{50} > 0.7$ mm) liet een directe relatie zien tussen de dwarshelling en de hoek van de lijzijde van de duinen die aanwezig waren in deze experimenten. Deze hoek was afhankelijk van de korrelgrootte. De relatie tussen de dwarshelling en de hoek van de lijzijde is mogelijk te verklaren doordat steile lijzijden zorgen voor permanente loslating van de stroming aan de duintop, wat de spiraalstroming versterkt in het dal tussen twee duinen. In experimenten met fijn sediment ($D_{50} < 0.7\ mm$) kwamen verschillende soorten beddingvormen voor, afhankelijk van de stroomsnelheid, variërend van ribbels, duinen met ribbels, duinen zonder ribbels, tot een vlakke bodem bij hoge stroomsnelheden. De afmetingen van deze beddingvormen lieten geen directe relatie zien met de spiraalstroming of de dwarshelling, en de hoeken van de lijzijden waren afhankelijk van het type beddingvorm in plaats van de korrelgrootte.

De experimenten met een sedimentmengsel lieten hetzelfde evenwicht zien tussen de spiraalstroming en de dwarshelling, wat aangeeft dat er geen terugkoppeling was tussen de sor-

tering en de grootte van de helling (Hoofdstuk 4). Om de sortering te kwantificeren werden er sedimentmonsters genomen over de dwarsrichting van 13 experimenten met verschillende dwarshellingen, waarna deze monsters werden gezeefd. De resultaten lieten zien dat alle fracties die mobiel waren efficiënt uitgesorteerd werden langs de dwarshelling. De verandering in het volume van de fracties over de dwarsrichting nam toe met de grootte van de fractie en met toenemende helling. Daarnaast lieten de monsters die over de gehele hoogte van de duin waren genomen weinig effect zien van verticale sortering langs de lijzijde van de duinen, omdat het verschil met oppervlakte monsters klein was. Dit betekent dat bochtsortering los van duinsortering gemodelleerd kan worden, wat gunstig is voor het gebruik van een actieve laag in morfologische modellen.

Hoewel de resultaten van de experimenten een nieuwe, niet-lineaire, relatie lieten zien tussen de bochtstroming en de dwarshelling, liggen de resultaten nog steeds rond de standaardwaarde voor de dwarshellingsparameter in morfologische modellen, of zelfs nog lager voor grof sediment. Dit suggereert dat het verhogen van de dwarshellingsparameter om de extreme insnijding in modellen tegen te gaan niet veroorzaakt wordt door de simpele implementatie van dwarshellingseffecten, maar dat dit waarschijnlijk nodig is om te compenseren voor andere tekortkomingen.

De modelresultaten lieten zien dat de mate van insnijding van de geulen met de standaard dwarshellingsparameter afhankelijk is van de gridcelgrootte en van de relatieve hoeveelheid sediment dat wordt getransporteerd in suspensie (Hoofdstuk 5). Met een fysisch realistische dwarshellingsparameter leidt een fijner grid tot meer insnijding, aangezien dezelfde afvoer door zo min mogelijk gridcellen wil stromen. De initiële balans tussen insnijding en transport in de dwarsrichting bepaalt of een geul zich gaat insnijden, of dat het naar een evenwicht gaat door de oevers te eroderen. De grootte van de dwarshellingsparameter die nodig is om extreme insnijding tegen te gaan, is afhankelijk van de hoeveelheid bodemtransport. De transportvoorspeller van Van Rijn maakt een onderscheid tussen bodemtransport en transport in suspensie, terwijl er in dit model vanuit gegaan wordt dat alleen bodemtransport onderhevig is aan dwarshellingseffecten. Hierdoor hangt de mate van insnijding af van de hoeveelheid sediment in suspensie. De transportvoorspeller van Engelund-Hansen maakt geen onderscheid en voorspelt tegelijkertijd een grotere hoeveelheid sedimenttransport dan de transportvoorspeller van Van Rijn. Aangezien hier al het sedimenttransport onderhevig is aan dwarshellingseffecten, hebben modellen met deze transportvoorspeller een lagere dwarshellingsparameter nodig om de onrealistische insnijding tegen te gaan.

De soort grootschalige morfologie die wordt gemodelleerd beïnvloedt de mate van insnijding en hoe gevoelig deze modellen zijn voor een toename in de dwarshellingsparameter. Om een dynamisch systeem te modelleren moet het model de grid-afhankelijke insnijding tegengaan op geul niveau door het dwarshellingseffect te verhogen. De geul kan namelijk alleen migreren als deze insnijding gebalanceerd is door sedimenttransport naar het midden van de geul. De modelresultaten lieten hierdoor zien dat geulen in modellen met de transportvoorspeller van Van Rijn niet meer migreerden nadat ze gevormd waren, terwijl geulen in modellen met de transportvoorspeller van Engelund-Hansen wel konden migreren en afsplitsen. Hiernaast lieten modellen met Van Rijn onnatuurlijke scherpe en hoekige bochten zien, die duidelijk het rechthoekige grid volgen. Systemen die op de grote schaal afhankelijk

zijn van een evenwicht tussen erosie en depositie, zoals rivieren en estuaria, hebben een hoge dwarshellingsparameter nodig om dynamisch te zijn, vooral wanneer het model gebruik maakt van de transportvoorspeller van Van Rijn. Verhogen van de dwarshellingsparameter zorgt hier voor langere en bredere zandbanken en een toename in actieve geulbreedte, en daardoor voor minder geulen en bifurcaties. Modellen van erosieve systemen, zoals een getijde bekken, hebben alleen een hoger dwarshellingseffect nodig wanneer het doel van het model is om dynamische geulen te krijgen. De grootte van de dwarshellingsparameter zal in dit soort modellen vooral de geuldimensies en migratiesnelheid bepalen, en niet zozeer de hoeveelheid geulen. In systemen waar vooral sediment afgezet wordt en waar laterale dynamiek initieel minder belangrijk is, zoals delta's en puinwaaiers, zullen zandbanken vormen met meer realistische dimensies met standaard dwarshellingseffecten. Echter, geulen die op deze afzettingen ontstaan, zullen wel insnijden en zullen ook de onnatuurlijke geuldimensies en hoekige bochten laten zien. De transportvoorspeller van Engelund-Hansen voorspelt een erg diffuse morfologie bij deze systemen, door de te grote hoeveelheid sedimenttransport dat voorspeld wordt.

Wanneer modellen ontworpen zijn om bestaande morfologie na te bootsen, bijvoorbeeld voor technische ingrepen of baggerstrategieën, zijn de modelresultaten sterk afhankelijk van de keuze in dwarshellingvoorspeller in combinatie met de transportvoorspeller (Hoofdstuk 5). De twee verschillende methodes om sedimenttransport in de dwarsrichting te berekenen in Delft3D, namelijk de methode van Ikeda of Koch Flokstra, resulteren in verschillende hoeveelheden en richtingen van sedimenttransport op dezelfde helling. Dit wordt veroorzaakt door de verschillende manier om de transportvector te berekenen en dit leidt tot een verschil in lokale geuldynamiek, zoals de snelheid van oevererosie en locaties van erosie en depositie. Op de grotere schaal leidt dit tot verschillende dimensies van banken en geulpatronen. Dit betekent dat wanneer een model gekalibreerd is op bestaande morfologie, maar gebruikt wordt om een schatting te maken van de snelheid van erosie of sedimenttransport, deze schatting afhangt van de keuze in dwarshellingvoorspeller. Aan de andere kant, wanneer een model gekalibreerd is op de snelheid van sedimenttransport zullen de morfologie en de lokale dwarshellingen verschillen tussen beide voorspellers. Dit zijn bijvoorbeeld modellen die focussen op de migratiesnelheid van gestort sediment, de verdeling van sediment over bifurcaties, of de snelheid van oevererosie. We kunnen hierdoor concluderen dat wanneer modellen gekalibreerd zijn door de dwarshellingsparameter te verhogen, het onmogelijk is om zowel sediment transport als morfologie te laten overeenkomen met gemeten data.

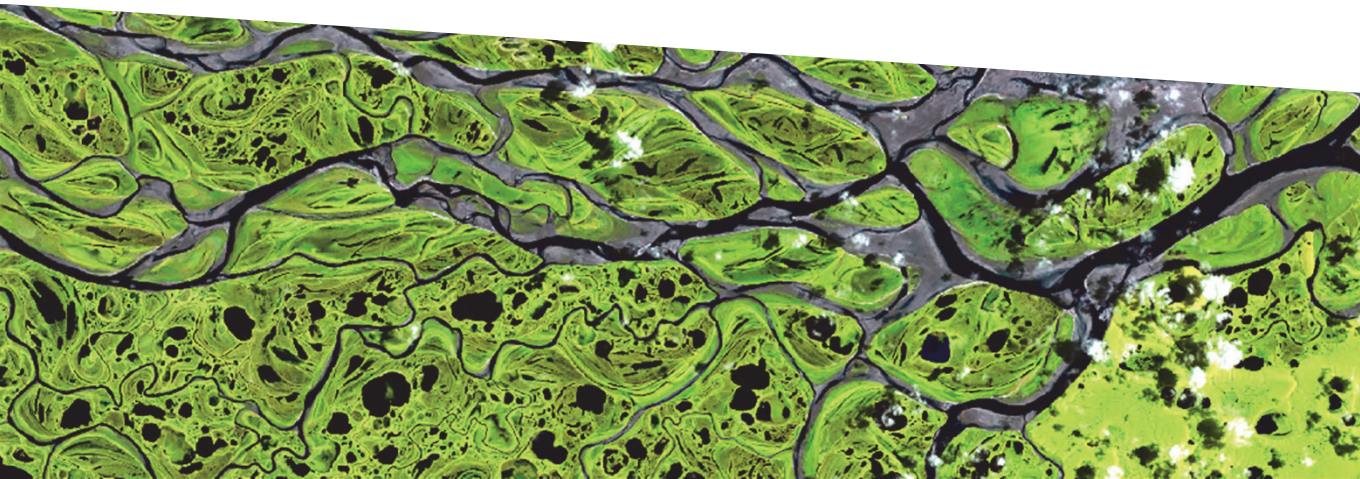

Chapter 1

Introduction

1.1 Problem definition and project aims

Flowing water forms channels that transport sediment from the mountains to the sea, forming rivers, deltas and estuaries (Fig. 1.1). These are dynamic fluvial and coastal landscapes harbouring a large part of the human population, that depend on rivers for transportation and as a source of water and food in many direct and indirect ways. Successful management of these systems requires reliable morphodynamic models, to predict the evolution of the system under the influence of pressures such as sea level rise and human interference, and to optimize for example engineering interventions, flood protection, sand mining and shipping fairway maintenance. However, current morphodynamic models are unreliable to accurately predict natural dynamics at the scale of bars and channels, due to a lack of understanding of local sediment transport dynamics. In particular models often predict unrealistically deep and narrow channels, and in practice all large-scale models need some form of calibration to converge to a stable morphology. However, this calibration leads to uncertainty in e.g. predicted sediment transport rates, channel dynamics and time scales of morphological change. Therefore, there is a need for a better physical understanding of sediment transport patterns at the channel scale that sets channel dimensions and determines bar and channel patterns.

Channel formation is initially the result of the balance of two processes: channel erosion and gravity-driven downslope sediment transport on the side slopes of the channel that counteracts this erosion. The formation of channels and bars start with minor perturbations that attract more flow, which leads to more erosion because sediment transport depends on velocity to a power larger than one. This nonlinearity of sediment transport leads to a positive feedback: once a shallow channel forms it attracts more flow and the channel deepens further. This positive feedback is strongest near the beginning of motion, where the nonlinearity of sediment transport is largest and therefore tends to carve and amplify channels. However, sediment is pulled down on the side slopes of this channel due to gravity, which counteracts the incision and is therefore an important feedback on channel formation (e.g. van Bendegom, 1947; Hasegawa, 1981; Struiksma et al., 1985; Sekine and Parker, 1992). As a result, the amount of downslope sediment transport strongly determines equilibrium channel dimensions and their dynamics, such as lateral channel migration.

When channel patterns evolve, downslope sediment transport is also essential in balancing secondary flows induced by bars and bends. Secondary flows in bends are inward directed near the river bed and therefore drag sediment upslope, but this is balanced by sediment traveling downslope due to gravity. The resulting equilibrium slope does not appear instantaneously downstream of the bend entry, but the bed adapts asymptotically (Struiksma et al., 1985). When there is a large amount of downslope sediment transport, the bend will adapt to an equilibrium slope over a relatively short reach and bars will disappear within a short

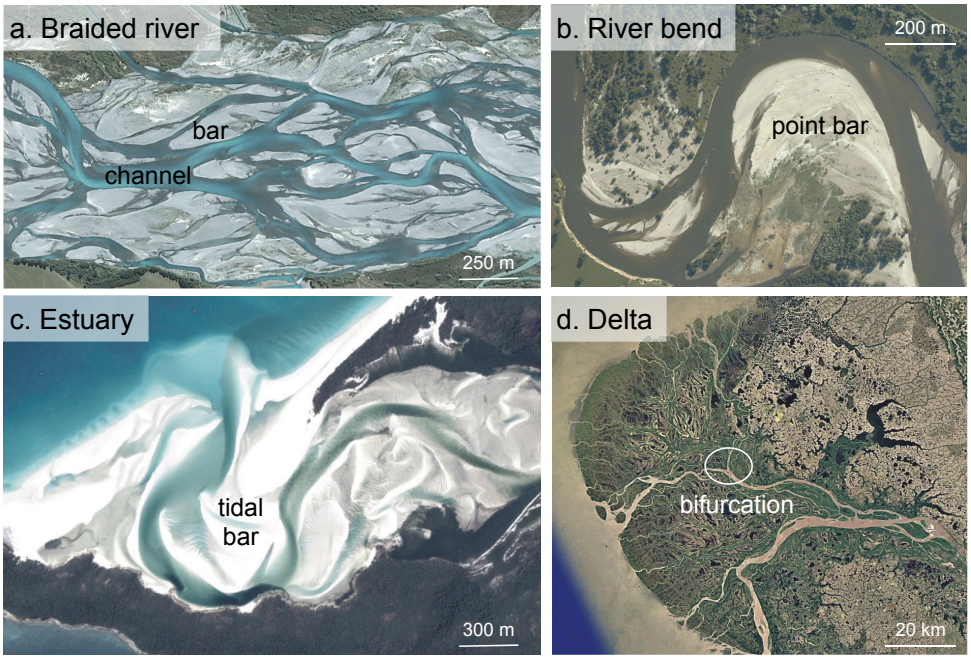

Figure 1.1: a) Fluvial channels and bars in the braided Rakaia River, New-Zealand. b) A meander bend in the Allier River, France. c) Tidal channels and bars in the estuary at Whitehaven beach, Australia. d) The Yukon Delta in Alaska, US, showing many bifurcations.

distance downstream, whereas smaller amounts of downslope sediment transport allow perturbations to propagate further downstream (Crosato and Mosselman, 2009; Kleinhans and van den Berg, 2011). Hereby, downslope sediment transport controls the adaptation of the morphology to changes in flow conditions (Struiksma et al., 1985; Johannesson and Parker, 1989).

By both counteracting incision and balancing secondary flow, the magnitude of downslope sediment transport determines the developed active channel width, orientation of channels, and the length and migration rates of fluvial and tidal bars (Seminara and Turbino, 2001; Dissanayake et al., 2009; Schuurman et al., 2013; Van Dijk et al., 2014), and controls the division of bedload over bifurcations (Kleinhans and van den Berg, 2011)(Fig. 1.1). On a larger scale, the amount of downslope sediment transport therefore has a major influence on channel and bar patterns, by determining braiding index(Parker, 1979; Struiksma et al., 1985; Crosato and Mosselman, 2009) and the stability of river bifurcations and the related tendency of channels on fans and deltas to avulse (Bolla Pittaluga et al., 2003; Kleinhans et al., 2008; Sloff and Mosselman, 2012; Bolla Pittaluga et al., 2015).

To accurately describe the interactions between sediment transport and large-scale morphology, it is essential to quantify the direction and magnitude of downslope sediment transport, but the underlying process is poorly understood and therefore overly simplified in morphodynamic models. At the same time, current morphodynamic models severely over-

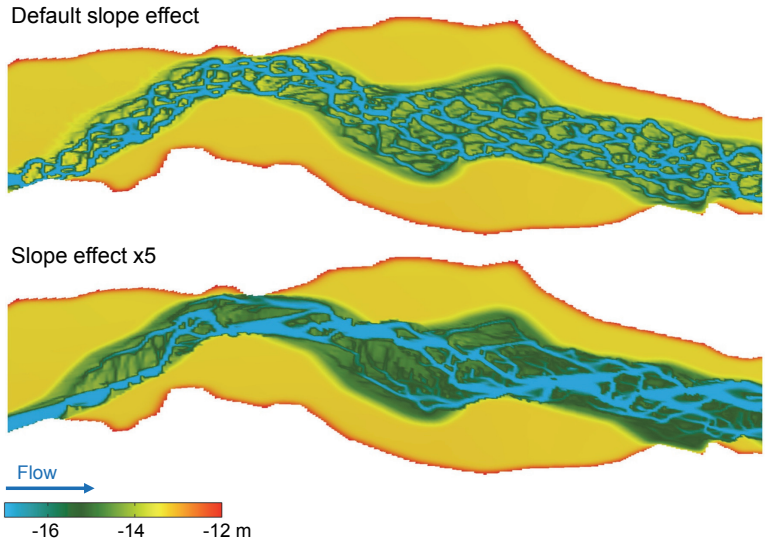

Figure 1.2: The Upper Yellow River modelled by Schuurman et al. (2016) with the default slope parameter, and with a slope parameter that is increased with a factor of 5.

predict channel depth and bar height, which means there is something wrong with the balance between incision and downslope sediment transport. The transverse bed slope parameter, which linearly increases downslope sediment transport, has proven to be an effective calibration parameter to counteract this unrealistic overdeepening of channels (Fig. 1.2) (Van Der Wegen and Roelvink, 2008; Schuurman et al., 2013; Schuurman et al., 2016, e.g.). As a result, the transverse bed slope parameter is seemingly arbitrary increased to obtain realistic bar and channel patterns, up to two orders of magnitude larger than the default value, meaning an increase of two orders of magnitude in downslope sediment transport. This results in better-looking morphology, but it is unknown how this large increase in local sediment transport affects bar and channel dynamics, the distribution of sediment over bifurcations, and therefore predicted large-scale channel patterns.

The severe incision in current morphodynamic models suggests the default transverse slope parameter is not realistic and should be better quantified. Even though the physical process of sediment transport on transverse bed slopes is not yet fully understood, the extremely large range in slope effects that is applied between different model studies seems highly unlikely to be realistic. The two main objectives of this thesis are therefore to:

1. Quantify the physical processes that influence sediment transport on transverse bed slopes to determine realistic ranges of the transverse slope parameter.
2. Identify the cause of the severe incision in morphodynamic models and why there are extremely large differences in transverse slope parameter needed to counteract this incision.

These two objectives will be answered through a series of subquestions, which are presented in section 1.5. In the following sections, the necessary context for these subquestions is pro-

vided, starting with the processes that influence sediment transport on slopes, followed by a review on previous transverse slope predictors, and an analysis on uncertainties related to transverse slope effects in morphodynamic models.

1.2 Sediment transport processes on transverse bed slopes

In a straight river section, the fluid drag on sediment particles is generally directed downstream along the river, while gravity pulls the particles in the direction of the slope. As a result, the particles are dragged along the flow while also traveling downslope, resulting in a net angle between sediment transport and the main flow direction (Fig. 1.3). This angle of deflection therefore depends on flow velocity in the downstream direction and sediment properties that determine the gravity component in the transverse direction (e.g. van Bendegom, 1947; Sekine and Parker, 1992; Talmon et al., 1995). In bends, flow patterns near the bed are modified by secondary flow patterns that alter the direction of the bed shear stress. As a result, bed shear stress is directed towards the inner bend. This leads to an equilibrium transverse slope when upslope directed drag force by secondary flow balances the downslope gravitational force on particles (e.g. Engelund, 1974; Struiksma et al., 1985). In this section processes that influence this balance between flow and sediment transport on transverse slopes are discussed.

In nature, sediment is never uniform but exists of a mixture of different grain sizes, which leads to sorting patterns due to different interactions with the flow. The size and density of the sediment determine the gravitational pull on the particles, while the drag force of the flow acts on the surface area. Therefore, on slopes, larger grain sizes are subject to a relatively larger pull of gravity than of flow shear, while finer particles are more easily dragged along by the flow, which leads to size-sorting along the slope (Ikeda, 1989). When an upslope-directed secondary flow is present in river bends, finer sediments are gradually dragged higher up the point bar by the secondary currents, while coarser sediments are deposited near the outer bend, which leads to the classic bend sorting pattern (e.g. Parker and Andrews, 1985; Bridge, 2003). This sorting becomes more pronounced when the standard deviation of the supplied sediment mixture is larger (Parker and Andrews, 1985). Possibly, sediment sorting influences the magnitude of the transverse slope and lowers the rate of channel incision, since coarser grains that are deposited lower on the slope need a higher shear stress to be entrained than fine sediment (e.g. Ashworth and Ferguson, 1989; Odgaard, 1981).

However, there are other processes that influence the balance between flow and gravity. Firstly, there are different modes of sediment transport. Just above the threshold of sediment motion, sediment stays in contact with the bed and is transported by the flow by rolling or sliding (Bagnold, 1977, e.g.). When flow velocity increases, particles start to hop over the bed and are only periodically in contact with the bed, which is called saltation (Bridge, 1992, e.g.). When the flow velocity further increases, sediment is transported in suspension and loses any contact with the bed (van Rijn, 1984, e.g.). The transition from one transport mode to another also depends on grain size and density. In theory, when particles are only periodically or not in contact with the slope, their movement direction is not constantly affected by the gravitational pull and therefore they do not always travel downslope (Sekine and Parker,

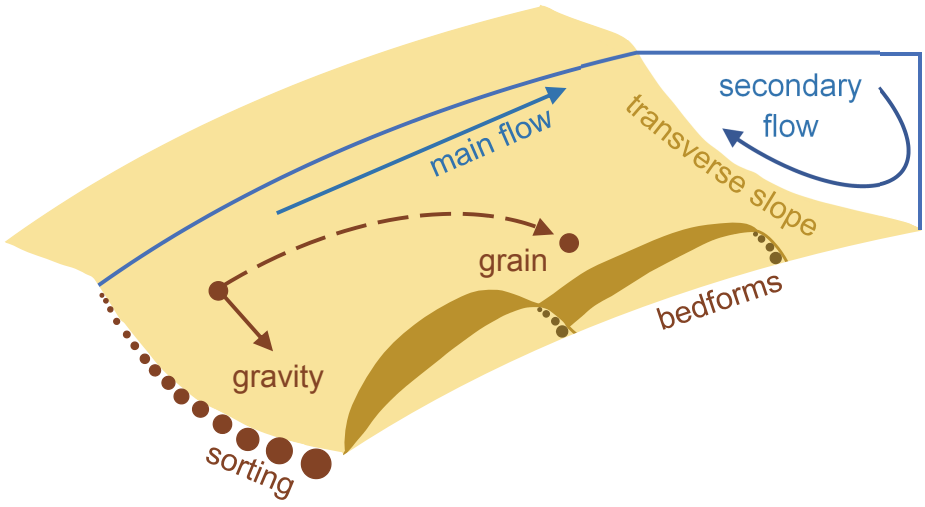

Figure 1.3: Sketch of the main processes that influence flow patterns and downslope sediment transport on slopes transverse to the main flow direction.

1992). Different modes of transport are therefore expected to lead to a different equilibrium transverse slope.

Secondly, in sand-bed rivers, bedforms ranging in scale from ripples to dunes are major contributors in determining how sediment is transported downstream and create large-scale turbulence in the flow (Allen, 1968; Bennett and Best, 1995; McLean et al., 1994; Best, 2005). The type of bedform that is present depends on flow velocity and sediment characteristics (Van den Berg and Van Gelder, 1993). At low transport rates, the sediment that is in motion travels over a flat bed, called the lower plane bed. Then, dunes start to develop in coarse sand (> 0.7 mm), where dune height will increase with increasing flow velocity and shear stress until they reach a certain height relative to the water depth (Van Rijn, 1984a; Julien and Klaassen, 1995). In fine sands first ripples start to form, transitioning into dunes at higher flow velocity. This transition phase is often characterized by dunes with ripples superimposed on the dune stoss side (e.g. Guy et al., 1966; Ashley, 1990; Ten Brinke et al., 1999; Venditti et al., 2005). At very high shear stresses, dunes flatten and upper stage plane beds are created (Van Rijn, 1984a; Naqshband et al., 2014; Bridge and Best, 1988)

Bedforms cause a strong variation in the flow field and the local streamwise and transverse slopes along the river bend. Due to their height, dunes may have a larger influence on the flow than ripples (Bennett and Best, 1995). Flow accelerates over the bedform stoss side and decelerates at the dune crest where, if the lee side is steep, flow detaches and reattaches further downstream and creates a zone of flow separation (e.g. Best, 2005; Lefebvre and Winter, 2016; Kwoll et al., 2017). By flow separation, bedforms generate turbulence and thereby exert friction on the flow (Best, 2005). Since dunes migrate with the flow downstream and transport sediment, they will influence the amount of transverse sediment transport and influence

sorting patterns. Sediment is transported over the dune stoss side and avalanches over the dune crest at the lee side (Best, 2005). Larger grains are deposited further downslope the lee side, which leads to vertical sorting over the height of a dune (Kleinhans, 2001; Blom and Parker, 2004). Because of their influence on flow, local bed morphology, and sorting patterns, dunes could potentially have a large influence on the balance between secondary flow and transverse sediment transport. However, to what extent and in what way is unknown. Observations in previous studies were based on a limited amount of experiments (Talmon et al., 1995; Wiesemann et al., 2006) or a specific field site (Kisling-Moller, 1993; Nanson, 2010), which means that the relations between varying bend radii, flow velocity, grain size and consequently changing bedform morphology were insufficiently quantitatively understood. Therefore, the influence of bedform morphology on flow patterns and transverse sediment transport was never incorporated in derivations of physics-based predictors for transverse downslope sediment transport. Their relative influence is most likely related to their height compared to the water depth (Talmon et al., 1995), and they could for example enhance secondary flow and thereby increase inward directed sediment transport by focusing flow in dune troughs (Kisling-Moller, 1993; Wiesemann et al., 2006), or increase downslope sediment transport by avalanching at the lee sides of the dunes (Sieben and Talmon, 2011).

1.3 Past research on predicting transverse sediment transport

The earliest relation between downslope sediment transport and secondary flow is described by van Bendegom (1947), who assumed a linear relation between the secondary flow intensity and the transverse slope:

$$\frac{\partial z_b}{\partial y} = Btan(\delta) = B\frac{u_n}{u_s} \tag{1.1}$$

Where $\frac{\partial z_b}{\partial y}$ = transverse slope, δ = direction of near-bed flow velocity, u = magnitude of the flow velocity $[m/s]$ in transverse direction (n) and streamwise direction (s) and B = a dimensionless slope factor. The secondary flow intensity is defined as the direction of the flow near the bed, i.e. the ratio between the magnitude of the normal flow and secondary flow.

Slope factor B relates the secondary flow intensity to the transverse slope, and thereby describes the equilibrium between upslope directed shear stress and downward directed gravity. Following research focused on determining this slope factor. They either developed a theoretical model validated with laboratory experiments or field data (e.g. Engelund, 1974; Koch and Flokstra, 1981; Ikeda, 1984), or based the slope factor on an empirical fit through experimental data (e.g. Talmon et al., 1995; Wiesemann et al., 2006). Theoretical models consist of a radial balance of forces acting on a grain moving on a transverse inclined bed. These forces consist of gravity pulling the particles downslope, a drag force on the particles in the direction of the bed shear stress, and friction between the particles and the bed (van Bendegom, 1947; Engelund, 1974; Koch and Flokstra, 1981). The frictional forces can consist of both dynamic friction between moving particles and the bed, and static friction between non-moving particles in the bed, which is frequently expressed as the angle of internal friction or angle of repose (Parker et al., 2003). Since the slope factor is assumed to be a function of sediment properties and fluid drag, in most studies B is a function of sediment mobility

(θ) (Talmon et al., 1995). Accordingly, the slope factor is often defined in the generalized form:

$$B = \alpha\theta^{\beta}, \tag{1.2}$$

or when the critical shear stress (θ_c) is included:

$$B = \alpha_c \left(\frac{\theta}{\theta_c} \right)^{\beta} \tag{1.3}$$

Where the sediment mobility θ, a dimensionless form of the bed shear stress, reads:

$$\theta = \frac{\tau}{(\rho_s - \rho)gD_{50}} \tag{1.4}$$

where τ = shear stress $[N/m^2]$, ρ_s = specific density of the sediment, g = gravitational acceleration $[m/s^2]$ and D_{50} = median grain size $[m]$.

The formulation of the parameters α or α_c and β in previous studies depended on the research objective but were generally a constant. Their magnitude was a result of the experimental conditions in empirical studies and the formulation of the forces on the grains in theoretical models. All studies focused on a specific process, related to sediment transport mode (Sekine and Parker, 1992; Parker et al., 2003, e.g) or bed state (Hasegawa, 1981; Ikeda, 1984; Talmon et al., 1995, e.g). Studies that wanted to avoid bedforms and focused on sediment transport on a lower plane bed included for example a critical sediment mobility and static friction to account for the beginning of motion (Hasegawa, 1981; Parker et al., 2003). Existing slope predictors based on an empirical fit through experimental data mainly focused on the effect of ripples and dunes (Talmon et al., 1995; Wiesemann et al., 2006), and saw a decrease in downslope sediment transport when dunes are present. They either included a calibration coefficient to the transverse bed slope predictor to account for the differences (Koch and Flokstra, 1981; Talmon and Wiesemann, 2006) or proposed a slope factor including a ratio between the water depth and the median grain size, to account for bedform height (Talmon et al., 1995). The dominant transport mode determines the effective gravity acting on the grains. The predictor of Sekine and Parker (1992) assumes that saltating particles are less influenced by gravity than rolling and sliding particles because they have less frequent contact with the bed, with the result that the slope factor B is less dependent on sediment mobility. When suspension is present, Talmon et al. (1995) found nearly half of the downslope sediment transport compared to bed-load dominant conditions with equal flow velocities.

A later refinement of this linear relation between the secondary flow intensity and the transverse slope is the non-linear model of Parker et al. (2003) and the approximation of this model by Francalanci and Solari (2008), in which the slope factor itself depends on the transverse slope. They state that linear theoretical models only apply for gentle slopes because dynamic and static friction are constant in this case and thereby do not depend on the magnitude of the transverse slope. However, their non-linear relation only holds for lower stage plane bed configurations, meaning no bedforms, and up to slopes of 14 degrees (Parker et al., 2003).

It is possible to calculate the transverse bed slope effect from morphological measurements in laboratory flumes. Experimental setup and conditions to validate the theoretical models

or to obtain an empirical fit depended on the process of interest. Firstly, past experiments were conducted in either a bended flume to study the equilibrium slope in river bends (e.g. Struiksma et al., 1985; Ikeda and Nishimura, 1986), or straight flumes initiated with a transversely sloped bed that relaxed to a horizontal bed (e.g. Ikeda and Nishimura, 1986; Talmon et al., 1995; Talmon and Wiesemann, 2006). Straight flumes have the advantage of reasonably isolating the transverse bed slope effect without strong bend flow. However, they have the disadvantage that the transverse bed slope effect is determined from the initial changes of the bed slope rather than an equilibrium morphology, and that the bedforms develop at the same timescale (Talmon and Wiesemann, 2006). In curved flumes and in the annular flume of Engelund (1975) a morphodynamic equilibrium is possible, which has the advantage of straightforward measurement of the transverse bed slope. However, this equilibrium depends on secondary flow patterns that need to be quantified and are only valid for one single bend radius. Secondly, the range of flow conditions and sediment properties corresponded with the sediment transport mode or bed state of interest. As a result, all experiments reported so far were performed with a limited range in flow conditions and sediment sizes, with a maximum of 11 unique experiments per study. The transition between bed states and sediment transport mode were mostly ignored, and the differences in experimental setup and assumptions made it impossible to compare the findings of different studies. Consequently, the need to develop experiments with appropriate conditions for testing certain predictors led in practice to limited and inconsistent experimental datasets to test and calibrate transverse bed slope relations.

Previous transverse bed slope predictors were not sufficiently tested, and there is therefore a need for a larger and consistent experimental dataset to obtain parameters for morphological modelling that cover all sediment transport modes and bedform regimes. This requires experiments with a large range in secondary flow intensity, leading to equilibrium transverse slopes from a nearly flat bed in gently curved channels to a steep transverse slope in tight river bends. Furthermore, grain size and flow velocity should be systematically varied, from the beginning of motion, across the ripple-dune transition, and up to a sediment mobility that results in an upper stage plane bed. In this study, experiments are conducted for a large range of near-bed flow velocities, secondary flow intensities and grain sizes, resulting in a total of 224 experiments.

1.4 Transverse bed slope effect in morphodynamic models

The severe channel incision in morphodynamic models is best known in the frequently-used morphological model code Delft3D (van der Wegen and Roelvink, 2012; Schuurman et al., 2013), but is also an issue in studies with other morphodynamic models, such as Telemac (Davies and Robins, 2017; Nnafie et al., 2016) and ROMS (Ganju et al., 2009). However, a quick inventory in typical geomorphology journals showed that only 13 (19%) out of 68 model studies discussed the imbalance between the severe incision and downslope sediment transport (Fig. 1.4a, Appendix D). The transverse slope parameter was only mentioned in 14 studies (21%), but the majority (41, 60%) ignored, or was unaware of, the importance of slope effects in their model. In this thesis, the problems that arise with bed slope effects

in morphodynamic models is illustrated with Delft3D, and therefore in this section the implementation of transverse slope predictors is explained for this specific model. However, the transverse bed slope predictors in other morphodynamic models are based on the same studies as mentioned in the previous section (Nnafie et al., 2016; Schuurman et al., 2016).

The uncertainty related to transverse slope effects in morphodynamic models is the result of four main issues: 1) the simplicity and unknown validity of the transverse slope predictor, 2) the implementation of this slope predictor, 3) the combination with the choice in sediment transport predictor, and 4) the interaction between horizontal and vertical sorting that is poorly constrained in morphodynamic models. The first cause of uncertainty, the simplicity and validity, is the result of using transverse slope predictors of previous experimental studies in the model. Downslope sediment transport is calculated by a transverse slope predictor that deflects the streamwise sediment transport vector as a result of the local bed slope. There are several options for transverse slope predictors in Delft3D which are all functions based on equation 1.2, i.e. a constant multiplied with the magnitude of the local transverse slope and a power function of sediment mobility. Since this power is a constant, the amount of downslope sediment transport is linearly related to sediment mobility throughout a model run. Even though this relation and corresponding slope factors were validated in literature for a specific process and corresponding range in flow conditions and sediment mobility, morphodynamic models apply these in a wide range of environments and conditions where all processes act together. Sediment sorting along a transverse slope in models with a sediment mixture is even more simplified. In this case, a factor is added to the transverse slope predictor that divides the diameter of the grain size fraction by the median grain size to the power of a user-defined coefficient. Morphodynamic models thus do not include physics-based relations for sediment sorting.

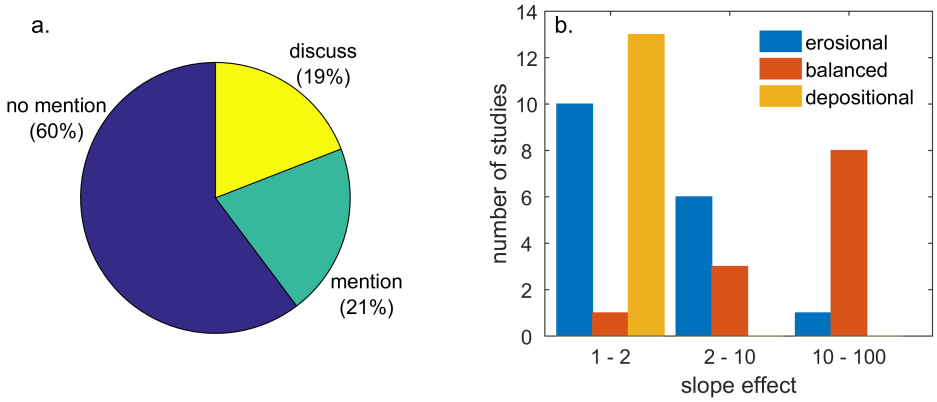

Figure 1.4: (a) Model studies that mentioned, discuss or overlooked the severe channel incision and the artificial increase in slope effect that was necessary to counteract this (see Appendix D for inventory). (b) Studies that mention the magnitude of the slope effect subdivided by modelled environment and the applied slope effect value (1=default).

The second cause of uncertainty is the way this transverse slope predictor is applied to calculate the resulting transport vector since there are different methods with important differences. The two most commonly used methods are the one by Ikeda (1984) and by Koch and Flokstra (1981). The method of Ikeda (1984) uses the transverse slope predictor with input parameter α_I to calculate an additional vector in transverse direction based on the magnitude of the streamwise vector (Fig. 1.5a). This vector is then added to the vector in streamwise direction to determine the resulting direction and magnitude of the transport vector. In contrast, for the method of Koch and Flokstra (1981) the direction of sediment transport is corrected for transverse gradients by rotating the transport vector, by using the transverse slope predictor with input parameter α_K to calculate an angle of deflection (Fig. 1.5b). Note that the way this transverse slope predictor is used in Delft3D means that α_K is the inverse of α_I. Another difference between both methods is that Ikeda (1984) uses a critical shear stress, which is absent in the method of Koch and Flokstra (1981). Equations and method to compare both slope parameterizations are given in Appendix B.

How the difference between these two methods affects morphology and the rate of change thereof remains unquantified, but the obvious hypothesis is that this has major implications for morphology, especially when the transverse slope parameter is increased in morphological calibration of models. Specifically, the method of Ikeda (1984) increases the direction and total magnitude of sediment transport when a transverse slope is present, while for the method of Koch and Flokstra (1981) only the direction is changed. The default value of α_I is set to 1.5, while the parameter α_K is not defined, but should also be 1.5 according to the study of Koch and Flokstra (1981). By increasing the α_I in the method of Ikeda (1984) by e.g. a factor of ten, the amount of downslope sediment transport is also increased by a factor of

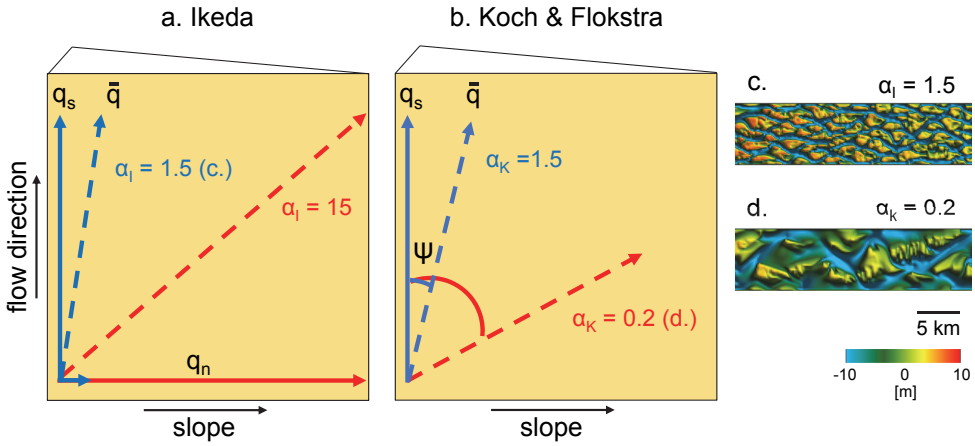

Figure 1.5: Two parameterizations for sediment deflection drawn on a transverse bed slope (Ikeda, 1984; Koch and Flokstra, 1981). Both methods are drawn on a top view of a bed sloping towards the right. Blue dashed arrows show transport vectors with default values for the slope effect, while red arrows represent transport vectors when the slope effect is increased to typical values used in current model studies. c+d) examples of the braided river model of Schuurman et al. (2013) with default (c) and high slope effect (d).

ten, which increases the total sediment transport significantly (Fig. 1.5). With the method of Koch and Flokstra (1981) sediment transport is not increased, but here, decreasing the α_K to values reported in literature could easily result in more downslope sediment transport than streamwise sediment transport.

The third cause of uncertainty relates to the choice in sediment transport predictor. Since the deflection of the transport vector is directly related to the magnitude of streamwise sediment transport, the amount of downslope sediment transport is very sensitive to the transport predictor that is used. Most commonly used predictors are the transport predictor of Meyer-Peter and Müller (1948), Engelund and Hansen (1967), or one of the predictors of Van Rijn (Van Rijn, 1984b; van Rijn, 1993; Van Rijn et al., 2004, e.g). One of the main distinctions between these sediment transport predictors is if they take suspended sediment into account. The predictors of Van Rijn make a distinction between bed load and suspended sediment, and only the bed load part is used to calculate downslope sediment transport, since it is assumed that gravity only acts on sediment in contact with the bed. In contrast, the predictors of Meyer-Peter and Müller (1948) and Engelund and Hansen (1967) are total load predictors, and therefore suspended load is treated as bed-load and the bed slope effect acts on all sediment in transport. Another important distinction is how they relate sediment transport to flow velocity, which defines the non-linearity of the sediment transport equation. For example, the predictors of Van Rijn and Meyer-Peter and Müller (1948) relate the sediment transport rate to the flow velocity to the power of 3, while the predictor of Engelund and Hansen (1967) relates this to the flow velocity to the power of 5. Therefore, Engelund-Hansen will predict a larger sediment transport rate at the same flow velocity. However, Van Rijn includes a critical flow velocity, and therefore the relation between flow velocity and sediment transport will be more non-linear near the beginning of motion.

The choice of sediment predictor thus directly influences the amount of downslope sediment transport, and therefore calibrating slope effects with different transport predictors lead to different magnitudes of the transverse bed slope parameter. For example, it is known that models with the predictor of Van Rijn need a higher bed slope parameter to counteract incision, which is assumed to be because slope effects only act on bedload (van der Wegen and Roelvink, 2012; Dissanayake et al., 2009; Braat et al., 2017). However, the literature study reveals that it is likely that the magnitude of the transverse bed slope parameter also depends on the environment that is modelled (Fig. 1.4b, Appendix D). Here, the environment means initial and boundary conditions, which determine sediment characteristics, flow conditions, channel pattern and bar regime. Models of environments with a large-scale balance between erosion and deposition, such as estuaries and rivers, particularly have the tendency to overpredict channel depth and braiding index and required very high slope effects up to a factor of 100 (e.g. Van der Wegen and Jaffe, 2014; Schuurman et al., 2018). In contrast, models of systems with dominant erosion such as a tidal channel network, usually had slope factors lower than 10 (e.g. Marciano et al., 2005; Dissanayake et al., 2009; Zhou et al., 2014), and depositional systems such as river deltas all used the default value (e.g. Edmonds and Slingerland, 2007; Leonardi et al., 2013; Caldwell and Edmonds, 2014). However, calibration of these erosional and depositional models did not necessarily focus on channel depth and bar dimensions, but for example on the rate of bank erosion and channel formation. Therefore,

both erosional and depositional models with default transverse slope parameters commonly show unrealistically deep channels and sharp angular bends Edmonds and Slingerland, 2009; Caldwell and Edmonds, 2014; Van der Vegt et al., 2016, e.g.

The fourth cause of uncertainty addressed in this thesis is the interaction between horizontal and vertical sorting that is poorly constrained in morphodynamic models and highly dependent on the thickness of a user-defined active layer. The relative importance of horizontal and vertical sorting and their characteristic timescales controls the degree of spatial sorting, which influences the flow by determining the distribution of friction, the sediment transport rate and maximum scour depth through mobility, and the morphology by downstream fining and sediment distribution over bifurcations when lateral slopes are present upstream of a bifurcation (Kleinhans, 2001; Mosselman et al., 1999; Frings, 2008). The active layer concept divides the bed in one active layer and immobile underlayers (Parker et al., 2000; Blom et al., 2008). Only the active top layer interacts with the flow and determines the amount of sediment transport, and there is only an exchange of sediment between the underlayers and the active layer in case of erosion or deposition. Therefore, the active layer determines the volume of each fraction that is available for sediment transport and consequently lateral sorting. As a result, spatial sorting and bed level changes are extremely sensitive to the user-defined thickness of this active layer, which sets the time scale of changes in bed composition. When the layer is relatively thin, sorting reacts fast to changes in the flow and will result in better developed sorting patterns. On the other hand, a relatively thick active layer results in slower adjustments, and therefore sediment sorting acts on the same timescale as morphological development (Sloff and Mosselman, 2007; Kleinhans, 2010). Lateral sorting therefore depends on the sediment that is available in the top layer of morphodynamic models and is incorporated in the transverse slope predictor. Vertical sorting by dunes is not included in the active layer concept. However, the thickness of the layer is often based on characteristic bedform height to simulate sorting processes on a time scale of multiple dunes migrating over the river reach (Ribberink, 1987; Armanini et al., 1989). Therefore, to be able to accurately model average lateral sorting, it is necessary to know the relative importance of vertical sorting on lateral sorting on the time scale that is modelled.

1.5 Specific research questions and thesis outline

The previous sections revealed several research gaps, related to the two main objectives of this thesis: 1) quantifying the physical processes that influence sediment transport on transverse bed slopes, and 2) identifying the cause of severe incision in morphodynamic models. These research gaps led to the following subquestions that will be answered in the chapters of this thesis:

1. *What is the relation between transverse slope and secondary flow intensity with varying grain size and sediment mobility?*

Previous studies on sediment transport on transverse slopes focused on a specific transport mode or bed state, and consequently experiments were performed with a limited range in

flow conditions and sediment sizes. In Chapter 2, the transverse bed slope effect is experimentally quantified in a rotating annular flume for a large range of near-bed flow conditions and uniform sediment sizes to obtain parameters for morphological modelling that cover all sediment transport modes and bed state regimes. This resulted in a total of 224 experiments, amounting in twenty times more experiments than reported in literature.

2. *What is the effect of bedform type and morphology on the relation between secondary flow and transverse slope?*

Bedforms could potentially have a large influence on the balance between secondary flow and transverse sediment transport, due to their influence on flow, local bed morphology, and sorting patterns. In Chapter 3 I focus on the different bedforms that developed in the annular flume experiments and study the interaction between their morphology and the equilibrium between secondary flow and transverse bed slope.

3. *What is the relation between transverse slope and bend sorting of a sediment mixture, and what is the relative importance of vertical sorting by dunes on the lateral sorting pattern?*

Current morphodynamic models do not include physics-based relations for sediment sorting on transverse slopes. Furthermore, to what extent vertical sorting by bedforms influences the classic bend sorting pattern is unknown. Therefore, experiments with poorly sorted sediment were conducted in the rotating annular flume, in which the transverse slope and dune dimensions were systematically varied. In Chapter 4, bend sorting is described as an empirical function of grain size fractions and transverse slope, and the relative influence of bedforms on these sorting patterns is determined. Additionally, de resulting relation is tested on published field data.

4. *What are possible causes and effects of the imbalance between incision and transverse sediment transport in morphodynamic models?*

Current morphodynamic models severely over-predict channel depth and bar height, which suggests that there is something wrong with the balance between incision and downslope sediment transport. To determine the tendency to incise independently of numerics, I developed an analytical model in Chapter 5 of a river channel cross-section. This analytical model calculates the balance and imbalance between channel incision and downslope lateral sediment transport on an initially perturbed bed (Appendix C), which is compared to a simple numerical model of three grid cells wide. the numerical model is run with typical combinations of sediment transport predictors and slope parameterizations to study differences in the tendency to incise.

5. *What is the effect of different combinations of slope parametrization and sediment transport predictor on local sediment transport dynamics and on the large-scale morphology of rivers, estuaries and deltas?*

The literature showed a large range in the magnitude of the transverse slope parameters that was needed to get realistic morphology in large-scale morphodynamic models. The magni-

tude depended on the environment that was modelled and the sediment transport predictor that was used. Therefore, in Chapter 5, five sets of numerical morphodynamic simulations are conducted for different scales and environments, to study the effect of typical combinations of sediment transport predictors and slope parameterizations on local sediment transport, bar and bend dimensions, and large-scale channel patterns. These results are then used to explain the extremely large differences in transverse slope parameters reported in literature.

Finally, Chapter 6 summarizes the main findings of this thesis in the context of the literature and model applications, and discusses specific needs for further research.

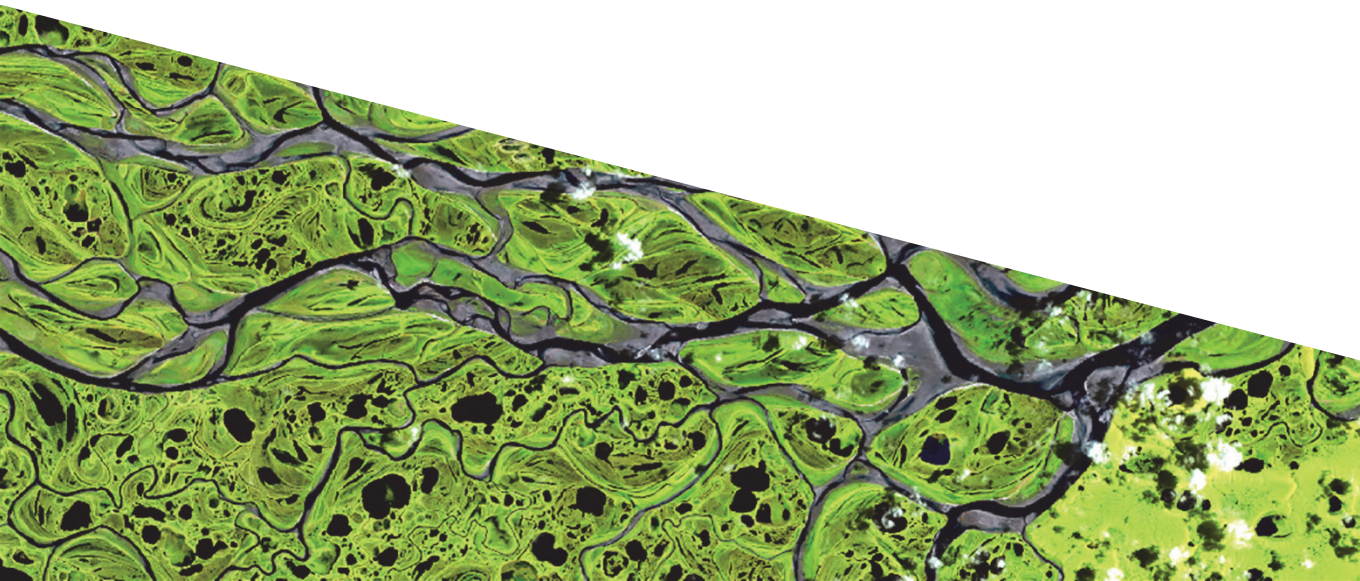

Chapter 2

Sediment transport of fine sand to fine gravel on transverse bed slopes in rotating annular flume experiments

Large scale morphology, in particular meander bend depth, bar dimensions and bifurcation dynamics, are greatly affected by the deflection of sediment transport on transverse bed slopes due to gravity and by secondary flows. Overestimating the transverse bed slope effect in morphodynamic models leads to flattening of the morphology, while underestimating leads to unrealistically steep bars and banks and a higher braiding index downstream. However, existing transverse bed slope predictors are based on a small set of experiments with a minor range of flow conditions and sediment sizes, and in practice models are calibrated on measured morphology. The objective of this research is to experimentally quantify the transverse bed slope effect for a large range of near-bed flow conditions with varying secondary flow intensity, sediment sizes (0.17–4 mm), sediment transport mode and bed state to test existing predictors. We conducted over 200 experiments in a rotating annular flume with counter-rotating floor, which allows control of the secondary flow intensity separate from the streamwise flow velocity. Flow velocity vectors were determined with a calibrated analytical model accounting for rough bed conditions. We isolated separate effects of all important parameters on the transverse slope. Resulting equilibrium transverse slopes show a clear trend with varying sediment mobilities and secondary flow intensities that deviate from known predictors depending on Shields number, and strongly depend on bed state and sediment transport mode. Fitted functions are provided for application in morphodynamic modelling.

Published as: Baar, A. W., De Smit, J.C., Uijttewaal, W.S.J., Kleinhans, M.G. (2018), Sediment transport of fine sand to fine gravel on transverse bed slopes in rotating annular flume experiments, *Water Resources Research*, 54(1), 19-45, DOI: 10.1002/2017WR020604.

2.1 Introduction

Subaqueous morphology arises from the interaction of flow and sediment transport. Starting from minor perturbations, the nonlinear dependence of sediment transport rate on flow shear stress at the bed causes growth of bedforms and bars, as deeper channels attract more flow, causing much more sediment transport, and the reverse for shallower areas. An important negative feedback on vertical growth is the direct pull by gravity on particles moving on gently sloping beds. Large-scale morphology in all aqueous environments with movable bed sediment is greatly affected by this. In particular, the bed slope effect determines wavelengths of coastal sandbanks and sandwaves (Hulscher, 1996; Blondeaux and Vittori, 2016), steepness of surfzone bars formed by gravity waves (Ruessink et al., 2007), length of fluvial bars and braiding index (Struiksma et al., 1985; Crosato and Mosselman, 2009), properties of tidal bars (Schramkowski et al., 2002; Seminara and Turbino, 2001; Leuven et al., 2016) and estuarine braiding (van der Wegen and Roelvink, 2012), and stability of river bifurcations (Bolla Pittaluga et al., 2015).

Here we focus on this transverse bed slope effect in curved channels with unidirectional flow and uniform sediment. In a straight river section, the fluid drag on sediment particles is generally directed downstream along the river, while the bed slope, usually the largest in transverse direction, causes sediment particles to also travel downslope across the channel. The net effect is an angle between the direction of sediment transport and the mean flow direction. The typical transverse slope that develops here is a balance between the shear stress in downstream direction and sediment properties that determine the gravity component in the transverse direction (e.g. van Bendegom, 1947; Sekine and Parker, 1992; Talmon et al., 1995). This is further modified by secondary flow patterns induced by bars and bends. These secondary currents alter the direction of the bed shear stress towards the inner bend. This leads to an equilibrium transverse slope towards the inner bend when the downslope gravitational force on particles is balanced by the upslope directed drag force by secondary flow (Fig. 2.1) (e.g. Engelund, 1974; Struiksma et al., 1985).

The transverse bed slope effect strongly influences bar patterns. Locally, slope effects determine bar height and active channel width (Schuurman et al., 2013). For example, a strong bed slope effect, i.e. a large deflection of sediment downslope, leads to low and wide bars. On a larger scale, transverse bed slope effects influence the adaptation of the bed to perturbations in the flow, as secondary currents are balanced by the transverse bed slope effect. The secondary flow patterns and the corresponding transverse bed slope do not appear instantaneously downstream of the bend entry, but adapt asymptotically (Struiksma et al., 1985). A strong bed slope effect causes the bend to adapt to an equilibrium slope over a relatively short reach and bars have the tendency to disappear within a short distance downstream, whereas weaker transverse bed slope effects allow perturbations to propagate further downstream (Crosato and Mosselman, 2009; Kleinhans and van den Berg, 2011). This process is illustrated by van der Wegen and Roelvink (2012) and Schuurman et al. (2013), who tested the sensitivity of a sandy estuary and of a morphodynamic model of a braided sand-bed river to the transverse bed slope effect. They showed that overestimating this effect leads to flattening of the morphology, while underestimating leads to unrealistically steep bars and banks

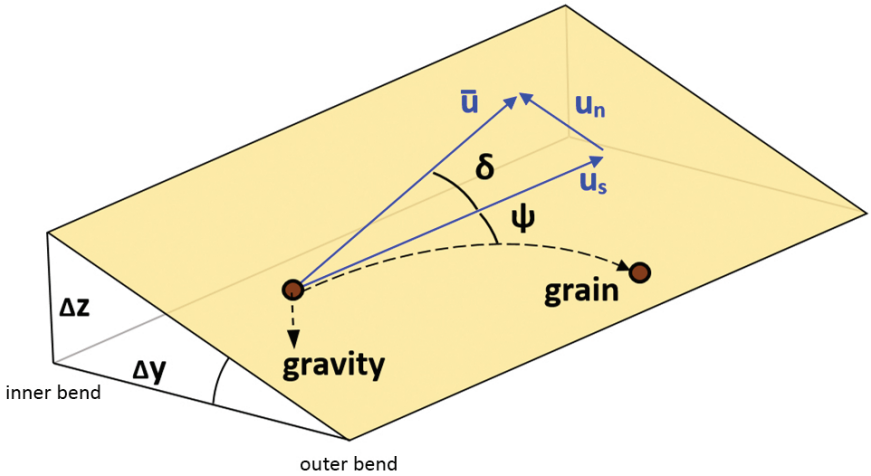

Figure 2.1: Definition of the main variables that determine the transverse bed slope effect. Grains on a slope transverse to the main flow direction (u_s) are deflected downslope due to gravity. When a secondary current is present, e.g. in bends, the inward and upslope directed shear stress drags particles upslope. In this case the equilibrium slope that develops ($\frac{\partial z_b}{\partial y}$) is a balance between the angle of deflection due to gravity (ψ) and the angle between the local flow velocity vector ($\vec{u}$) and the main flow direction (δ) near the bed, which represents the secondary flow intensity (after Sekine and Parker, 1992; Schuurman, 2015).

and a higher braiding index downstream. An incorrect setting thus has major consequences for the predicted large-scale morphology, bank protection works and dredging volumes for fairway maintenance (van der Wegen and Roelvink, 2012; Schuurman et al., 2013).

The stability of bifurcations is also highly sensitive to the bed slope effect. Just upstream of the bifurcation, a transverse slope also develops as a result of a bed level difference between the distributaries, which develops when one of the branches aggradates while the other erodes. The distribution of sediment over the branches is influenced by the direction of sediment transport on this transverse slope, which affects the further development of the bifurcation (Bolla Pittaluga et al., 2003; Kleinhans et al., 2008; Sloff and Mosselman, 2012; Bolla Pittaluga et al., 2015). Whether a bifurcation is stable depends on whether the sediment transport capacity difference between the downstream branches is balanced by sediment transport in downslope direction feeding into the deeper channel. The societal relevance is that bifurcations divide water, sediment and thus flood risk over fluvial plains and deltas.

The literature reports starkly different magnitudes of the bed slope effect. Previous studies isolated a specific transport mechanism or bed state and study its separate effect on the transverse bed slope effect. Consequently, the resulting predictors are based on a small set of experiments, with a maximum of 11 unique experiments (Talmon et al., 1995) and a minor range of flow conditions and sediment sizes depending on the process that is studied (e.g. Struiksma et al., 1985; Ikeda and Nishimura, 1986; Talmon and Wiesemann, 2006). However, these predictors are now used in numerical morphodynamic modelling where all processes act in combination. As a result, current models often over-predict channel depth and bar height, so that the transverse bed slope parameters in current models in practice need to

be calibrated on measured morphology. This means that the most important results of morphological models depend critically on a poorly quantified parameter representing a poorly understood combination of processes. Unfortunately, calibrating morphology on bed slope parameters also compensates for other model weaknesses such as poorly parameterized or absent processes, e.g. bank erosion, bedform effects on sediment transport and flow resistance. To some degree, calibration parameters account for the effect of sediment mobility and transport mode (rolling or saltating bed load to sheet flow), presence of bedforms of different types (ripples and dunes) with strong subgrid variations in transverse and streamwise slopes, and transverse sediment sorting effects, such as the classic bend sorting (Wiesemann et al., 2006; Sekine and Parker, 1992). To test whether poor model behavior and the need for calibration beyond expected parameter ranges is caused by poor bed slope predictors or other model issues, we urgently need a comprehensive set of data for a large range of sediment mobility and grain size, covering all sediment transport modes and bed state regimes. The key problem is the scarcity of experimental data covering all these processes to test and calibrate process specific transverse bed slope relations.

The objective of this research is to experimentally quantify the transverse bed slope effect for a large range of near-bed flow conditions and sediment sizes to obtain parameters for morphological modelling that cover all sediment transport modes and bed state regimes. We conducted experiments with a set of sediments in a rotating annular flume, which allows control of the secondary flow intensity independently from the streamwise flow velocity. Therefore, all important parameters could be isolated and their separate effect on the transverse slope can be determined. Below we first review transverse bed slope predictors and their limitations, followed by a description of our experimental set-up, data reduction of the 224 experiments conducted in fine sand to fine gravel, and finally discuss the results and draw conclusions.

2.2 Existing transverse slope predictors

An inclination of the bed in streamwise as well as transverse direction affects the magnitude of sediment transport, and additionally a transverse slope causes a deviation of the direction of the transport vector from the applied bed shear stress (Parker et al., 2003; Francalanci et al., 2009). Furthermore, an inclined bed lowers the critical shear stress for the beginning of motion compared to a horizontal bed (Fernandez Luque and Van Beek, 1976; Seminara et al., 2002). In this paper, we will focus on the effect of transverse slopes because these typically are orders of magnitude larger than average streamwise slopes.

The simplest relation used in literature for the change in sediment transport direction due to slope effects in transverse direction was formulated for river bends by van Bendegom (1947) as:

$$tan(\psi) = tan(\delta) - \frac{1}{B}\frac{\partial z_b}{\partial y} \tag{2.1}$$

where ψ = direction of sediment transport, δ = direction of near-bed flow velocity, affected the intensity of the secondary current, and B = a dimensionless slope factor. See Figure 2.1 for definition of parameters. This equation shows that the secondary flow intensity, which is

directed upslope in curved channel sections, counteracts slope effects. Consequently, when equilibrium is attained in an infinitely long bend of constant curvature because net transverse sediment transport is zero, this equation reduces to a balance:

$$\frac{\partial z_b}{\partial y} = Btan(\delta) = B\frac{u_n}{u_s} \tag{2.2}$$

where u = magnitude of the flow velocity $[m/s]$ in transverse direction (n) and streamwise direction (s). A later refinement of this linear relation between the secondary flow intensity and the transverse slope is the non-linear model of Parker et al. (2003), in which the slope factor itself depends on the transverse slope. Francalanci and Solari (2008) approximated the non-linear equation of Parker et al. (2003) with polynomial functions of the local transverse bed slope, which was tested experimentally together with the linear model of Parker et al. (2003) by Francalanci et al. (2009). Results suggested that linear transverse bed slope predictors lead to an underestimation of lateral sediment transport.

Current transverse bed slope predictors are either based on theoretical model studies validated with laboratory experiments or field data (e.g. Engelund, 1974; Koch and Flokstra, 1981; Ikeda, 1984), or are based on an empirical fit through experimental data (e.g. Talmon et al., 1995; Wiesemann et al., 2006). Important differences between these studies relate to the factors included in the bed slope factor B. Theoretical models follow the reasoning of van Bendegom (1947), and base the slope factor on the radial balance of forces acting on a grain moving on a transverse inclined bed. These forces consist of gravity pulling the particles downslope, a drag force on the particles in the direction of the bed shear stress, and friction between the particles and the bed (van Bendegom, 1947; Engelund, 1974; Koch and Flokstra, 1981). The frictional forces can consist of both dynamic friction between moving particles and the bed, and static friction between non-moving particles in the bed, which is frequently expressed as the angle of internal friction or angle of repose (Parker et al., 2003).

Table 2.1 lists variations of the slope factor B. The variations broadly fall into four categories. Firstly, since the slope factor is assumed to be a function of sediment properties and fluid drag, in most studies B is a function of sediment mobility (θ) (Talmon et al., 1995). Accordingly, the slope factor is often defined in the generalized form:

$$B = \alpha\theta^{\beta}, \tag{2.3}$$

or when the critical shear stress (θ_c) is included:

$$B = \alpha_c \left(\frac{\theta}{\theta_c}\right)^{\beta} \tag{2.4}$$

Where the sediment mobility θ, a dimensionless form of the bed shear stress, reads:

$$\theta = \frac{\tau}{(\rho_s - \rho)gD_{50}} \tag{2.5}$$

where τ = shear stress $[N/m^2]$, ρ_s = specific density of the sediment, g = gravitational acceleration $[m/s^2]$ and D_{50} = median grain size $[m]$. Table 2.1 shows that β varies between 0 and

1, but is usually 0.5 based on the relation between shear stress and flow velocity. Henceforth, the ratio of sediment mobility θ and critical sediment mobility θ_c will be referred to as relative sediment mobility. Several studies include a critical sediment mobility for the beginning of motion (e.g. Ikeda and Nishimura, 1986; Talmon and Wiesemann, 2006; Francalanci et al., 2009), which according to Odgaard (1981) is necessary to relate the transverse slope to bed surface characteristics, instead of only bed load properties. Parker et al. (2003) included a ratio between the critical sediment mobility for the cessation of sediment transport and for the beginning of motion (λ), which is generally below 1. Similar differences in formulation of relative and excess sediment mobility exist between sediment transport predictors, which implies that transverse bed slope relations should be formulated consistently with the sediment transport relation that is used.

Secondly, the dominant mode of transport determines the effective gravity acting on the grains. Sekine and Parker (1992) discuss that previous theoretical relations are only valid for rolling or sliding transport, since particles are assumed to be continuously in contact with the bed. Therefore, they propose a transverse slope predictor that is based on a stochastic model of saltating particles, resulting in a β of 0.25. However, their resulting relation has a number of simplifications and is still only valid for small transverse slopes and a low sediment mobility, since the number of saltating particles needs to be low to avoid particle collision. When suspension is present, Talmon et al. (1995) found a slope effect that is two times larger than under bed-load dominant conditions with equal flow velocities. However, in current models suspended load is not influenced by bed slope effects (Talmon et al., 1995; van der Wegen and Roelvink, 2012), or, alternatively, suspended load is treated as bed-load when a total load sediment transport predictor is used as in van der Wegen and Roelvink (2012) and Schuurman et al. (2013).

Thirdly, most studies only include a dynamic friction coefficient (μ_d) to balance the fluid drag force (Talmon and Wiesemann, 2006; Ikeda and Nishimura, 1986), and thereby ignore the effects of a lower threshold of sediment motion due to a transverse slope, which depends on static friction (μ_s) (Fernandez Luque and Van Beek, 1976; Seminara et al., 2002). Engelund (1974) even assumes a slope effect that only depends on dynamic friction and is therefore independent of flow conditions and sediment size. Consequently, he concludes this predictor is only valid for small sediment transport rates. Only the predictor of Hasegawa (1981) includes static friction directly, while the predictor of Francalanci et al. (2009) takes the friction angle into account indirectly since their experiments used for calibration were designed with steel particles with a high friction angle. The values of these friction coefficients are based on experimental findings. In the predictors of Ikeda (1984) and Ikeda and Nishimura (1986) the dynamic friction depends on a ratio of lift to drag coefficient (γ), which is also a constant. In general, linear theoretical models only apply for gentle slopes, because dynamic and static friction are constant and thereby do not depend on the magnitude of the transverse slope (Sekine and Parker, 1992; Parker et al., 2003). For higher slopes, the dynamic friction changes due to the increase in slope, and thus the equation should be non-linear.

Table 2.1: Transverse slope predictors and the experimental conditions for which they were determined. c.p. = study specific calibration parameter, of which the range is determined when validating the predictor with experiments.

author	B	α/α_c	β	flume	runs nr	D_{50} $[mm]$	θ	transport mode	bed state	c.p. (range)
independent of sediment mobility										
Engelund (1974)	μ_d	0.51	0	bended	2	0.3	0.28, 0.40	bedload	dunes	μ_d
Engelund (1975)	μ_d	0.47	0	annular	2	3 ($\rho = 1400$)	0.25,0.75	bedload	lower plane bed	μ_d
dependent on sediment mobility										
Koch and Flokstra (1981)	$\frac{3}{2}\theta f_b$	1.5	1	bended	3	0.21, 0.78	0.67, 0.34	-	ripples	$f_b(\sim 1)$
Struiksma et al. (1985)	$f_s\theta$	1	1	bended	6	0.3-0.78	0.16-0.52	bedload	dunes	f_s(0.4-1.5)
Talmon et al. (1995)	$9(\frac{D_{50}}{H})^{0.3}\sqrt{\theta}$	1.7	0.5	straight	11	0.09-0.78	0.1-0.8	bedload, suspended	dunes, ripples	-
Wiesemann et al. (2006)	ripples: $\sqrt{\theta}$ dunes: 0.9	1 0.9	0.5 0	straight	3	0.25,0.96	0.16-0.5	bedload, suspended	dunes, ripples	-
including critical sediment mobility										
Hasegawa (1981)	$\sqrt{\frac{\mu_s\mu_d\theta}{\theta_c}}$	0.67	0.5	straight	9	0.425	0.05-0.3	-	lower plane bed	-
Ikeda (1984)	$\frac{\mu_d}{1+\gamma\mu_d}\sqrt{\frac{\theta}{\theta_c}}$	0.31	0.5	straight	2	0.18, 0.42	0.23, 0.10	-	dunes	-
Ikeda and Nishimura (1986)	$\frac{f_{sh}\mu_d}{1+\gamma\mu_d}\sqrt{\frac{\theta}{\theta_c}}$	0.19	0.5	bended	1	0.15	0.3	suspended	ripples	$f_{sh}(\sim 0.59)$
Sekine and Parker (1992)	$1.33(\frac{\theta}{\theta_c})^{0.25}$	1.33	0.25	straight	11	0.425, 1.3	$<$0.2	bedload (saltation)	lower plane bed	-
Parker et al. (2003)	$\frac{1}{\lambda}\sqrt{\frac{\theta}{\theta_c}}$	1.43	0.5	straight	5	1.5-3.3	low	bedload (saltation)	-	-
Talmon and Wiesemann (2006)	$\frac{\mu_d}{f_b}\sqrt{\frac{\theta}{\theta_c}}$	0.27	0.5	straight	6	0.09-0.96	0.1-0.9	bedload, suspended	dunes, ripples	f_b (1-1.06)
non-linear relation										
Francalanci et al. (2009)	$\alpha_\psi(\frac{\theta}{\theta_c})^{\beta_\psi}$	$\alpha_\psi(\frac{\partial z_b}{\partial y})$	$\beta_\psi(\frac{\partial z_b}{\partial y})$	straight	5	3 ($\rho = 7850$)	0.03-0.12	bedload (saltation)	lower-stage plane bed	$b_\psi, d_\psi, h_\psi, m_\psi$

Fourthly, validation of the theoretical models with experimental data with varying bed states and particle properties lead to the need for several calibration parameters and the adjustment of the dynamic friction coefficient. Predictors based on forces acting on the grains have grain-related calibration factors to ensure an agreement with the model, namely a shape factor of the grains (f_s) (Struiksma et al., 1985) and a sheltering coefficient (f_{sh}) (Ikeda and Nishimura, 1986). Bed state was ignored in the theoretical models. Therefore, in several experimental studies either flow conditions were chosen such that bedforms were avoided (Hasegawa, 1981; Engelund, 1975), or the presence of bedforms caused a calibration parameter for the transverse bed slope predictor (Koch and Flokstra, 1981; Talmon and Wiesemann, 2006).

Dunes in particular may have large effects that are incompletely understood. In particular, the local bed streamwise and transverse slopes vary strongly along a dune as do the flow field and flow turbulence intensity, none of which is incorporated in derivations of physics-based predictors for transverse bed slope effect. In fact, bedforms occur in almost none of the current morphodynamic models meaning that their effects on flow and sediment transport is somehow calibrated into parameters for flow resistance, sediment transport and predictors for slope effects. Existing predictors based on an empirical fit through experimental data mainly focused on the effect of different bed states, which in the case of Wiesemann et al. (2006) lead to a different trend for a bed with ripples or with dunes, since they observed that downslope sediment transport decreased when dunes were present and became independent of sediment mobility. In contrast, Sieben and Talmon (2011) used artificial dunes to show that the slope effect is enhanced when oblique dunes are present, due to avalanching at the lee sides of the dunes. Talmon et al. (1995) manually prepared dunes based on earlier experiments, since the development of natural dunes required the same time as the duration of their bed leveling experiments. They conclude that the scale of bedforms has a significant influence on the slope factor, and this value is twice as small in the experimental setting with relatively high bedforms compared to natural rivers, but this conclusion may have been affected by the initial condition. They therefore proposed a slope factor including a ratio between the water depth and the median grain size, to account for bedform height.

Another cause for variations in B may be the type of experimental facility used to collect calibration data (see Table 2.1). To validate the theoretical models or to obtain an empirical fit, past experiments were conducted in either a bended flume (e.g. Struiksma et al., 1985; Ikeda and Nishimura, 1986) or an annular flume (Engelund, 1975), or straight flumes initiated with a transversely sloped bed that relaxed to a horizontal bed (e.g. Ikeda and Nishimura, 1986; Talmon et al., 1995; Talmon and Wiesemann, 2006). Straight flumes have the advantage of reasonably isolating the transverse bed slope effect without strong bend flow, but have the disadvantage that the transverse bed slope effect is determined from the initial changes of the disequilibrium bed slope rather than an equilibrium morphology, and that the bed state, e.g. dunes, develops at the same timescale (Talmon and Wiesemann, 2006). In curved flumes and in the annular flume of Engelund (1975) a morphodynamic equilibrium is possible, which has the advantage of straightforward measurement of the transverse bed slope but the disadvantage that this result depends on secondary flow patterns that need to be quantified and are only valid for one single bend radius. An annular flume additionally has the

advantage that it avoids boundary effects and the flow does not have to adapt to changes in channel curvature, and therefore the transverse slope that develops in the flume is in equilibrium with the established flow conditions along the entire flume. This requires that the flow conditions are well known. To study the effect of different bend radii, a rotating annular flume was used in the current research, in which the intensity of the secondary flow can be controlled and varied by counter-rotating the floor and side walls of the flume (Booij, 2003). Thereby, the effect of the secondary flow can be isolated by simulating infinite bends with various bend radii. This concept will be explained in more detail in the next section.

The need to develop experiments with appropriate conditions for testing certain predictors led in practice to limited experimental datasets. In the case of validation of a theoretical model, the conditions were chosen such that they fit the model assumptions, for instance absence of bedforms. As a result, all experiments reported so far were performed with a limited range in flow conditions and sediment sizes depending on the studied process, with a maximum of 11 unique experimental settings (Table 2.1). As a side effect, the effects of varying bed states and sediment transport modes on slope effects were mostly ignored in past studies. Consequently, the amount of data to test and calibrate transverse bed slope relations is too scarce and inconsistent.

Estimates of the magnitude of the transverse slope factors α or α_c and β in Equation 2.3 are given in Table 2.1, based on reported theoretical and calibration parameters by the corresponding studies. The range of α varies between 0.47 and 1.7, and is comparable with the range of α_c, which varies between 0.19 and 1.43. These ranges comprise constant values typically used in morphodynamic models, and consequently transverse slope factors are linearly related to sediment mobility throughout a model run. Even though the magnitudes of the transverse slope factors were validated for a specific process and corresponding range in flow conditions and sediment mobility, current morphodynamic models apply these values in a wide range of environments and conditions. We illustrate the problems that arise in applications here with the implementation of bed slope effects in the state-of-the-art morphodynamic model Delft3D. Typically, a predictor based on either Koch and Flokstra (1981) or Ikeda (1984) is used to calculate bed load transport on transverse slopes, with the main difference that in the predictor of Ikeda (1984) a critical shear stress is used, which is absent in the predictor of Koch and Flokstra (1981). However, the resulting transport vector is calculated in different ways for these predictors. Firstly, the magnitude of sediment transport is predicted, based on a situation of a flat bed with a single grain size. Secondly, for Koch and Flokstra (1981) the direction of sediment transport is corrected for transverse gradients by rotating the transport vector:

$$tan(\psi) = \frac{1}{\alpha\theta^{\beta}} \frac{\partial z_b}{\partial y} \tag{2.6}$$

On the other hand, for Ikeda (1984) an additional transport vector is calculated perpendicular to the flow direction (van Rijn, 1993; van der Wegen and Roelvink, 2012):

$$q_n = q_s \frac{1}{\alpha_c} \sqrt{\frac{\theta_c}{\theta}} \frac{\partial z_b}{\partial y} \tag{2.7}$$

where q = sediment transport load $[m^2/s]$. α, β and α_c are user defined adjustable parameters. Here the default value of α in Delft3D is set to 1.5, which is directly taken from Koch and Flokstra (1981). β_k is set to 0.5, which differs from the value of 1 proposed by Koch and Flokstra (1981), but is equivalent to most other predictors (Table 2.1). Schuurman et al. (2013) varied α between 0.35 and 1.5 and eventually used a value of 0.7. Based on the experiments of Ikeda (1984) in a straight flume, van Rijn (1993) concluded α_c should be around 0.67, which is thus the default value for the second bed slope option in Delft3D. Details on the default values for both α and α_c, and how compare them are given in Appendix B. However, in practice both slope factors are reduced to one or two orders of magnitude smaller than the default values in the calibration to measured morphology, to correct for the tendency of the model to overdeepen channels and exaggerate bar length (e.g. van der Wegen and Roelvink, 2012; Schuurman et al., 2013), and the absence of physics-based bank erosion (e.g. Grenfell, 2012; Schuurman et al., 2013). For example, the modelled braided sand-bed river of Schuurman et al. (2013) showed an increase of more than 60 percent in channel depth and an increase in braiding index from 2.4 to 3.5 after 25 months when using his optimal value of 0.7 for α compared to a model run with the lower value of 0.35. They therefore concluded that the model results are very sensitive to a change in this parameter value. The study of van der Wegen and Roelvink (2012) compared two model runs based on an existing morphology of a sandy estuary with an α_c of 0.1 and 0.2, which showed an increase of 8 percent in channel depth and a higher braiding index than the morphology when using the higher value despite the fact that this is still significantly lower than the default value of 0.67. This sensitivity of predicted long-term morphology to the transverse bed slope parameters, even when a measured bathymetry is used for calibration, illustrates the need for a better understanding of the transverse bed slope effect.

2.3 Methods

2.3.1 Experimental methodology

We conducted experiments in a rotating annular flume (Fig. 2.2) which allows control of the secondary flow intensity independently from the streamwise flow velocity. Rotation of the flume lid drives the flow by applying a shear stress on top of the water column. This not only generates streamwise flow, but also causes a secondary circulation to develop due to the curvature of the flume. The centrifugal force generated by rotating the lid causes water to be pushed outwards at the top of the water column which creates a pressure gradient from the outer to the inner bend. This pressure gradient drives the secondary flow and thereby creates an inward-directed bed shear stress near the bed, which corresponds with the development of secondary flow patterns in natural river bends. However, in a rotating annular flume the secondary flow can be counteracted by rotating the floor of the flume plus attached sidewalls in opposite direction. By counter-rotating the floor, an outward-directed centrifugal force is added on the flow low in the water column, which decreases the pressure difference over the water column at the outer bend, and thereby decreases the secondary flow and the inward-directed bed shear stress (Booij, 1994; Booij, 2003). Both the lid and floor of the flume can rotate over a continuous range of angular velocities in both directions. By controlling lid

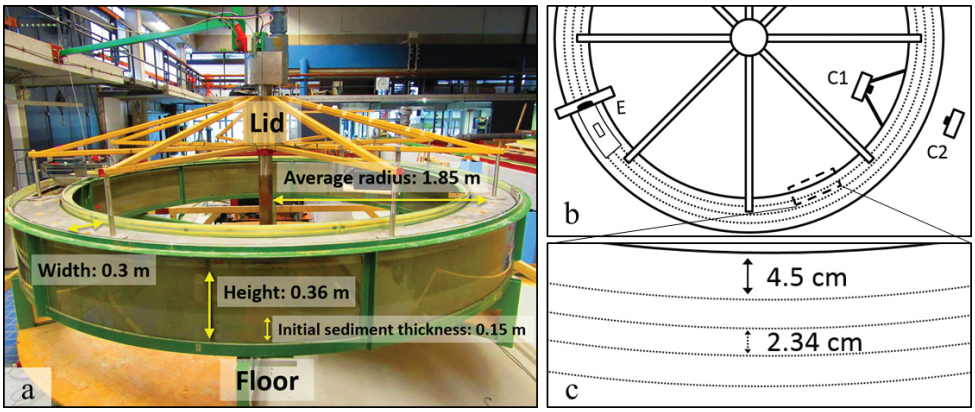

Figure 2.2: Experimental setup. a) The dimensions of the rotating annular flume. Floor and sidewalls are attached; lid rotates independently. b) Schematic drawing of the measurement set-up (top view). The morphological development during the experiments was captured with a camera attached to the inside of the flume (C1) and a static camera at the outside of the flume (C2). Bed elevation was measured in still flow with an echosounder (E) along ten transects (dashed lines). Flow velocities were measured separately with a Vectrino-II, which was installed at the channel centerline. c) Ten transects were measured along the circumference of the flume, each 2.34 cm apart in transverse direction, starting at 4.5 cm from the walls of the flume.

and floor angular velocities, the streamwise flow velocity as well as the secondary flow can be isolated and thus the ratio between these parameters can be varied as well. Changing this ratio alters the direction of the flow velocity vector near the bed, which determines the secondary flow intensity and corresponds to different bend radii in nature. Most studies until now (e.g. Booij, 1994; Yang et al., 2015) sought the ratio of lid and floor rotation at which the centrifugal force of the floor rotation balances the centrifugal force of the lid rotation, with the result that the secondary flow is minimalized and the flume can be used as an infinite straight river reach. Booij (1994) reports an optimal ratio of about 1.8, independent of the magnitude of the lid and floor rotation. Additionally, he measured a uniform streamwise shear stress across the width of the flume at this ratio. Here we employ the possibility to not only minimalize secondary flow, but also to control the secondary flow magnitude, without which no large transverse bed slope would develop.

Rotation of the flume floor also adds an outward-directed centrifugal force on the sediment, which effectively results in a rotation of the gravity vector. This can be expressed as a slope towards the outer bend related to this effective direction of gravity ($tan(\eta)$):

$$tan(\eta) = \frac{\omega_f^2 r}{g} \tag{2.8}$$

where ω_f = angular velocity of the flume floor $[rad/s]$ and r = radius of the flume [m]. However, with the current experimental settings this results in maximum slopes of 0.01 m/m, which is insignificant compared to the much steeper (up to 0.5 m/m) equilibrium transverse slopes in the morphodynamic experiments. Therefore, we will ignore the effect of centrifugal forces on the sediment in the remainder of this paper.

To determine near-bed streamwise and normal flow velocity without intrusive measurement techniques in flows with suspended sediment, analytical relations were derived as a function of the rotation rates of flume lid and floor. For verification and calibration we ran 186 experiments for basic flow measurements in the center of the channel over flat bed conditions. More sophisticated numerical flow modelling representing details of this 3D-flow is outside the scope of this paper.

We conducted 224 morphodynamic experiments for several sediments ranging from fine sand to fine gravel, including low-density walnut grains, and the technically largest possible range of sediment mobilities and secondary flow intensities. We ran each experiment until morphological equilibrium, meaning that neither transverse slope nor bedform dimensions changed appreciably. With the resulting average transverse bed slope and the estimate of the near-bed normal and streamwise flow velocity, the slope factor B of each experiment could be determined (Eq. 2.2). Slope factors of all experiments were then used to find a general relation between slope factor and sediment mobility for the entire experimental range (Eqs. 2.3, 2.4), and compared to the values for α, α_c and β found in literature for specific ranges of sediment mobility. Below we detail methods of flow measurement and modelling, sediment properties, experimental conditions and measurement of morphology.

2.3.2 Measurement and analytical approximation of flow conditions in the annular flume

Flow velocities in streamwise and transverse direction were measured with a Vectrino-II, an acoustic Doppler velocity meter, at the center of the flume during two minutes. The Vectrino-II collects 16 data points in vertical direction in a range of 3 cm, with the most accurate measurement in the middle of this range. We chose to measure 0.5 - 3.5 cm above the bed, since in this range the highest normal flow velocities were recorded and furthermore, the objective is to study the effect of near-bed flow characteristics on sediment transport. Flow velocity measurements were done separately from the slope experiments and only on a flat bed, since it was not possible to measure near the bed when bedforms were present. In total, 186 flow velocity measurements were conducted under systematically varied angular velocities of both the lid and the floor, and above flat sediment beds without bedforms with median grain sizes of 0.26 mm and 1 mm. Angular velocities of the lid ranged from 0.16 to 0.90 rad/s, which corresponds with tangential velocities at the centerline between 0.30 and 1.67 m/s, and floor rotation was varied between 0 and -0.42 rad/s (0.78 m/s). Henceforth, lid and floor rotation will be expressed in tangential velocity at the centerline. The range in rotation velocity was restricted by the measurement range of the Vectrino-II, which gave large scatter at high angular velocities and when saltation or suspension concentration was too high. Measured flow velocities were reduced to a median streamwise and normal flow velocity, to be able to relate them to measured transverse slopes in the morphodynamic experiments. Vectrino-II data were then filtered by removing data points with a correlation less than 80 percent, taking the median of the timeseries per elevation and using the maximum value. This method of determining the average flow velocity produced significant scatter for unclear reasons, especially in normal flow velocities, and it was therefore not possible to fit a clear trend through the data to extrapolate for higher angular velocities. Therefore, a simple analytical model was

developed to predict streamwise and normal flow velocities at any combination of angular velocities.

Our analytical flow model is based on the assumption that shear stresses and centrifugal forces caused by lid and floor rotation, which drive the flow in the annular flume, are balanced by frictional forces of the lid and the walls of the flume. The trend in streamwise flow velocity is based on the model of Booij (1994), who found a reasonable agreement with flow velocity measurements in the same annular flume, but with a smooth bed without sediment. He assumed that shear stresses should cancel around the axis of rotation and therefore used the average value of the absolute tangential velocity (U) of the lid (l) and floor (f) at the center of the flume, multiplied with the ratio in surface area of the lid and flume. This ratio accounts for the larger surface area of the floor and sidewalls that apply shear to the water, and therefore have a larger influence on the average flow velocity than the lid. For the dimensions of the flume in this study, this ratio would be 0.78. However, in the current model this ratio is represented by a factor A_{s1} and is calibrated on measured data to account for unknown effects of three dimensional flow patterns on the non-linearity of the velocity profile. Furthermore, due to the sediment bed, in the current experiments the floor has a higher friction coefficient than during the measurements of Booij (1994), and therefore only a fraction of the floor velocity is transferred to the flow. This fraction is indicated with a second calibration parameter A_{s2}, which is absent in the model of Booij (1994). The resulting approximation for the streamwise flow velocity is:

$$u_s = A_{s1} \frac{U_l + A_{s2}|U_f|}{2} \tag{2.9}$$

The trend in normal flow velocity is determined using a model of a cross-section of the flume. Here, it is assumed that the centrifugal force generated by the lid affects the top half of the water column, while floor rotation influences the bottom half. Since the pressure difference between the top half and the bottom half of the water column at the outer bend drives the secondary flow, the difference in lid and floor centrifugal acceleration is used as driving centrifugal force. This force is balanced by friction exerted along the lid, side walls and sediment bed. The resulting approximation of the normal flow velocity is as follows:

$$u_n = \frac{A_{n1} HW(U_l - A_{n2}|U_f|)}{r(c_w(W+H) + c_b W)} \tag{2.10}$$

where H = water depth [m], W= width of the flume [m] and c = friction coefficient for the walls and lid (w), and the bed (b). A_{n1} and A_{n2} are calibration factors, accounting for non-linearity of the velocity profile and the relatively larger influence of floor rotation on the average flow velocity due to a larger cross-sectional surface, respectively. The full derivation is given in Appendix A. When the ratio of lid to floor rotation is equal to A_{n2}, secondary flow is minimal and an infinite straight river section can be simulated. Booij (1994) stated this ratio is around 1.8 for the dimensions of the flume used in the current experiments.

Since only lid and floor tangential velocities are included in these equations as characteristic flow velocities for parts of the cross-section, the magnitude of the resulting streamwise

and normal flow velocity are only a coarse approximation. Therefore, the measured flow velocities are used to calibrate the magnitude of the predicted flow velocities, while the trend of the analytical flow model is considered to correctly represent that of the measured flow velocities. We consider this the most parsimonious method as lid and floor tangential velocities and grain size are the only variables.

2.3.3 Experimental conditions and data collection

The annular flume used for the experiments described here has a radius of 1.85 m at the centerline and a rectangular cross-section with a width of 0.30 m and an adjustable height up to 0.47 m (Fig. 2.2a). In our experiments, the lid is fixed at a height of 0.36 m above the flume floor. Each experiment started with a uniform horizontal sediment bed with a thickness of 0.15 m, resulting in an average water depth of 0.21 m. Lid rotation can be varied over a continuous range up to 3.7 m/s. For safety reasons an angular floor velocity of 1.2 m/s was not exceeded.

Sediment size, floor rotation and lid rotation were systematically varied in order to isolate the effect of a large range of near-bed flow conditions and sediment mobilities on the transverse slope, covering all sediment transport modes and bed state regimes. In Table 2.2 the range in sediment characteristics, sediment mobility and secondary flow intensity is summarized, together with the number of experiments per sediment type. Values for all experiments are given as supporting information. The parameter space covered by the experiments was designed and determined using the bedform stability diagram of Van den Berg and Van Gelder (1993), which plots sediment mobility against non-dimensional grain sizes, and distinguishes bed state stability fields of no motion, ripples, dunes and upper-stage plane bed (USPB). Grain sizes have been normalized as described by Van Rijn (1984b) to remove the effect of fluid viscosity and density. We assume that lower-stage plane bed occurs around the beginning of motion as observed in some bed slope experiments. We chose uniform sediments with median grain sizes of 0.17, 0.26, 0.37, 1.0, 2.0 and 4.0 mm and a density of 2650 kg/m^3, to ensure a transition from both hydraulic smooth to hydraulic rough conditions and across the ripple-dune threshold. Additionally, we used low-density granular walnut shell with a density of 1300 kg/m^3 and a median grain size of 1.55 mm to test the effect of centrifugal forces generated by the flume floor. Henceforth we collectively name the sands < 0.5 mm fine sand and the coarser sediments coarse sand and fine gravel.

Morphological development was registered using time-lapse photography and echosounding. Photographs were taken on both the inside and outside of the flume with a constant time interval, ranging from 5 to 300 seconds depending on the expected duration of the experiment. The camera on the outside was not attached to the flume and thus captured the development of the entire flume when floor rotation was added, while the camera at the inside was attached to the floor, consequently registering the development of a fixed segment (Fig. 2.2b). The experiment was ended when the transverse bed slope and the bedforms were in equilibrium with the flow conditions. This took of the order of an hour for the high mobility experiments to a few days for the lowest mobility experiments. Experiments where dune troughs touched the solid flume floor were excluded. Afterwards, the morphology was measured in still flow with an echosounder over ten transects in streamwise direction, each

Table 2.2: Range in sediment characteristics, sediment mobility and secondary flow intensity of each sediment type, summing to a total of 224 experiments.

ρ	D_{50}	D_{10}	D_{90}	nr runs	θ	$\tan\delta = \frac{u_n}{u_s}$
kg/m^3	$[mm]$	$[mm]$	$[mm]$	$[-]$	$[-]$	$[-]$
2650	0.17	0.12	0.21	34	0.02-1.59	-0.24-0.19
2650	0.26	0.19	0.33	23	0.03-1.16	-0.04-0.17
2650	0.37	0.23	0.63	30	0.02-0.90	-0.11-0.16
2650	1.0	0.85	1.16	45	0.02-0.41	-0.10-0.13
2650	2.0	1.7	2.5	31	0.02-0.29	-0.03-0.11
2650	4.0	3.15	5.6	37	0.04-0.19	-0.02-0.08
1300	1.55	1.25	1.66	24	0.02-0.31	0.01-0.11

2.34 cm apart in transverse direction (Fig. 2.2c). To allow filtering for sonic noise, the effective spacing of echosounder recordings was between the 1.2 mm and 1.4 mm in streamwise direction, depending on the circumference of the measured transect. The footprint of the echosounder is about 2 cm at average bed level.

Data were gradient-filtered for outliers and gridded for presentation, but the full dataset was used for data reduction of resulting morphologies to one transverse slope value per experiment in the following steps. For each transect the median bed level over the entire flume length was determined. A linear trend was fitted by least-squares through eight of the ten data points across the flume to obtain the average transverse slope, excluding the two transects near the flume wall. Average transverse slopes of all experiments are reported in the online supplement. Additionally, the $16-84$ and $5-95$ percentiles of the bedlevels along the transects were determined to represent spatial variation including bedforms along the flume. These values are used for analysis in combination with modelled flow velocity.

2.4 Results

In this section, we first evaluate the trend in flow velocity at specific ratios of lid and floor angular velocities, and then describe the trends in the spatially averaged transverse bed slopes. Finally, we seek relations between near-bed flow conditions, sediment mobility and average equilibrium transverse bed slope.

2.4.1 Flow velocity and bed state at specific angular velocities

The best fit of the analytical flow velocity model on the measured flow velocities was obtained with calibration parameters $A_{s1} = 0.65$ and $A_{s2} = 0.5$ for streamwise flow velocities, and $A_{n1} = 0.025$ and $A_{n2} = 2.5$ for normal flow velocities. Results show that streamwise velocities increase both with increasing lid rotation (Fig. 2.3b) and with increasing counter-rotation of the floor (Fig. 2.3d), due to the larger difference between absolute lid and floor angular velocities. The linear relation of Equation 2.9 shows a reasonable similarity with the data (Fig. 2.3f) and an A_{s1} of 0.65 is similar to the 0.78 obtained by Booij (1994) and lower as expected because of higher bed friction.

Normal flow velocities increase when lid rotation is increased and can be described with a linear relation for a given floor rotation (Fig. 2.3a). When lid rotation is constant and the

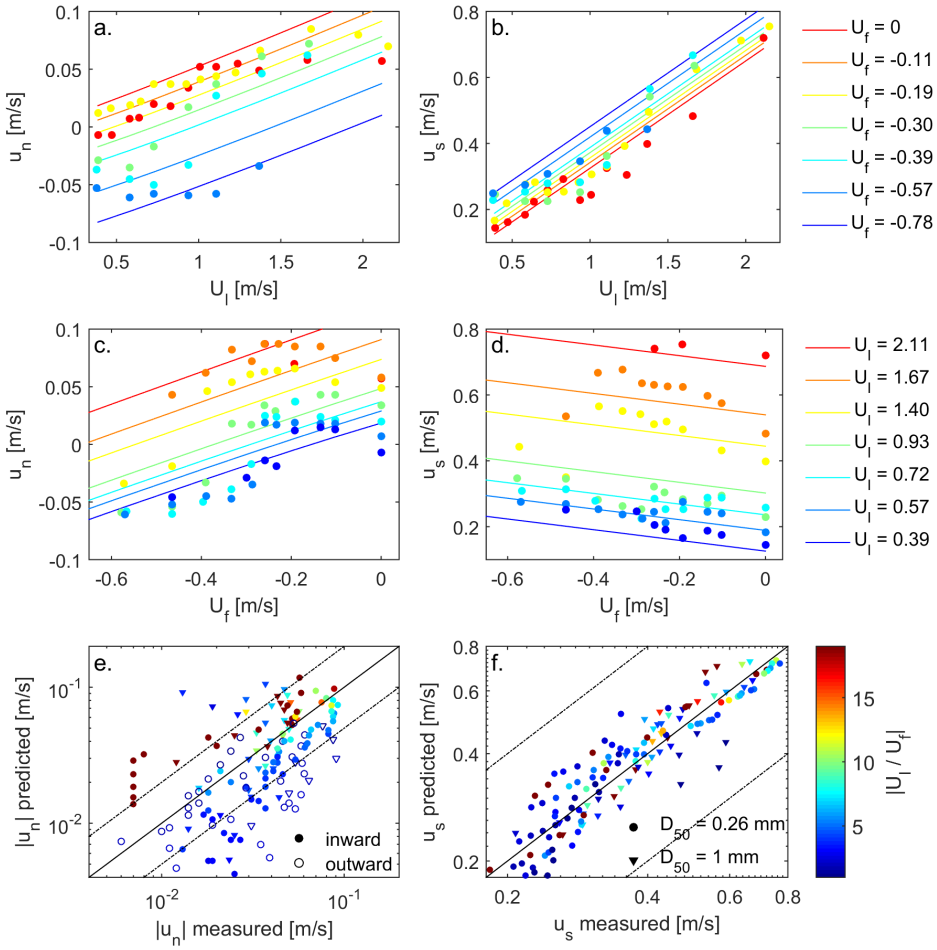

Figure 2.3: Measured (scatter) and predicted flow velocities (lines) for a range of lid and floor angular velocities used in the experiments. a, b) Variation in normal and streamwise flow velocity with lid rotation, where separate lines and colors indicate a constant floor rotation. c, d) Variation in normal and streamwise flow velocity with increasing counter-rotation of the floor, where separate lines and colors indicate a constant lid rotation. e) Predicted against measured normal flow velocities for a range in lid to floor rotation ratios (color scale). Flow is either directed towards the inner bend (positive values) or towards the outer bend (negative values). $R^2 = 0.78$. f) Predicted against measured streamwise flow velocities, $R^2 = 0.90$. Dashed lines indicate deviation of a factor of 2.

counter-rotation of the floor increases, normal flow velocities generally decrease as modelled (Fig. 2.3c). Our data show that the ratio of lid to floor angular velocity for which the secondary flow intensity is minimal and reverses towards the outer wall is about 2.5 (A_{n2}), where Booij (1994) found a ratio around 1.8. Our ratio is higher due to the added roughness of the sediment bed. When floor rotation is increased even further, and this ratio therefore further decreases, the centrifugal force created by the floor rotation is dominant and as a result, secondary flow reverses and the normal flow velocity is directed towards the outer

bend near the bed. However, when the flow velocity vector changes direction from the inner bend towards the outer bend the data deviates from the model, since the data shows a sharp transition in normal flow velocities. Furthermore, the data also deviates from the model for low counter-rotation rates, where a local increase is observed before flow velocities decrease. As a result, the modelled linear trends look similar to the measured data except for the initial increase in velocity and the sharp transition when normal flow velocities change direction. Consequently, normal flow velocities are underpredicted for low ratios of lid to floor rotation where secondary flow reverses towards the outer bend, and overpredicted for low floor rotation, i.e. high ratios of lid to floor rotation (Fig. 2.3e). This will be considered in later interpretations of bed slope data. Since negative normal flow velocities do not occur in natural river bends, the morphodynamic experiments with a flow velocity vector directed towards the outer bend will not be taken into account when determining the trend in transverse slope parameters.

The parameter space covered by the morphodynamic experiments contains a large range in secondary flow intensity (Fig. 2.3) and sediment mobility for each grain size, and therefore covers most bedform stability fields (Fig. 2.4). Figure 2.5 shows examples of the typical bedform morphologies in the experiments. With fine sand we obtained bed states ranging from a lower-stage plane bed, across the ripple-dune threshold, to an upper-stage plane bed (USPB). In the experiments with coarse sand and fine gravel, including the experiments with low-density sediment, dunes developed and USPB was not reached. Observed beginning of sediment motion occurred at Shields numbers around the Shields curve for the beginning of sediment motion (Soulsby and Whitehouse, 1997; Kleinhans et al., 2017). The transition from ripples to dunes in the fine sand experiments is characterized by dunes with superimposed ripples (e.g. Ashley, 1990; Ten Brinke et al., 1999; Venditti et al., 2005). The lines separating the ripple and dune fields therefore indicate a transition zone rather than a hard threshold (Kleinhans et al., 2017).

2.4.2 Equilibrium morphologies

During the experiments a transverse slope developed towards either the inner wall or the outer wall. When flow conditions favored bedforms, they started to develop immediately at the start of each experiment (Fig. 2.5). Dune height developed at the same rate as the transverse slope, but dune length needed more time to attain equilibrium because of dune splitting and merging processes. In the absence of dunes, on plane bed or with ripples, the transverse slope was fairly uniform along the flume. When dunes were present, the equilibrium transverse slope was largest in the dune trough but almost horizontal on the dune crest (Fig. 2.5a). Furthermore, dune crests were aligned obliquely to the streamwise flow direction.

When sediment mobility was low, the transverse slope did not develop over the entire width. Since flow velocities are lower at the inner bend than at the outer bend, the inner part of the flume was still below the threshold of sediment motion. This effect was most clearly observed in the experiments with relatively coarse sediment, but was also present at the experiments with finer sediment. Thus, sediment mobility has a large effect on the average transverse slope near the threshold for motion. The effect of the glass walls of the flume on the morphology was limited to about 2 cm from the walls, while the outer bed level

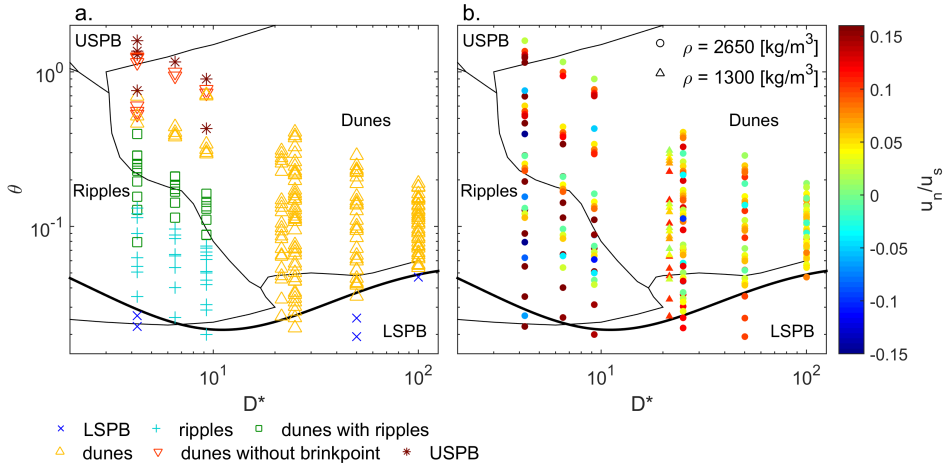

Figure 2.4: Parameter space covered by the experiments plotted in the bedform stability diagram of Van den Berg and Van Gelder (1993), with stability fields of lower-stage plane bed (LSPB), ripples, dunes and upper-stage plane bed (USPB) indicated. The thick black line indicates the Shields curve for the beginning of sediment motion of Soulsby and Whitehouse (1997). a) Observed bed states in the experiments (symbols). b) Experimental range in secondary flow intensity (color scale) calculated from lid and floor rotation. For the experiments with coarse sand and fine gravel, sediment mobilities were limited by the maximum angular velocity of the lid.

measurements start at 4.5 cm from the wall. However, to make sure we did not include any wall effects, the two measurement transects near the walls were excluded from analyses.

Figure 2.6 illustrates the morphology of several experiments with different grain sizes, sediment mobilities and secondary flow intensities, as well as the corresponding quantile bed levels in transverse direction. When lid rotation increased without floor rotation, the average transverse slope did not increase significantly from low to high mobility (Fig. 2.6a,b). However, bedforms increased in height with increasing lid rotation and therefore the variation in bedlevels increased.

On the other hand, when the inward-directed secondary flow decreased through increasing floor rotation whilst sediment mobility (θ) was kept constant, the average transverse slope depended strongly on secondary flow intensity (Fig. 2.6c,d). When the secondary flow intensity became negative, and thus normal flow velocities near the bed were directed outwards, a steep slope developed towards the outer wall of the flume. As observed in the flow direction data, this transition from a slope towards the inner bend to a slope towards the outer bend was rather sudden, so that gentle slopes towards the outer bend are uncommon in our data. In addition, bedforms also decreased in height with decreasing secondary flow intensity and increased again when secondary flow was directed towards the outer wall, even though average sediment mobility remained the same. Furthermore, the orientation of dunes crests varied with changing secondary flow intensity.

Figure 2.6e,f isolates the effect of changing mobility whilst keeping secondary flow intensity constant. The average transverse slope hardly changes with sediment mobility once the sediment is mobile over the entire flume width. However, bed level variation, i.e. the area be-

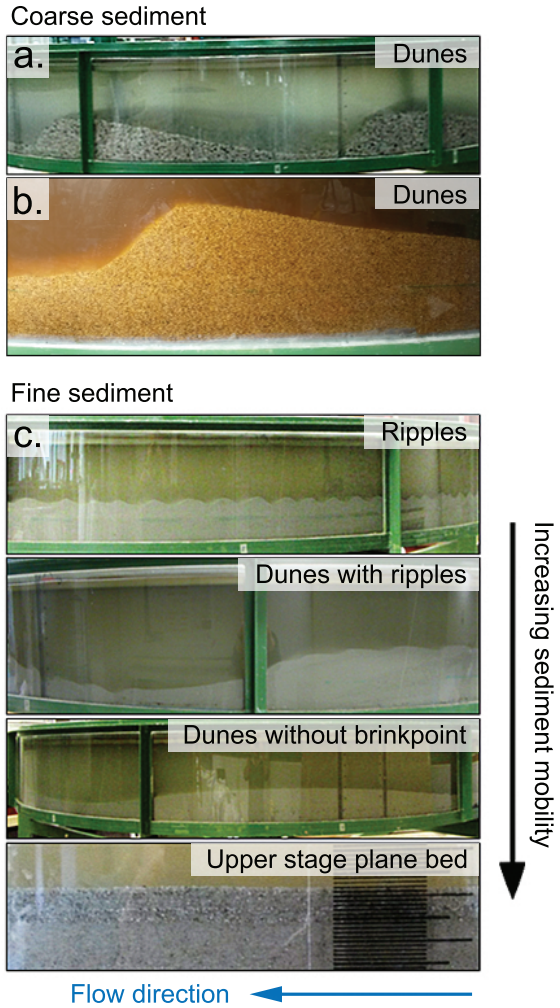

Figure 2.5: Examples of typical equilibrium bed states. a) Dunes developed during experiments with coarse sand and fine gravel, b) and with low-density sediment. c) With fine sands the entire range of bed states from lower-stage plane bed, across the ripple-dune threshold, to upper-stage plane bed were obtained with increasing sediment mobility.

tween the 5 and 95 bed elevation percentiles, varied strongly with mobility in fine sediment, which is the result of bed state transitions. With increasing sediment mobility, bedforms developed from ripples to dunes with superimposed ripples, plane dunes, and low-angle dunes without brinkpoints on the transition to USPB. As a result, the variation in bed levels increased when dunes developed and decreased again when sediment mobility increased towards USPB. In coarse sand on the other hand, variation in bed levels merely increased due to an increase in dune height. Dunes did not flatten as only intermediate sediment mobility was reached.

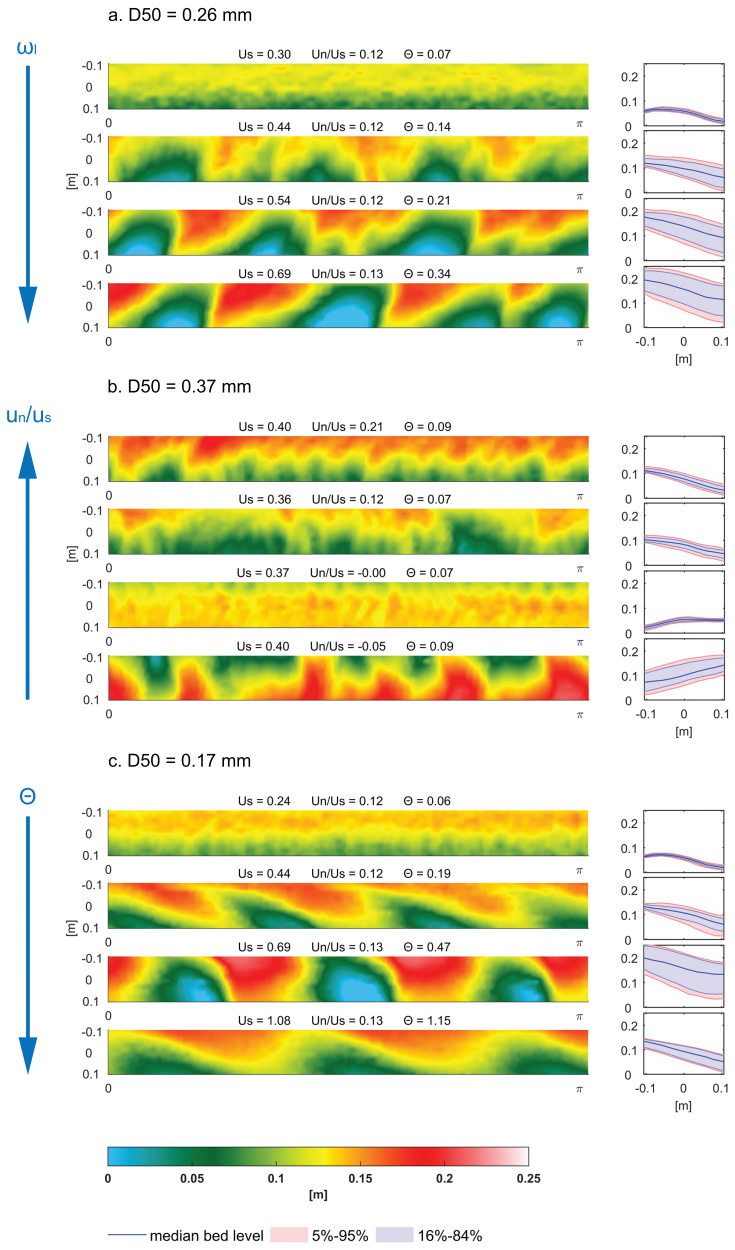
a. D50 = 0.26 mm
ωl
Us = 0.30 Un/Us = 0.12 Θ = 0.07
Us = 0.44 Un/Us = 0.12 Θ = 0.14
Us = 0.54 Un/Us = 0.12 Θ = 0.21
Us = 0.69 Un/Us = 0.13 Θ = 0.34
b. D50 = 0.37 mm
un/us
Us = 0.40 Un/Us = 0.21 Θ = 0.09
Us = 0.36 Un/Us = 0.12 Θ = 0.07
Us = 0.37 Un/Us = -0.00 Θ = 0.07
Us = 0.40 Un/Us = -0.05 Θ = 0.09
c. D50 = 0.17 mm
Θ
Us = 0.24 Un/Us = 0.12 Θ = 0.06
Us = 0.44 Un/Us = 0.12 Θ = 0.19
Us = 0.69 Un/Us = 0.13 Θ = 0.47
Us = 1.08 Un/Us = 0.13 Θ = 1.15
[m]
0 0.05 0.1 0.15 0.2 0.25
median bed level
5%-95%
16%-84%

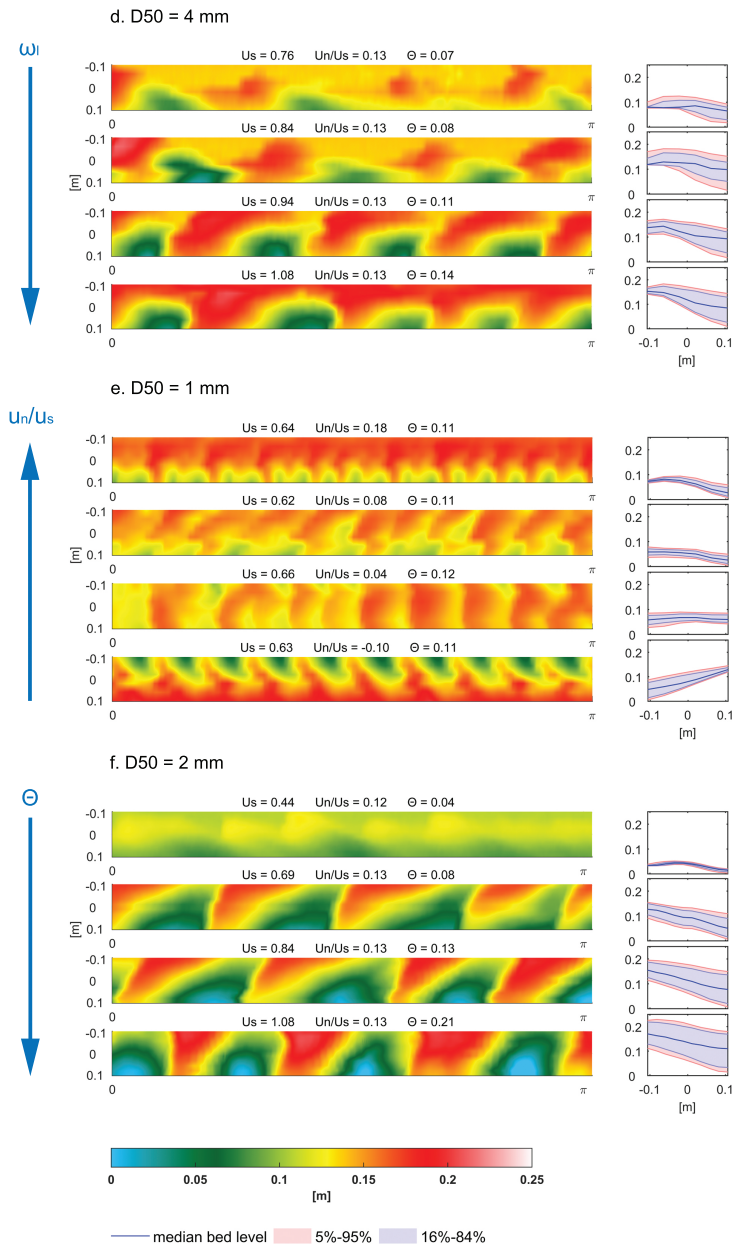

Figure 2.6: Example maps of bed elevation above the flume floor (color scale) on streamwise and normal coordinates, and data reduction to bed elevation percentiles across the flume. Flow is to the left; the inner bend is towards negative normal coordinates and only a semicircle of the bed is shown. Experiments are grouped to illustrate trends with grain sizes, lid rotation, secondary flow intensity or sediment mobility with other factors kept constant. The average transverse bed slopes used in the remainder of this paper were calculated by linear regression on the median bedlevels across the flume, excluding the outermost transects. Experiments where dune troughs touched the solid flume floor were excluded. Left page shows fine sediments and right page shows coarse sediments with similar behaviors. a, d) Experiments with increasing lid rotation with static floor. b, e) Experiments with decreasing secondary flow intensity, while sediment mobility remains constant. c,f) Experiments with increasing sediment mobility and constant secondary flow intensity.

2.4.3 Effect of isolated parameters on average transverse slope

The above examples suggest relations of sediment mobility and secondary flow intensity with average transverse slope. Here we combine transverse bed slope, modelled secondary flow intensity and sediment mobility of all experiments to explore the trends, and calculate slope factor B (Eq. 2.2) for the experiments with secondary flow directed towards the inner bend..

Sediment mobility varied from just above the threshold of sediment motion up to 1.59 for the finest sand (Fig. 2.7a). Despite this large range, no clear trend in average slope against sediment mobility is discernable, as a large variation in transverse slopes occur at various ranges of sediment mobility. However, when sediment mobility approaches the beginning of motion, transverse slopes reduce. At the other extreme end of the possible slope range, transverse slopes never increased above 0.5 m/m, or about 29°, which is about the angle of repose of loose granular sediment.

On the other hand, transverse slope against secondary flow intensity shows a clearer trend. Slopes increase with secondary flow intensity, i.e. when the normal flow velocity component increases relative to the streamwise velocity (Fig. 2.7b). However, there is still considerable scatter. The data, color-coded with sediment mobility in Figure 2.7b, suggest relatively lower increase in bed slope with secondary flow intensity with increasing sediment mobility. Furthermore, the restriction on transverse slope at relatively low sediment mobility is visible by the average slopes just above zero regardless of the secondary flow intensity. This shows there is no simple similarity collapse for transverse bed slope as a function of secondary flow and sediment mobility.

For the experiments with fine sand, the bed slope factor B increases monotonously with increasing relative sediment mobility up to a relative sediment mobility of about 6 (Fig. 2.8A). This means that, given a constant secondary flow intensity, transverse slopes steepen with sediment mobility. For relative sediment mobilities higher than 6, the slope factor reaches a constant value for a given secondary flow intensity, suggesting independence of sediment

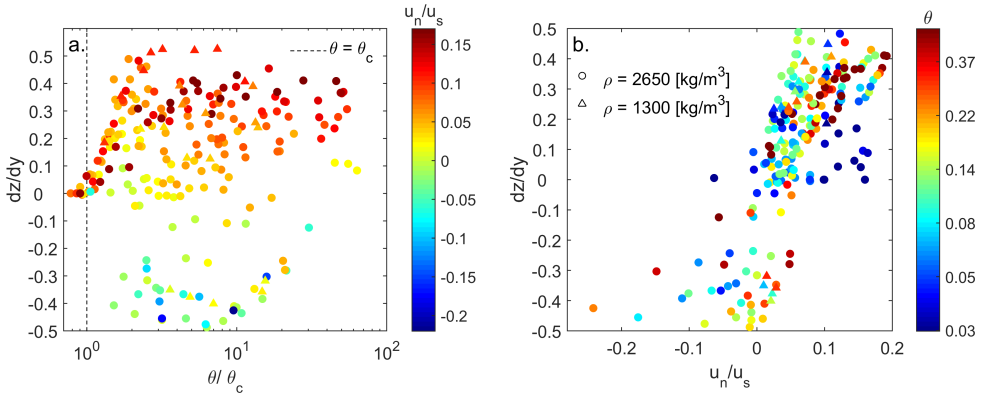

Figure 2.7: Average transverse bed slopes of all experiments. a) Transverse slope against relative sediment mobility. Color scale indicates secondary flow intensity and direction. b) Transverse slope against secondary flow intensity. Color scale indicates sediment mobility.

mobility. For the coarse sediments, the slope factor first increases rapidly with increasing sediment mobility, but then abruptly decreases (Fig. 2.8B). This local maximum is more pronounced for lower secondary flow intensities and coarser sediment. Above a relative sediment mobility of about 4, the slope factor appears independent of sediment mobility. However, for relatively low secondary flow intensities, the slope factor of a few experiments continues to decrease at relatively high sediment mobility.

The different trends of fine and coarse sediments and the existence of a local maximum bed slope factor B at intermediate sediment mobility suggests a relation with bed state. Various bed states were observed which appeared to influence the average transverse slope significantly, especially when dunes were present (Fig. 2.5a). For experiments with almost equal

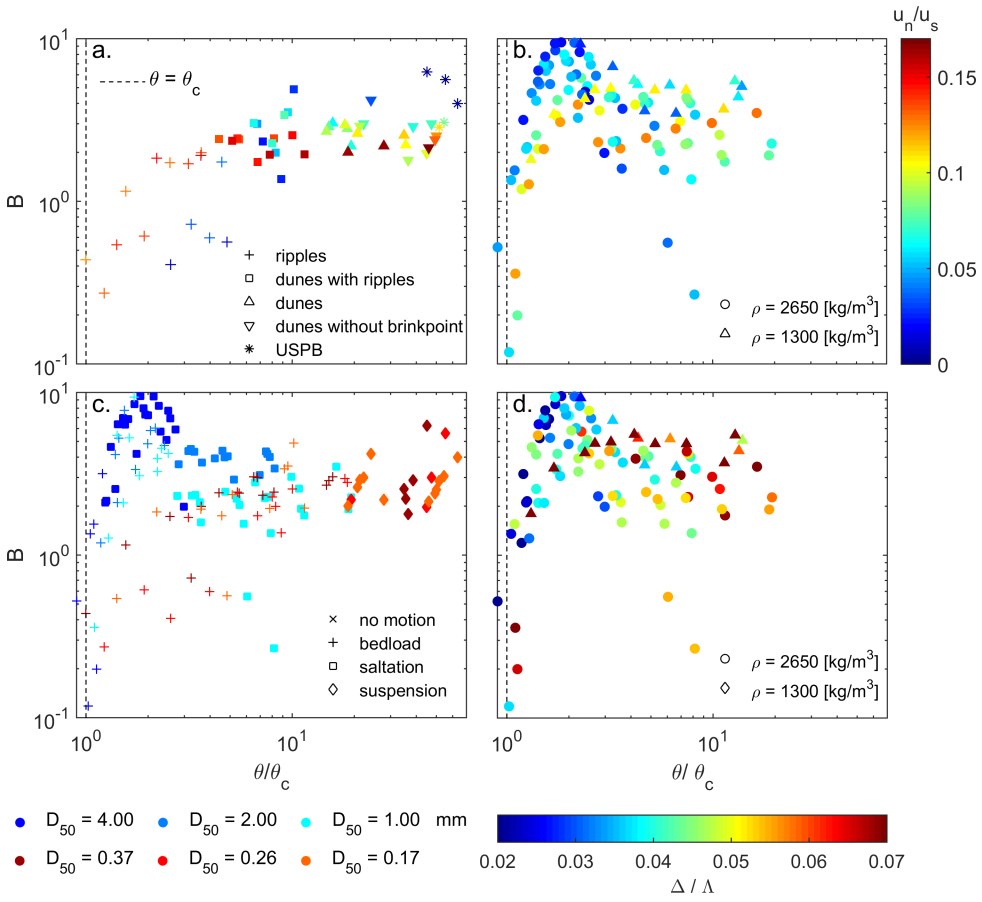

Figure 2.8: Trends in slope factor (Eq. 2.4) against relative sediment mobility of all experiments with transverse slopes towards the inner bend. a) Slope factor of the experiments with fine sands. Color bar indicates secondary flow intensity. b) Slope factor of the experiments with coarse sands and fine gravel, including the low-density sediment. Color bar indicates secondary flow intensity. c) Observed sediment transport mode of all experiments. Color indicates grain size. d) Dune dimensions of the experiments with coarse sand and fine gravel. Colorbar indicates dune height to length ratio (Δ/Λ).

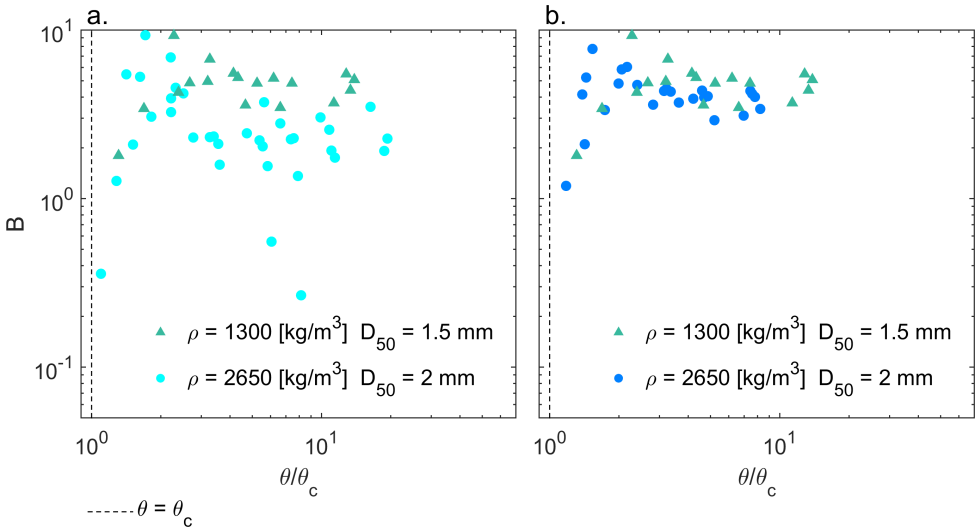

Figure 2.9: Trend in slope factor (B) against relative sediment mobility for experiments with low-density sediment, compared with experiments with normal sediment with median grain sizes of a) 1 mm and b) 2 mm

secondary flow intensities, transverse slope increased with mobility when ripples are present, but upon dunes initiation the transverse slope hardly increased (Fig. 2.8a). However, similar trends were observed for experiments with coarse sediment and only dunes (Fig. 2.8b). Here, the local maximum in slope factor seems to coincide with low dune height to length ratio (Fig. 2.8d), as well as the transition from rolling sediment transport to saltation (Fig. 2.8c). We attempted normalization by a number of bedform dimensions and bedform-related friction parameterizations but none resulted in a similarity collapse of the data of fine and coarse sediment.

Experiments with low-density sediment followed the same trend in bed slope factor B with changing relative sediment mobility, indicating that sediment density has no first-order effect on equilibrium slopes. This is confirmed by the observation that the magnitude of the slope factor of the low-density experiments corresponds best with the experiments with a median grain size of 2 mm (Fig. 2.9b), rather than the experiments with a median grain size of 1 mm (Fig. 2.9a) which have corresponding non-dimensional grain sizes (Fig. 2.4), since grain sizes are normalized with relative density (Van Rijn, 1984b).

2.5 Discussion

We first discuss the relation between the transverse bed slope and the secondary flow intensity and the sediment mobility (expressed as Shields number) observed in the experiments, and then compare the observed trends with predictors found in literature and comment on the implications for morphodynamic modelling.

2.5.1 Influence of secondary flow intensity and sediment mobility on transverse slope

Average transverse bed slope shows a relation with secondary flow intensity and proportionality factor B, as Equation 2.2 by van Bendegom (1947) suggests. However, there are two slope-limiting conditions not included in this relation. The first limit is the maximum angle that can be reached under the influence of gravity. Here this is slightly lower than the typical value for the angle of repose due to dilatancy of the sediment during transport (Kleinhans et al., 2011). The morphology was measured in still flow, while during the experiments this maximum slope could have been higher under stronger secondary flows driving the sediment upwards. Secondly, the transverse slope cannot fully develop when width-averaged sediment mobility is close to the threshold of sediment motion and below it in the inner bend. Hence, the cross-sectionally averaged transverse slope remains low when sediment mobility is low, regardless of secondary flow intensity (Figure 2.7).

The limiting role of sediment mobility is also visible in Figure 2.8. Below a relative sediment mobility of 6, the slope factor B of fine sands depends on relative sediment mobility. For coarse sand and fine gravel this dependence is visible up to a relative sediment mobility of 3. The proportionality factor B is lower than unity at small sediment mobilities, with lowest values of around 0.2 for fine sediments and 0.1 for coarse sediments, and rapidly increases above 1 for larger sediment mobilities. For coarse sediments, this increase in slope factor is even more pronounced, especially for experiments with relatively weak secondary flow and low transverse bed slopes. The nonlinearity of the relation between sediment mobility and slope factor suggests other processes covarying with sediment mobility also affect the proportionality of transverse slope to secondary flow intensity. We found that including the critical Shields number led to a better similarity collapse of trends in average slope of experiments with different grain sizes under the same conditions, which makes sense as the different sediments have different critical Shields numbers and therefore a different offset (Fig. 2.10).

Furthermore, Figure 2.8 shows that the magnitude of the slope factor varies with different secondary flow intensities, suggesting the transverse slope is not linearly related to the secondary flow intensity with constant sediment mobility (Eq. 2.2). However, low secondary flow intensities were underpredicted by the analytical flow model (Fig. 2.3), so it remains unclear whether this trend is significant.

2.5.2 Influence of bedforms and sediment transport mode

The scatter in the data described above suggests that other processes are important. Here we discuss four processes: sediment transport mode, modified turbulence over the ripple-dune transition, the net effect of avalanching at dune slipfaces migrating on a transverse bed slope, and flow steering in the troughs of oblique dunes.

Firstly, the dominant mode of sediment transport changed with increasing sediment mobility (Bridge, 1992; Bennett et al., 1998). The transition from rolling bed load towards saltating particles coincides with the local maximum in transverse slope observed during the experiments with coarse sand and fine gravel (Fig. 2.8c). For fine sands there is no local maximum, but instead the slope factor gradually increases with increasing mobility until

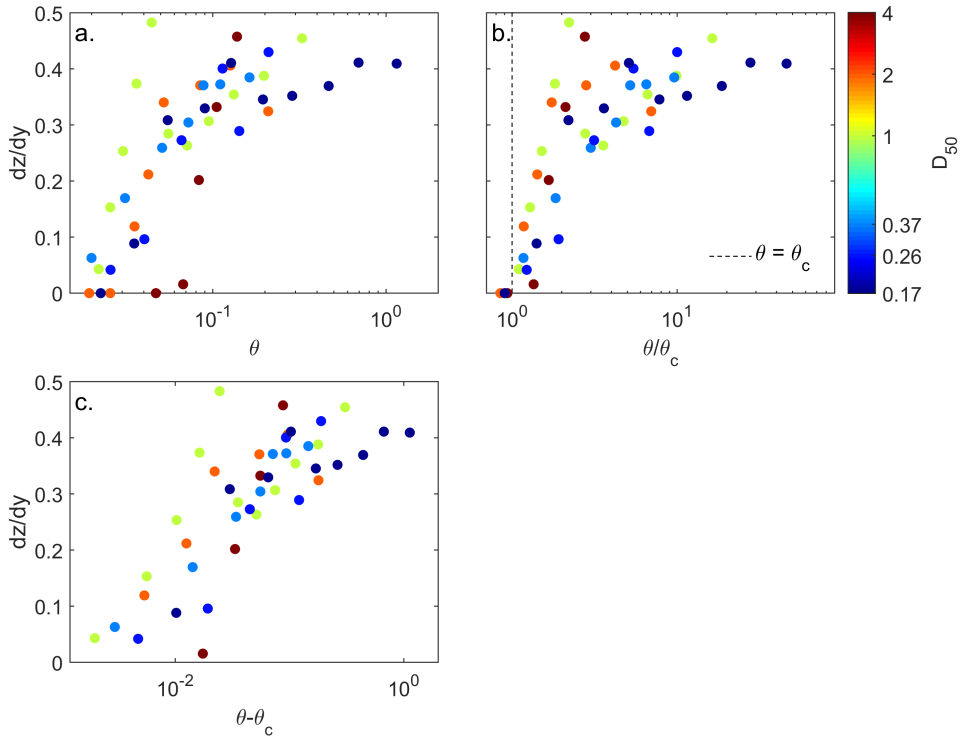

Figure 2.10: Average transverse bed slopes of experiments with only lid-rotation against (a) absolute sediment mobility, (b) relative sediment mobility and (c) excess sediment mobility for all grain sizes (colorscale). The best similarity collapse is attained for relative sediment mobility.

suspension of sediment is present. Here, the slope factor is constant, which means that in this range transverse slopes are independent of sediment mobility and increase linearly with increasing secondary flow intensity (Fig. 2.8a). However, this transition to a constant slope factor is not clearly related to the transition from dominant bed load transport to suspended transport and therefore it remains unclear if this is a causal relation.

Secondly, bedforms were prominent in many experiments. When the bed state of the fine sand experiments transitions from ripples to dunes at higher sediment mobilities, the increase in average slopes decreases and as a result the slope factor reaches a constant value (Fig. 2.8a). Compared to the ripple regime, this means a relative increase in downslope sediment transport with increasing sediment mobility that linearly depends on dune height. Sieben and Talmon (2011) found that the increase in downslope sediment transport on lee sides of dunes resulted in lower transverse slopes, which is caused by the fact that avalanching on the dune slip face is in downward direction rather than perpendicular to the bed or in the direction of dune migration. In our experiments, long dunes, and thus fewer dunes, were observed at intermediate sediment mobilities, where also the maximum slope factor was observed during experiments with coarse sediments (Fig. 2.8d).

Thirdly, in the case of fine sands, the independence of sediment mobility when dunes are present could be explained by a change in turbulence as ripples transition to dunes (e.g. Bennett et al., 1998), which would affect flow through the friction, and sediment transport through the near-bed turbulence. This agrees with the observations of Wiesemann et al. (2006), who found that transverse bed slopes become independent of sediment mobility when dunes start to develop, although they observed a decrease in downslope sediment transport. However, our comprehensive dataset shows a similar independence of transverse slope on higher sediment mobility for coarse sediment where ripples cannot form, so the ripple-dune transition in itself cannot be the explanation.

Fourthly, Dietrich and Smith (1984) and Kisling-Moller (1993) qualitatively observed that the near-bed transverse flow is affected by the presence of oblique dunes in curved flow. In the annular flume, slope was largest in the dune trough and almost horizontal on the dune crest, so that the maximum slope in the dune trough was about two times larger than the average slope. These large variations in transverse slopes along the flume show that average values for flow velocities and slopes are not necessarily representative, and possibly cause unexplained scatter in our trends. Dunes must have had a substantial influence on flow patterns because of their large height relative to water depth. As a result, transverse flow may have lined up with, and concentrated in the troughs of oblique dunes. Indeed, differences in the obliquity of dune crests were observed between experiments, which could have been an effect of secondary flow and this flow concentration, or the cause of enhanced secondary flow. Alternatively, the obliquity was the result of the secondary flow affected by bedforms. The above discussion shows a potentially large influence of dunes on secondary flow patterns. Also, the transverse bed slope strongly depended on the position on the dunes. Future analysis of flow velocity patterns over large dunes is needed to unravel which of the above hypotheses really matter for the transverse bed slopes in the experiments, and how such trends hold for full-scale natural systems with lower dunes relative to water depth.

2.5.3 Comparison with existing bed slope predictors

Published predictors were derived for one sediment transport mode or bed state to study its separate effect on the transverse bed slope effect, and were calibrated and verified with experiments within a specific range in flow conditions and sediment mobility to isolate this mode or bed state. The predictors are therefore only valid for the parameter space of these experimental conditions, which are indicated in Table 2.1. For example, the predictor of Ikeda (1984) that is used in Delft3D is only valid for median grain sizes around 0.15 *mm* and a sediment mobility between 0.10 and 0.23. All predictors include slope factors which are based on a linear relation with slope, i.e. a constant α or α_c, and a power function of sediment mobility, which means that friction parameters and calibration parameters are constant. However, our objective is to obtain parameters that cover all sediment transport modes and bed states, so that this relation can be used in large-scale and long-term modelling where all processes act in concert. The current results show a non-linear relation for the slope factor when plotted as a function of relative sediment mobility (Fig. 2.8) as they cover the limiting effect of low sediment mobility, the effect of the angle of repose and effects of different bed states and sediment transport mode due to experiments with grain sizes varying between 0.17 and

4 *mm* and sediment mobility between 0.018 and 1.59. Consequently, the trend of the slope factor with sediment mobility from this study is more complex than that of the existing predictors, with an α or α_c and β that are not constant. Based on current results, the slope factor should thus be described with a different function than Equation 2.4 to adequately describe the non-linear dependence on sediment mobility. However, to be able to compare the slope parameters of existing predictors to the experimental results, a preliminary fit of the slope factor over relative sediment mobility is plotted in Figure 2.11 with constant values for α_c and β per median grain size:

$$B = 25 D_{50}^{0.37} \left(\frac{\theta - \theta_c}{\theta_c} \right)^{0.2} \tag{2.11}$$

In view of our understanding of the sediment transport process reflected in transport predictors, it is necessary to include a critical shear stress, especially when different sediment sizes are considered. Additionally, it is necessary to start at a relative sediment mobility of 0, to start with a flat bed at the beginning of motion. Consequently, the resulting formulation of relative sediment mobility is the same as the mobility parameter in the sediment transport predictor of Van Rijn (1984b). Furthermore, the fit is grain size dependent due to significant differences in the magnitude of the slope factor. To further account for the difference

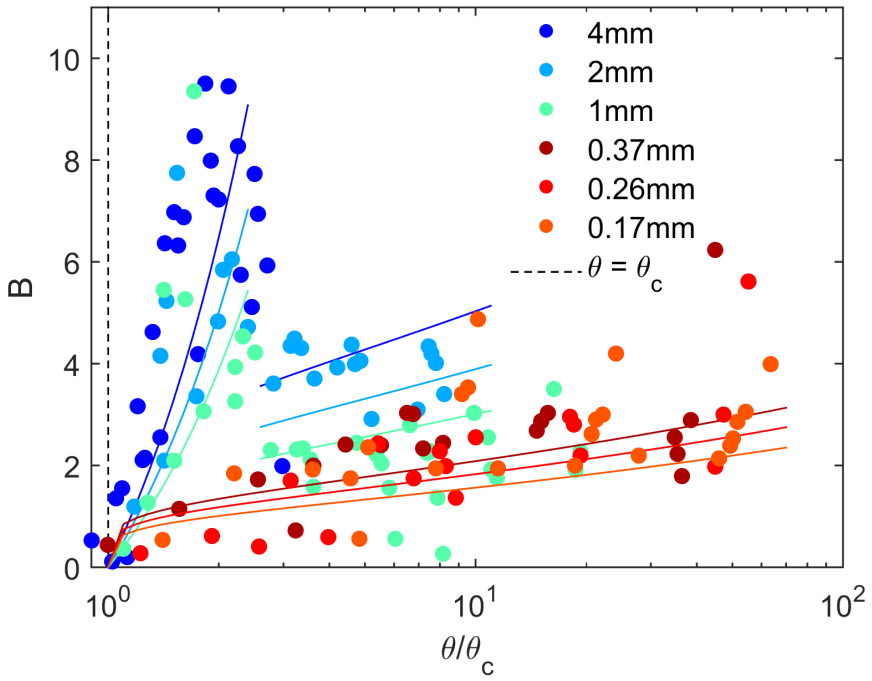

Figure 2.11: Empirical fits to experimentally determined slope factors as a function of relative sediment mobility and grain size. The fitted functions have a similar shape as existing relations found in literature (Eqs 2.11, 2.12).

between fine sediment and coarse sediment, a different function is plotted for experiments with coarse sediment and a relative sediment mobility lower than 2.5:

$$B = 50 D_{50}^{0.37} \left(\frac{\theta - \theta_c}{\theta_c} \right) \tag{2.12}$$

which empirically covers the abrupt transition observed in the data but is as yet unsatisfactory for modelling purposes where sudden transitions and thresholds may cause instability.

This fit indicates α_c varies between 1 (0.17 mm) and 1.34 (0.37 mm) for fine sand, and between 1.94 (1 mm) and 3.24 (4 mm) for coarse sand and fine gravel with relatively higher sediment mobility. However, this fit does not describe the independence from sediment mobility of the slope factor, which is reached at a lower sediment mobility for coarse sands and fine gravel than for fine sands. For a relative sediment mobility lower than 2.5 and coarse sediment, α_c varies between 3.9 (1 mm) and 6.5 (4 mm) and β is equal to 1, representing the sharp increase in slope factor at low sediment mobility. Compared to literature the predictors based on a power function of Shields number all underestimate the slope factor significantly and thus overestimate the downslope sediment transport and therefore lead to flatter slopes than we observed (Fig. 2.12c). Predictors that include a critical sediment mobility more adequately describe the amount of downslope sediment transport for fine sands, but still overestimate slope effects for coarse sand and fine gravel (Fig. 2.12c). The predictors of Engelund (1974) and Engelund (1975) are independent of sediment mobility and therefore cannot be valid for low Shields numbers. The value of 0.2 for β is lower than in literature, resulting in a lower increase in slope factor with increasing sediment mobility.

We can now examine the trends in our data in view of the assumptions behind the process-specific predictors (Table 2.1). Firstly, in literature several predictors are specified for low sediment mobility and a plain bed configuration, with either bed load transport (Engelund, 1975; Hasegawa, 1981) or saltation (Sekine and Parker, 1992; Parker et al., 2003; Francalanci et al., 2009). In the current experiments, no plain bed was observed above the threshold of sediment motion, but we can compare these predictors with the trend in our data for experiments with bedload transport and saltation below a sediment mobility of 0.2, which is the maximum sediment mobility for which the predictor of Sekine and Parker (1992) is validated. Hasegawa (1981) defined a predictor based on both dynamic and static friction for bedload transport of fine sediment, with an α_c that is comparable to our fine sediment data in this range (Fig. 2.12d). Parker et al. (2003) defined a predictor for coarse sediment based on a ratio between the critical sediment mobility for the cessation of sediment transport and for the beginning of motion, which is generally below unity and results in a slope factor that is comparable to our coarse sediment data around the transition to saltation. Therefore, we can conclude that for low sediment mobility the influence of transverse slopes on the beginning and cessation of motion mainly determines the equilibrium slope. However, the strong observed increase in slope factor with increasing sediment mobility for coarse sediment is not explained by existing predictors for low sediment mobility.

The predictor of Sekine and Parker (1992) assumes that saltating particles are less influenced by gravity than rolling and sliding particles because they have less frequent contact with the bed, with the result that the slope effect is less dependent on sediment mobility.

Consequently, due to a β of 0.25, this predictor most accurately describes the trend in the current data for relative sediment mobilities higher than 4, for both fine sand and coarse sand and fine gravel. In this range, all coarse sand and fine gravel experiments showed saltation for which the predictor of Sekine and Parker (1992) was developed (Fig. 2.8). At lower sediment mobilities, sediment mobility has a larger influence on slope effects, as described above, and here the predictor deviates from the data.

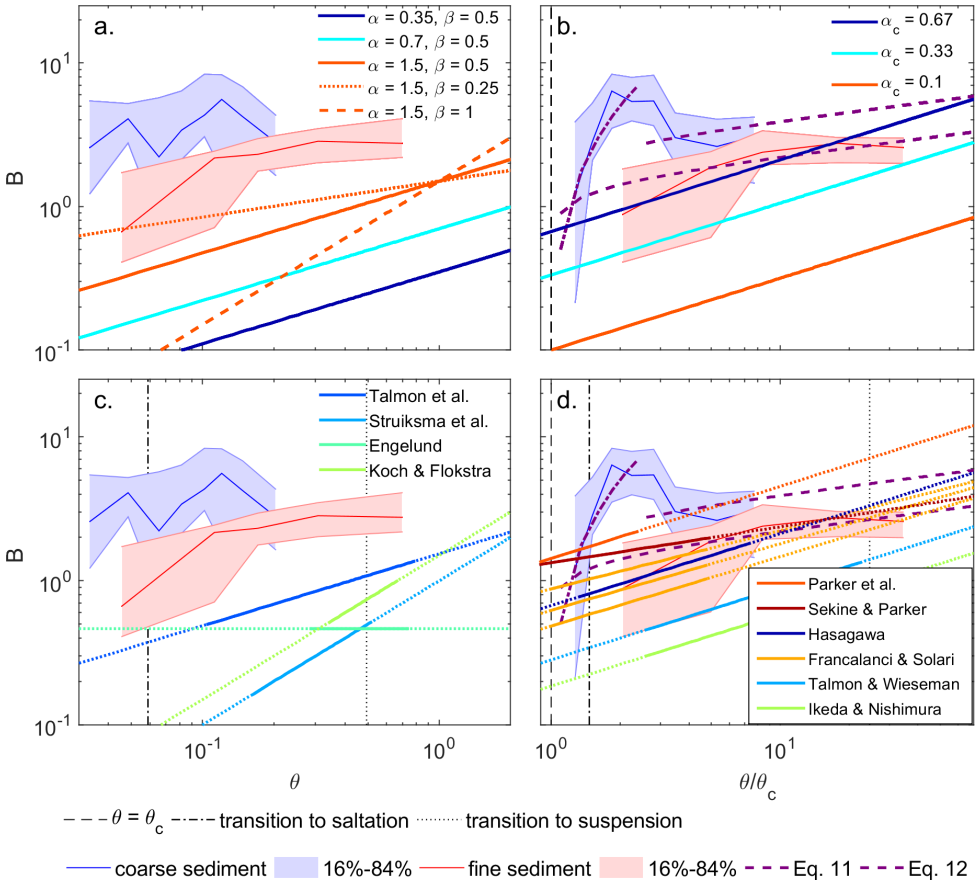

Figure 2.12: Comparisons of experimentally determined slope factors and predictors found in literature for sediment mobility ranging between the beginning of sediment motion and upper-stage plane bed. The experimental data is reduced to slope factor percentiles for small intervals of (relative) sediment mobility, split in two grain size classes with distinct behaviors. The fitted functions based on the experimental data (Eqs 2.11, 2.12) are also shown. a,b) Experimental data compared with generic predictors (Eqs 2.3,2.4) with typical parameter values as used in morphological modelling based on either sediment mobility (a) or relative sediment mobility (b). c,d) Experimental data compared with specific existing predictors (Table 2.1), based on either sediment mobility (c) or relative sediment mobility (d). The condition range for which an existing predictor is valid is indicated with a solid line, while outside this range the predictor is plotted with a dotted line. The non-linear predictor of Francalanci and Solari (2008) is plotted for transverse slopes of 0.3 (upper line), 12 (middle line) and 25 degrees (lowest line). Theoretical transition zones to saltation as defined by Bridge (1992) and to suspension as defined by Van Rijn (1984a) are also indicated by vertical dashed lines.

Ikeda (1984) and Ikeda and Nishimura (1986) have a similar predictor, based on the balance between friction and drag force. The only difference between these two predictors is the addition of a sheltering coefficient by Ikeda and Nishimura (1986) that improves the fit with their experimental data. The resulting difference in α_c can thus be explained by the difference in experimental settings which were used to validate the theoretical model. Namely, the model of Ikeda and Nishimura (1986) is validated with conditions that favored ripples, while during the experiments of Ikeda (1984) dunes formed. Although these predictors deviate significantly from our slope parameters, this confirms that bed state can have a significant effect on the slope factor, as is observed in the current experimental data set and described in the previous section.

The difference in slope factor due to bedforms is also observed in the study of Talmon et al. (1995) and the empirical study of Talmon and Wiesemann (2006) who added a specific bedform calibration parameter to account for this. Talmon et al. (1995) showed that the difference between slope factors in natural rivers are in the order of two lower than slope factors in experiments with dunes, due to the relatively high bedforms compared to the water depth. Therefore, they used a slope factor based on the bedform height predictor of van Rijn (1984) to account for the increased bed friction. van Rijn (1984) predicts bedform height to depend on relative sediment mobility and a ratio between median grain size and water depth: $\left(\frac{D_{50}}{H}\right)^{0.3}$. Interestingly, our trend in slope factor also depends on a median grain size to the power of about 0.4 (Eq. 2.11, 2.12). In Figure 2.13, dune height as observed in the experiments with a median grain size of 4 *mm* and 0.17 *mm* is compared with dune height as predicted by van Rijn (1984). The predicted dune height for coarse sediment agrees with the observed dune heigth. The magnitude of the predicted dune height for fine sediment does not correspond with the data, but the increase in dune height with increasing relative sediment mobility is visible, as is the maximum around a relative mobility of 10 and the decrease when dunes are flattened towards an upper stage plane bed. This, together with the conclusion that bed state has a significant influence on the slope factor, confirms the use of an α_c that depends on the median grain size to account for bedform friction.

2.5.4 Implications for morphodynamic modelling

Pending a more complete process explanation and better transverse bed slope relation, we here briefly interpret what the implications of our findings are for large-scale morphology and for morphodynamic modelling. At lower sediment mobility slope effects are relatively high, resulting in smoother morphologies than expected from existing relations, while at environments with larger sediment mobilities slope effects have less influence, which is reflected in a higher slope factor and will result in steeper transverse slopes in otherwise the same conditions and in the absence of processes not studied here, such as lateral diffusion of suspended sediment. For coarse sediments, slope effects are the smallest at intermediate sediment mobility and here slopes are even steeper than at high sediment mobility under the same secondary flow conditions. This will result in for example a higher braiding index than expected from existing relations. Furthermore, current results suggest a change in sediment mobility has a larger effect at lower mobilities, compared with relatively high mobilities were the slope factor is almost constant with increasing sediment mobility. This effect is therefore

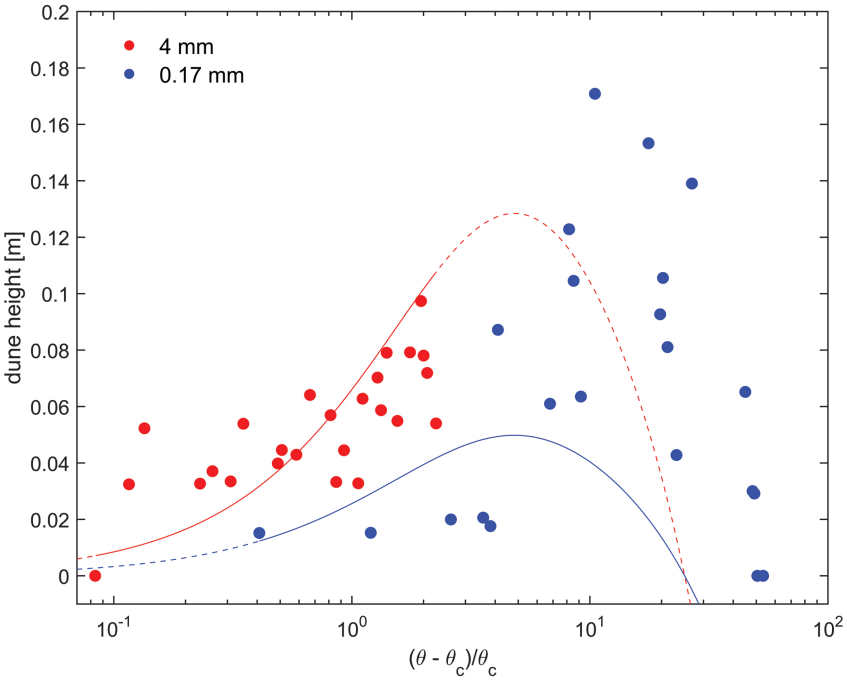

Figure 2.13: Comparison between the dune height observed in the experiments with a median grain size of 4 *mm* and 0.17 *mm* (scatter) and the dune height as predicted by van Rijn (1984) (lines). Solid lines represent the predictor for relative sediment mobility in the range of the experiments, while dashed lines show the whole trend of the dune height predictor from lower stage plane bed to upper stage plane bed.

especially important in areas with low sediment mobility where a significant difference in sediment mobility over time or space occurs, e.g. near channel banks and shoal margins. How exactly a nonlinear bed slope relation changes this local morphology remains to be studied by modelling.

The objective of this study was to obtain a general relation that is valid for all systems where various sediment transport processes and bed states can occur together, instead of the process-specific predictors subject to model operator choice. This relation is therefore more suitable for application in a morphodynamic model like Delft3D that is used across a wide range of environments and conditions in science and in engineering practice. As long as current morphodynamic models do not include a transverse slope relation that describes the non-linearity with sediment mobility and the dependence on grain size as found in our dataset, it is therefore tentatively advised to adjust input parameters α_c and β to the system that is modelled. This is a simplification in that changes in mobility away from channels and up bars are ignored. Equations 2.11 and 2.12 can be used as guidelines when determining these input parameters. In general, for systems with low sediment mobilities and grain sizes larger than 0.8 *mm*, where only dunes are expected to occur, β should be 1 and α_c around

5. For systems with higher sediment mobilities, a β of 0.2 and an α_c around 2.5 is advised. For fine sediments and all systems, α_c is lower, around 1. A calibration range of a factor 2 is acceptable to account for the uncertainty of the influence of relatively high bedforms in flume experiments. Appendix B describes the input parameters for Delft3D in more detail, and a guideline to switch between the two methods for sediment transport deflection on transverse slopes.

Surprisingly, the magnitude of experimentally determined slope factors is similar or higher than slope factors in predictors used in Delft3D, which also means the parameter α_c is higher than the default value of 0.67 for most sediment mobilities and only lower than 0.33 near the beginning of motion (Fig. 2.12b). Likewise, the α is always higher than a value of 1.5 (Fig. 2.12a). This is at odds with the need to increase the slope effects by decreasing α or α_c in model calibration on measured bathymetry (e.g. van der Wegen and Roelvink, 2012). Under all assumptions made in our work, this leads to the conclusion that the tendency of models to overdeepen channels is not a direct result of the shortcomings of current transverse bed slope predictors. Rather, it suggests that such calibration is necessary to compensate for other, hitherto unidentified model weaknesses such as issues with numerical schemes or missing processes.

Past work hints at a combination of processes and parameters that affect bed slopes indirectly (e.g. Kleinhans et al., 2008). Firstly, the prediction of flow resistance can be improved, including the effect of bedforms. In Delft3D, a constant Nikuradse roughness coefficient results in steeper gradients between river banks and channels, while a uniform Chezy roughness implies a changing Nikuradse roughness coefficient with water depth and results in shallower channels and smoother morphology in general (Schuurman et al., 2013). Secondly, sediment transport predictors have different degrees of nonlinearity due to different power functions and different choices of including the threshold for motion. Thirdly, the choice in sediment transport predictor determines if suspended sediment is taken into account. van der Wegen and Roelvink (2012) decreased the α_c by an order of magnitude for the Van Rijn sediment transport predictor which includes suspended sediment, compared to the total-load Engelund-Hansen predictor which was entirely treated as bed-load in their model. Fourthly, current morphodynamic model simulations generally use only one sediment fraction, while Dastgheib and Roelvink (2010) shows that using multiple fractions in long-term model simulations leads to channel depth reduction, as would a larger bed slope effect, because of bed armouring effects. Finally, lower values for α or α_c, and thus more downslope sediment transport, may be necessary to compensate for subgrid bank erosion processes that usually are not incorporated in the numerical models (Grenfell, 2012; Schuurman et al., 2013).

2.6 Conclusions

We experimentally tested the effect of a large range in secondary flow intensity and sediment mobility on equilibrium transverse slopes using a rotating annular flume, covering all sediment transport modes and bed states for a wide range of secondary flow intensity.

The resulting trend in slope effect deviates from typical power relations with Shields number and is grain size dependent. An increase in secondary flow intensity resulted in an increase in transverse slope until the angle of repose of loose granular sediment was reached. On the other hand, when secondary flows were minimal, the average transverse slope was also minimal. Sediment mobility limited the development of transverse slopes just above the beginning of motion and influenced slope effects by affecting sediment transport mode and bed state. Downslope sediment transport increased when ripples transitioned to dunes in fine sands, and with coarse sand and fine gravel slope effects were minimal when dune height-to-length ratios were low. The presence of dunes had a large influence on flow patterns because of their large height relative to water depth and possibly enhanced secondary flow. Future analysis of flow velocity patterns over large dunes is needed to unravel the exact effect of dunes on transverse bed slope effects and to translate the current results to natural systems.

Downslope sediment transport is significantly lower than in existing transverse slope predictors, especially for coarse sand and fine gravel. Furthermore, the change in slope effect with increasing sediment mobility is higher at low sediment mobility, but significantly lower at higher sediment mobility. Eventually, slope effects become independent of sediment mobility, which is not yet taken into account in current models. The lower downslope sediment transport is in contrast with the tendency to increase slope effects in morphodynamic modelling to compensate for overdeepening of channels. This suggest calibrating the slope effects in current practice is necessary to compensate for other model weaknesses, such as roughness, the choice of sediment transport predictor or the absence of bank erosion.

Acknowledgements

This research was partly supported by Deltares and by the Dutch Technology Foundation STW (grant Vici 016.140.316/13710 to MGK, which is part of the Netherlands Organisation for Scientific Research (NWO), and is partly funded by the Ministry of Economic Affairs). This work is part of the Ph.D. research of AWB and M.Sc. research of JdS. We are grateful to Sander de Vree and Hans Tas of the Environmental Fluid Mechanics Laboratory at the TU Delft for technical support. Discussion with Kees Sloff, reviews by two anonymous reviewers and steer by Associate Editor Christophe Ancey helped to improve the manuscript. The authors contributed in the following proportions to conception and design, data collection, flow modelling, data analysis and conclusions, and manuscript preparation: AWB(50,70,50,60,80)%, JCdS(0,30,0,10,0)%, WSJU(10,0,40,0,0)%, MGK(40,0,10,30,20)%. Supporting data are included in Appendix E.

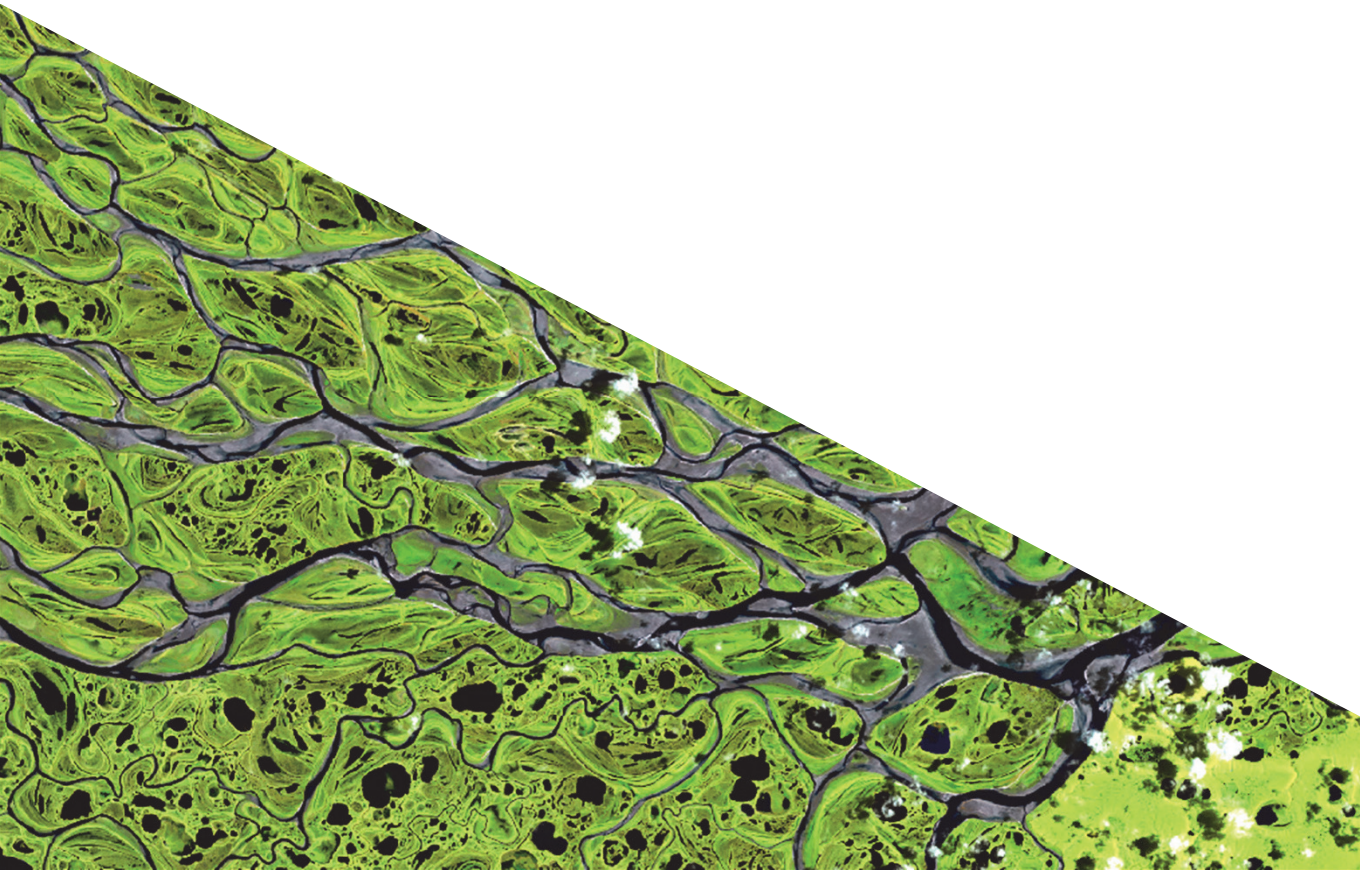

Chapter 3

Influence of grain size-dependent bedform morphology on flow and transverse slope in river bends

Bedforms transport sediment and influence near-bed flow by modulating the near-bed shear stress distribution. Dunes can create a zone of permanent flow separation which causes an increase in friction, depending on relative height and lee-side angle. However, while the interaction between bedform morphology and flow is relatively well known in straight river reaches, research on the influence of bedforms on the interaction between sediment dynamics and flow in river bends is limited and only qualitatively described. Recent research suggested that different bedforms led to a magnitude of difference in sediment transport on slopes towards the inner bend. The objective of this study is to unravel the difference in interaction between different bedform types and the balance between secondary flow and transverse sediment transport in curved channels. To this end, we use experimental data from 142 experiments in a rotating annular flume, with a large range in grain size, streamwise and transverse flow velocity. This resulted in bedforms ranging from a lower-stage plane bed, across the ripple-dune transition, to an upper-stage plane bed, and transverse slopes from a nearly flat bed to the angle-of-repose. Results show that dunes in coarse sediment steepen the transverse slope by enhancing secondary flow in dune troughs, controlled by grain size-dependent lee-side angles. Bedforms in fine sediment did not show an interaction with the equilibrium between transverse slope and secondary flow, and lee-side angles depended on bedform type. These findings imply that friction and transverse slope in river bends depend on grain size controlled bedform morphology.

Based on: Baar, A. W., Cisneros, J. (2018), Influence of grain size-dependent bedform morphology on flow and transverse sediment transport in river bends. *Submitted to:* Journal of Geophysical Research: Earth Surface.

3.1 Introduction

In sand-bed rivers, bedforms ranging in scale from ripples to dunes and larger bar-forms are major contributors in determining how sediment is transported downstream and creating large-scale turbulence in the flow (Allen, 1968; Bennett and Best, 1995; McLean et al., 1994; Best, 2005). Turbulence is generated via eddy shedding in the shear layer between free flow and recirculating flow where flow separates at the bedform crest and reattaches downstream (Best, 2005). Consequently, these bedforms have a direct relation with water depth through exerting friction on the flow (Allen, 1968). Furthermore, bedforms cause hydraulic heterogeneity within rivers, thus creating areas of local deposition and erosion that influence riverbank erosion by producing areas of aggradation and degradation in channels (Ashworth et al., 2000; Hickin, 1974).

In coarse sand ($> 0.7\ mm$), dunes will develop, where dune height and length will increase with increasing flow velocity and shear stress until they reach a certain height relative to the water depth (Van Rijn, 1984a; Julien and Klaassen, 1995). At very high shear stresses, dunes become washed out and upper stage plane beds are created (Van Rijn, 1984a; Naqshband et al., 2014; Bridge and Best, 1988). In fine sands ($< 0.7\ mm$) and low shear stresses, first ripples start to form then these bedforms transition into dunes at higher shear stress. This transition from ripples to dunes is depicted in phase space diagrams as being a sharp transition, whereas often ripples and dunes will coexist in this transition (Van den Berg and Van Gelder, 1993; Guy et al., 1966). Flow accelerates over the bedform stoss side and decelerates at the crest where, if the lee side is steep, flow detaches and reattaches further downstream and creates the zone of flow separation (Best, 2005). Thus, the major features of flow over an asymmetrical bedform include flow separation, a shear layer dividing the free stream flow and recirculating flow above the zone of flow separation, and turbulent eddy shedding in the form of Kelvin-Helmholtz vortices within the shear layer (Best, 2005). Whereas both ripples and dunes undergo flow separation, the turbulent eddies produced in the shear layer of ripples are of lower magnitude and less frequent, and the turbulent eddies advected off ripple crests diffuse well below the water surface (Bennett and Best, 1995). Due to the larger magnitude turbulent eddies and larger flow separation zone, dunes may have a larger influence on the flow than ripples – this is reflected in the field where dunes have been proposed to break down channel-scale secondary flow cells in a large river when the dune height was large compared to flow depth (Parsons et al., 2005).

Previous studies have linked lee-side angle to the strength and length of these flow separation zones and have shown that permanent flow separation is absent in dunes with lee-side angles less than 10 degrees (Best and Kostaschuk, 2002; Best, 2005; Motamedi et al., 2012; Motamedi et al., 2014; Lefebvre and Winter, 2016; Kwoll et al., 2017). Specifically, Lefebvre and Winter (2016) showed with numerical modelling that permanent flow separation zones start to develop and grow in size between 11 and 18 degrees depending on relative bedform height and aspect ratio, i.e. the ratio between height and length, and these zones are fully developed at lee-side angles higher than 24 degrees. Therefore, bedform dimensions have a large influence on flow dynamics near the bed, and thus on the shear stress distribution that can potentially influence near-bed sediment transport. However, in current flow rough-

ness predictors for dunes in river channels, known morphologic parameters such as height and wavelength are commonly used whereas dune lee-side angle is often assumed as a steep, straight line connecting the dune crest and trough (i.e. simple, triangular dunes) (Einstein, 1950; Nelson and Smith, 1989; Van Rijn, 1984a; Vanoni and Hwang, 1967).

Many studies have focused on 2D bedforms in straight river channels (Best, 2005), while research on the influence of bedforms on the interaction between sediment dynamics and flow in river bends is limited, even though this has implications for flow patterns through the bend, fairway depth, and bank erosion. In river bends, transverse downslope sediment transport on the point bar is balanced by secondary flows dragging the sediment upslope, and this equilibrium determines the transverse slope towards the inner bank (e.g. Engelund, 1974; Struiksma et al., 1985). Dunes are expected to influence this balance depending on their relative height compared to the water depth (Talmon et al., 1995) since they cause a strong variation in the local streamwise and transverse slopes, flow field and flow turbulence intensity along the river bend. However, how dunes influence the transverse slope is under debate since they could either enhance secondary flow and thereby increase the transverse slope by focusing flow in dune troughs (Kisling-Moller, 1993; Wiesemann et al., 2006), or increase transverse downslope sediment transport by avalanching at the lee sides of the dunes and thereby lower the slope (Sieben and Talmon, 2011). Furthermore, the aspect ratio of dunes is observed to increase in a tight bend (Nanson, 2010) which implies there is a feedback between flow conditions and bedform characteristics. Observations in previous studies were based on limited experiments (Talmon et al., 1995; Wiesemann et al., 2006) or a specific field site (Kisling-Moller, 1993; Nanson, 2010), which means that the relation between varying bend radii, flow velocity, grain size and consequently changing bedform morphology was never quantitatively understood. Therefore, the influence of bedform morphology on flow patterns and transverse sediment transport was never incorporated in derivations of physics-based predictors for transverse downslope sediment transport.

A recent comprehensive set of experiments (Baar et al., 2018) ranging from fine sand to fine gravel near the beginning of sediment motion up to sheet flow (upper-stage plane bed) showed a significant difference in equilibrium transverse slope in river bends between coarse and fine sediment under the same flow conditions, which is likely to be caused by a difference in bedform type. More specifically, experiments with grain sizes larger than 0.7 mm showed higher equilibrium transverse slopes than experiments with finer sediment. These results indicate that different bedform types potentially have a significant effect on transverse downslope sediment transport and/or secondary flow patterns. However, it is unclear what bedform characteristics cause the difference in transverse sediment transport between coarse and fine sediments, and how this will change when a bedform transitions from one type to another. It is hypothesized herein that dunes interact with the secondary flow patterns in the bend, and thereby influence the equilibrium transverse slope that develops, while a rippled bed does not influence the interaction between secondary flow and transverse sediment transport.

The main objective of this paper is therefore to unravel the interaction between bedform characteristics, secondary flow, and sediment transport on transverse slopes. To this end, we analyzed bedform characteristics of 142 experiments in a rotating annular flume with a wide

range of flow velocities in the subcritical regime, secondary flow intensities, and sediment sizes around the transition between sand and gravel systems. We used a new method that analyses dune lee sides across the width of the channel along transect lines, but also notes that the maximum slope will not always dip in the direction parallel to the transect line. In this way, lee side slopes are measured as the maximum sloping surface on the lee side and not along a line that may be oblique to the dune crest. Ultimately, the aim is to describe the difference in magnitude of transverse downslope sediment transport between bends with different bedform states, and to explore implications for roughness compared to straight river reaches.

3.2 Methods

3.2.1 Experiments in a rotating annular flume

Experiments were conducted by Baar et al. (2018) in a rotating annular flume, which represents an infinite river bend and therefore has the advantage that flow and sediment transport do not have to adapt to inflow and outflow, resulting in a morphology that is in equilibrium with the flow conditions. Furthermore, the rotating annular flume allows control of secondary flow intensity separately from the main flow velocity, by the possibility to control the centrifugal forces on the water by separately rotating both the lid and the floor of the flume. Lid rotation drives the streamwise flow by applying shear on top of the water column and generates a centrifugal force that creates a pressure gradient from the outer to the inner bend which drives secondary flow. Counter rotation of the floor of the flume adds an additional outward directed centrifugal force on the lower half of the water column, thereby decreasing the near-bed secondary flow that is inward directed. In this way, different bend radii can be simulated independent of the main flow velocity, and thus the characteristics of bedforms can be isolated from the transverse slope and secondary flow intensity. Baar et al. (2018) derived an analytical model based on flow velocity measurements with a Vectrino-II, an acoustic Doppler velocity meter. This analytical model describes near-bed streamwise and normal flow velocity as a function of lid and floor rotation and flume dimensions, which will be used in this paper to characterize shear stress, sediment mobility and secondary flow intensity. Secondary flow intensity is defined as the magnitude of streamwise flow velocity $[m/s]$ divided by the inward-directed normal flow velocity $[m/s]$. Sediment mobility θ, a dimensionless form of the bed shear stress, is defined as:

$$\theta = \frac{\tau}{(\rho_s - \rho)gD_{50}} \tag{3.1}$$

where τ = shear stress $[N/m^2]$, ρ_s = specific density of the sediment, g = gravitational acceleration $[m/s^2]$ and D_{50} = median grain size $[m]$.

In total, 142 experiments were conducted with sediments with a median grain size of 0.17, 0.26, 0.37, 1.0, 2.0 and 4.0 mm and a density of 2650 kg/m^3, to ensure a transition from both hydraulic smooth to hydraulic rough conditions and across the ripple-dune transition defined in previous literature (Van den Berg and Van Gelder, 1993; Southard and Boguchwal, 1990). Henceforth we name the sands with median grain sizes smaller than 0.7 mm fine sand,

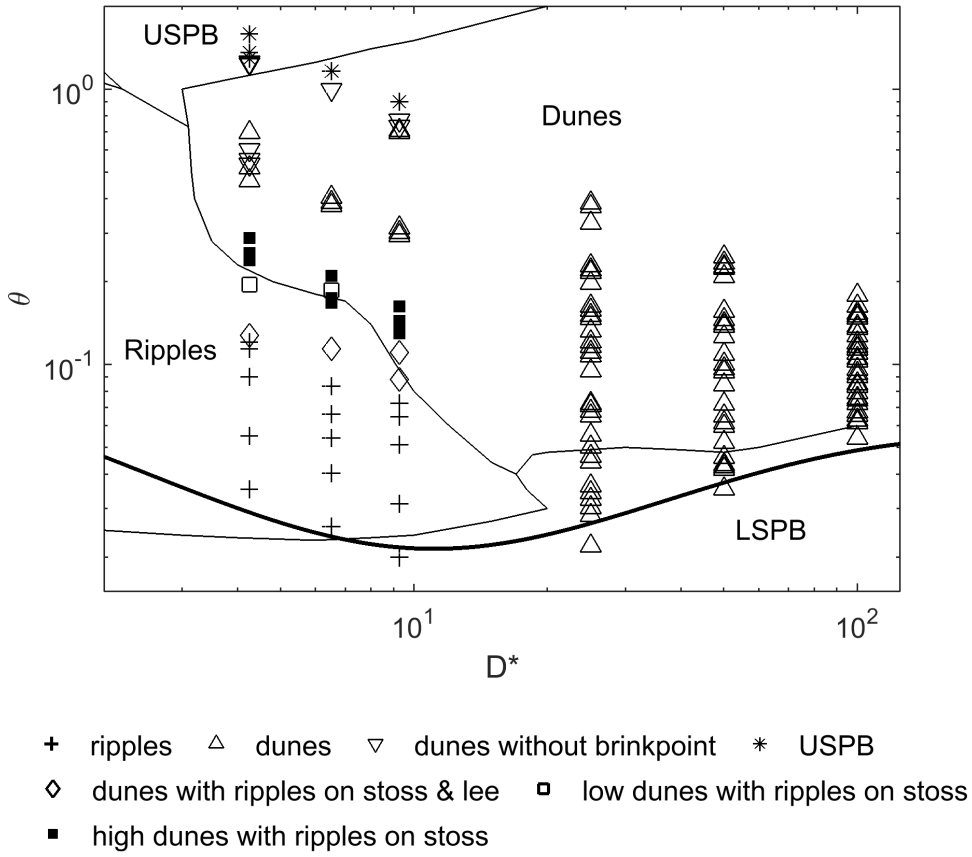

Figure 3.1: Parameter space as observed in the experiments (symbols) plotted in the bedform stability diagram of Van den Berg and Van Gelder (1993), with stability fields of lower stage plane bed (LSPB), ripples, dunes and upper stage plane bed (USPB) indicated. The thick black line indicates the Shields curve for the beginning of sediment motion of Soulsby and Whitehouse (1997). Symbols indicate the observed bed states in the experiments.

and the coarser sediments coarse sand ($0.7 - 2\ mm$) and fine gravel ($> 2\ mm$). Sediment mobilities ranged from the threshold of motion up to 1.59 for the finest sand, covering all sediment transport modes and bed states in the subcritical regime. Each experimental condition is plotted in the Shields diagram in Figure 3.1 to illustrate the experimental range. The transverse slope was varied by changing the lid to floor rotation ratio, resulting in secondary flow intensities from 0 (a straight river reach), to 0.15, where 1 would mean the normal flow velocity is equal to the streamwise flow velocity.

All experiments started with a flat bed, and with a water depth of $0.21\ m$. Experiments were run until both the transverse bed slope and the bedform dimensions were in equilibrium with the flow conditions. We assumed this equilibrium was reached when transverse slope, bedform wavelength and height were stable over time. This was assumed to be the case when

there was no change in bedform morphology, bed level, and number of bedforms present along the length of the channel for at least one hour. Morphology was observed during the experiments with time-lapse photography through the sidewall windows and observed by eye to be consistent within the channel by oblique viewpoints through the sidewall windows. After the experiment ended, the bedform morphology was measured by an echosounder in static flow over ten transects in the streamwise direction spaced 2.34 cm apart. These transects were then converted from a curvilinear grid to a rectilinear grid and interpolated in the cross-stream direction between measured transects where the cell resolution was equal in the x and y directions. Thus, a pseudo-bathymetric map was created of the flume bed to be used in the bedform analysis method detailed below.

3.2.2 Bedform analyses and data reduction

The digital elevation models from the flume experiments were used as input for the bedform analysis tool of Cisneros et al. (In prep). This analysis tool identifies all bedforms along longitudinal transects (Fig. 3.2b) and determines their height and lee-side angle. lee-side angle is determined as the mean angle for all grid cells that are located in a lee side, by calculating the angle between the maximum bed level differences with neighboring cells, and choosing only cells whose dip directions are within the boundaries of a user-defined looking angle centered around the average flow direction. This is therefore different than the classic method to only calculate lee-side angles along one transect in the longitudinal direction, since it takes three-dimensionality of a lee side into account by measuring the steepest sloping lee side in each transect even if the dip of the lee side is oblique to the transect line. As a result, the output of the bedform analysis tool is a large data set with the height and wavelength of all bedforms encountered along all transects of the digital elevation model, and the lee-side angles of each bedform identified.

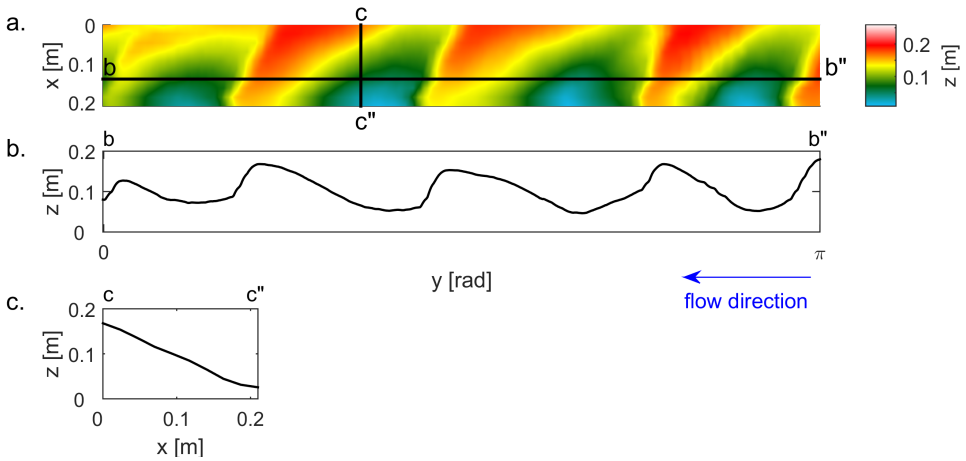

Figure 3.2: (a) Example map of bed elevation above the flume floor (color scale) of an experiment with dunes (Fig. 3.3a.). (b) Longitudinal profile (b - b″) along the horizontal black line in (a). (c) Transverse profile (c - c″) along the vertical black line in (a).

Since the objective of the present study is to compare characteristic bedform dimensions and lee-side angles to the average transverse slope and secondary flow intensity, all these data points needed to be reduced to one characteristic value of each experiment. First, the dataset was filtered for angles that were caused by the transverse slopes instead of dune lee-side angles by comparing the slope distributions of the transverse slope and the slope distribution of the dune lee sides. Then, for each experiment the most abundant combination of dune height and lee-side angle was determined by identifying hotspots in a 2D histogram (Fig. 3.4), and these values were selected as the characteristic height and angle for that experiment. Two experiments resulted in unrealistic results, with lee-side angles higher than the angle of repose, which was caused by a bad interpolation between the echosounder transects to a bathymetric map resulting in very high slopes along the edges of the bathymetric map that were impossible to filter out. These results were ignored in further analyses. Furthermore, the results of the experiments with no bottom rotation were also excluded, since the analytical model that calculates flow velocities (and thus the sediment mobility) was less accurate and did not match the flow velocity measurements via the Vectrino-II in these conditions (Baar et al., 2018).

To compare the characteristic dune dimensions and lee-side angle with the corresponding transverse slope and secondary flow intensity, the slope factor (B) as defined in Baar et al. (2018) is used to define the balance between downslope transverse sediment transport under the influence of gravity and the upslope sediment transport by secondary flow:

$$\frac{\partial z_b}{\partial y} = B\frac{u_n}{u_s} \tag{3.2}$$

where $\frac{\partial z_b}{\partial y}$ = the transverse slope [m/m], u = magnitude of the flow velocity $[m/s]$ in transverse direction (n) and streamwise direction (s). Consequently, by comparing the trend in slope factor with changing sediment mobility, the effect of varying bedform dimensions on transverse sediment transport under the same flow conditions can be compared. The conditions of all experiments and resulting slope and characteristic bedform dimensions are given as supporting information.

3.3 Results

3.3.1 General bedform morphology

In experiments with coarse sand and fine gravel, bedforms developed (Fig. 3.2, Fig. 3.3a) ranging from very low and long sheets of sediment in the lower stage plane bed regime to high dunes that occupied a large portion of the water depth. In experiments with fine sands, bedforms developed ranging from ripples to dunes, and an upper stage plane bed at very high sediment mobilities (Fig. 3.3b). When dunes were present in the fine sediment, with increasing sediment mobility first ripples were present on both the stoss and the lee side of the dune (Fig. 3.3c). Then, dunes developed with ripples only on the stoss side and with a relatively low dune height compared to ripple height. Last, dunes increased in height and were significantly larger than the ripples on the stoss side. Histograms of all lee-side angles and corresponding bedform height show that an experiment with ripples had very consistent

Figure 3.3: Examples of the different bedform types in coarse (a) and fine (b) sediment. (c) Three different types of dunes with superimposed ripples. Dunes had either ripples on stoss and lee side, or only on the stoss side. A dune is ripple dominated when dunes are relatively low compared to ripple height, and as a result ripples influence the lee-side angle. When dunes are relatively high compared to ripple height, ripples have no significant influence on the lee side, and the experiment is therefore dune dominated.

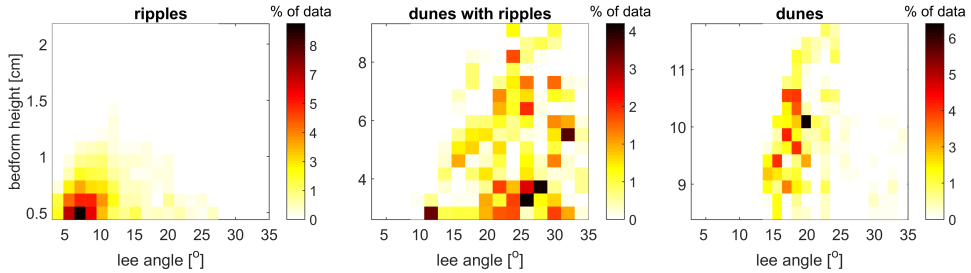

Figure 3.4: Examples of histograms with bedform height [cm] against lee-side angle [degrees] for experiments with three different types of bedforms. Note the bedforms scales for ripples are $\sim \frac{1}{40}$ flow depth whereas dunes range between $\frac{1}{6} - \frac{1}{2}$ flow depth. The scales of bedforms are distinctly different and thus represent flume scale equivalents of respective bedform types. The color indicates the percentage of the data where darker colors mean more abundant combinations of dune height and lee-side angle. Note: bedform height axis changes between plots.

lee-side angles and bedform height over the entire flume (Fig. 3.4). Experiments with dunes show more scatter, but there is still clearly a characteristic lee-side angle and bedform height. In contrast, dunes with superimposed ripples can have multiple hotspots. In experiments with ripples or a plane bed (USPB and LSPB), the transverse slope was uniform along the flume. In experiments with dunes, the transverse slope was steep in dune troughs (Fig. 3.2c), and nearly horizontal on dune crests. Furthermore, most dune crests were aligned obliquely to the main flow direction (Fig. 3.2a), varying between 1 and 89 degrees, where zero is defined as perpendicular to the flow. An oblique dune crest led to lee sides that were directed towards the inner bend. The orientation of the dune crests showed no relation with secondary flow velocity or transverse slope (Fig. 3.5a).

Different bedform types were previously identified as the reason for different trends in equilibrium transverse slope between experiments with the coarser and finer sediments under the same flow conditions (Baar et al., 2018). Figure 3.6 shows the trend in slope factor, i.e. the equilibrium between transverse slope and secondary flow, with increasing sediment mobility for all bedform types. Here, we observed a peak in slope factor at intermediate sediment mobility, which coincides with relatively low and long sheets of sediment in the lower stage plane bed regime, while fine-sand experiments with ripples show low slope factors at the same mobility. To understand the influence of grain size and the difference in transverse sediment transport between different bedform types, we first investigate the bedform characteristics and their effect on the equilibrium slope of the experiments with coarse sands and fine sands separately.

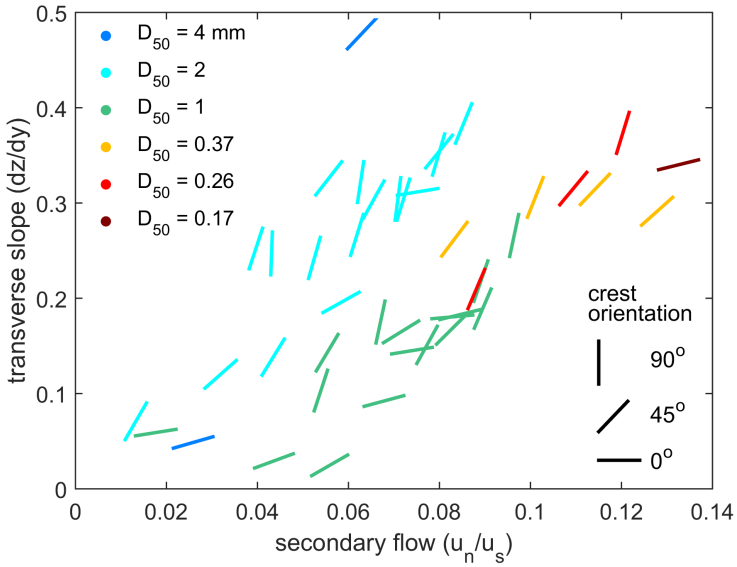

Figure 3.5: Average transverse slope (dz/dy) against secondary flow intensity (u_n/u_s) for all experiments with dunes, where the orientation of the lines represents the median crest orientation in the experiment. Color indicates grain size.

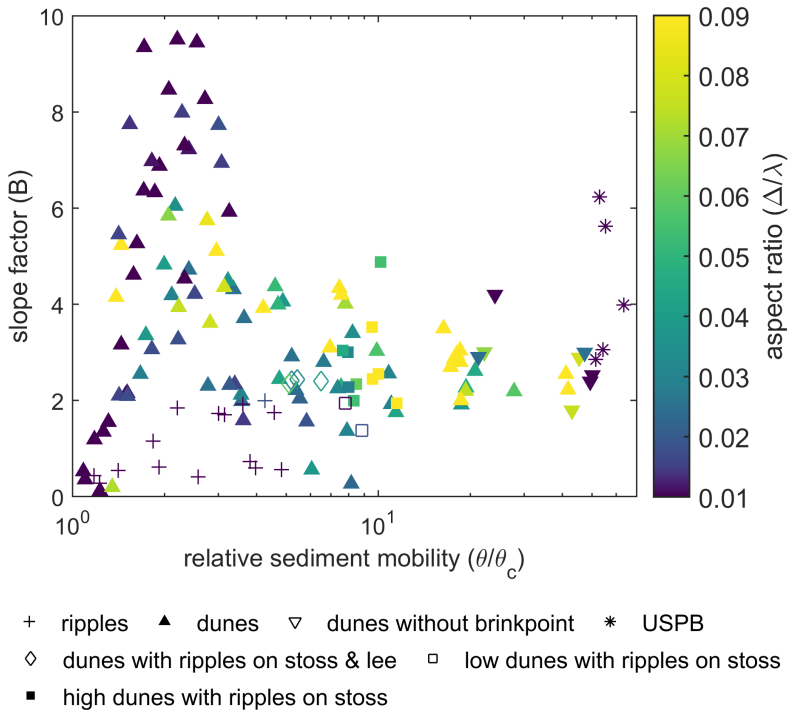

Figure 3.6: Slope factor (B) of all experiments against relative sediment mobility (θ/θ_c). The slope factor is defined as the average transverse slope divided by the secondary flow intensity. Symbols represents bedform type and colors represent bedform aspect ratio.

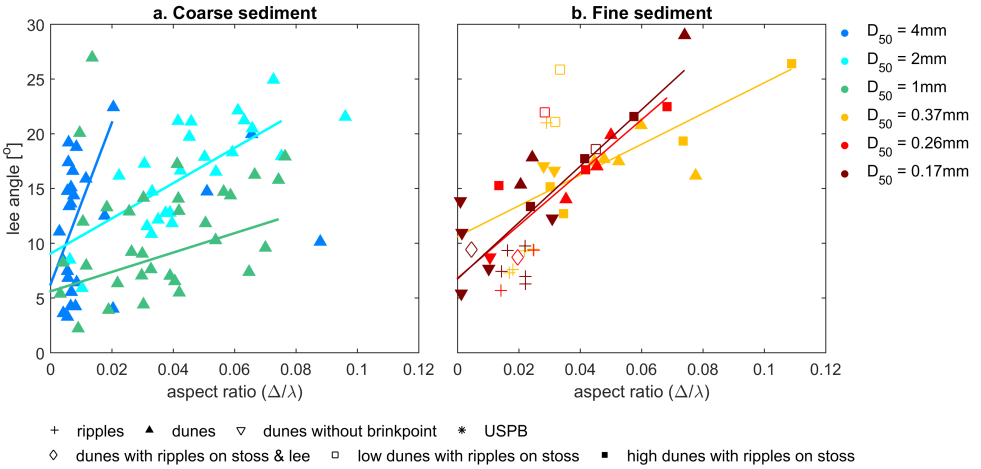

Figure 3.7: lee-side angle against bedform aspect ratio (Δ/λ) for (a) all experiments with coarse sediment and (b) all experiments with fine sediment. Colors represent grain size and symbols indicate bedform type. The lines represent a linear interpolation through all data of the same grain size to show whether trends differ (coarse sediment) or align (fine sediment).

3.3.2 Coarse sediment

Dune dimensions in coarse sand and fine gravel show increasing lee-side angles with increasing aspect ratios for grain sizes of 1 *mm* and 2 *mm*, where aspect ratio is defined as bedform height divided by bedform length (Fig. 3.7a). However, dunes with 2 *mm* size grains have higher lee-side angles than those with 1 *mm* size grains with the same aspect ratio. In contrast, the experiments with 4 *mm* size grains generated dunes with low aspect ratios, notably dune lengths were a hundred times longer than their height and have no relation with lee-side angle. These dunes behave more like sheets of sediment than dunes and appear to be more in the stability space of a lower stage plane bed (Leeder, 1980). These bedforms with very low aspect ratios are the cause of the peak in slope factors at intermediate sediment mobilities as seen in Fig. 3.6, and since they occupy a space in the stability diagram outside of the interest in this paper, bedforms with aspect ratios lower than 0.01 are ignored in further analyses.

The increase in transverse slope with increasing secondary flow intensity also differs with grain size, since the experiments with a median grain size of 2 *mm* show larger transverse slope than the experiments with 1 *mm* at the same secondary flow intensity (Fig. 3.8a). Furthermore, Figure 3.8c shows that lee-side angles are more dependent on the transverse slope than on average secondary flow since high lee-side angles only occur at high transverse slopes, but at a larger range of secondary flow intensity. As a result, higher lee-side angles in coarse sediment are related to higher slope factors, meaning that there is less sediment transport downslope in the transverse direction than in experiments with lower lee-side angles (Fig. 3.9a). This trend is independent of sediment mobility since high lee-side angles occur at any sediment mobility.

3.3.3 Fine sediment

The trend in lee-side angle against bedform aspect ratio in the experiments with fine sands is independent of grain size (Fig. 3.7b), unlike the experiments with coarse sand and fine gravel. However, in these experiments, this relation shows a different behavior for different bedform types. Experiments with ripples or dunes follow the same trend as the coarser sediments and show an increase in lee-side angle with an increasing aspect ratio. Dunes with superimposed ripples show three different types of behavior. Firstly, dunes with ripples on stoss and lee side have a low aspect ratio and low lee angle due to the ripples that are also present at that lee side. Secondly, dunes with ripples only on the stoss side and with a relatively low dune height compared to ripple height show a constant aspect ratio, but the existence of the superimposed ripples steepen the lee side. Dunes with ripples only on the stoss side with a relatively large dune height show the same trend as the experiments with dunes without superimposed ripples. Dunes that were observed not to have a brinkpoint (Fig 3.3b) show a low aspect ratio, since the dunes are flattened at high sediment mobility, but can still show relatively steep lee-side angles, which are remnants of dunes. Experiments with an upper stage plane bed did not show a bedform length and thus a relationship of aspect ratio cannot be made with this data.

The increase in transverse slope with increasing secondary flow is linear and is independent of grain size because the curves overlap (Fig. 3.8b). Moreover, the difference in bed form types seems to have no effect on this trend, which is underlined by the experiments with an

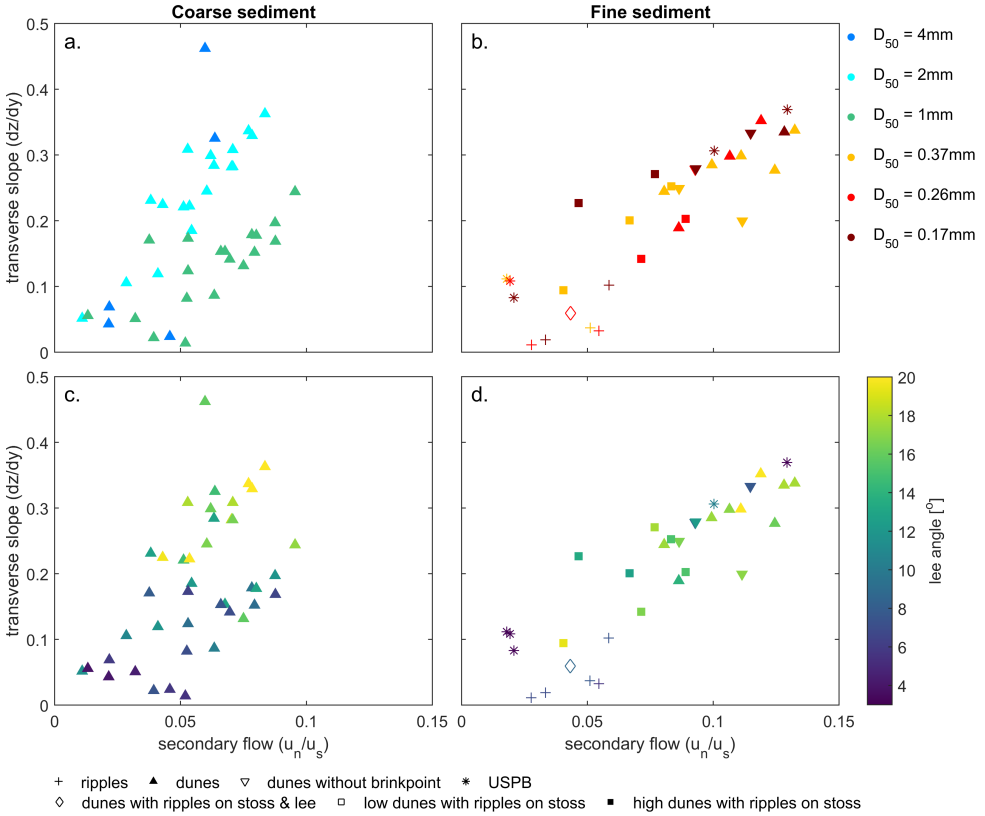

Figure 3.8: Average transverse slope (dz/dy) against characteristic secondary flow intensity (u_n/u_s). Panels on the left show experiments with coarse sediment and an aspect ratio higher than 0.01. Panels on the right represent all experiments with fine sediments. Colors either represent grain size (a,b), or lee-side angle (c,d).

upper stage plane bed that follow the same trend. In further analyses, the experiments with an upper stage plane bed are left out for the same reasons as the lower plane bed in the coarse sediment experiments. Fig. 3.8d shows that lee-side angles seem independent or only weakly dependent on slope or secondary flow. As a result, dunes and dunes without a brinkpoint show the same equilibrium between transverse slope and secondary flow, independent of lee-side angle and sediment mobility (Fig. 3.9b). Dunes with superimposed ripples show a larger variation in slope factor, but this is also unrelated to lee-side angle.

3.4 Discussion

3.4.1 Feedback between bedform morphology and equilibrium transverse slope

The experiments showed that there is a distinct difference in interaction between bedforms, bend flow and equilibrium transverse slope between experiments with fine sand and with coarse sand and fine gravel. Experiments with coarse sediment showed that an increase in

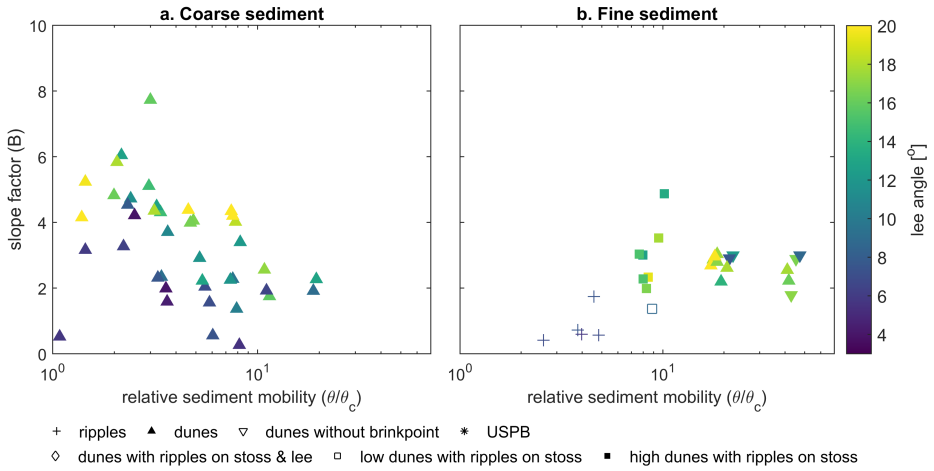

Figure 3.9: Slope factor (B) against relative sediment mobility (θ/θ_c), for (a) experiments with coarse sediment and a characteristic aspect ratio higher than 0.01, and (b) experiments with fine sediment, excluding experiments with an upper stage plane bed. The slope factor is defined as the transverse slope divided by the secondary flow intensity. Colors represent lee-side angles.

median grain size resulted in an increase in lee-side angle for dunes with equal aspect ratios (Fig. 3.7a). Transverse slopes were steeper in experiments with increased lee-side angles (Fig. 3.8c), which we assume is the result of the enhancement of secondary flow in the dune troughs. Recirculating flow within the zone of flow separation was steered towards the inner bend (see Movie S1 in supporting information for an example), as was also qualitatively observed by Kisling-Moller (1993). Steeper lee-side angles will result in stronger intensity and larger size flow separation zones (Lefebvre and Winter, 2016), and this thereby controls the enhancement of secondary flow in the dune troughs. Therefore, transverse slopes were higher with increasing grain size for experiments with equal average secondary flow intensity, and consequently resulted in higher slope factors. Furthermore, lee-side angles were independent of sediment mobility, since the same trend was observed at any sediment mobility (Fig. 3.9). Finally, previous literature suggested that the orientation of a bedform crest is expected to influence flow patterns (e.g. Dietrich and Smith, 1984; Kisling-Moller, 1993; Hasbo, 1995; Parsons et al., 2005), but crest orientation showed no relation with secondary flow, transverse slope or bedform morphology in the experiments, but instead is likely to depend on interactions between bedforms within the experiment by local increases in crest-to-crest distance via dune kinematics (Reesink et al., 2018).

In experiments with fine sediment, there was no feedback between bedform morphology and the equilibrium between secondary flow and transverse slope, since this equilibrium shows a linear relation independent of bedform characteristics or grain size (Fig. 3.8b,d). In contrast to the coarse sediment experiments, lee-side angle was independent of grain size, but depended on the presence and interaction of different bedform scales (Fig. 3.7b). For dunes, ripples, and relatively large dunes with ripples only on the stoss side, lee-side angle showed the same increase with increase in aspect ratio as in the experiments with coarse se-

diment. Relatively small dunes with ripples did not follow this trend due to the influence of these superimposed ripples. In this case, the dunes and ripples co-exist and have feedbacks in their effects towards each other. Ripples are present and migrate within the boundary layer of the larger dune (Smith and McLean, 1977). However, the ripples also have their own flow dynamics and have a faster migration than the larger dune (Raudkivi and Witte, 1990; Venditti et al., 2005), and thus can modify the morphology of the larger dunes (Allen and Collinson, 1974). As a result, relatively small dunes with ripples only on the stoss side were observed to show a cyclic behavior in steepening lee-side angle similar to previous work of Reesink and Bridge (2007). First, ripples locally build up the dune near the crest and steepened the lee side. Then, when the lee side passed the angle of repose, sediment of the ripple avalanched down the lee of the dune, before the next ripple started steepening the lee again (see Movie S3 in the supporting information). This cyclic, and process-based behavior is captured in Figure 3.4: 'dunes with ripples' as there are multiple 'hotspots' in this 2D histogram plot which likely represent dunes at different stages of this cycle at this snapshot in time. When ripples were also present on the lee side, i.e. at lower sediment mobility, they lowered the lee-side angle and bedform height. In this case, the ripples are the dominant bedform and have a much faster celerity than the larger bedform. In contrast, when ripples are relatively low compared to dune height, they barely interact and therefore the trend in increase in lee-side angles with increasing bedform aspect ratio show the same trend as normal dunes. Interestingly, we note these multi-scale bedforms were stable over time, rather than transitional, as this data was taken at least one hour after equilibrium was reached.

It is unknown how median grain size influences the lee-side angle in coarse sediments, and possible explanations could relate to saltation lengths, sediment porosity or the angularity of the sediment. Theoretically, saltation length increases with smaller grain sizes (Bridge, 1992), and therefore grains could travel a longer distance over the dune crest, resulting in lower lee-side angles - this is known as sediment bypassing (Reesink et al., 2018). However, differences in saltation length were not measured, and existing saltation length predictors only depend on grain size and sediment mobility, therefore it is impossible to establish a causal relation with lee-side angle in the current experiments. Furthermore, sediment porosity, which was presumably higher for the coarser sediments and could therefore dissipate energy by water flowing through grains (hyporheic flow) is reported by Blois et al. (2014) to cause a decrease in pressure difference in the lee of gravel dunes, which prevents lee side scour just above the entrainment threshold. As a result, gravel dunes are low, two-dimensional, and have an irregular wavelength at initial formation, which could therefore also explain the formation of the very low and long sheets we observed at low sediment mobility during the 4 *mm* experiments (Dinehart, 1992; Carling, 1999). Another explanation could be differences in angularity of the sediment, which influences the angle of repose, although the angle of repose for sand is around 30 degrees (Coulomb friction theory) and angularity is thought to increase this angle due to interlocking of grains (Carrigy, 1970).

3.4.2 Implications for friction and sediment transport in natural river bends

From the coarse sediment experiments in the rotating annular flume, it follows that lee-side angle is the main bedform characteristic that influences the flow and consequently trans-

verse slope in river bends. In straight river reaches, previous studies related lee-side angle to form drag, since lee-side angles determine the strength of flow separation behind the bedform crest (Lefebvre and Winter, 2016; Kwoll et al., 2017). According to Lefebvre and Winter (2016), permanent flow separation starts to develop for angles between 11 and 18 degrees, which in general also summarizes the current experiments, since experiments with lee-side angles higher than 11 degrees showed higher slope factors and thus steeper transverse slopes (Fig. 3.10). In bends, friction is already increased compared to straight sections due to the secondary flow and curvature-induced increase in turbulence (Leopold, 1960; Blanckaert and de Vriend, 2003). Rivers with coarse sand will most likely experience an additional increase in friction due to the interaction between lee-side angle, flow and transverse slope. However, lee-side angles also steepened in fine sands when dunes are present which coincided with steeper transverse slopes, meaning roughness is expected to increase in all bends with dunes compared to straight reaches.

These findings furthermore have implications for sediment transport in natural river bends. In the case of coarse sand, the coarser the sediment, the more interaction there is between the dunes and the flow because of steeper lee-side angles associated with coarse sediment. This will result in steeper slopes towards the inner bend compared to bends with fine sand, and therefore more erosion in the outer bend. On the other hand, bedforms in fine sands

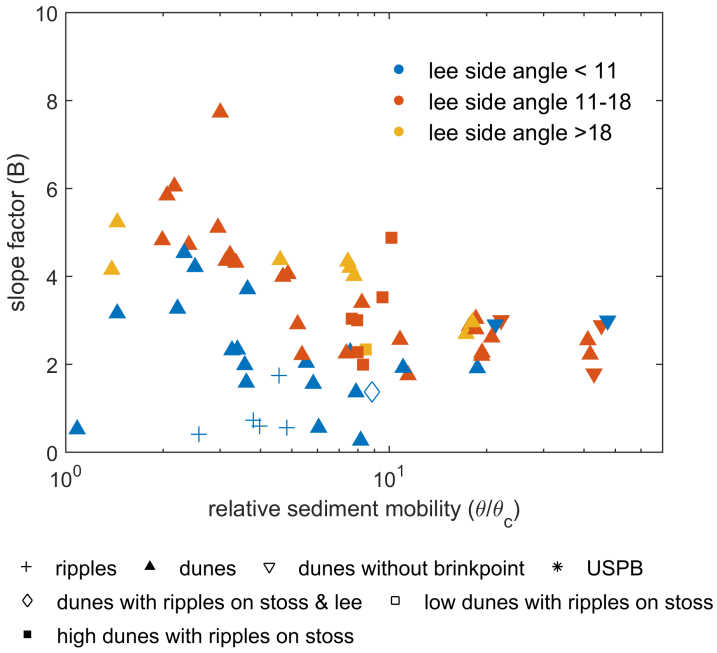

Figure 3.10: Slope factor (B) against relative sediment mobility (θ/θ_c) for both coarse and fine sediment experiments, where the color indicates the range of lee-side angles [degrees]. Theoretically, permanent flow separation starts to develop between 11 and 18 degrees(e.g. Lefebvre and Winter, 2016).

showed no direct interaction with the flow and show less steep transverse slopes for intermediate sediment mobilities. Bedforms are very mobile and occupy the entire river width and only locally influence flow dynamics near the bed. The predictor of Talmon et al. (1995) for the deflection of sediment transport on transverse slope includes relative dune height, but this should be extended by a distinction between fine and coarse sediment as a first step to account for the different bedforms as the morphology of these bedforms could exhibit different flow behavior.

In the current experiments, bedforms are relatively large compared to the water depth (up to $\frac{1}{2}$ of the water depth) and dunes in natural rivers. Talmon et al. (1995) showed that the equilibrium between downslope sediment transport and secondary flow is twice as large in experiments than natural rivers, due to the relatively high bedforms. Furthermore, recent work has observed that dunes with lee sides less than 15 degrees (low angle dunes) are common in natural large rivers (e.g. Roden, 1998; Kostaschuk and Villard, 1996). As flow separation is only permanent for lee sides greater than 10 degrees and not fully developed until lee-side angle is greater than 24 degrees (Lefebvre and Winter, 2016), the possible lack of flow separation in low angle dunes may not create the same enhancement of bend flow as in the experiments. These differences in height and possible lee-side angles imply the relative influence by bedforms on the flow and sediment transport in natural rivers could also be significantly lower than in experiments. However, it is unclear if lee-side angles are also generally lower in bends as these field observations were analyzed for straight reaches (Kostaschuk and Villard, 1996; Lefebvre and Winter, 2016; Roden, 1998). An interesting study would be to compare the effect of bends on natural dune morphology similar to the current analysis. Furthermore, the experimental dune height ranged from $\frac{1}{20}$ to $\frac{1}{2}$ of the water depth, yet the same increase in transverse slope with increasing lee-side angle is observed for any dune height. This suggests the trend would also hold for natural river bends.

3.5 Conclusions

We experimentally determined the interaction between bedform morphology, secondary flow and transverse slope in a rotating annular flume, using a large range in near-bed flow conditions and covering all bed states. We found there is a significant difference in interaction between flow conditions and bedforms in fine and coarse sand, due to the different bedform types that develop. Coarse sediment ($D_{50} > 0.7\ mm$) showed a direct relation between grain size-dependent dune lee-side angle and transverse slope, since sufficiently high lee-side angles theoretically result in permanent flow separation that enhances secondary flow in the dune troughs. In experiments with fine sediments ($D_{50} < 0.7\ mm$), different bedforms developed, ranging from ripples, dunes with superimposed ripples, dunes, to an upper stage plane bed. These bedforms showed no direct interaction with the secondary flow, and lee-side angles mainly depended on bedform type instead of grain size and bedform aspect ratio. As a result, transverse slopes in fine sediment did not depend on bedform morphology but rather the presence and interactions between bedform scales, in contrast to the coarse sediment experiments. These findings imply that form roughness will increase in bends with dunes in coarse sand compared to straight river reaches. Furthermore, in rivers

with coarse sand this will result in steeper transverse slopes and more erosion in the outer bend, due to the interaction with the bend flow. Future work should focus on studying the effect of bends on natural river dune morphology, specifically focusing on dune lee-side angles. Furthermore, for modelling purposes, predictors for the deflection of sediment transport on transverse slopes should be grain size dependent.

Acknowledgements

This work is part of the Ph.D. research of AWB and JC. AWB is partly supported by Deltares and by the Dutch Technology Foundation (STW) of the Netherlands Organization for Scientific Research (NWO) (grant Vici 016.140.316/13710 to Maarten Kleinhans). JC is supported by National Science Foundation Graduate Research Fellowship (NSF GRF). This material is based upon work supported by the National Science Foundation Graduate Research Fellowship under Grant No. DGE - 1746047. Any opinion, findings, and conclusions or recommendations expressed in this material are those of the author(s) and do not necessarily reflect the views of the National Science Foundation. Supporting data are included in Appendix E.

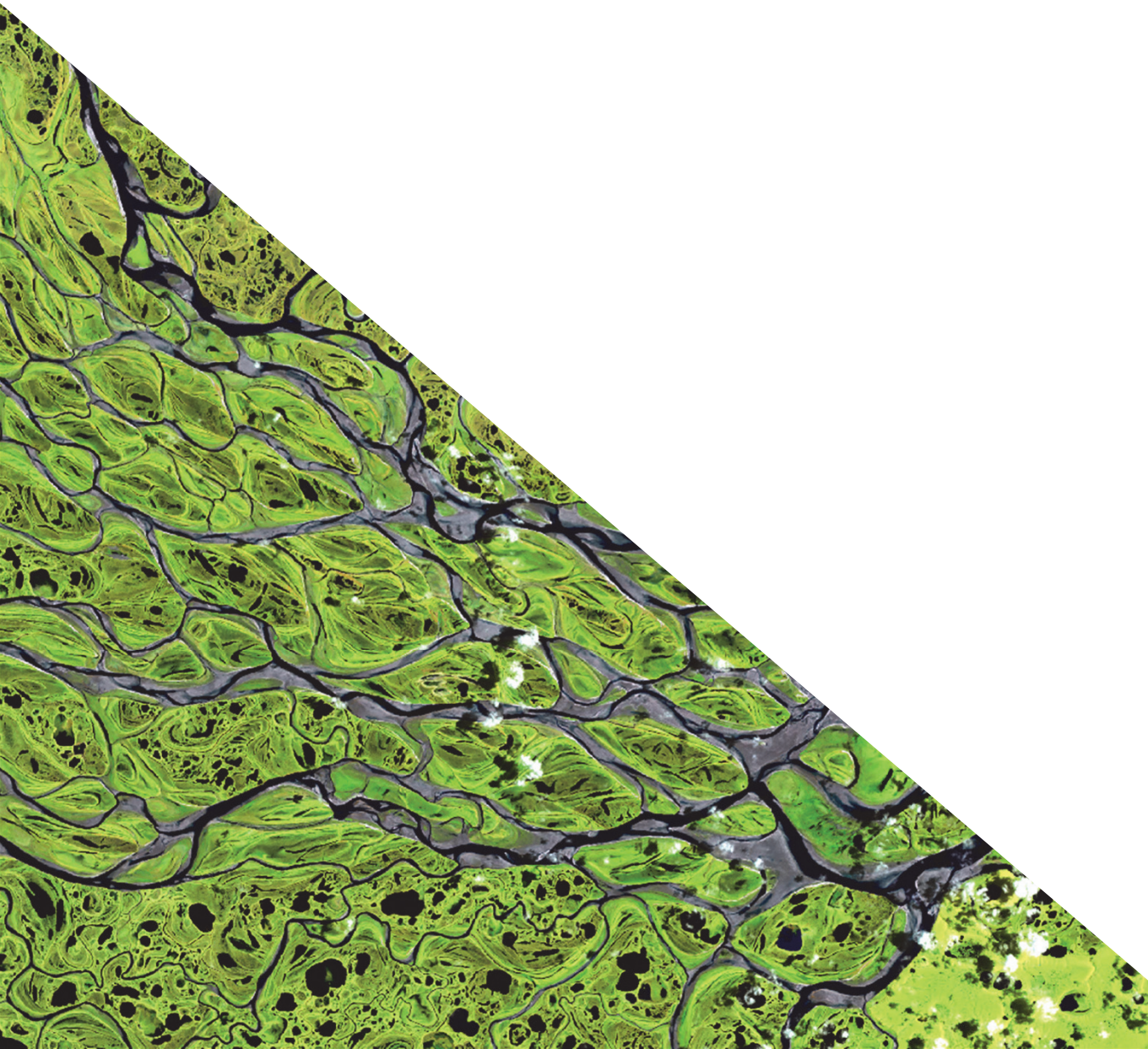

Chapter 4

Interaction between lateral sorting in river bends and vertical sorting in dunes

Sediment is sorted in river bends under the influence of gravity that pulls the heavier grains downslope and secondary flow that drags the finer grains upslope. Furthermore, when dunes are present, sediment is also sorted vertically by grain size dependent deposition at the dune lee side. However, sorting functions in morphodynamic models are poorly defined, as relation to transverse slope and the interaction between lateral and vertical sorting is not yet understood for lack of data under controlled conditions. The objective of this study is to gain understanding of the interaction between lateral and vertical sorting in river bends. To this end, we conducted experiments with a sediment mixture in a rotating annular flume in which secondary flow intensity can be controlled separately from the main flow velocity, and therefore transverse slope towards the inner bend and dune dimensions can be systematically varied. We sampled along cross-sections at the surface of dune troughs and dune crests, and over the entire depth at the location of dune crests (bulk samples), which allowed us to compare the relative contribution of vertical sorting by dunes to lateral sorting by the transverse slope. The data show that lateral sorting is always the dominant mechanism, and bulk samples showed minor effects of vertical mixing by dunes as long as all grain size fractions are mobile. We fitted an empirical bend sorting model that redistributes the available sediment fractions over the cross-section as a function of transverse slope. Comparison with field data showed that the model accurately reproduces spatially-averaged trends in bend sorting in single-thread channels. The implication for numerical modelling is that bend sorting mechanisms can be modelled independently of dunes, allowing application of the active layer concept.

Based on: Baar, A. W., Weisscher, S. A. H., Kleinhans, M.G. (2018), Interaction between lateral sorting in river bends and vertical sorting in dunes, *Submitted to:* Sedimentology

4.1 Introduction

Sediment sorting patterns in curved river channels arise from grain size-dependent interactions between sediment transport processes and local secondary flow patterns. The morphology of river bends is mainly the result of helical flow that is directed inward near the bed and drags sediment upslope on the point bar, which is balanced by the transverse bed slope effect deflecting grains downslope towards the outer bend under the influence of gravity (e.g. Engelund, 1974; Struiksma et al., 1985). Here, the imbalance between flow drag, depending on particle surface area, and gravity, depending on particle volume and density, leads to size-sorting. Finer particles are gradually dragged higher up the point bar by the secondary currents, while coarser grains are pulled further down by gravity and are deposited near the outer bend (e.g. Parker and Andrews, 1985; Bridge, 2003). This is the same sorting pattern as observed in inclined heterolithic strata (IHS) in meander channel belt deposits (Thomas et al., 1987). These sorting patterns are important for a range of processes. For example, grain size differences influence the flow by determining the distribution of friction, the sediment transport rate and maximum scour depth through mobility, and the morphology by determining the distribution of sediment over bifurcations when lateral slopes are present upstream of a bifurcation (Kleinhans, 2001; Mosselman et al., 1999; Frings, 2008). While quite relevant for river bends with shipping fairways and in river bifurcations with a bend just upstream (Frings, 2008), most current morphodynamic models do not include physics-based relations for sediment sorting.

Sediment is actively sorted during transport, both laterally and vertically. Lateral sorting results from differences in interaction between shear stress and gravity on different grain sizes. During transport, shear stress exerts drag as a function of the exposed surface area of particles, while gravity acts on particle weight as a function of volume and density. Therefore, larger grain sizes are subject to a relatively larger pull of gravity than of flow shear, while finer particles are more easily dragged along by the flow (Ikeda, 1989). Given an upslope-directed flow component forced by channel curvature, this leads to the classic bend sorting pattern with fine sediment in the inner bend and coarse sediment in the outer bend. This sorting becomes more pronounced when the standard deviation of the supplied sediment mixture is larger (Parker and Andrews, 1985). Active vertical sorting is the result of dunes that mix the sediment vertically, by grain size dependent deposition of particles that are transported over the lee side (Kleinhans, 2001; Blom and Parker, 2004). Coarser particles are deposited further downslope the lee side, which results in upward fining and possibly in the formation of coarse bed layers beneath dunes when not all fractions are mobile (Kleinhans et al., 2007; Frings, 2008). The degree of vertical sorting depends mainly on the standard deviation of the sediment mixture (Blom and Parker, 2004; Kleinhans, 2005). Therefore, it is expected that larger bedforms at higher flow velocities have relatively larger influence on bend sorting. Additionally, large bedforms possibly influence secondary flow patterns through their troughs (Dietrich and Smith, 1984; Kisling-Moller, 1993), which would influence the lateral sediment distribution.

Several analytical and empirical relationships to describe lateral bend sorting exist. Analytical solutions focus on lateral forces on individual sediment particles for active sorting

during transport (Bridge and Jarvis, 1982; Parker and Andrews, 1985; Ikeda, 1989) or on differences in critical shear stress of individual grains (Odgaard, 1981). However, these equations were never directly incorporated in morphodynamic models. Ikeda et al. (1987) and Yen and Lee (1995) conducted few experiments with a coarsely skewed mixture and developed an empirical relation that describes the change in median grain size over a cross-section along the bend radius, instead of considering grain size distributions. However, these experiments were conducted in a flume with a fixed curvature, and therefore the effect of changing transverse slope was not directly quantified. Furthermore, both their experiments ignored the effect of bedforms and suffered from hiding exposure effects due to the large skewness of the sediment mixture. Moreover, these relations describe the effect of transverse slopes on sediment sorting, but it is unknown how sorting influences the magnitude of the slope itself. In conclusion, these analytical and empirical relations are not yet suitable to include in spatial models.

Horizontal and vertical sorting and their interaction are poorly constrained in morphodynamic models. However, their relative importance and characteristic timescales determine both the degree of sorting and the degree of morphological change. Horizontal sorting on the large scale is approached with the active layer concept (Parker et al., 2000; Blom et al., 2008), which divides the bed in one active layer and immobile underlayers. Only the active top layer interacts with the flow and determines the amount of sediment transport, and there is only an exchange of sediment between the underlayers and the active layer in case of erosion or deposition. Therefore, the active layer determines the volume of each fraction that is available for sediment transport and consequently lateral sorting. As a result, spatial sorting and bed level changes are extremely sensitive to the user-defined thickness of this active layer, which sets the timescale of changes in bed composition. When the layer is relatively thin, sorting reacts fast to changes in the flow and will result in better developed sorting patterns. On the other hand, a relatively thick active layer results in slower adjustments, and therefore sediment sorting acts on the same time scale as morphological development (Sloff and Mosselman, 2007; Kleinhans, 2010).

Lateral sorting therefore depends on the sediment that is available in the top layer of morphodynamic models, and is incorporated in the transverse slope predictor. This predictor adjusts the direction of sediment transport of specific grain sizes based on the bed slope. However, sediment deflection on slopes in general is poorly defined in morphodynamic models (e.g. van der Wegen and Roelvink, 2012; Schuurman et al., 2013; Baar et al., 2018) and grain sorting due to lateral gradients is even more simplified. Vertical sorting by dunes is not included in the active layer concept. However, the thickness of the layer is often based on characteristic bedform height to simulate sorting processes on a time scale of multiple dunes migrating over the river reach. Therefore, to be able to accurately model average lateral sorting, it is necessary to know the relative importance of vertical sorting on lateral sorting on the time scale that is modelled.

The objective of this study is to experimentally determine this relative importance of lateral sorting in river bends and vertical sorting by dunes. To this end, we conducted experiments with poorly sorted sediment in a rotating annular flume, in which the transverse slope and dune dimensions can be systematically varied (Baar et al., 2018). As a result, we describe

bend sorting as an empirical function of grain size fractions and transverse slope, and we determine the relative influence of bedforms on these sorting patterns. Additionally, we analyze the feedback of sediment sorting on the transverse slope, by comparing transverse slopes to experimental results with uniform sediment in the same flume. Finally, we compared the resulting bend sorting model with published field data.

4.2 Methods

4.2.1 Experimental set-up and data collection

We conducted experiments in a rotating annular flume (Fig 4.1a), which allows control of secondary flow intensity separately from the main flow velocity (Booij, 2003; Baar et al., 2018). Both the lid and the floor of the flume can rotate separately over a continuous range of rotation velocities in both directions. Rotation of the lid of the flume drives the streamwise flow by applying shear on top of the water column, and drives the secondary flow by generating an outward directed centrifugal force. This centrifugal force causes a pressure difference between the inner and outer bend, which results in an inward directed bed shear stress near the bed, similar to the flow field observed in natural river bends. Rotation of the floor and attached side-walls of the flume adds an additional outward directed centrifugal force near the bed, resulting in a decrease of the pressure difference and thereby a decrease in secondary flow intensity. By varying the rotation velocities of the lid and the floor of the flume, and the ratio between them, the streamwise and normal flow velocity can be isolated and controlled (Fig 4.1a). As a result, different bend radii can be simulated from straight river reaches to very sharp bends, and as a result the transverse slope that develops towards the inner bend can be controlled. Baar et al. (2018) derived an analytical model based on flow velocity measurements describing near-bed streamwise and normal flow velocity as a function of lid and floor rotation and flume dimensions. Furthermore, they describe the relation between secondary flow intensity, i.e. the ratio between streamwise and normal flow velocity, and the transverse slope that develops.

Since the objective of this study is to determine the relative influence of transverse slope and dune dimensions on bend sorting, a series of 28 experiments were conducted with slopes varying between 0 and 0.38 m/m, and sediment mobility varying between $\theta = 0.025 - 0.63$, which determines the dune dimensions (van Rijn, 1984). Here, sediment mobility, i.e. the nondimensional shear stress, is defined as:

$$\theta = \frac{\tau}{(\rho_s - \rho) g D_{50}} \tag{4.1}$$

where τ = shear stress $[N/m^2]$, ρ_s = specific density of the sediment, g = gravitational acceleration $[m/s^2]$ and D_{50} = median grain size $[m]$. Both sediment mobility and transverse slope were varied by systematically changing the ratio of lid and flume rotation, which determines the magnitude of streamwise and transverse slope. These ratios were based on the results of Baar et al. (2018). Different combinations of sediment mobility and transverse slope were used, to study their separate effect on bend sorting. The sediment mixture was chosen such that dunes dominated and ripples were rare and that all sediment fractions were mobile over

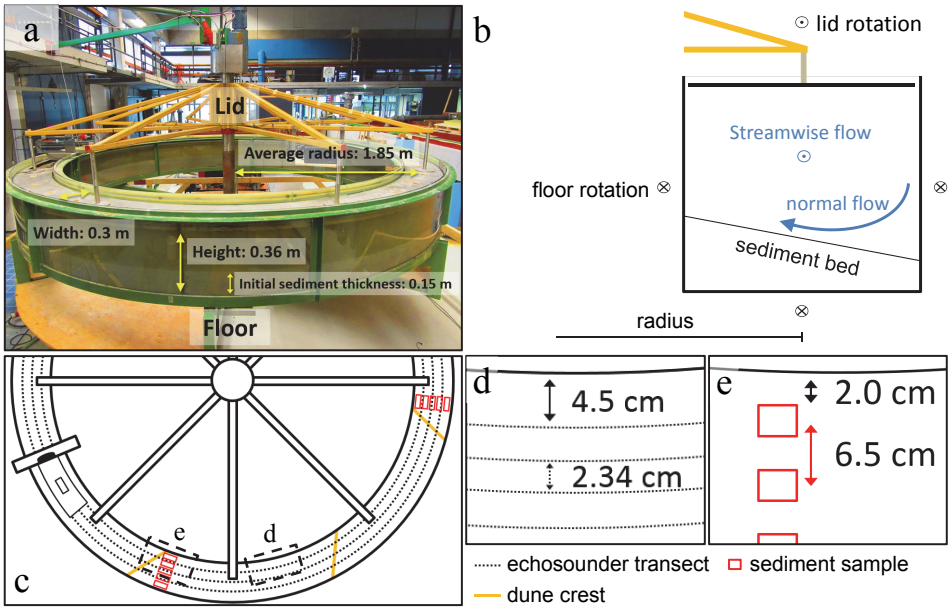

Figure 4.1: Experimental setup. a) The dimensions of the rotating annular flume. The lid rotates independently from the floor and attached side walls. b) Schematic drawing of the flow vectors and rotation directions. The floor and attached side walls rotate in the opposite direction of the lid, which allows control of the centrifugal forces in the flume and thereby the magnitude of the normal flow velocity. c) Schematic top view of the measurement set up, with transects of the echosounder, which measured bed elevation in still water, and the sampling locations of the bulk samples and surface samples on top of the dune crest. d) Ten echosounder transects were measured, each 2.33 cm apart in transverse direction, starting at 4.5 cm from the walls. e) Five sediment samples were taken along a cross-section, with their centers 6.5 cm apart, starting at 2 cm from the wall. 4x5 Samples were taken both at the surface of a dune crest and at the surface of a dune trough, and 5 samples over the entire height of the dune (bulk samples). This resulted in a total of 45 samples per experiment.

a wide range of average mobilities, to avoid selective transport, hiding exposure effects and bed armouring. This resulted in a sediment mixture with a median grain size of 0.78 *mm* and a standard deviation of 0.73 *mm*.

Experiments started with a flat and a well-mixed sediment bed, and with a water depth of 0.21 *m*. Experiments were run until both the transverse bed slope and the bedform dimensions were in equilibrium with the flow conditions. We assumed this equilibrium was reached when transverse slope, bedform length and height were stable over time. Generally, an experiment ran for two to three days. After the experiment ended, the equilibrium morphology was registered by an echosounder in still flow over ten transects in streamwise direction (Fig. 4.1c,d). The bedlevels along each transect were reduced to a median bed level, and the average transverse slope was obtained by fitting a linear trend through these values. To determine if sediment sorting also influences the average transverse slope compared to bends with uniform sediment, the average transverse slopes were compared to experiments with an uniform grain size of 1 *mm* in the same flume (Baar et al., 2018). In order to compare

equilibrium transverse slopes, the average transverse slope of each experiment was divided by the characteristic secondary flow intensity and plotted against sediment mobility. This ratio represents the transverse slope effect (B).

After slowly draining the water, 13 of the 28 experiments were sampled. Samples were taken at the surface of four dune troughs and dune crests, and over the entire depth at the location of dune crests (Fig. 4.1c), which allowed us to compare the relative contribution of dunes to observed bend sorting. At these locations, five samples were taken over the cross-section, with the center of the samples 6.5 cm apart (Fig. 4.1e). As a result, for each experiment there were four samples that were taken at the same relative location at a cross-section and along a dune. These samples were combined to one sample, to get an average value per experiment. The grain size distribution of each sediment sample was determined by sieving in 15 size fractions between 0.16 *mm* and 3.96 *mm* . The volume of each sediment fraction was used as input for the bend sorting model.

4.2.2 Development of bend sorting model

The bend sorting model described in this study is consistent with the dune lee face sorting model of Blom and Parker (2004), which redistributes the available volume of a sediment fraction that is transported over the dune crest over the lee side of that dune, as a function of sediment mobility. As a result, their model describes vertical sorting by bedforms with conservation of mass by size fraction, which is a critical requirement for application in numerical modelling. Our sorting function for lateral sorting redistributes the available volume of a sediment fraction over the cross-section as a function of transverse slope. The imperfectly sorted sediment in the cross-section could then be vertically sorted by the dune sorting model but that is beyond the scope of this paper. The bend sorting model predicts the volume (F) of a specific sediment fraction (i) at a certain location (r) along a transverse slope, relative to the volume of that sediment fraction that is available along the cross-section, which is defined as the reference volume ($F_{i,ref}$). We assume that the logarithm of the relative fraction increases or decreases linearly over the cross-section:

$$Log\left(\frac{F_i}{F_{i,ref}}\right) = \delta_i R_{rel} + \gamma_i \tag{4.2}$$

A schematic representation of the model is visible in figure 4.2.

The reference volume depicts the volume of a sediment fraction that would theoretically be present at each location if the sediment was well-mixed over the cross-section. This volume is therefore defined as the sum of the volume fractions over the cross-section, divided by the number of samples (N) along that cross-section:

$$F_{i,ref} = \frac{\sum_R^N F_i}{N} \tag{4.3}$$

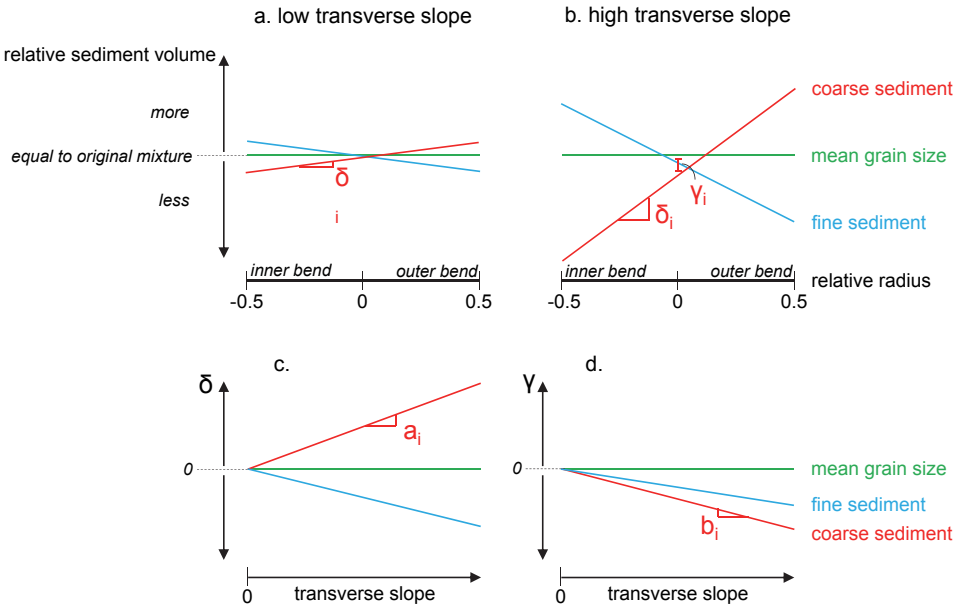

Figure 4.2: Schematic representation of the bend sorting model (Eq. 4.2). a) Theoretical change in relative volume over the cross-section of fractions that are coarser and finer than the median grain size. The volume of coarser sediment increases toward the outer bend due to the pull of gravity, while finer sediment will be transported towards the inner bend by the secondary flow. δ and γ represent the parameters in equations 4.2. b) An increase in transverse slope will cause more pronounced sorting and therefore a larger change in volume of these fractions (δ) over the cross-section, and a larger offset at the channel centerline (γ). The relation of the parameters δ and γ with transverse slope is visible in panel c and d (Eq. 4.5, 4.6).

R_{rel} is the relative location along the cross-section, which is used to make the location non-dimensional and relative to the center of the cross-section:

$$R_{rel} = \frac{R - R_{mean}}{W} \tag{4.4}$$

where R_{mean} is the radius at the centerline of the channel, and W is the width of the cross-section. The width should be measured from the lowest point at the outer bend to the water line at the inner bend, since we assume all sediment fractions present along the cross-section are mobile and available for sorting. Since the location is relative to the center of the flume, this means that when sediment is perfectly linearly sorted over the cross-section of the flume, the volume of a sediment fraction at the centerline is equal to the initial sediment mixture.

The parameter δ_i in Eq. 4.2 determines the change in relative volume over the cross-section, while γ_i denotes the relative volume at the centerline (Fig. 4.2a,b). These parameters depend on slope and grain size, since coarser fractions will be deposited downslope, resulting in an increase in relative volume towards the outer bend and thus a positive δ_i, while finer fractions are mainly deposited at the inner bend, and therefore will have a negative δ_i. A larger slope is expected to result in a larger change in volume of a certain fraction over the cross-section, which results in a larger absolute magnitude of δ_i (Fig. 4.2c). When γ_i is zero,

the volume of a sediment fraction at the centerline is equal to the initial sediment mixture and the sorting is perfectly linear over the cross-section. However, when sorting is more distinct, the offset at the channel centerline is higher and γ_i is will be lower than 0. This offset will therefore also depend on grain size fraction and transverse slope (Fig. 4.2d). A constraint for the model is that when the transverse slope is equal to zero, i.e in a straight river section, fractions are equally distributed over the cross-section, and thus δ_i and γ_i are equal to zero. The resulting definitions are as follows:

$$\delta_i = a_i \frac{\partial z}{\partial y} \tag{4.5}$$

$$\gamma_i = b_i \frac{\partial z}{\partial y} \tag{4.6}$$

where:

$$a_i = c_1 \frac{\psi_{rel}}{\sigma} \tag{4.7}$$

$$b_i = c_2 \left(\frac{\psi_{rel}}{\sigma} \right)^2 \tag{4.8}$$

where σ is the standard deviation of the initial mixture, defined as:

$$\sigma = \sqrt{\sum_i^N \psi_{i,rel}^2 F_{i,ref}} \tag{4.9}$$

Ψ_{rel} is the relative grain size in the Ψ scale, defined as:

$$\psi_{i,rel} = \psi_i - \psi_{mean} \tag{4.10}$$

Which relates to grain size as follows:

$$\psi_{i,rel} =^2 log \left(\frac{D_i}{D_{mean}} \right) \tag{4.11}$$

where D = grain size in mm. In this study, the mean grain size is determined by:

$$\psi_{mean} = \sum_i^N \psi_i F_{i,ref} \tag{4.12}$$

where n = the number of sediment fractions. The relative grain size is divided by the standard deviation to be able to use the sorting function for different sediment mixtures. The Ψ scale is used so that sediment fractions that are finer than the median grain size are negative, and coarser sediment fractions are positive.

The resulting equation for relative volume per sediment fraction at a location along the cross-section then reads:

$$\frac{F_i}{F_{i,ref} \sum_i^N F_i} = exp \left\{ \left[c_1 \frac{\psi_{i,rel}}{\sigma} R_{rel} - c_2 \left(\frac{\psi_{i,rel}}{\sigma} \right)^2 \right] \frac{\partial z}{\partial y} \right\} \tag{4.13}$$

where the parameters c_1 and c_2 are constants that determine the change in volume fraction over the cross-section and offset at the channel centerline, which will be determined with the experimental data. The relative volume of each grain size fraction is divided by the total volume of all fractions, to make sure the sum of all fractions is 1.

4.2.3 Field data

To study natural deviations in the sorting patterns compared to the experimental data, the model is tested against scarce field data that is available in literature. Grain size distributions from three previous studies are used, with different median grain sizes, channel dimensions, and transverse slopes (Table. 4.1).

Firstly, Bridge and Jarvis (1976) studied the flow and sedimentation in the small meandering river South Esk during a discharge peak, from bankfull conditions to low water. They sampled along several cross-sections along the bend, but here we focus on the cross-section at the bend apex, to minimalize possible effects of flow adaptation on sediment transport processes. Here, the transverse slope was 0.1 m/m. During high water dunes were present over the entire cross-section, while during falling discharge these dunes disappeared and ripples started to form near the inner bend and expanded towards the pool at the outer bend.

Secondly, data from a gently curved reach with a transverse slope of 0.06 m/m in the gravel bed river Severn, as described by Hey (1991), is used to test the bend sorting model with larger grain sizes (Table. 4.1). They sampled the bed load transport four times during two months, to study the shear stress distribution over the cross-section with varying discharge. At one occasion, all fractions were mobile over almost the entire cross-section, in contrast to the other three measurement campaigns when only the silt to fine gravel fractions were in transport, and only at the center of the channel. We compared the bend sorting model to all measurement campaigns.

Thirdly, the model was tested on data from the lower Rhine river, a gravel-sand bed river with protected banks, at the bend where the river bifurcates into the Waal river and the Pannerdensch Kanaal. This data was obtained by Guijters et al. (2001), who took samples along a total of 15 cross-sections in all three rivers (also see Kleinhans, 2001). For this study we use the grain size data of the first 40 cm of the bed, along the cross-section just upstream of the bifurcation and along the first cross-section of the Pannerdensch Kanaal just after the bifurcation. This case is extremely relevant for morphodynamic modelling, since this bend upstream of the bifurcation determines the sediment size distribution over the bifurcates. The Waal river is located at the inner bend and therefore receives a larger volume of the finer fractions, while the Pannerdensch Kanaal is located at the outer bend and receives a larger volume of the coarser sediment. However, the bend radius of the upstream bend is relatively large, and therefore transverse slopes are relatively low. The transect in the Rhine has a transverse slope of 0.01 m/m, while the transect just downstream of the bifurcation has a slope of 0.035 m/m.

Table 4.1: Characteristics of field sites and measured sediment distributions found in literature.

	D_{50} [mm]	σ [mm]	W [m]	$\partial z/\partial y$ [m/m]
South Esk	1.36	2.89	7.5	0.1
Severn	63.40	1.88	10	0.05
Rhine	2.25	3.67	280	0.01
Pannerdensch Kanaal	3.67	3.54	70	0.035

4.3 Results

In this section, we first describe the development of the morphology and evaluate the degree of sorting over the cross-section at equilibrium conditions for varying transverse slope and dune height. Then, we use the resulting trend in grain size fractions to calibrate the bend sorting model, and finally compare this model to the field data described in literature.

4.3.1 Observations in the experiments

After the start of experiments developing transverse bed slopes, the outer bend eroded and this eroded sediment was transported by sediment lobes towards the inner bend under the influence of secondary flow. These lobes of sediment extended laterally as they moved towards the inner bend and thereby gradually transformed into dunes. Experiments were run until the dune dimensions were in equilibrium with the flow conditions, which was reached faster in experiments with relatively high sediment mobility. For experiments with low sediment mobility and relatively weak secondary flow, dunes did not expand over the entire cross-section, and instead ripples formed near the inner bend, since here sediment mobility was below the ripple-dune transition (Fig. 4.3b). Dune height increased with increasing sediment mobility, but showed a smaller increase with transverse slopes lower than about 0.1 (Fig. 4.4a).

While these bedforms were forming, a transverse slope developed towards the inner bend, and sorting became more pronounced. Mainly finer sediment was transported in the lobes of sediment over the dune towards the inner bend by the secondary flow (Fig. 4.3a). Relatively coarse sediment rolled downslope under the influence of gravity, and the coarsest fractions remained in the dune troughs. At the end of most experiments a clear sorting pattern could be observed with fine sediments in the inner bend and coarse sediment at the outer bend (Fig. 4.3b). Average transverse slopes showed the same trend with increasing sediment mobility as uniform sediment experiments (Fig. 4.4b).

These sorting patterns caused by transverse slopes and dunes were quantified by the sieve data. The bulk samples taken over the entire depth of the dune show that median grain size is about equal or slightly lower than the original mixture at the channel centerline, and increases rapidly towards the outer bend for transverse slopes larger than 0.15 m/m, while for lower transverse slopes this increase seems more gradual (Fig. 4.5a). A more gradual decrease in median grain size is observed towards the inner bend, and this is less dependent on average transverse slope. Increasing bedform height with equal transverse slopes had no significant effect on the sorting patterns, since the trend in median grain size does not differ significantly (Fig. 4.5b,c,d). However, dunes mainly affected both the D_{10} and D_{90}, which showed a larger variation over the cross-section with varying bed forms heights. Nevertheless, lateral sorting by slope effects is clearly the dominant mechanism, as the general trend related to the transverse slope is always visible.

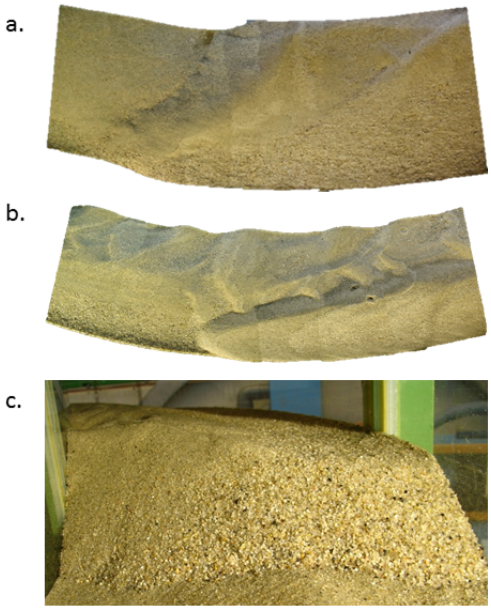

Figure 4.3: Examples of equilibrium morphology and sorting patterns of experiments visible on photomosaics with a) high transverse slope, and b) low transverse slope in combination with low sediment mobility. c) Frontal view on a dune crest and slipface, where coarse sediment is located in the outer bend (right) and fine sediment in the inner bend (left).

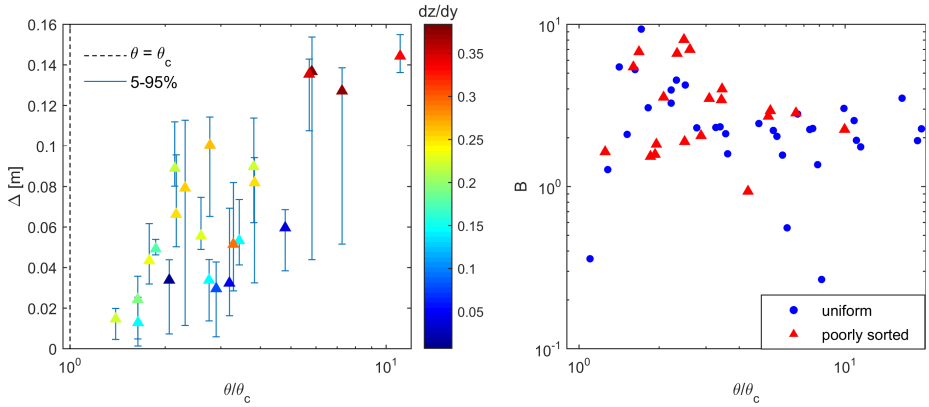

Figure 4.4: a) Average dune height (Δ) of all experiments against relative sediment mobility (θ/θ_c), including the variation in dune height in each experiment. Color scale indicates average transverse slope. b) Slope factor B (transverse slope / secondary flow intensity) against relative sediment mobility, for the experiments in this study with a sediment mixture and experiments with uniform sediment with comparable grain size from Baar et al. (2018).

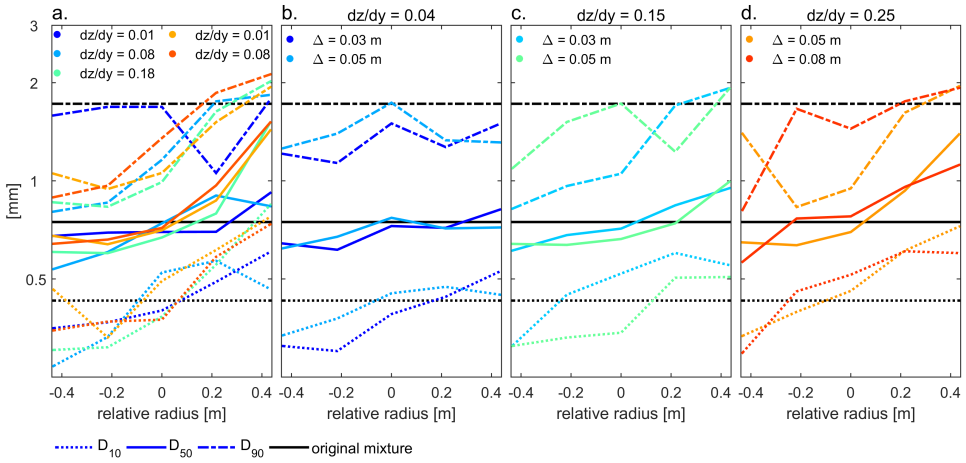

Figure 4.5: Bulk sediment distribution of D_{10}, D_{50}, D_{90} over the entire cross-section of the flume for bulk samples in experiments with varying transverse slope and dune height. Black lines indicate values from the original mixture at the beginning of the experiment. Radius is relative to the center of the flume (0).

Surface samples in dune troughs and on dune crests show in general the same trend in sorting with increasing transverse slope (Fig. 4.6, 4.7). However, samples in dune troughs show the same sharp increase in median grain size towards the outer bend for all transverse slope magnitudes, and also the trend in $D10$ and $D90$ shows a more distinct sorting for low transverse slopes than in the bulk samples. Furthermore, for both trough and crest samples, sorting is even less dependent on dune height with increasing transverse slope, since also the $D10$ and $D90$ show the same trend for experiments with the same transverse slopes but different dune height.

The variation in D_{10} and D_{90} between experiments is caused by small deviations in the most extreme fractions that alter the trend over the cross-section, and also the sharp increase in median grain size towards the outer bend is the results of a couple of coarse grains that are more likely to end up in the outer bend. This shows that the only way to describe and predict bend sorting is by using grain size fractions instead of percentiles.

4.3.2 Testing of bend sorting model on experimental data

The sieving data of the bulk samples were used to calibrate the bend sorting model. Figure 4.8 shows four examples of the relative volumes of the sieved fractions over the cross-section and the fitted linear function through these volumes to determine coefficient δ_i, which is the slope of the fitted function, and γ_i, which is the offset at the center of the channel (Eg. 4.2). For fractions coarser than the median grain size, relative volumes increase towards the outer bend, resulting in positive values for δ_i. On the other hand, fractions finer than the median grain size show a decrease in relative volume towards the outer bend, corresponding to negative values for δ_i. Furthermore, the offset of the relative volume of all sediment fractions is always negative, but this offset also increases, i.e. becomes more negative, towards the

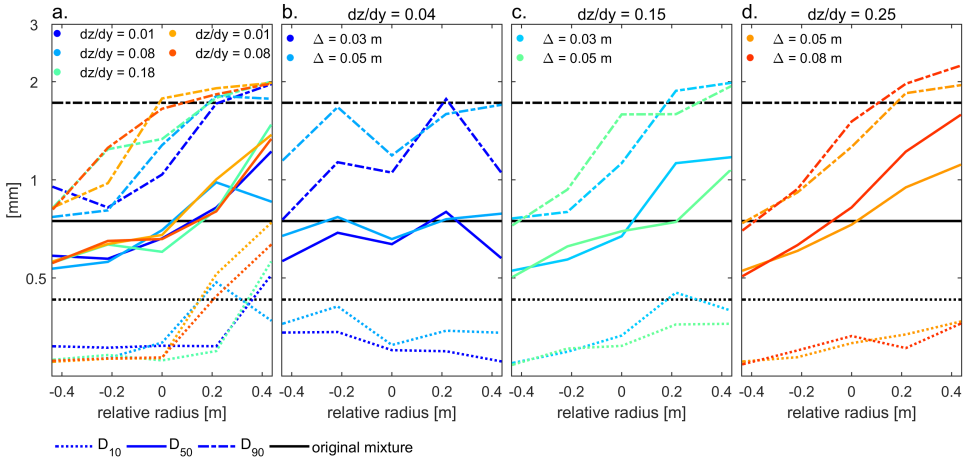

Figure 4.6: Dune trough distribution of D_{10}, D_{50}, D_{90} over the cross-section of the flume for surface samples in dune troughs in experiments with varying transverse slope and dune height. Black lines indicate values from the original mixture at the beginning of the experiment. Radius is relative to the center of the flume (o).

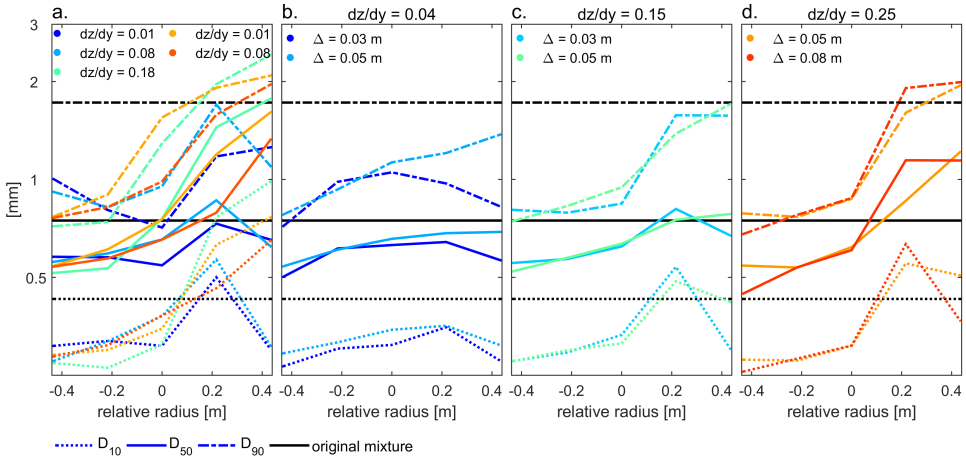

Figure 4.7: Dune crest distribution of D_{10}, D_{50}, D_{90} over the cross-section of the flume for surface samples at dune crests in experiments with varying transverse slope and dune height. Black lines indicate values from the original mixture at the beginning of the experiment. Radius is relative to the center of the flume (o).

finer and coarser fractions. These trends increase with increasing slope, while the effect of sediment mobility is not significant.

The change of δ with increasing transverse slope for specific fractions is characterized by the variable a_i (Eq 4.5), and the change of γ by b_i (Eq 4.6). These variables are plotted in figure 4.9 for each grain size fraction, together with their values for the samples that were taken in the dune trough and on the dune crest. For the bulk samples, coefficients c_1 and c_2 (Eq. 4.13) can be determined by fitting a function through the trend in a_i and b_i against

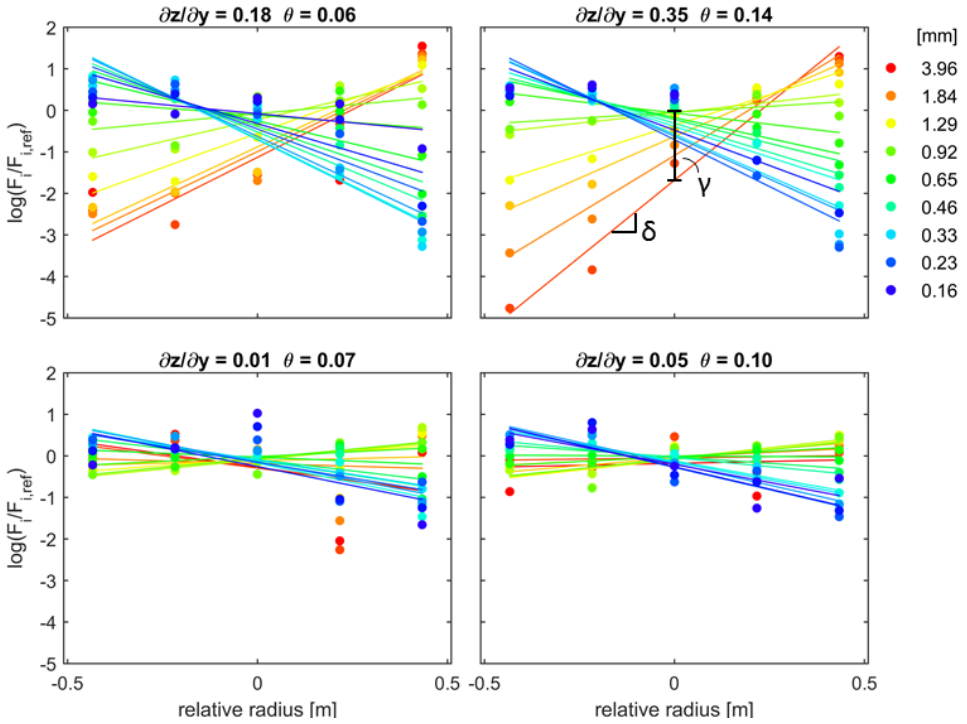

Figure 4.8: Four examples of measured relative volume of grain size fractions (scatter) over the cross-section and the fitted linear function trough these volumes (lines) to determine coefficient δ_i, which is the slope of the fitted function, and γ_i, which is the offset at the center of the channel (Eg. 4.2).

grain size fraction according to Equations 4.7 and 4.8, which are input for the bend sorting model (Eq 4.13). These fitted functions result in a c_1 of 5.5 and a c_2 of -0.5. Both the coarsest and finest sediment fractions show a slight deviation from the bend sorting model. However, these fractions have a much smaller total volume than the fractions near the median grain size, as showed by the sediment distribution of the initial mixture (Fig. 4.9). Furthermore, using more complex functions to describe these trends did not result in a more accurate prediction of the resulting sediment volumes.

For trough and crest samples, the curves show a slightly different behavior. For a_i the trend is steeper towards the coarser fractions and more constant towards the finer fractions. This means that the volume change over the cross-section with increasing transverse slope is larger for coarser grains, and thus sorting is more pronounced, while the volume change of finer sediment over the cross-section does not change significantly for increasing slope. The more pronounced sorting of coarser grains is also visible in the curve of b_i, which is steeper towards the coarser fraction, which means that the offset is increasingly larger at the center of the flume. Again, the offset of sediment volumes of the finer fractions are less influenced by increase in slope.

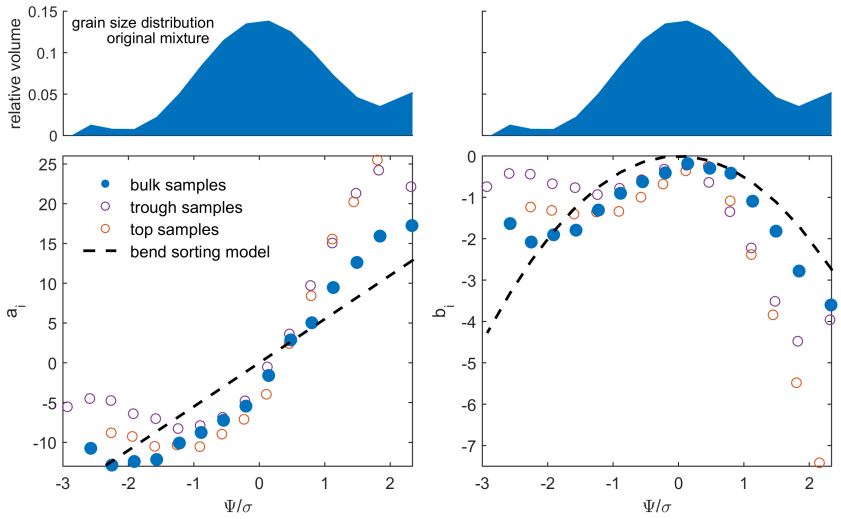

Figure 4.9: Change in parameters a_i (Eq 4.5) and b_i (Eq 4.6) with increasing relative grain size fraction (ψ/σ), for bulk and surface samples (scatter) and the trend described by the bend sorting model (dashed lines). a_i represents the change in volume change over the cross-section with increasing transverse slope, while b_i represents the change in offset at the channel centerline with increasing transverse slope. The grain size distribution on top shows the relative amount of grain size fractions present in the initial mixture.

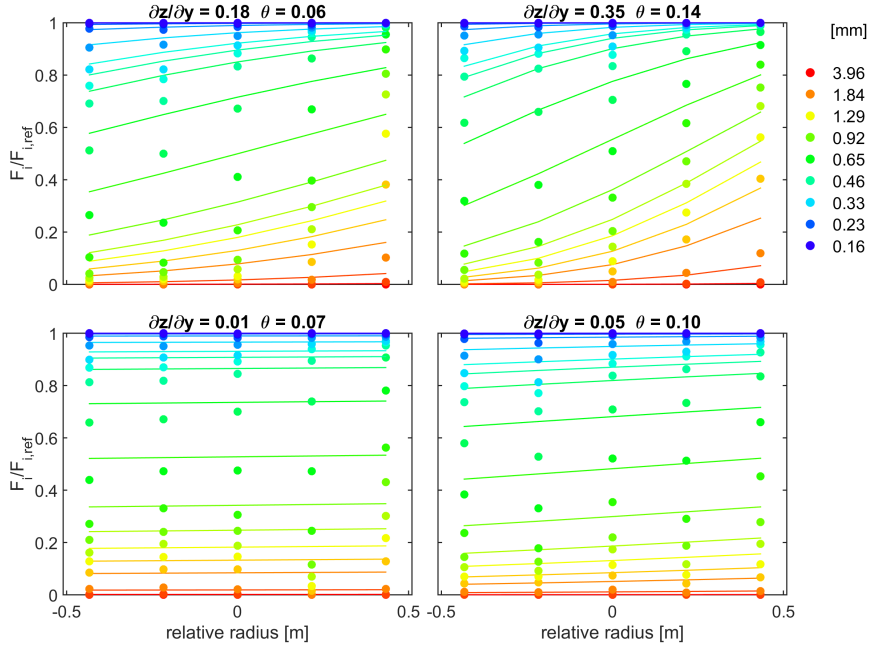

Figure 4.10: Comparison between measured (scatter) and predicted (lines) relative grain size fractions (color scale) over the cross-section of the flume, for four examples of experiments with varying transverse slope and sediment mobility.

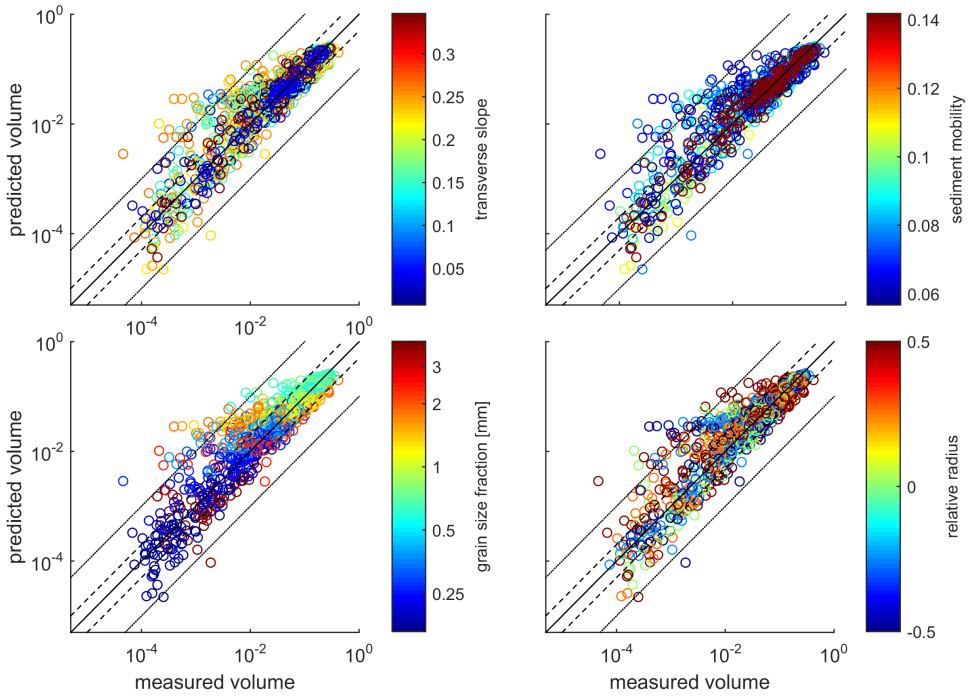

Figure 4.11: Predicted against measured volumes of all grain size fractions from all bulk samples. Color scales show the average transverse slope or sediment mobility of the experiment during which the sample was taken, grain size fraction, and the cross-sectional location of the sample.

The bend sorting model, with the coefficient c_1 and c_2 included according to the experimental data, predicts the measured volumes well (Fig 4.10, 4.11), with a R^2 of 0.85. However, for low sediment mobilities, predicted relative volumes can be significantly higher than measured, especially in combination with high slopes. Furthermore, the model underpredicts low volumes of fine sediment.

4.4 Discussion

4.4.1 Interaction between lateral and vertical sorting

The experimental data showed that lateral sorting strongly increases with transverse slope. However, the average transverse slope shows the same trend with secondary flow and sediment mobility as the experiments with uniform sediment, showing that the transverse bed slope effect is unaffected by transverse sorting in experiments where all fractions are mobile. The sharp increase in median grain size and D_90 towards the outer bend, especially for slopes steeper than 0.15 m/m, and the more gradual decrease towards the inner bend shows the larger tendency of coarser grains to travel downslope due to gravity than the finer sediment upslope due to secondary flow. This difference is more enhanced for steeper slopes. Qual-

itatively, the experimental observations are in agreement with Parker and Andrews (1985), who observed the locus of sediment coarser than the median grain size to be at the channel centerline at the bend apex.

The difference between bulk samples and surface samples tells us the relative importance of lateral sorting by the transverse slope and vertical sorting by dunes. Bulk samples show a sorting pattern averaged over a longer time, since this pattern is the result of multiple dunes passing, and thereby filter out local or temporal variations. Surface samples show local trends that depend on the location on the dunes. Dunes were as efficiently vertically sorted as found in Kleinhans (2005) and determined the availability of sediment fractions in the surface samples. In dune troughs, secondary flow was enhanced and as a result transverse slopes were steeper than the average slope, and sorting was more efficient than in the bulk samples (Fig. 4.9). In contrast, finer fractions showed a smaller change with increasing slope at the surface, possibly due to lateral mixing by suspension. The bulk samples therefore showed that vertical sorting by dunes dampens lateral sorting of the coarsest fractions and slightly enhances sorting of the finest fraction. However, the overall trend of dependency on transverse slope between bulk and surface samples is similar, and the influence of vertical mixing was not sufficient to depend on dune height or sediment mobility. Therefore, the relative influence of vertical sorting by bedforms on lateral bend sorting is relatively low, and the bend sorting model is calibrated on the bulk samples collected from the experiments.

4.4.2 Application of the empirical bend sorting model to field data

Comparison of the bend sorting model with field data shows that the bend sorting model generally works on other data as well, since it redistributes all sediment that is available over the cross-section. The trend in volume change over the cross-sections of specific fractions is similar to that of the experiments. Nevertheless, deviations from the model are observed. In general, figure 4.15 shows that the model can overestimate lower relative volumes. This overestimation is larger than with the experimental data. Other deviations can be explained by differences in field and experimental conditions.

Firstly, the bend sorting model redistributes available sediment assuming all fractions are mobile, while this was not the case when discharge was lower in the gravel bed river Severn (Fig. 4.12), and at the inner bend at the lowest discharge in the river South Esk (Fig. 4.13). When only the finer fractions were in transport, the volume of fine sediment fractions at the inner bend is considerably larger than the bend sorting model predicts. The measured volumes of the coarser fractions at the outer bend did not change compared to when all fractions were mobile, but since the model redistributes the fractions that are present, it now underestimates these volumes.

Secondly, in case of the Severn and the South Esk surface samples were taken, and therefore show interaction with bedforms and present flow conditions. Just like the surface samples in the experiments, data from the South Esk shows relatively more fine sediment in the inner bend and a larger amount of coarser sediment at the outer bend when all fractions were mobile. The data of the Severn show a slight deviation when all fractions were in transport because of a bar that was located in the middle of the cross-section.

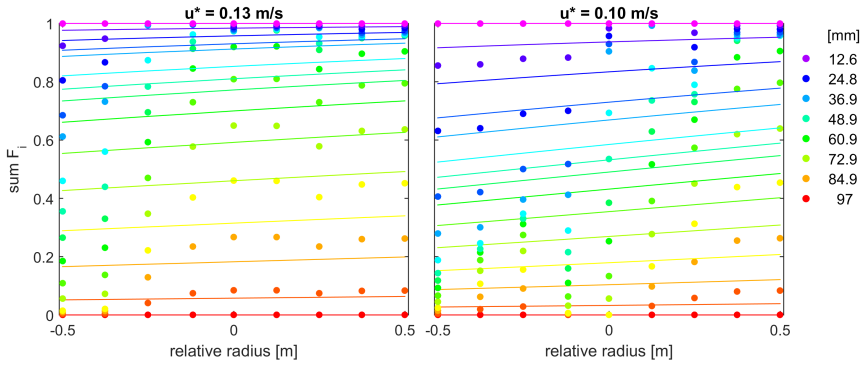

Figure 4.12: Comparison between measured (scatter) and predicted (lines) relative grain size fractions (color scale) over the cross-section of the river Severn (Hey, 1991), at different flow conditions.

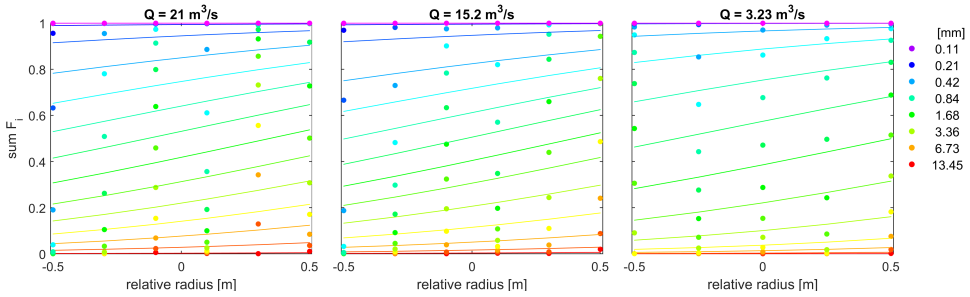

Figure 4.13: Comparison between measured (scatter) and predicted (lines) relative grain size fractions (color scale) over the cross-section of the river South Esk (Bridge and Jarvis, 1976), during falling discharge.

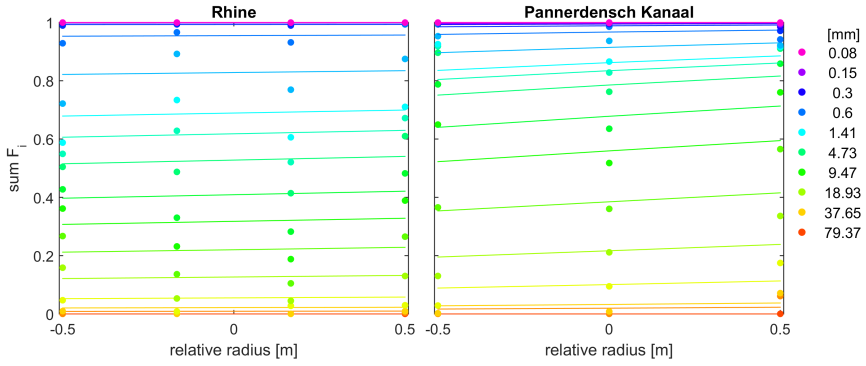

Figure 4.14: Comparison between measured (scatter) and predicted (lines) relative grain size fractions (color scale) over the cross-section of the Rhine and Pannerdensch Kanaal. The transect of the Rhine is just upstream of a bifurcation, while the transect at the Pannerdensch Kanaal is the first after the bifurcation.

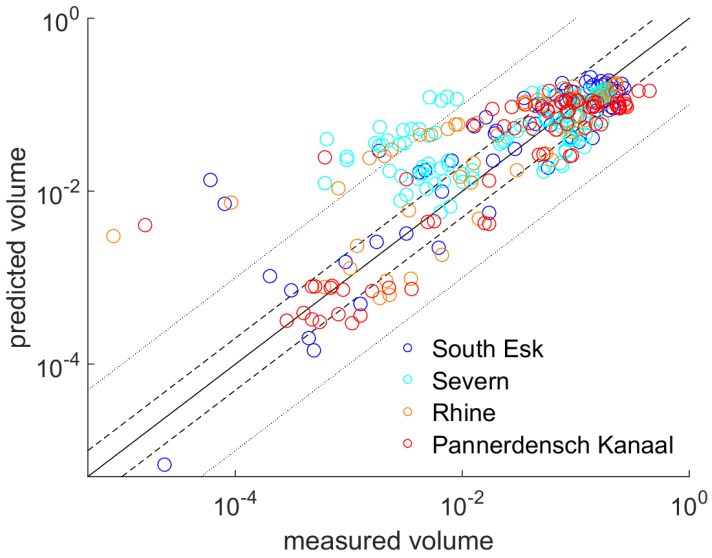

Figure 4.15: Predicted against measured volumes of all grain size fractions from fielddata found in literature. Color indicates the river that was sampled.

Thirdly, sorting patterns of the Rhine river seem to be more pronounced in the data compared to the model (Fig. 4.14). Furthermore, the river Rhine is heavily managed, which might influence local sediment characteristics near the banks. Grain size samples from the Rhine river just upstream of the bifurcation into the Waal river and the Pannerdensch Kanaal show that sorting is gradual over the cross-section in the first 40 cm of the bed, since there is only a mild transverse slope. Nevertheless, the volume of coarse sediment fractions is indeed larger in the Pannerdensch Kanaal, which is the bifurcation originating in the outer bend of the Rhine river.

4.4.3 Static sorting

The bend sorting model redistributes available sediment assuming all fractions are mobile, but as the field data shows this is not always valid. When not all fractions are mobile, static sorting can occur due to differences in critical sediment mobility, since larger particles are less mobile than finer grains and need higher shear stresses to be entrained (e.g. Odgaard, 1981; Ashworth and Ferguson, 1989). This can lead to vertical sorting by armouring of the bed when selective entrainment removes all fines from the bed and supply is limited (e.g. Powell, 1998; Kleinhans, 2001), and also hiding exposure effects become important when coarser grains shelter finer particles from the flow (e.g. Wilcock and Crowe, 2003). When coarser fractions are immobile, lateral sorting is hampered. However, static sorting is most prominent in gravel-bed rivers with wide sediment distributions, and therefore selective entrainment presumably has less influence on sorting patterns than active sorting during transport (e.g. Hoey and Ferguson, 1994).

Differences in critical sediment mobility and resulting static sorting will have an influence on the transverse slope and consequently on bed morphology. In case all fractions are mobile, the river bend responds to changes in shear stress by adjusting the bed level, and in this case the transverse slope. In case of selective entrainment, the river will adjust to a gradient in shear stress by adjusting the sorting pattern before it can adjust bed level (Dietrich and Whiting, 1989). This will thereby result in a different bed slope than when all fractions would be mobile, and influences the dynamics of river bars and the amount of bed and bank erosion (Ikeda, 1989). Due to both differences in sorting patterns and bed morphology, our bend model that only describes active sorting is less applicable in model cases where sorting due to selective entrainment plays an important role. Rather, the empirical model best represents the end member case of fully mobile sediment mixtures in infinite bends.

The effect of size selective entrainment was almost absent in the experiments due to the choice in sediment mixture. However, comparison between measurements and the bend sorting model showed that sorting was less pronounced with low sediment mobility, especially in combination with steep transverse slopes, which indicates that sediment was not mobile enough to fully develop the sorting pattern. However, this effect was only minor, and the two experiments for which this was the case did not influence the trend in the bend sorting model.

4.4.4 Implications for modelling bend sorting

The relatively simple bend sorting model can be used for multiple applications, since it can be included in any model that already predicts transverse slope and flow conditions. For example, it can be an addition to analytical models that predict bifurcation dynamics based on upstream transverse slope (Bolla Pittaluga et al., 2003; Kleinhans et al., 2008). Furthermore, an existing transverse slope predictor based on bend radius can be used to predict the slope of lateral accretion surfaces in a point bar, after which the bend sorting model can predict grain size distribution along this surface (van de Lageweg et al., 2014). The current model predicts lateral sorting along the transverse slope at the bend apex, but this pattern can have a large influence on morphology by different trajectories of the different grain sizes through the bend and towards bends downstream (Parker and Andrews, 1985). The current bend sorting model could therefore be a starting point to predict spatial distribution of sediment fractions along the bend, and thereby improve predictions of sediment transport, bed level elevations and point bar connectivity models by predicting the dimensions and spatial distribution of stratigraphic units (Willis and Tang, 2010).

The relatively low influence of vertical sorting on the trend in lateral sorting has important implications for morphodynamic models with the active layer concept. These findings show that over a longer time period, i.e. longer than the migration of a few dunes, the effect of vertical sorting can be ignored. This shows that the use of the active layer is still valid when modelling lateral sorting, which should make it easier to model sediment transport processes realistically. However, before lateral sorting can be described accurately, a more physics-based predictor needs to be implemented to calculate the deflection of the available grain size fractions in the active layer as a function of transverse slope (Sloff and Mosselman, 2012). In model scenarios where the active layer concept is not sufficient, e.g. when the ob-

jective is to look at smaller scale processes at a shorter time scale, recent studies suggested to replace the active layer by a continuous bed distribution, and to include the entire particle size distribution (Powell, 1998; Parker et al., 2000; Blom et al., 2008; Frings, 2008). In this case, the fraction-based lateral sorting function of this study can be a useful addition to the already existing formulations for streamwise (Parker et al., 2000) and vertical sorting Blom and Parker (2004). However, these more advanced continuous sorting models have not yet been applied in 2D horizontal modelling because of its mathematical and numerical complexity (Chavarrías et al., 2018).

4.5 Conclusion

We experimentally determined the trend in lateral sorting of grain size fractions as a function of transverse slope, and described the relative influence of vertical mixing by dunes. We found that all sediment fractions that are mobile are efficiently sorted along the transverse slope, where the volume change over the cross-section of specific fractions increases with grain size and magnitude of the slope. There was no feedback between sorting and the magnitude of the slope itself.

Bulk samples that were taken over the entire height of a dune showed minor effects of vertical sorting along the lee side of dunes, since the difference with surface sample were small. Only the coarsest fractions were more evenly distributed over the cross-section as a result of dune migration, while sorting of the extremely fine fractions was enhanced. Therefore, lateral sorting can be modelled independently of dunes, which allows application of the active layer concept in morphodynamic models.

We developed a bend sorting model that redistributes the available sediment over the cross-section as a function of transverse slope and grain size fraction. This model is calibrated with the bulk samples, which show an average trend over a longer time period, instead of local trends that depend on interactions with bedforms and present flow conditions. Comparison with field data showed that the model is only valid when all grain size fractions that are sampled are mobile under the present flow conditions, and therefore the model is less applicable in rivers with wide sediment distributions. The resulting bend sorting model can be used in any analytical model that predicts the transverse slope, and is a reference for morphodynamic models that predict sediment sorting patterns of mobile sediment in bends.

Acknowledgements

This research was partly supported by Deltares and by the Dutch Technology Foundation (STW) of the Netherlands Organization for Scientific Research (NWO)(grant Vici 016.140.316/13710 to Maarten Kleinhans). This work is part of the Ph.D. research of AWB and M.Sc. research of SAHW. We are grateful to Wim Uijttewaal, Sander de Vree and Hans Tas of the Environmental Fluid Mechanics Laboratory at the TU Delft for technical support. Supporting data are included in Appendix F. Sieve curves of all samples are available online.

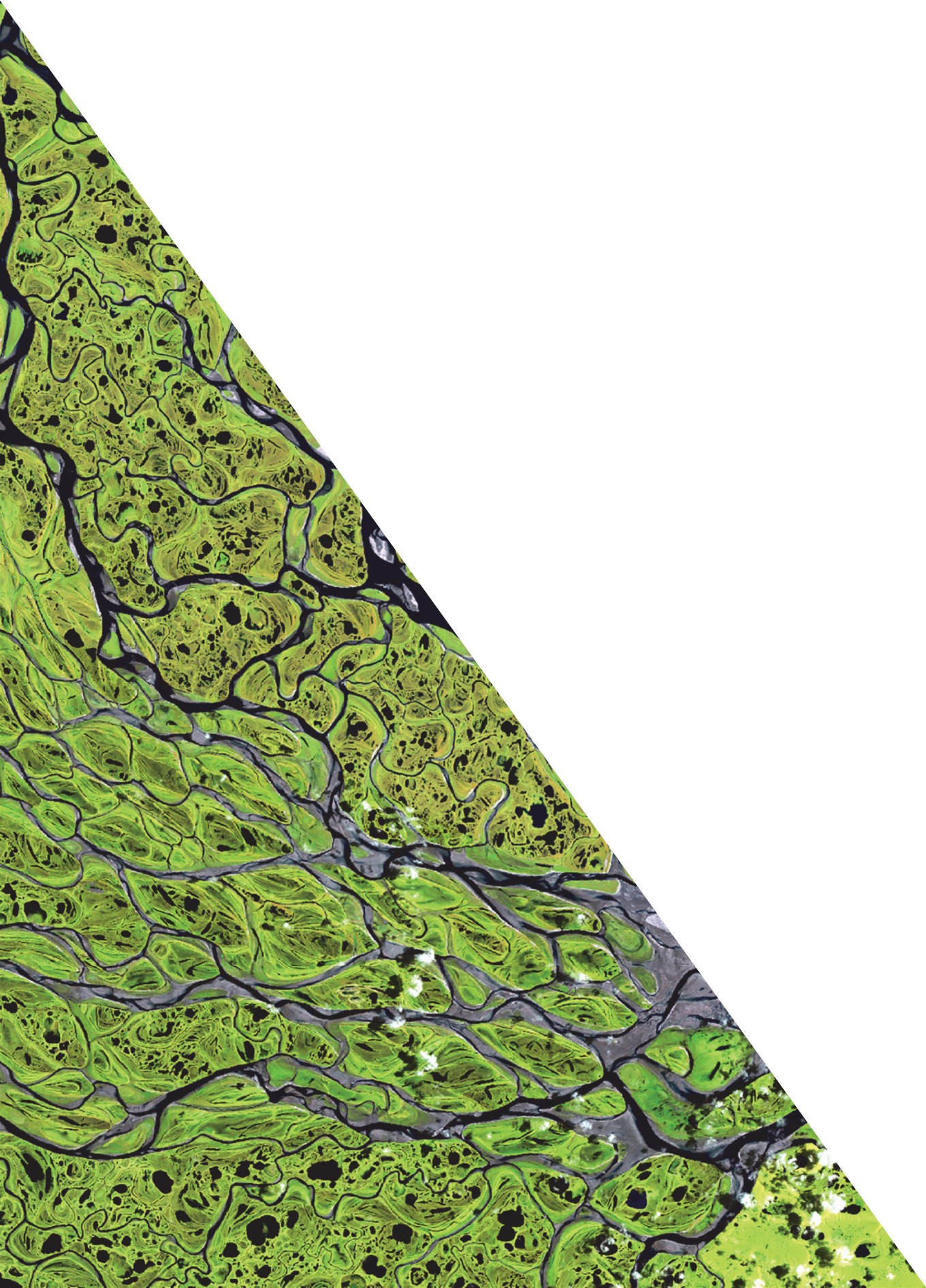

Chapter 5

Critical dependence of morphological models of fluvial and tidal systems on empirical downslope sediment transport

Morphodynamic models are essential tools to predict the development of fluvial and tidal systems in scientific and engineering studies, and are increasingly used for decision making regarding climate change mitigation, flood control, navigation and engineering works. However, many existing morphodynamic models predict unrealistically high channel incision, which is masked by increased numerical diffusion or gravity-driven downslope sediment transport up to two orders of magnitude too high. Here we show that such arbitrary calibrations dramatically change local sediment dynamics, bar and channel patterns, and rate of morphological change. For five different models bracketing a range of scales and environments, we found that it is impossible to calibrate a model on both sediment transport magnitude and morphology. Present calibration practice may cause an order magnitude error in channel depth, bed slopes and bar dimensions. We show how model design can be optimized for different applications. This has major implications for model interpretation and applications and suggests a critical knowledge gap.

Based on: Baar, A. W., Boechat Albernaz, M., Van Dijk, W.M., Kleinhans, M.G. (2018), Slip-sliding away: critical dependence of morphological models of fluvial and tidal systems on empirical downslope sediment transport. *To be submitted to:* Nature Communications

5.1 Introduction

River valleys, coastal plains and deltas are changeable landscapes with a large part of the human population that will be at risk from climate change effects and sealevel rise. Adaptation requires a systems approach (Brown et al., 2014, e.g.) with combinations of hard engineering measures and sediment attrition (Smajgl et al., 2015). Reliable forecasting of effects of combined measures requires morphodynamic models for rivers, estuaries, deltas and coasts. Morphodynamic models are therefore widely used tools to study and forecast the development of these landscapes. However, model results depend on the balance between channel incision due to the nonlinearity of sediment transport, and processes counteracting this deepening. In practice, all large-scale models need some form of calibration to converge to a stable morphology, for example by tuning roughness coefficients, grain size distributions, and increasing the transverse bed slope parameter which determines the sediment transported on channel side-slopes. The latter has proven to be most effective, since the bed slope parameter linearly increases downslope sediment transport and thereby directly affects channel depth and braiding index, and therefore has the largest effect on large-scale morphology (Schuurman et al., 2013).

The problem is that models require artificially and seemingly arbitrarily slope factors up to a 100 times higher (van der Wegen and Roelvink, 2012; Schuurman et al., 2013; Braat et al., 2017) than physically correct (Baar et al., 2018) to prevent unrealistic channel incision and to obtain realistic bar and channel patterns. A recent comprehensive set of experiments showed that a physically realistic value for the slope parameter is in the order of 1 and a realistic calibration range is within a factor of two (Baar et al., 2018). This calibration range is therefore much smaller than needed in recent model studies. Increasing the transverse slope effect by more than an order of magnitude to compensate for these weaknesses, raises doubts about the physical validity and predictive power of these models. The need to apply unrealistically intense bed slope effects implies a flaw in the balance between the non-linearity of sediment transport that carves out channels, and downslope sediment transport. This begs the question whether these models converge to a balance between erosion and deposition for the right reasons, whether the dynamics due to sediment motion can be correct at the same time, and what aspects of the forecasts on timescales of a century are most unreliable.

Part of the uncertainty is due to different parameterizations for the deflection of sediment transport on transverse slopes. The two most commonly used methods, by Ikeda (1984)(IK) and by Koch and Flokstra (1981)(KF), calculate the downslope sediment transport vector differently (Fig. 5.1). For KF the streamwise transport vector is rotated as a function of the transverse bed surface gradient, while for IK the normal transverse transport vector is enhanced before combination with the streamwise transport vector. As a result, the method of IK not only changes the direction, but also increases the flux of sediment transport. How this affects morphology and the rate of change thereof remains unquantified.

The severe channel incision is best known for sensitive codes such as Delft3D (van der Wegen and Roelvink, 2012; Schuurman et al., 2013), but is also an issue in studies with other morphodynamic models. For example, the estuary model of Ganju et al. (2009) was modelled with the Regional Ocean Modeling System (ROMS) in combination with the Commu-

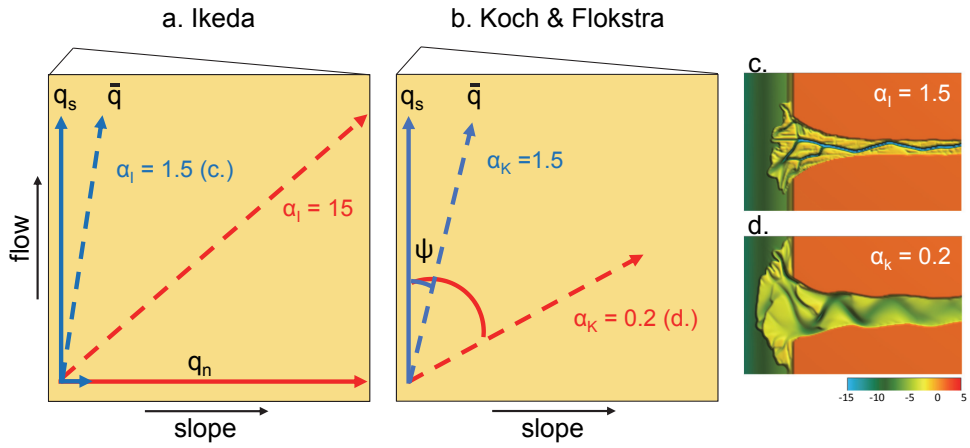

Figure 5.1: Two parameterizations for sediment deflection drawn on a transverse bed slope (Ikeda, 1984; Koch and Flokstra, 1981). Both methods are drawn on a top view of a bed sloping towards the right. Blue dashed arrows show transport vectors with default values for the slope effect, while red arrows represent transport vectors when the slope effect is increased to typical values used in current model studies. See Appendix B for detailed calculation method. c+d) examples for default and high slope effect.

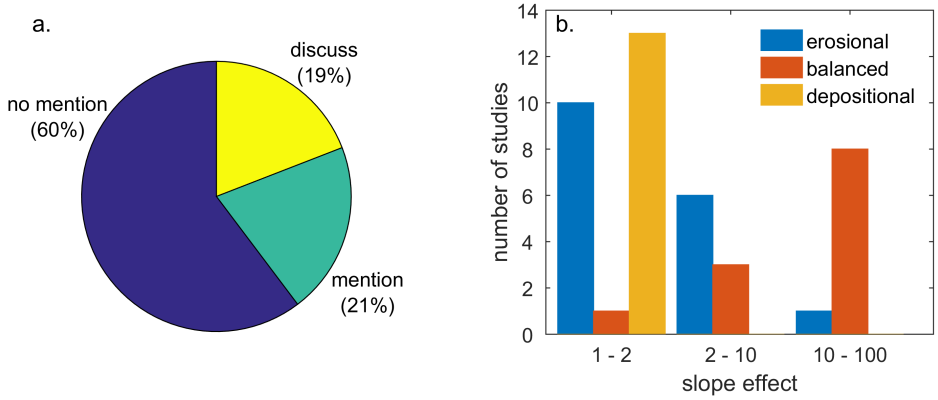

Figure 5.2: (a) Model studies that mentioned, discuss or overlooked the severe channel incision and the artificial increase in slope effect that was necessary to counteract this (see online supplement for inventory). (b) Studies that mention the magnitude of the slope effect subdivided by modelled environment and the applied slope effect value (1=default).

nity Sediment Transport Modeling System (CSTMS), and needed the bed to be coarsened to reduce unimpeded erosion in deeper channels. Furthermore, a tidal channel (Davies and Robins, 2017) modelled in Telemac with the sediment transport predictor of Van Rijn et al. (2004) (VR) needed a coarse sediment underlayer to prevent unrealistic bed erosion. On the other hand, Telemac in combination with the predictor of Engelund and Hansen (1967) (EH) showed extreme morphological diffusion (Nnafie et al., 2016), showing the sensitivity of the chosen combination of sediment transport predictor and downslope sediment transport pa-

rameterization. Regardless, a quick inventory in typical geomorphology journals showed that only 13 (19%) out of 68 model studies discussed the imbalance between severe incision and downslope sediment transport (Fig. 5.2,online supplement).

Additionally, the review suggested sensitivity to incision depends on the environmental settings. Here, environment means initial and boundary conditions, which determine sediment characteristics, flow conditions, channel pattern and bar regime. Models of environments with a large-scale balance between erosion and deposition, such as estuaries and rivers, particularly have the tendency to overpredict channel depth and braiding index and required very high slope effects up to a factor of 100 (Van der Wegen and Jaffe, 2014; Schuurman et al., 2018, e.g.). In contrast, models of systems with dominant erosion such as a tidal channel network, usually had slope factors lower than 10 (Marciano et al., 2005; Dissanayake et al., 2009; Zhou et al., 2014, e.g.), and depositional systems such as river deltas all used the default value (Edmonds and Slingerland, 2007; Leonardi et al., 2013; Caldwell and Edmonds, 2014, e.g.) (Fig. 5.2,online supplement) . However, this emphasis on channel depth and bar dimensions masks effects of downslope sediment flux on the rate of bank erosion, channel formation and migration in erosional models, while default transverse slope parameters in both erosional and depositional models commonly show unrealistically deep channels and sharp angular bends (Edmonds and Slingerland, 2009; Caldwell and Edmonds, 2014; Van der Vegt et al., 2016, e.g.).

Here we conduct five sets of numerical morphodynamic simulations for different scales and environments to quantify the effects of increased downslope sediment transport on morphology (Fig 5.3). The objective is firstly to identify possible causes of the imbalance between incision and transverse sediment transport on the channel scale for typical combinations of sediment transport and slope parameterizations. Secondly, we quantify the effects on local sediment transport rates and on large-scale morphology. Finally, we will discuss sensitivity to environment, and consequently give recommendations for an appropriate design of models depending on research objectives of future studies given the present limitations and uncertainties. Results demonstrate that arbitrary bed slope calibration to obtain better-looking morphology may cause an order of magnitude error in rate of morphological change, channel depth, degree of braiding and bar dimensions. Furthermore, we found that it is impossible to calibrate a model on both sediment transport magnitude and morphology.

5.2 Results

5.2.1 Effects of combinations of slope parameterization and sediment transport predictor

All five models (Fig. 5.3) generally showed deep incision and oversteepened morphology with physically correct slope effects, leading to deep and narrow channels, a higher number of channels and shorter bars than typically observed in nature. Increasing the bed slope effect resulted in wider and shallower channels, longer bars, a smaller braiding index, and fewer bifurcations and a greater similarity to natural systems, although a very high slope effect caused overly subdued relief (Fig. 5.4, 5.5). However, different combinations of sediment

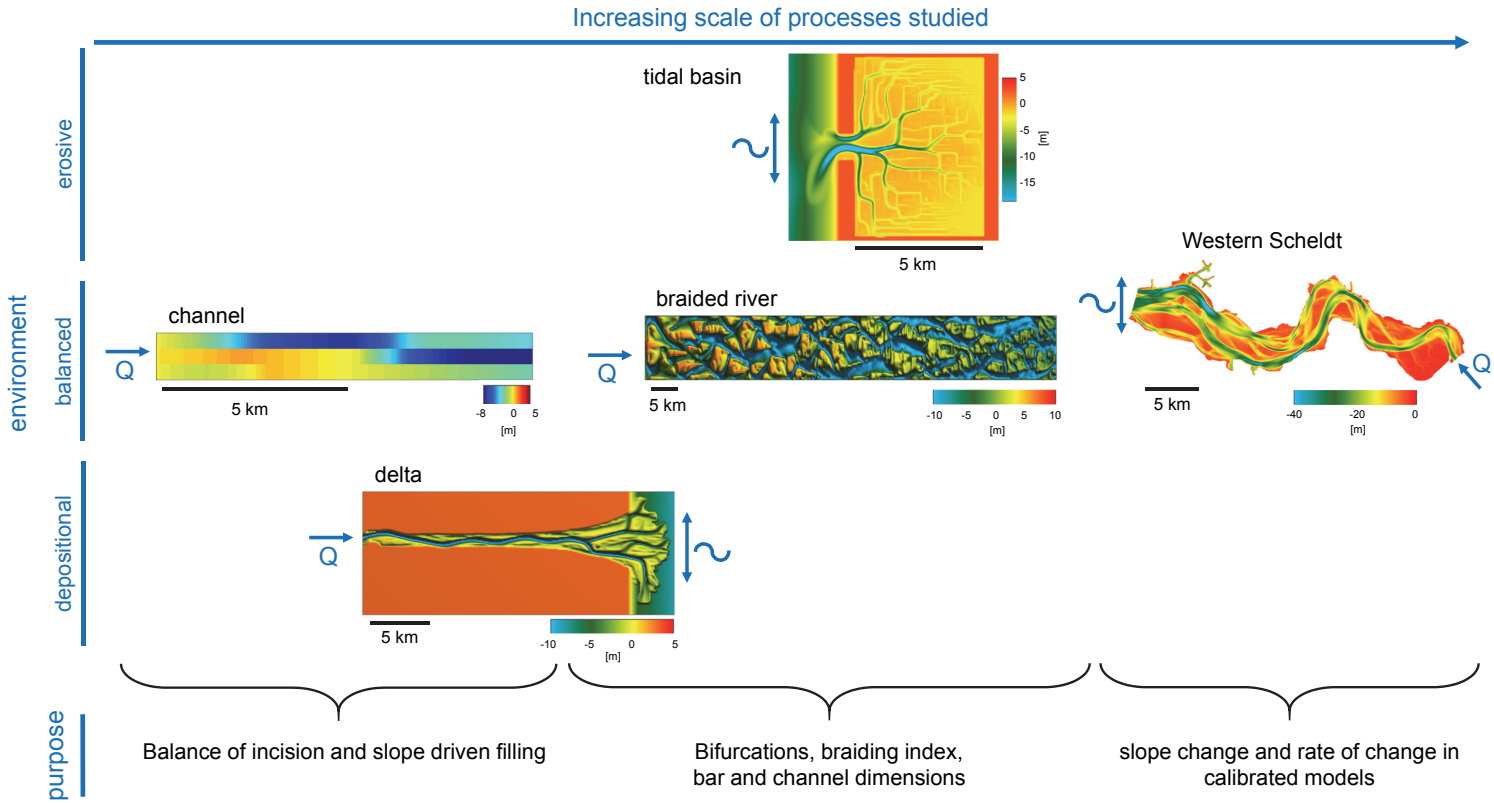

Figure 5.3: Overview of model environments and objectives in this study. The narrow channel model and the river in the delta model are used to study local sediment transport processes. The delta model, the braided river model, and the tidal basin model quantify the effects of different methods on bifurcation dynamics, braiding index and channel dimensions, and the combinations of slope predictors with sediment transport predictors. The calibrated Western Scheldt estuary model shows differences in dynamics relevant for fairway dredging depth and intensity.

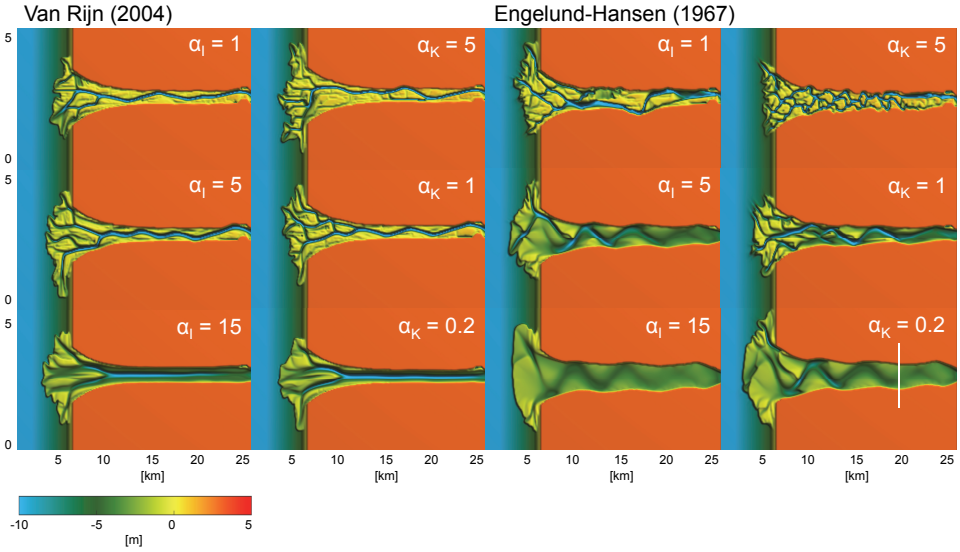

Figure 5.4: Morphology of 12 delta model runs after 1000 years for combinations of slope effect and sediment transport predictors. Maps on the horizontal axis have an equal slope effect, with slope effect increasing downwards. The α_I is the input parameter of the method of Ikeda (1984), while the α_K is the input parameter of the method of Koch and Flokstra (1981). The models in the first two columns were run with the VR sediment transport predictor, while the models in the last two columns were run with the EH predictor. The average sediment transport rates plotted in Figure 5.8 were computed for all model runs over a cross-section at 20 km, represented by the white line in the bottom right panel.

transport predictor and method to calculate downslope sediment transport lead to starkly contrasting morphologies. To quantify the difference in effect of both slope options on sediment transport processes and morphology, the parameter that determines the magnitude of the transverse slope effect was systematically increased. Henceforth, the term slope effect refers to the magnitude of this parameter, which is the α_I in the method of Ikeda and the α_K in the method of Koch and Flokstra (Appendix B). Note that the parameter α_K is roughly the inverse of α_I. To be able to compare the differences between both options, the values for these parameters were not simply proportionately varied, but determined by requiring equal sediment transport in the transverse direction as explained in Appendix B.

The cumulative slope distributions (Fig. 5.6) show that a higher slope factor causes a smoother and more subdued morphology, and shows one to two orders of magnitude variation between slope and transport combinations for parameter ranges between physically correct and typically used in the literature. The braided river model showed a wider range in the distribution of slopes with increasing slope effect and changing slope and sediment transport predictor than the delta model, since the latter is less confined and more dynamic. Models with the parameterization of KF, which merely rotates the transport vector, had steeper slopes and deeper channels than models with the parameterization of IK. Models with the VR sediment transport predictor also had much steeper slopes and deeper channels than with EH. The most worrying conclusion is that the braided river model with α_K of 0.7 (slope

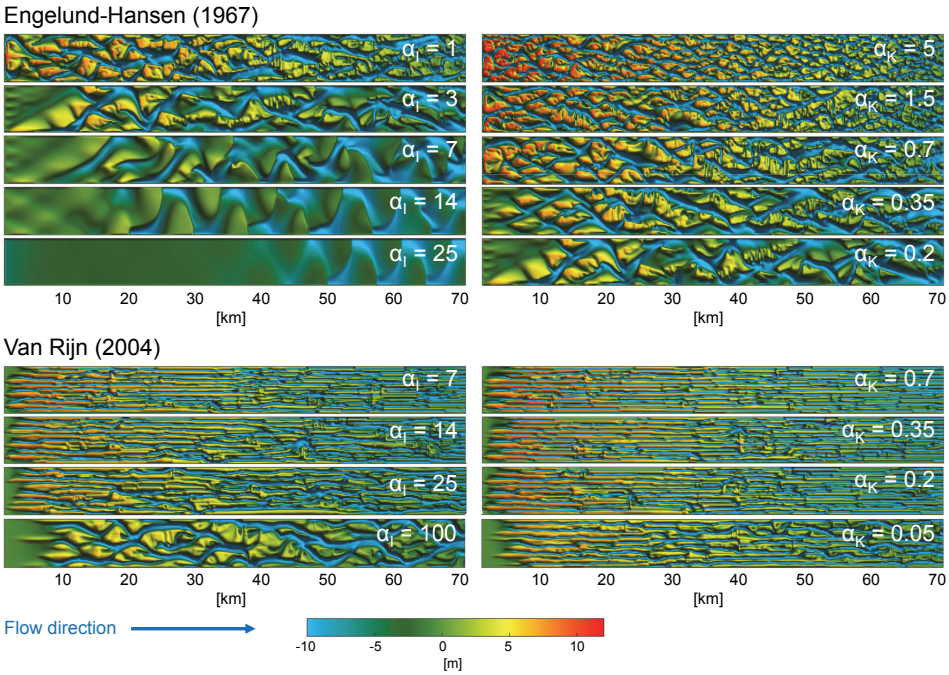

Figure 5.5: Morphology of 18 braided river model runs for all combinations of slope effect and sediment transport predictors. Models on the horizontal axis have equal slope effect, which increases downwards for each transport predictor. The α_I is the input parameter of the method of Ikeda (1984), while the α_K is the input parameter of the method of Koch and Flokstra (1981), both with defaults of order 1.

effect = 7) has similar morphology as with α_I of 1 (slope effect = 1) (Fig. 5.6b), but has seven times larger transverse sediment fluxes, since the slope effect is seven times larger. The consequence could be that the time scale of morphological adaptation differs considerably, which has consequences for management and dredging.

5.2.2 Sediment transport at the channel scale

Here we examine the effect of varying slope effect and sediment transport predictor on sediment transport processes across scales for different environments (Fig 5.3). Firstly, we study differences in sediment transport processes at the channel scale, then we explain the effect on bifurcation and bar dynamics of using different slope options, and lastly we quantify the change in dynamics in calibrated large-scale models.

We designed a very simple numerical model scenario of three grid cells wide that can also be solved analytically to study the magnitude and direction of sediment transport. This prevents formation of complex patterns so that channel and bar formation are fundamentally the result of the balance of two processes: channel erosion and gravity-driven sediment motion towards the channels. In particular we are interested whether a perturbation grows or decays. Growing means channel erosion that is the result of the nonlinear dependence of the sediment transport rate on flow shear stress at the bed, since sediment transport is en-

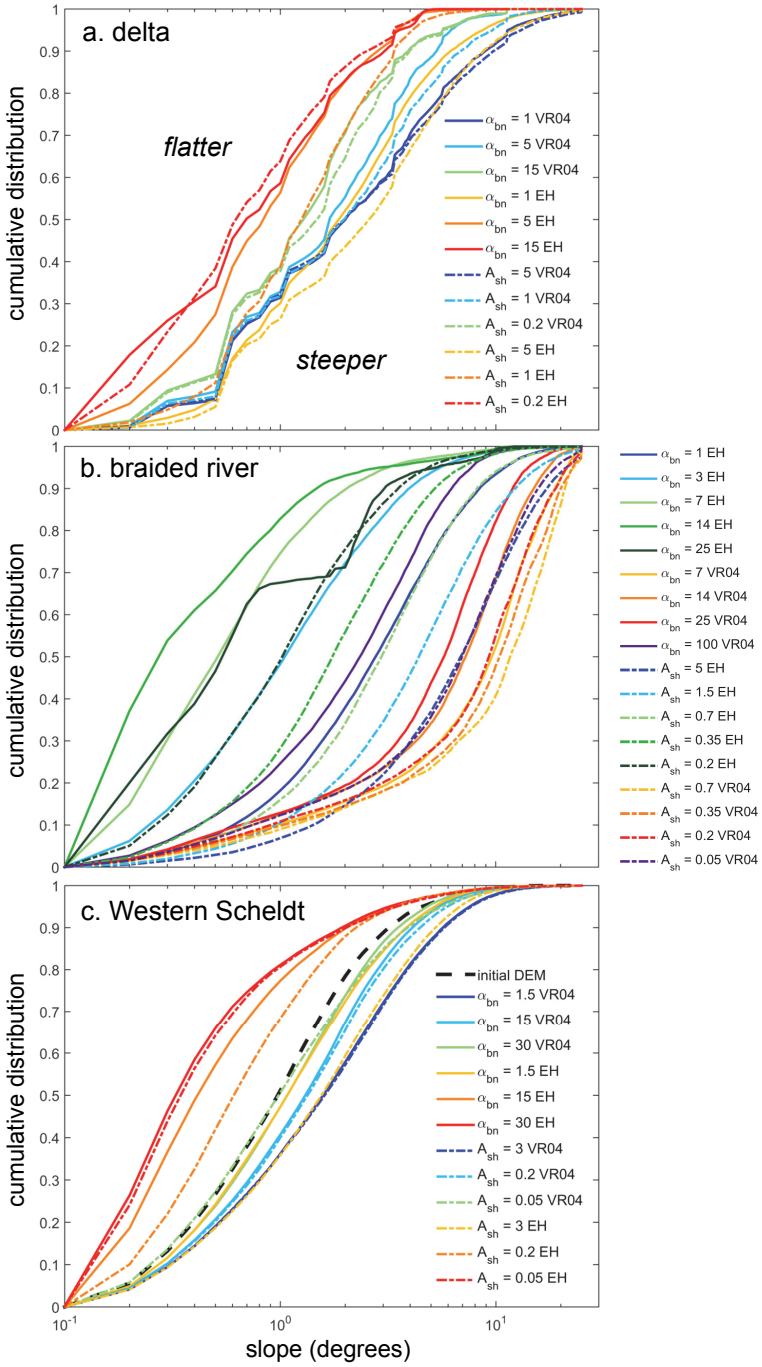

Figure 5.6: Cumulative slope distributions of (a) the delta model runs, (b) the braided river model runs, and c) the Western Scheldt model runs. Solid lines are results with IK and dashed lines are results with KF. Colors indicate equal transverse sediment transport magnitudes and the same sediment transport predictor. The black dashed line in the Western Scheldt plot represents a measured bathymetry used as input.

hanced in deeper channels that attract more flow. This positive feedback is strongest near the beginning of motion, where the non-linearity of sediment transport is largest and therefore tends to deepen channels, albeit at a low rate. The most important negative feedback on channel formation is sediment transport deflection on the side slopes towards the center of the channel under the influence of gravity (van Bendegom, 1947; Sekine and Parker, 1992; Talmon et al., 1995), which is thus a crucial feedback in forming equilibrium channels. However, numerical diffusion in the flow model would have a similar effect. To determine the tendency to incise independently of numerics, we use an analytical model of a river channel cross-section. This calculates the balance and imbalance between channel incision and downslope lateral sediment transport on an initially perturbed bed (Appendix C), which we compared to the simple numerical model of three grid cells wide. Channel width was varied between 21 and 210 m. In addition to the sediment transport predictors of Van Rijn et al. (2004)(VR04) and Engelund and Hansen (1967)(EH), we also ran the numerical model with a general total-load sediment transport predictor, in which the non-linearity of sediment transport and the addition of a critical sediment mobility was specified (Appendix B). This allowed us to determine whether imbalances are related to sediment transport nonlinearity or to the implementation of a specific transport predictor in the model. For VR, we only take the bed load part into account in the analytical model.

The analytical model at the channel scale tells us when incision is theoretically balanced by downslope sediment transport. In general agreement with bar theory, wider and shallower channels tend more to incise, so that larger bed slope effects are needed to prevent growth of channels. We plotted a combined dimensionless parameter that collapses the marginal curves above which growth commences. This parameter is the width-to-depth ratio of the channel multiplied with the bed slope effect, which we will therefore call the channelization factor. The analytical model identifies the equilibrium channelization factor, which means that perturbations in numerical models plotted below this line should theoretically decay, while models plotted above the line should have growing perturbations (Fig. 5.7). With the default value for the slope effect ($\alpha_I = 1.5$), the VR models corresponded reasonably well with the analytical model, since the transition from a dampened system towards a channel where the perturbation grows is around the theoretical equilibrium line (Fig. 5.7a). There was no effect of the depth of the initial perturbation in the numerical model. However, with increased slope effect, the numerical models significantly deviated from the analytical model. Here, the numerical model with wider channels required a disproportionately larger slope effect to dampen the initial perturbation (more than 30 times higher than the default factor as opposed to 4 times the default in the analytical model). On the other hand, the initial perturbation in models with the models with the EH predictor immediately decayed (Fig. 5.7b), until the channel has a width-to-depth ratio around 36, which is more than 15 times higher than the theoretical model. This behavior was very similar to that of the models with the general predictor (Fig. 5.7c,d). Even when sediment transport is related to flow velocity to the power of 10, perturbations did not start to grow at a lower width-to-depth-ratio, while this was expected based on the analytical model. The two slope parameterizations differed only slightly and removing the critical sediment mobility from the generic transport predictor had no effect on equilibrium morphology. These results demonstrate a stronger tendency

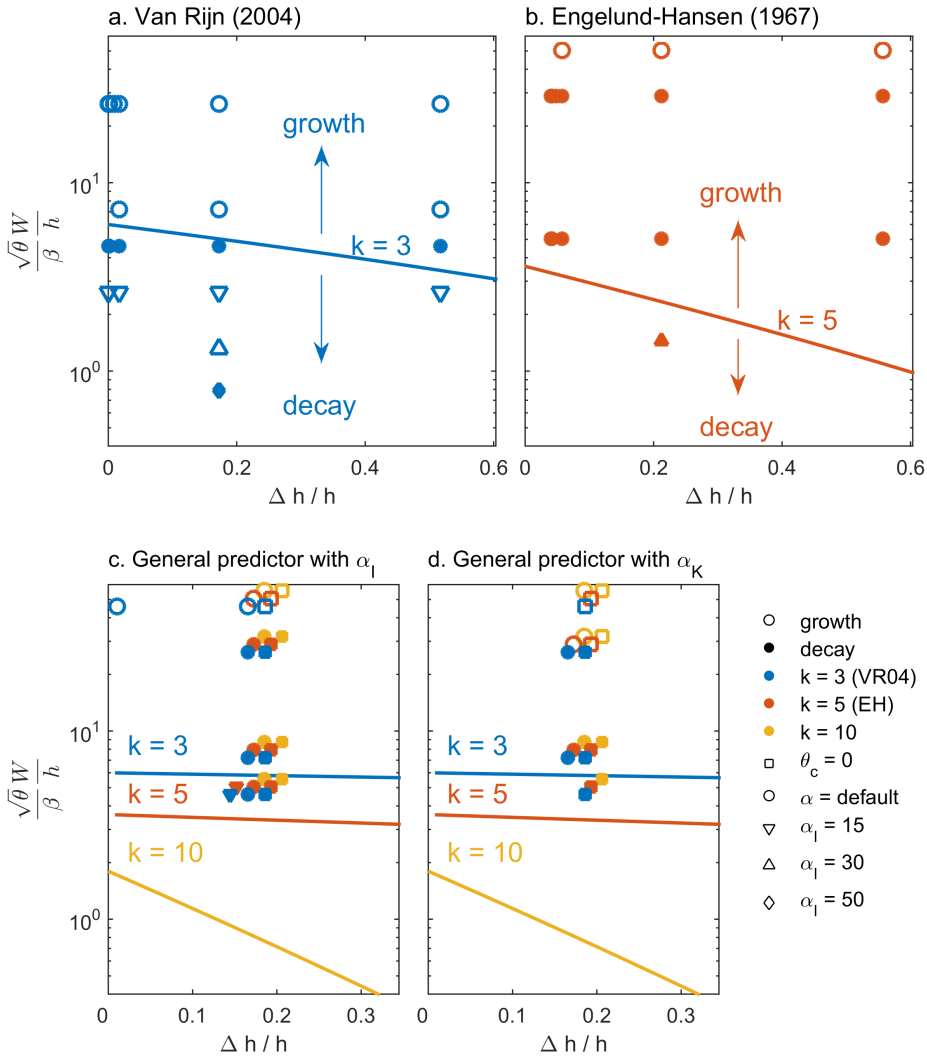

Figure 5.7: Comparison between the behavior of the analytical model (lines) and the numerical channel (symbols) with (a) the VR sediment transport predictor, (b) the EH sediment transport predictor, (c) the general transport predictor with the IK slope parameterization, and (d) the general transport predictor with the KF slope parameterization. The analytical model predicts the width-to-depth ratio (W/h) for a certain non-linearity of sediment transport (power k on shear stress) at which incision and downslope sediment transport are in balance (Appendix C). The channelization factor ($W/h\sqrt{\theta}/\beta$) is plotted against the relative depth of the initial perturbation ($\Delta h/h$). The perturbation in the numerical models either grows (open symbol), or decays (filled symbol). Colors represent non-linearity of the sediment transport predictor and symbols represent the magnitude of the slope effect based on the IK slope parameterization, or in case of the general transport predictor the absence of a critical sediment mobility.

to incise in the numerical model with VR than expected from theory, and a weaker tendency to incise in numerical models with EH.

5.2.3 Slope effect-dependent sediment transport

The rate of morphological change depends on sediment transport magnitude, which finds applications in fairways kept out of equilibrium by dredging. To test whether different slope parameterizations have similar transport rates and can have similar morphologies at the same time, we compared results of several combinations of parameterizations at a cross-section in the laterally unconfined river reach of the delta model (Fig. 5.8). The delta model is similar to that of Geleynse et al. (2010), with a 20 km long river that deposits its sediment in a 10 by 10 km basin. The river can freely migrate and forms its own topographic forcing by incising and forming meander bends.

Streamwise sediment transport rates were independent of transverse components for the first 100 years, after which more complex morphology developed and channel dimensions began to depend on the magnitude of the transverse slope effect. Models with the EH predictor had an order of magnitude higher sediment transport rates in streamwise and lateral direction than with the VR predictor. When morphology developed, the magnitude of sediment transport of models with corresponding slope effect and the same sediment transport predictor were similar, except for the model with the KF method and a very low slope effect. Here, a braided river developed when combined with the EH sediment transport predictor (top-right panel in Fig. 5.4), resulting in multiple channels that transport sediment and therefore average sediment transport rates were impractical to compare with the other models. Transverse sediment transport rates of models with equal slope effect were also similar in general, and when it deviated, it could be explained by different trends in streamwise sedi-

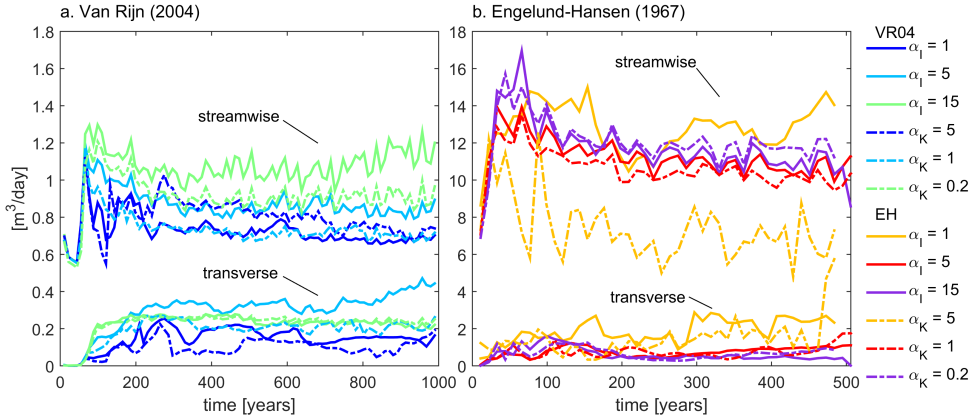

Figure 5.8: Total sediment transport over a transect at km 20 in the river part of the delta model, integrated over the active channel width. (a) Streamwise and transverse sediment transport over time for all models with the VR sediment transport predictor, and (b) for all the model runs with the EH predictor. Note different vertical scales. Solid lines represent model runs with the IK method to calculate downslope sediment transport, while the dashed lines represent the models with the KF method. Lines with the same colors represent corresponding slope effects and sediment transport predictors.

ment transport magnitude. Models with a higher slope effect had a higher average transverse sediment transport rate at the start of the model run, resulting in channel widening and development of gentle sloping morphology. This eventually resulted in lower transport rates than models with a lower slope effect with steeper slopes and deeper channels.

While sediment transport rates are equal for models with equal slope effect but different slope parametrizations, models with the slope parameterization of KF showed steeper bed slopes and a larger number of avulsions downstream at the delta (Fig. 5.4, 5.6. These results demonstrate that even though it is possible to calibrate models on sediment transport magnitude with different slope parametrizations, bed slopes and morphology will differ. Additionally, an order of magnitude difference in sediment transport rates results from predictor choice.

5.2.4 Slope effect-dependent bar and channel pattern properties

Having established that combinations of slope and transport parameterizations result in different morphological patterns and sediment transport magnitudes, we now quantify effects on critical elements of fluvio-deltaic patterns in erosive, balanced and sedimentary environments: bars and the degree of braiding. Here, the delta in the delta model is a perfect depositional environment. The braided river model represents a Brahmaputra-sized braided sand-bed river with a 3.2 km wide and 80 km long braidplain where erosion and deposition are on average in balance, and is exactly the same as the model of Schuurman et al. (2013). The tidal basin model consists of a channel network that is incised by the tidal motion, and therefore this model represents an erosional environment.

Downslope sediment transport is essential in balancing helical flows in curved channel sections. In nature, secondary currents alter the direction of the bed shear stress towards the inner bend, which leads to a balance between the upslope directed drag force by the secondary flow and the downslope sediment transport under influence of gravity (Engelund, 1974; Struiksma et al., 1985). By balancing secondary flows, downslope sediment transport controls the adaptation of the morphology to changes in flow conditions (Struiksma et al., 1985; Crosato and Mosselman, 2009; Kleinhans and van den Berg, 2011). Therefore, by both counteracting incision and balancing secondary flow, the magnitude of downslope sediment transport determines the developed active channel width, orientation of channels, and the length and migration rates of fluvial and tidal bars (Seminara and Turbino, 2001; Dissanayake et al., 2009; Schuurman et al., 2013; Van Dijk et al., 2014), and controls the division of bedload over bifurcates (Kleinhans and van den Berg, 2011). On the larger scale, the amount of downslope sediment transport therefore has a major influence on channel and bar patterns, by determining braiding index (Parker, 1979; Struiksma et al., 1985; Crosato and Mosselman, 2009) and the stability of river bifurcations and related tendency of channels on fans and deltas to avulse (Bolla Pittaluga et al., 2003; Kleinhans et al., 2008; Sloff and Mosselman, 2012; Bolla Pittaluga et al., 2015).

Braided river models with KF had a larger braiding index and shorter bars than the models with IK with the lowest slope effect, and the braiding index decreased with increasing the slope effect for both sediment transport predictors (Fig. 5.9b). Models with the EH sediment transport predictor showed braiding indices that were lower than predicted with

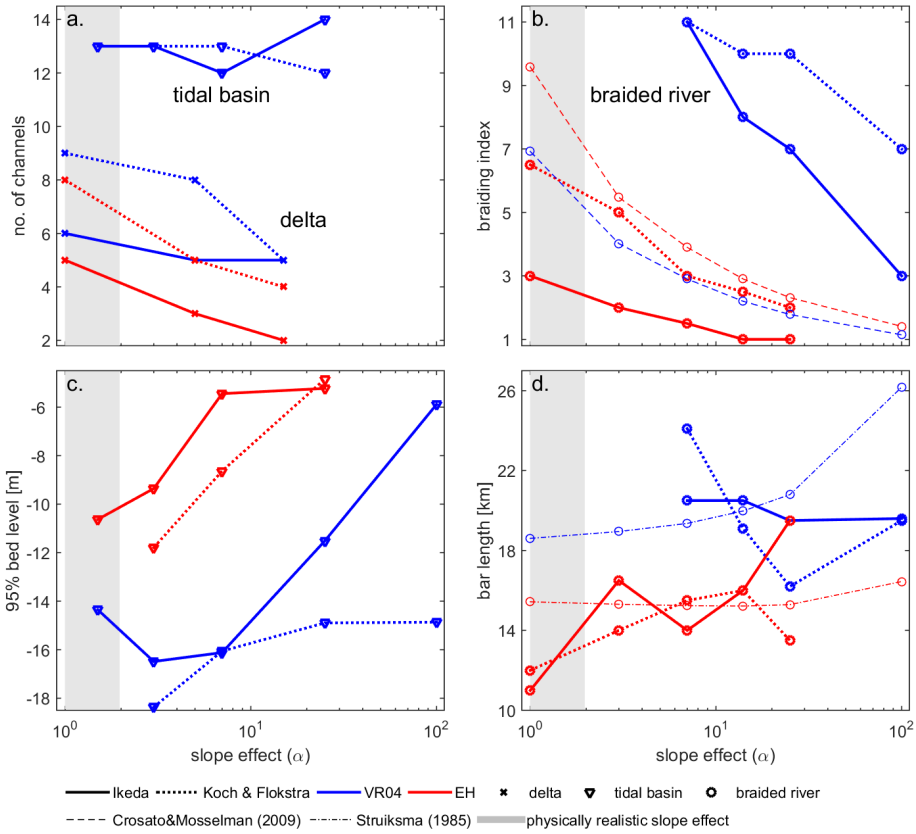

Figure 5.9: a) Number of channels at the delta front in the delta models, and the number of channels in the tidal basin models, against increasing slope effect. b) Braiding index with increasing slope effect in the braided river model, with the semi-analytical predictor for braiding index from Crosato and Mosselman (2009) in corresponding colors for comparison. c) The 95% depth of all tidal channels in the tidal basin models against slope effect. d) Mean bar length in the braiding river model when increasing the slope effect, including the predictor of Struiksma and othersStruiksma et al., 1985 for wave lengths of bars. Braiding index and bar length are computed according to the methods described in Schuurman et al. (2013). The method of determining the number of channels in the tidal basin models is explained in Section 5.4.4. Slope effect is given as the α_I for IK and transformed for KF.

the braiding index predictor of Crosato and Mosselman (2009), especially at a lower slope effect. However, models with the KF slope parameterization had braiding indices that were only slightly lower with a higher slope effect than the braiding index predictor, and generally showed the same trend in decreasing braiding index with increasing slope effect. Models with the VR sediment transport predictor theoretically should have lower braiding indices due to the lower non-linearity of sediment transport, but in these models many deep and narrow channels developed separated by long bars (Fig 5.5). Only with downslope sediment transport that was almost a hundred times larger than with the default value, realistically shaped bar patterns developed, but the braiding index was still too high.

In general, bar length in the braided river model increased with increasing slope effect in models with the EH sediment transport predictor, but for the models with the IK slope parameterization bar length showed a local decrease with an intermediate slope effect (Fig. 5.9d). For strong slope effects, a subdued morphology is visible with short and wide bars. Bar length also decreased slightly in the model with the KF slope method and with the largest amount of downslope sediment transport. Predicted bar length by Struiksma et al. (1985) is in the same range as the models, but show a much more stable bar length with an increase in slope effect. As a result, bars in the braided river model are theoretically longer when the slope effect is weak, and shorter when the slope effect is strong. Models with the VR predictor showed a decreasing bar length with increasing slope effect, since here cross bar channels started to dissect the unnaturally long bars separating the deep channels, or started show realistically shaped bar patterns in the case of the model with the IK slope parameterization. The bar length predictor predicts increasing bar lengths with increasing slope effect, which is therefore not comparable with bar lengths in the braided river models with the VR predictor.

The number of avulsions in the delta models is larger for runs with the KF bed slope predictor compared to runs with the IK parameterization, even though sediment transport rates were equal for models with an equal downslope sediment transport. Models with VR had a larger number of avulsions compared to models with the EH predictor with equal slope effect (Fig. 5.9a). In contrast, the tidal basin model shows that the number of channels is not significantly affected by increasing downslope sediment transport in an erosive environment (Fig. 5.9a). Furthermore, the amount of incised channels was also similar between models with different slope parameterizations. The magnitude of the bed slope effect did have an influence on channel dimensions, since in general channels became shallower with increasing downslope sediment transport (Fig. 5.9c). However, models with the VR transport predictor and IK slope predictor needed a much larger slope effect to counteract severe incision than models with the EH transport predictor, and in combination with the KF parameterization there is no significant effect of increasing the slope parameter on channel depth.

5.2.5 Slope effect-depended dynamics in the calibrated model of the Western Scheldt

The fifth set of models is a detailed case study of the topographically forced Western Scheldt estuary in the Netherlands, to test the sensitivity of a calibrated model with two different slope parameterizations in comparison with measured bathymetry. This topographic forcing is typical for many natural and engineered systems and is important because it limits free bar and pattern formation, rendering models less sensitive in large-scale pattern to chosen parameterizations. Here, we focused on differences in local sediment transport dynamics in two model runs with different slope predictors that showed the same large-scale morphology in view of the need to predict sediment transport rates for fairway maintenance dredging. After 10 years of morphological development, these models reproduced the cumulative slope distributions that were closest to the actual morphology of the Western Scheldt that was used as input (Fig. 5.6c). The models had a strong slope effect, namely an α_I of 30 and an α_K of 0.05, which again shows that a higher than physical slope effect is needed when calibrating the Western Scheldt model on existing morphology.

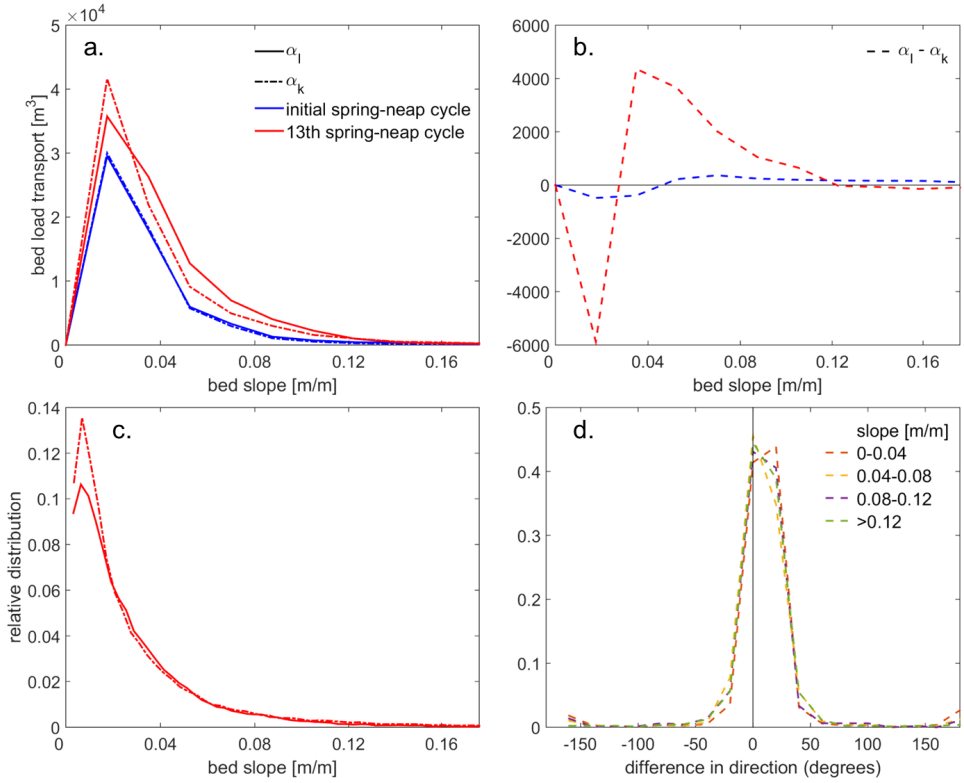

Figure 5.10: (a) Total amount of sediment transported on specific bed slopes for both Western Scheldt models with different slope parameterizations, at the beginning and at the end of the model run. (b) The difference in sediment transport between both slope parameterizations on specific bed slopes. (c) relative distributions of bed slopes in both Western Scheldt models. (d) Difference in direction of sediment transport between the models with different slope parameterizations. This distribution shows the relative abundance of these differences for all grid cells in the model.

While large-scale morphology is similar between both models after ten years (Fig. 5.6d), the dynamics differ in local sediment transport. The model with the IK method has higher bed load transport rates on steeper slopes, while the model with the KF method has higher transport rates on lower slopes (Fig. 5.10). Furthermore, there is a significant difference in direction of the transport vectors in more than half of all grid cells in the model (Fig. 5.10d), which is independent of slope. These differences in direction and magnitude imply locally channels can be orientated differently and location and speed of bank erosion will differ. For fairway maintenance dredging this means that predicted time scales can significantly differ when models are calibrated with a different slope parametrization on the same measured morphology.

5.2.6 Effect of grid size on incision

Finally, grid size is systematically varied for the tidal basin model and braided river model, to study if the overdeepening of channels is a numerical diffusion issue. For the braided river

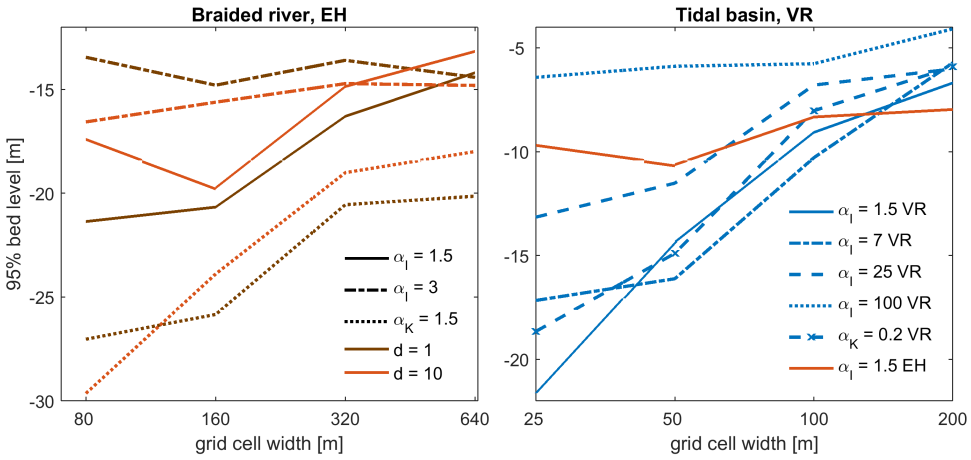

Figure 5.11: Tendency to incise quantified as 95% depth against size of the grid cells of (a) the braided river model modelled with the EH transport predictor in combination with a horizontal eddy diffusivity (d) of 1 or 10, and (b) of the tidal basin model with the VR04 transport predictor compared with the model with the EH predictor and default slope effect ($\alpha_I = 1.5$).

model with the EH transport predictor, channel depth in the model with the KF method decreased with increasing grid cell width (Fig. 5.11a), while the model with the IK method with the same slope effect ($\alpha_I = 3$) did not show a significant decrease. However, the model with the default value for the IK method ($\alpha_I = 1.5$), and therefore with an even lower slope effect, did show a decrease in channel depth. In these braided river models also the horizontal eddy diffusivity was changed from 10 to 1, and this resulted in slightly different distributions of channel depth, but did not have the same amount of influence as increasing grid size or changing slope effect. Increasing grid cell width in the erosional tidal basin model resulted in less incision with increasing grid size for all models with the VR transport predictor, except with a very high slope effect (α_I=100) (Fig. 5.11b). In contrast, channel depth in the model with the EH transport predictor and default slope effect does not show a trend with grid size.

5.3 Discussion

The emerging explanation for unrealistic channel incision and high braiding index common in morphological models is twofold. Firstly, the sediment transport predictor sets the balance between transverse sediment transport and channel incision, which explains why the choice of sediment transport predictor has a major influence on large-scale morphology. Simple transport predictors such as EH and the general predictor overdampen perturbations due to the high sediment transport rate and because slope effects act on all sediment transport. On the other hand, VR initially predicts the correct balance between incision and downslope transport in accordance with the analytical model. However, once incision commences, it needs much higher slope effects to counteract incision than in theory. This can be explained by the distinction of suspended and bedload transport, since bed slope effects only act on

bedload. Consequently, the tendency to incise depends on grain size and sediment mobility (Dastgheib and Roelvink, 2010; Nicholas, 2013; Schuurman et al., 2013). Several studies commented on the uncertainty of how slope effects act on suspended sediment and how the vertical distribution in the water column affects this (Talmon et al., 1995; Schuttelaars and De Swart, 1999; Walstra et al., 2007), and concluded that the parameterization of transverse sediment transport is therefore complicated in sand-bed rivers. Secondly, the amount of incision is highly depended on grid size, suggesting strong resolution and numerical diffusion effects. When a channel incises, the channel will attract more flow and will experience a positive feedback. The flow seems to prefer flowing through as few grid cells as possible, and when grid cell width is smaller this means that there is more discharge flowing through a smaller area, which therefore results in more incision. The initial response will determine this positive feedback and dependency on grid size, and therefore especially models with weak slope effects experienced a more extreme deviation in channel depth, braiding index and bar length. With a sufficiently high slope effect this grid size-dependent incision is counteracted (Fig. 5.11), which thus depends on transport predictor, slope parametization and sediment mobility as described above. Numerical diffusion is also the reason why the model of Nnafie et al. (2016) experienced extreme subdued morphology, and on the other hand why the model of Dam et al. (2016) showed realistic bed slopes even though the model did not include any slope effects, since all sediment was assumed to be transported in suspension.

The methods of Ikeda (1984) and Koch and Flokstra (1981) to calculate downslope sediment transport indeed cause different sediment transport magnitudes and directions, even though the amount of downslope sediment transport are equal, due to the different methods of calculating the deflection of the transport vector. This affects the timescale of morphological adaptation, sediment division at bifurcations and frequency of avulsion (Kleinhans and van den Berg, 2011), meander migration rates (Van Dijk et al., 2014) and braid plain reworking.

Pending further investigations into sediment transport parameterizations and numerical effects, we here develop recommendations for model setup depending on environment and research objectives to help avoid inadvertent artifacts due to arbitrary choices. Our recommendations based on the results of this study are summarized in figure 5.12. Firstly, the environment determines the sensitivity of the morphodynamic model to changes in bed slope effect. Environments that depend on a balance between erosion and deposition, e.g. estuaries and dynamic rivers, are the most sensitive, and therefore we will discuss these first. In balanced systems, the characteristic adaptation length of the bed to the flow conditions (Struiksma et al., 1985) increases with slope effect, resulting in longer and wider bars and increasing active channel width, which therefore can result in weaker braiding and fewer bifurcations. Secondly, the objective of the model study should determine the choice of sediment transport predictor. The total load EH predictor is much more sensitive to an increase in slope effect and needs much lower slope effects to counteract incision, due to its tendency to overdampen perturbations. Even though theoretically sediment transport rates are too high, this predictor will therefore lead to more realistically shaped bars and channel networks in systems were the balance between incision and downslope sediment transport is essential. However, if the objective is to have sediment transport magnitude and morpho-

logical adaptation right, the VR transport predictor works better. Furthermore it makes the distinction between bed load and suspended load which is important for example in tidal environments with waves, varying flow directions, or mud. A downside is that models with the VR transport predictor need extremely high slope effects to balance incision since slope effects only act on the bed load, as shown by the results from the channel model. As a result, the morphology was unnaturally shaped with extremely high braiding index and bar length. Thirdly, the method to calculate transverse sediment transport should be considered. As was observed with the braided river models with the EH transport predictor, the dramatic increase of total sediment transport when slope effects were increased with the IK method had a very different effect on bar shapes compared to a larger rotation of the transport vector with the method of KF. This increase in sediment transport results in a more subdued morphology with a lower braiding index than predicted, and wide and relatively short bars since a larger part of the sediment is deflected transversely. The KF method does not increase the total sediment transport, and braiding index therefore showed more similarity with the braiding index predictor of Crosato and Mosselman (2009). Practically, it is only advisable to combine the VR predictor with the IK slope method and an extremely high slope effect, which in the braided river model resulted in a significant decrease in braiding index and more realistically shaped bars. The KF method only rotates the transport vector and does

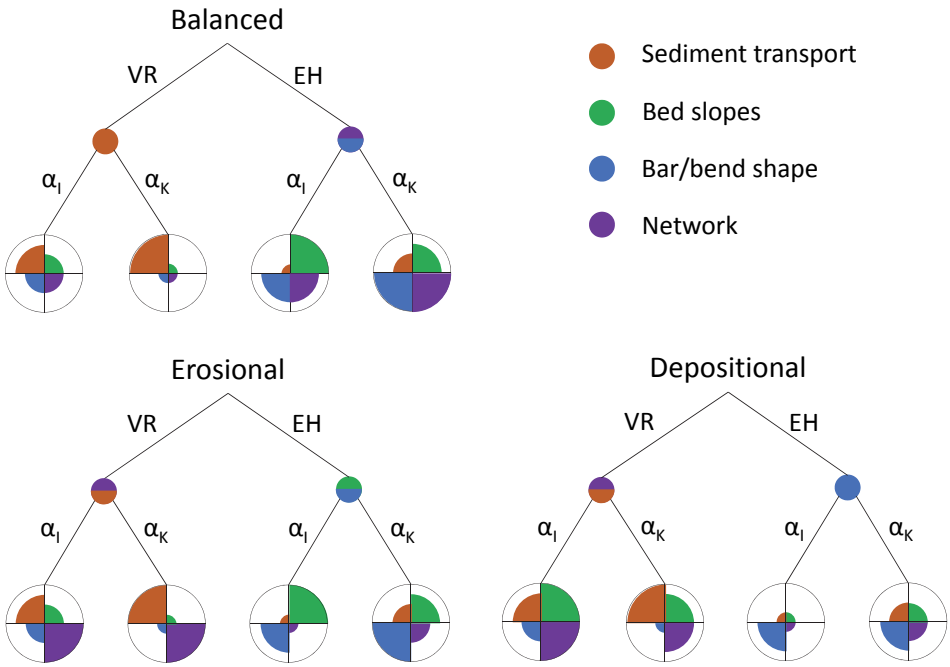

Figure 5.12: Relative performance for each combination of transport predictor and slope method in models of different environments. Relative performance is divided in four categories, such that the choice of predictors can be made depending on the research objective.

not increase total sediment transport, and thereby cannot balance severe incision by the VR transport predictor, so that it results in unnatural bar and channel patterns.

Erosional and depositional models show different behavior with both sediment transport predictors. Models with the EH transport predictor are too diffusive to model channel networks realistically, and in case of depositional models it is also difficult to get realistic channel dimensions and bed slopes. On the other hand, models with the VR transport predictor show a more realistic channel network and sediment transport magnitudes. However, also these models show steeper bed slopes due to the imbalance between incision and downslope sediment transport. This is exacerbated with increasing sediment mobility and decreasing sediment size which also leads to more suspension (Nicholas, 2013; Schuurman et al., 2013). This is the reason that models with a relatively large amount of suspended sediment and default slope effects show unrealistically sharp bends with up to 90 degree angles, since there is less downslope sediment transport to counteract secondary flow. These sharp bend are for example visible in many depositional model results like the delta model of Van der Vegt et al. (2016), who studied the effect of decreasing the ratio between bed load and suspended load, and the delta model of Edmonds and Slingerland (2009) and Caldwell and Edmonds (2014), who studied the effect of different grain sizes. In depositional and erosional models the difference in effect of both slope options on large-scale morphology is smaller than in environments that depend on the balance when increasing slope effect. At the delta deposit, the number of channels and the bifurcation angles decrease, but at a similar rate for both slope options. However, in the erosive tidal basin model the number of channels is not determined by the magnitude and direction of downslope sediment transport, but seems to be related to the dimensions of the basin. Nevertheless, the slope effect does determine channel dimensions, and again models with the KF parameterization show deeper and narrower channels. Altogether, it seems that when the slope effect is increased with an order of magnitude or even larger, the extreme increase in sediment transport with the IK parameterization will have the largest impact on large-scale morphology.

All these observations have major implications for models that are used for management decisions about, for example, navigation and engineering, as the direction and time scales of sediment transport are heavily dependent on the choices made for downslope sediment transport in combination with the choice of sediment transport predictor. When these models are calibrated on morphology, different methods to calculate downslope sediment transport will lead to locally deviating transport magnitudes and direction, which therefore affects the time scale of for example fairway maintenance dredging and the migration rate and direction of dumped sediment, and different channel migration rates and locations of bank erosion. For example, calibrating the Western Scheldt model with different methods to calculate slope effects resulted in differences in local sediment dynamics, even though models had the same large-scale morphology and cumulative slope distributions. However, when a model is calibrated to sediment transport time scales, meaning streamwise and transverse sediment transport rates are similar to measured values, morphology and bed slopes will differ between different methods. We can therefore conclude that when models are calibrated by increasing downslope sediment transport, either sediment transport magnitude or bed slopes match to measured data, while both is not possible. Furthermore, it is highly neces-

sary to further research the effect of numerical diffusion and grid size on incision, and the parameterization of transverse sediment transport on suspended sediment transport.

5.4 Methods

The morphodynamic modelling package DELFT3D FLOW2D3D version 6.02.13.7658 was used in all models in this study. For all models, the depth-averaged version with parameterization of secondary flow was used. In this chapter, we describe the set-up of each model in detail. in Table 5.1 the physical and numerical parameters of interest are summarized for all five models.

5.4.1 Channel model

We set up a simple river channel in Delft3D for comparison to the analytical model to study the tendency to incise due to imbalance between incision and downslope sediment transport (Appendix C. This river channel has 3 grid cells across the channel, and two additional outer cells with a bed level that is 7 meters higher than the inner three cells to avoid boundary effects. This means that these outer two cells are above the water level and do not interact with the channel. As a result, the active channel has the same cross-section as the analytical model (Fig. C.1). The discharge is equally partitioned over the three grid cells as three upstream boundary conditions.

The default model run has a channel with a length of 10 km, a slope of 0.5 m/km, a Chezy coefficient of 40 $\sqrt{m}/s$, a ratio between discharge Q and channel width W of Q/W=12.5 m^2/s, and a grain size of 0.5 mm, which is all equal to the default analytical model. As a result, the average water depth is 5.8 m. The IK method is used for slope effect, with an α_I of 1.5. To be able to compare the model behavior to the analytical model results, we varied the channel width between 21 and 210 m, the bed level difference of the middle grid cell and the surrounding cells between 0.01 and 3 m, and the α_I between 1.5 and 50. Furthermore, we either used the VR sediment transport predictor, which relates the transport rate to the flow velocity to the power of 3 (k=3) at higher mobility, or the EH predictor, where the transport rate is related to the flow velocity to the power of 5 (k=5). To test if the model results depend on the varied parameters or on the implementation of the specific transport predictor, we

Table 5.1: Overview of the default physical and numerical parameters of interest for all five Delft3D models used in this study.

model	channel	braided river	river delta	tidal basin	Western Scheldt
environment	river	river	river with tides	tides	estuary
grain size [mm]	0.5	0.2	0.25	0.125	0.2
roughness coefficient	C=40	k_s=0.15	C=50	C=50	n=0.022 -0.028
time step [min]	0.1	0.1	0.5	0.5	0.25
morphodynamic run time [yr]	0.33	2	1000	200	10
MorFac	1	25	200	200	20
grid size LxW [m]	7x7 to 67x67	200x80	100x50	50x50	250x120 120x50

run the same models with the general transport predictor in combination with both the IK and KF slope parameterization, with and without the critical shear stress, and varied the non-linearity between 3 and 10. The models were run for two months, after which either the perturbation caused larger bed level differences and 1 grid cell wide bars to form, or the perturbation decayed and the three grid cells showed the same bed level.

5.4.2 Braided river

The braided river model was inspired by the Jamuna river and is the same model that is used and described in detail in the study of Schuurman et al. (2013). The model consists of a 3.2 km wide and 80 km long braidplain, with a slope of 0.093 mm/m. The total discharge was 40000 m^3/s, partitioned over 20 cells at the upstream boundary, with an initial water depth of 5 m. The initial bed and the discharge were slightly perturbated to stimulate bar development. The bed level of the upstream grid cells differed by 1 cm, and the partitioning of the discharge between the upstream grid cells varied sinusoidally through time over the cross-section, with an amplitude of 200 m^3/s and a period of 2.28 days. In this study, the model was run for 2 years at the morphodynamic time scale.

5.4.3 River delta model

The river delta model was inspired by the Old Rhine river mouth at Leiden, The Netherlands, from the mid-late Holocene (Geleynse et al., 2010). It consists of a 20 km long river that flows into the coastal domain delimited as a 10 km by 10 km sloping bed, where the sediment is deposited and a delta is formed. Initially, the river is a 7 m deep channel with a width of 0.5 km for the first 15 km from the upstream boundary, after which it exponentially expands over the last 5 km towards a width of 3 km at the river mouth. The sea has a depth around 4 meters at the river mouth, increasing towards the end of the model domain. The upstream boundary consists of a constant discharge of 1750 m^3/s and at the downstream water level boundary a M2 tide is prescribed with an amplitude of 0.7 m. The model is run for 5 years at the hydrological time scale with a morphological scale factor of 200, resulting in a morphological run time of 1000 years.

5.4.4 Tidal basin model

The tidal basin model consists of a coastal domain of 7 by 3 km and a tidal basin of 7 by 5 km, connected by a 1 km wide inlet. The water depth at the basin is initially 1 m, and the coastal domain slopes up to 15 meters depth. A 0.75 m amplitude M2 tide is prescribed at the north and south coastal boundary with a phase difference in order to create an alongshore tidal current. The initially flat tidal basin, evolves with incisions due to the tidal induced currents, promoting a rich channel network. The model is run for 12 months at the hydrological time scale with a morphological scale factor of 200, resulting in a morphological run time of 200 years. Figure 5.13 shows two bathymetries of model runs with the default slope parameter in the IK method ((α_I = 1.5), and with an α_I of 25. A characteristic number of channels is determined at a fixed distance from the inlet of 2.5 km.

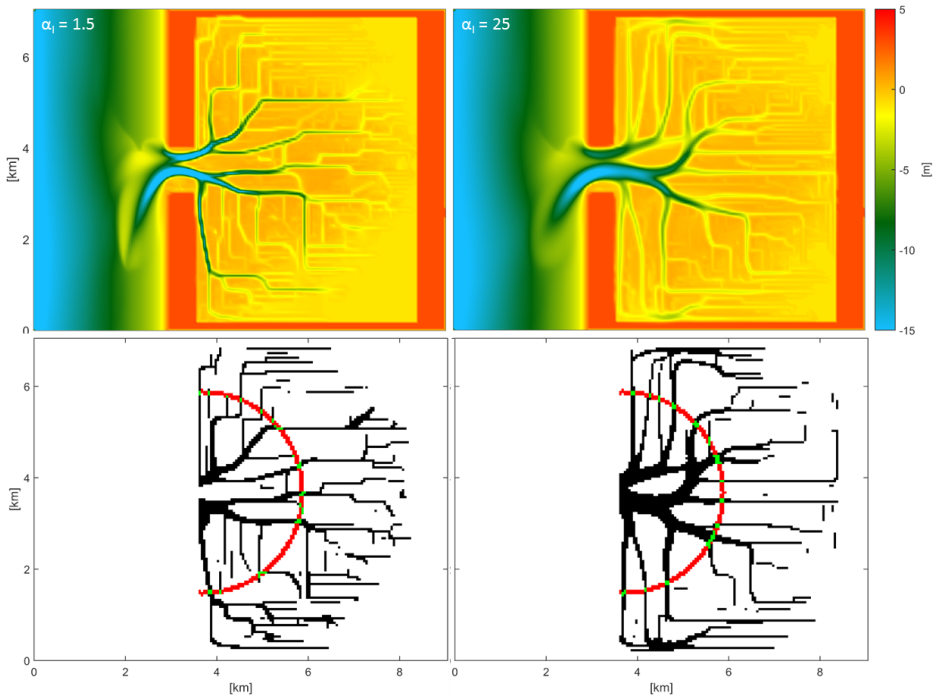

Figure 5.13: Bathymetries of the tidal inlet model with the IK method in combination with an α_I of 1.5 (default) and 25, and their corresponding binary image, where channels are black and the surrounding area is white.

5.4.5 Western Scheldt estuary

The Western Scheldt estuary model is based on the NeVla-Delft3D schematization of the Scheldt estuary, which includes the upstream Flemish branches of the estuary, the Western Scheldt and part of the North Sea. The NeVla-Delft3D model is a schematization from the fluid-flow behavior of the Simona simulation used by Rijkswaterstaat (the Netherlands) combined with the Delft3D component for sediment transport and morphodynamics. The NeVla model is a state-of-the-art numerical model that has been optimized for hydrodynamics (Maximova et al., 2009b; Vroom et al., 2015) and morphology (Grasmeijer et al., 2013; Schrijvershof and Vroom, 2016) and is applied by the Dutch and Belgian government.

Here, we used a nested model of the NeVla-Delft3D schematization focusing on the Western Scheldt partly for reducing the computational time, which is also used by Van Dijk et al. (subm). The model boundaries include the Western Scheldt from the mouth at Vlissingen to the Belgian border, in which the seaward boundary includes a water level fluctuation due to tides and the landward boundary a current. For simplification the boundaries consist of a repeating spring-neap tidal cycles. Sediment fraction was uniform with a median grain size of 200 μm. The roughness field in the model is defined in Manning n and is variable over the model domain, which was 0.022 $s \cdot m^{-1/3}$ for the eastern part, and 0.027 $s \cdot m^{-1/3}$ for the western partMaximova et al., 2009b; Maximova et al., 2009a; Maximova et al., 2009c;

Vroom et al., 2015; Van Dijk et al., subm. The bed consisted of erodible and non-erodible layersGruijters et al., 2004; Dam and Bliek, 2013, and therefore sediment thickness varies within the Western Scheldt model, which reduces the morphological changes but not the transverse bed slopes. To reduce computational time the wind direction and magnitude as well as salinity were excluded because of they have no effect on the transverse bed slope. We applied a morphological factor of 20, to reduce computational time and evaluated the model runs after 10 years of morphological changes.

We assessed the effect of sediment transport, and the transverse bed slope predictor and its calibration parameter α_I or α_K on the sediment transport and morphodynamics within the Western Scheldt model.

Acknowledgements

The authors declare that they have no competing financial interests. Correspondence and requests for materials should be addressed to A.W.B. (email:annebaar@gmail.com).

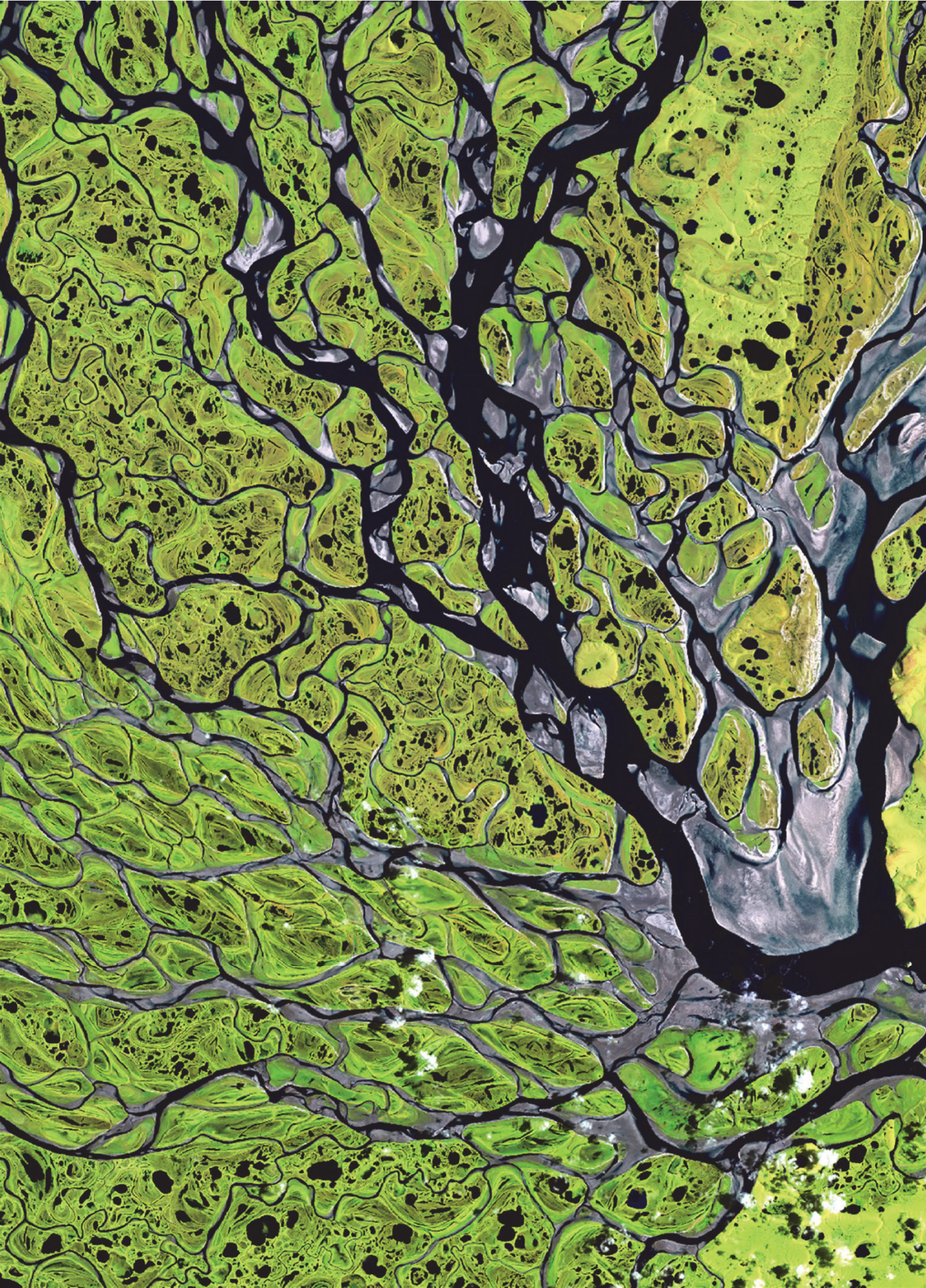

Chapter 6

Improving large-scale morphodynamic models starts at small-scale bed slope effects: a discussion

6.1 Introduction

The two main objectives of this thesis were 1) to quantify the physical processes that influence sediment transport on transverse bed slopes, and 2) to identify the cause of the severe incision in morphodynamic models and why there are extremely large differences in transverse slope parameter needed to counteract this incision. Firstly, the influence of bend flow, sediment characteristics and bedforms on the equilibrium between secondary flow and transverse sediment transport were quantified with experiments in a rotating annular flume (Chapter 2, 3, 4). Secondly, long-term numerical simulations bracketing a range of scales and environments were conducted (Chapter 5).

The general findings are illustrated in Figure 6.1, which shows the trend in slope factor (B) with increasing sediment mobility for the experimental results, and illustrates the range in typical values for the transverse slope parameter used in current model studies. The slope factor represents the equilibrium between transverse slope and secondary flow intensity, and is defined as:

$$\frac{\partial z_b}{\partial y} = B\frac{u_n}{u_s} \tag{6.1}$$

Where $\frac{\partial z_b}{\partial y}$ = average transverse slope, u = average magnitude of the near-bed flow velocity [m/s] in transverse direction (n) and streamwise direction (s). The secondary flow intensity for each experiment is defined as the direction of the flow near the bed, i.e. the ratio between the magnitude of the normal flow and secondary flow.

This thesis has shown that the balance between secondary flow intensity and transverse slope is a non-linear relation with sediment mobility (Chapter 2), which is grain size dependent due to differences in bedform morphology (Chapter 3, Fig. 6.1a,b). This is in contrast with the linear relations described in previous literature (e.g. Ikeda, 1984; Hasegawa, 1981; Sekine and Parker, 1992) that are implemented in morphodynamic models. Furthermore, sediment sorting is quantified as a function of transverse slope, but sorting had no effect on the average transverse slope (Chapter 4). Even though the experimental results show a new relation with sediment mobility, the resulting transverse slope parameter is in the same order as default values in morphodynamic models (α 1) which was based on literature (Ikeda, 1984; Koch and Flokstra, 1981). The increase of the transverse slope parameter up to two orders of magnitude that is needed to obtain realistic morphology is therefore well outside the range of the experimental findings, and implies an imbalance between incision and downslope sediment transport in the models due to another cause. The tendency of models to incise depends on the suspended sediment transport rate and on grid size, and arbitrary bed

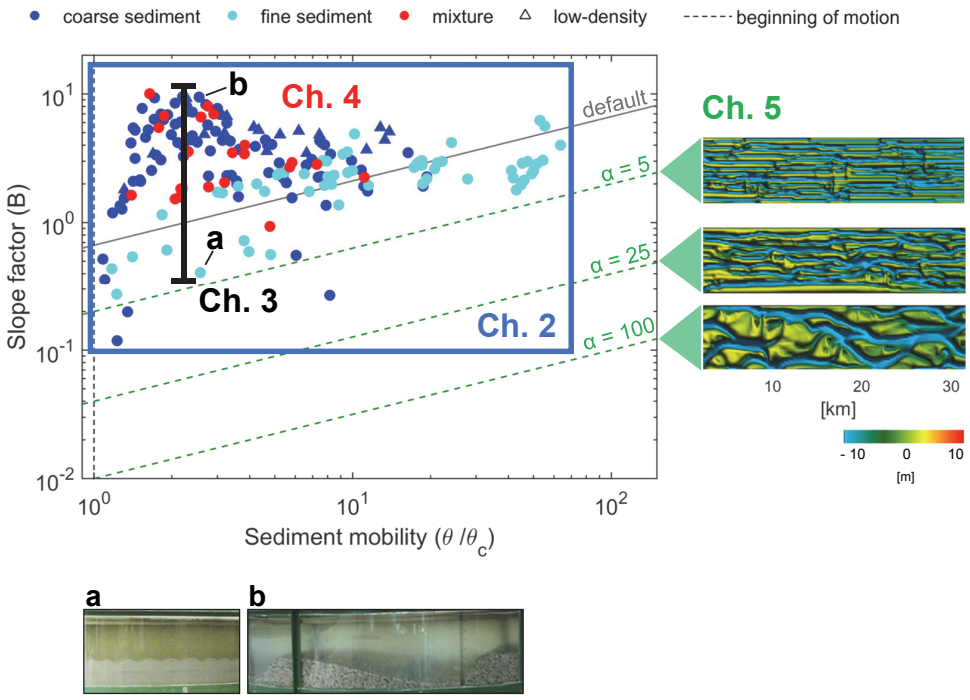

Figure 6.1: Trend in slope factor (B, Eq. 6.1) against relative sediment mobility (θ/θ_c) for all experiments described in this thesis (scatter). a and b show examples of an experiment with ripples (a) and with dunes (b). This experimental data is compared with the generic predictor of van Bendegom (1947) with typical parameter values as used in morphological modelling (lines).

slope calibration to counteract this incision may cause an order of magnitude error in rate of morphological change, channel depth, degree of braiding and bar dimensions (Chapter 5).

In order to seek the explanation for the sensitivity of large-scale morphology to local sediment transport direction and magnitude, in this chapter I first focus on the imbalance between transverse sediment transport and incision, by discussing both the new non-linear relation with sediment mobility that was found in the experiments and the cause of extreme incision in morphodynamic models. Then, I examine the effect of this imbalance on channel dynamics and consequently on the larger scale morphology, analyze the role of environment and discuss the implications for calibrating large-scale models for decision making. I end with recommendations for further research to improve both the unrealistic incision in morphodynamic models and the relation of transverse sediment transport.

6.2 Transverse slope effect: a non-linear relation with sediment mobility

This thesis shows that the balance between the transverse slope effect and secondary flow is not linearly related to a power function of sediment mobility, as suggested in previous literature, but severely depends on several sediment transport processes that act together

(Chapter 2). This means that with increasing sediment mobility, the transverse slope will not be proportionally increased, due to a different interaction between bed state or sediment transport mode with the flow conditions. In this section, the influence of these sediment transport processes on the equilibrium between secondary flow and transverse slope is discussed, thereby explaining the non-linear relation with increasing sediment mobility. This new-found relation is limited by gravity in two ways. Firstly, there is a minimum shear stress needed to entrain sediment, i.e. the threshold of sediment motion, since the transverse slope cannot fully develop when not all sediment is in motion over the channel cross-section. Secondly, gravity sets the maximum angle that can be reached, leading to a transverse slope that is equal to the angle of repose.

The equilibrium between secondary flow and transverse slope with increasing sediment mobility is grain-size dependent, since this determines the mobility of the sediment, bed state (Van den Berg and Van Gelder, 1993) and the dominant mode of sediment transport (Bridge, 1992; Bennett et al., 1998). Firstly, to accurately describe the trends in average slope of experiments with different grain sizes under the same conditions it is necessary to include a critical sediment mobility, as the different grain sizes have different critical sediment mobilities and therefore a different offset. This is assuming the sediment is uniform, or sorted out spatially. The poorly sorted sediment mixture in this thesis was chosen such that it was unimodal and all sediment fractions were mobile over a wide range of sediment mobilities to avoid size selective transport. This means that in this case the critical bed-shear stress did not vary much with size fraction, and the D_50 is an accurate representation of the sediment mixture (Kleinhans and van Rijn, 2002).

Secondly, the bed state is the cause of a difference in equilibrium slope at low and intermediate sediment mobility between grain sizes larger and smaller than 0.7 *mm* (Chapter 3). Dunes in coarse sediment showed a direct relation between transverse slope and grain size dependent dune lee side angle, as sufficiently high lee side angles likely resulted in flow separation (e.g. Lefebvre and Winter, 2016) that enhanced secondary flow in the dune troughs. As a result, transverse slopes were steeper than in the experiments with fine sediment with the same streamwise and secondary flow (Fig. 6.1). In experiments with fine sediments, different bed states developed, ranging from ripples, dunes with superimposed ripples, dunes, to an upper stage plane bed. These bedforms showed no direct interaction with the secondary flow, and lee side angles mainly depended on bedform morphology instead of grain size.

Thirdly, grain size determines the dominant mode of transport. The mode of transport theoretically influences the transverse slope by determining the effective gravity acting on the grains, since saltating or suspended particles have less contact with the bed than rolling or sliding grains (Sekine and Parker, 1992). Saltating grains would be dragged further along with the flow, resulting in a smaller angle of deflection, while suspended particles do not interact with the slope at all. However, both the transition from rolling bed load towards saltating particles and from saltation to suspension show no clear relation with changes in the trend of transverse slope with increasing sediment mobility. Experiments with coarse sand (1 and 2 mm) did show a decrease in transverse slope at the transition to saltation, but experiments with fine gravel (4 *mm*) already showed saltation at much lower sediment mobility and in combination with higher transverse slopes. This observation is counter-intuitive,

since larger grain sizes theoretically need a higher sediment mobility to loose contact with the bed (Bridge, 1992). Around the transition to suspension in the experiments with fine sediment, the equilibrium between transverse slope and secondary flow intensity became independent of sediment mobility and could reflect the smaller influence of gravity. However, transverse slopes in the experiments with coarser sediment were in the same order of magnitude at high sediment mobilities and also suggested to go towards a constant trend.

Sediment transport mode has an effect on the transverse slope due to the change in contact with the bed, and thus how far the flow can drag along the grains before they are deflected downslope. In morphodynamic models, the bed load effect does not act on the suspended sediment load, which is why models with a large suspended sediment fraction need higher transverse slope parameters to increase downslope sediment transport to counteract severe incision (van der Wegen and Roelvink, 2012; Dissanayake et al., 2009; Braat et al., 2017). Further research is needed into the relation between sediment transport on transverse slopes and the relative amount of suspended sediment. Furthermore, sediment transport mode possibly controls transverse slope effects indirectly by influencing bedform dimensions and vice versa. For example, it is not yet explained why dune lee side angles are lower with smaller grain sizes, which could be related to a longer travel distance over the dune crest, since saltation length theoretically increases with smaller grain sizes (Bridge, 1992). Additionally, bedform lee side angles could also explain the observation that fine gravel experiments showed saltation at low sediment mobility. Chapter 3 showed that these experiments were characterized by long bed load sheets with steep lee sides, that theoretically should have permanent flow separation (e.g Best, 2005; Lefebvre and Winter, 2016). During the experiments, grains detached at the bedform crest and followed the recirculating flow above the zone of flow separation. These experiments were therefore classified as experiments with saltation, but actually say more about the presence of flow separation.

The new, process dependent, relation between bend flow and transverse sediment transport that was found in the experiments is expected to have a significant effect on modelled local bed slopes, channel and bar dimensions, and consequently on channel patterns. At low and intermediate sediment mobility, experiments with coarse sediments ($> 0.7\ mm$) show up to six times steeper transverse slopes than the experiments with fine sediments, which show the same slope parameter as the default value in morphodynamic models (Fig. 2.12b). The model study in Chapter 5 shows that this will result in narrower and deeper channels, shorter bars, and a larger braiding index (Fig. 5.9). Furthermore, at high sediment mobilities the slope effect is constant with increasing sediment mobility for all sediment sizes, which means that a change in sediment mobility has a larger effect at lower mobilities. This is therefore especially important in areas with low sediment mobility where a significant difference in sediment mobility over time or space occurs, e.g. near channel banks and shoal margins. How exactly a nonlinear bed slope relation changes the local morphology remains to be studied.

Even though the experimental results show a new relation between bend flow and transverse sediment transport, resulting transverse slope parameters are still in the same order of the default values in morphodynamic models in case of the fine sediment experiments, or even lower for most of the coarse sediment experiments (Fig. 6.1). This implies that the need

to artificially increase the transverse slope parameter in models to counteract severe incision is not caused by the oversimplified implementation of the transverse slope effect. Furthermore, experiments with a sediment mixture showed that bend sorting had no influence on the magnitude of the transverse slope when all sediment fractions were mobile, which means that the use of a uniform grain size in models can also not explain the overdeepening of channels of all modelled environments. Therefore, the use of coarser sediment fractions in morphodynamic models might be effective to counteract incision (e.g. Davies and Robins, 2017; Dastgheib and Roelvink, 2010) but is not physically realistic and likely hampers the dynamics of the system.

Since the experimental results show that the new-found relation of the slope parameter lies around the default value in morphodynamic models, this new relation will not solve the imbalance between incision and transverse sediment transport in morphodynamic models. This suggest that calibration by arbitrary increasing the transverse slope parameter up to two orders of magnitude is necessary to compensate for other model weaknesses. The question is what weaknesses, such as issues with numerical schemes or missing processes, could lead to unrealistic incision. The next section will therefore focus on identifying these processes that affect the balance between incision and transverse slope effect.

6.3 Imbalance between incision and transverse slope effect in morphodynamic models

The extreme incision in morphodynamic models is the result of an imbalance at the channel scale between the non-linearity of sediment transport that carves out channels and transverse sediment transport, and depends on grid size and the relative amount of sediment in suspension (Chapter 5). With the default transverse slope parameter, the flow seems to prefer flowing through as few grid cells as possible, and when grid cell width is smaller this means that there is more discharge flowing through a smaller area, which therefore results in more incision. This initial response determines whether a system tends to incise or goes towards an equilibrium channel by eroding the banks. The transition from grid size-depended incision to a more dynamic system is determined by the transverse sediment transport rate and can therefore be reached by increasing the transverse slope parameter (Fig. 5.11).

The magnitude of slope parameter that is needed to overcome grid size-dependent incision is determined by the bed load transport rate that is initially available for deflection downslope. This transport rate is calculated by the sediment transport predictor, which determines both the sediment transport rate and the ratio of bed load versus suspended load. The sediment transport predictor of Engelund-Hansen that relates sediment transport rate to flow velocity to the power of 5, has a higher sediment transport rate than the predictor of Van Rijn, which relates sediment transport rate to flow velocity to the power of 3. The predictor of Van Rijn furthermore makes a distinction between bedload and suspend load, and assumes the bed slope effect only acts on the bedload part. As a result, the predictor of Engelund-Hansen will deflect more sediment downslope than the predictor of Van Rijn at the same flow velocity, which will therefore need a lower slope parameter to counteract incision.

However, to understand which predictor behaves more naturally, it is necessary to compare these predictors to the theoretical equilibrium between incision and downslope sediment transport. In nature, the width-to-depth ratio determines if a perturbation grows or decays (Struiksma et al., 1985). Wider and shallower channels tend more to incise, so that larger bed slope effects are needed to prevent growth of channels, and this equilibrium determines the development of bars and sets the braiding index (Struiksma et al., 1985; Crosato and Mosselman, 2009). The transition between decay and growth of a perturbation is therefore a function between width-to-depth ratio and the transverse sediment flux, and was analytically described in Chapter 5 and Appendix C. Morphodynamic models with the sediment transport predictor of Van Rijn predict this transition reasonably well on the channel scale with default transverse slope values. However, once perturbations start to grow and channels start to incise the numerical models significantly deviate from the analytical model. Here, the numerical model with wider channels required a disproportionately larger slope effect to dampen the initial perturbation where the analytical model predicted this to occur. An extremely high slope effect is needed to generate enough downslope sediment transport from the bed load transport vector to counteract the disproportionately larger grid size-dependent incision. Since the transverse sediment transport rate depends on how much sediment is in suspension, the magnitude of the slope parameter that is needed to balance incision depends on grain size and sediment mobility, which was also observed by Dastgheib and Roelvink (2010) and Schuurman et al. (2013). From these results, it follows that even though the predictor of Van Rijn predicts the most realistic sediment transport rate, the absence of slope effects acting on suspended sediment transport leads to severely unrealistic model results. This again highlights the need for further research into the relation between sediment transport on transverse slopes and the relative amount of suspended sediment.

On the other hand, the predictor of Engelund-Hansen overdampens perturbations due to the high sediment transport rate, and therefore needs width-to-depth ratios that are significantly larger than the theoretical values for perturbations to grow. On the larger scale, this for example leads to a subdued morphology in depositional environments like the delta model in Chapter 5. This means that even though the predictor of Engelund-Hansen needs significantly lower slope parameters to counteract grid size-dependent incision due to the high bedload transport rates and therefore results in better-looking large-scale morphology, it does not necessarily predict the right bar and channel stability.

6.4 Transverse slope effect controls channel dynamics

The environment that is modelled controls the growth or decay of perturbations at the channel scale. Here, environment means the initial and boundary conditions, which determine sediment characteristics, flow conditions, channel pattern and bar regime. The environment therefore influences how likely models are to incise and how sensitive they are to changes in bed slope effect (Chapter 5). Environments with a large-scale balance between erosion and deposition, such as estuaries and rivers, particularly have the tendency to overpredict channel depth and braiding index and require very high slope effects to overcome the severe incision. With increasing slope effect, the characteristic adaptation length of the bed to

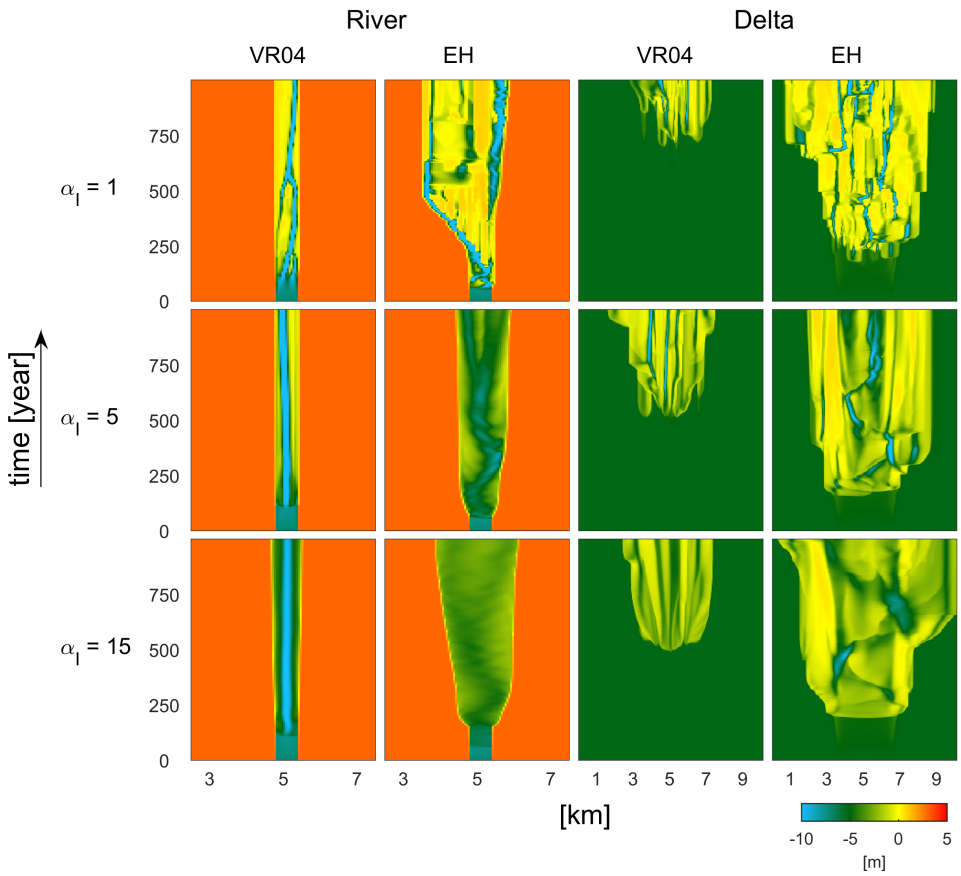

Figure 6.2: Development of the bathymetry of a cross-section at the river and at the delta over time in the delta model (for model setup, see Chapter '5), for different combinations of sediment transport predictor and magnitude of the slope parameter with the method of Ikeda (1984).

the flow conditions increases (Struiksma et al., 1985), resulting in longer and wider bars and increasing active channel width, which therefore can result in weaker braiding and fewer bifurcations. In contrast, depositional models like the delta model in Chapter 5 will show more natural looking bars with default slope parameters, although channels that form on the deposits will incise during the model run and can show unnaturally sharp angular bends that clearly follow the rectangular grid, as observed in model results by e.g. Edmonds and Slingerland (2009), Caldwell and Edmonds (2014), and Van der Vegt et al. (2016). Models of systems with dominant erosion, such as the tidal basin model, also show large incision and unnaturally shaped bends, but here increasing the transverse slope parameter will set these channel dimensions but not necessarily the number of channels (Fig. 5.9). These differences between environments can be explained by differences in lateral dynamics.

To model a dynamic system, the model has to overcome extreme incision at the channel scale by increasing slope effects. Only when this is balanced by downslope sediment trans-

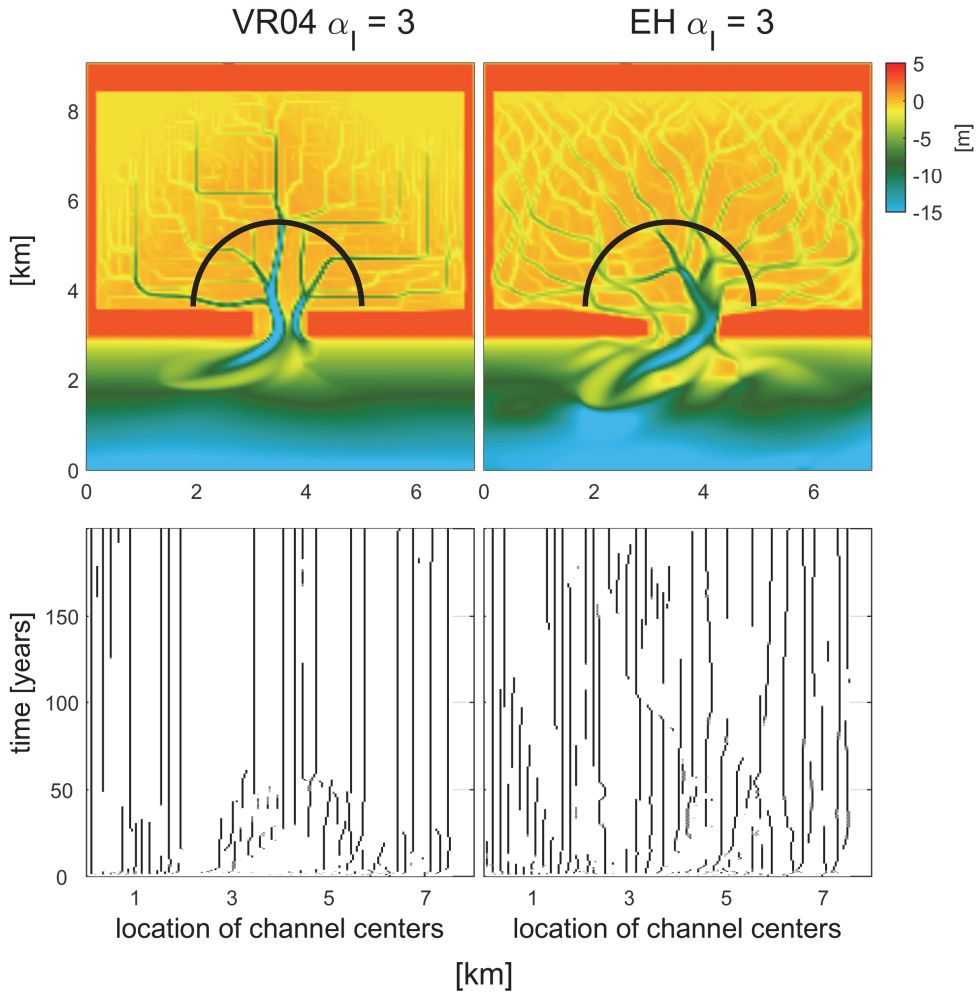

Figure 6.3: Difference in morphology between the tidal basin model (for model setup, see Chapter '5) with either the sediment transport predictor of Van Rijn or Engelund-Hansen. The lower two panels show the locations of the channel centers over time at the cross-section that is indicated with the black circle in the upper two DEMs. The slope parameter is constant and modelled with the method of Ikeda (1984).

port, the channel can migrate sideways. Large-scale morphology critically depends on these local lateral dynamics, which is illustrated in Figure 6.2 and 6.3. The delta model described in Chapter 5 initially exists of only a straight channel, before it starts transporting sediment and depositing it in the sea basin. However, over time, the river in the models with the transport predictor of Van Rijn stays within that initial channel without moving sideways, and only at a high slope parameter it starts to erode the initial banks (Fig. 6.2). In contrast, models with the sediment transport predictor of Engelund-Hansen are immediately much more dynamic. This illustrates the effect of the difference in slope effect needed to balance incision at the channel scale between both transport predictors. On the other hand, the delta is a depo-

sitional environment and depends on sedimentation instead of the non-linear incision, and therefore initially does not have to erode banks. As a result, depositional models with the sediment transport of Engelund-Hansen show a subdued morphology due to the large sediment transport rates, which is enhanced with increasing slope effects. However, the channels on the delta show similar dynamic behavior as in the river part of the model, since they incised in the deposited material. Once channels start to form in the models with Van Rijn, their location seems to be fixed due to the transverse sediment transport rate that is too low, while channels on the delta in models with Engelund-Hansen show lateral movement and regular avulsions. Channels in the erosive tidal basin model showed the same behavior: once a channel was formed in models with Van Rijn it was fixed to that location, while channels in models with Engelund-Hansen were still able to migrate (Fig. 6.3). Grid size-dependent incision and the resulting lack of channel migration also explains the angular bends that are observed in many models with the transport predictor of Van Rijn. The channels follow the grid configuration which is rectangular in this study, and therefore it is expected that models with an irregular shaped grid will show other bend shapes, but this does not mean that the problem of grid size-dependent incision and lack of channel migration is solved in this case.

The magnitude of the transverse slope parameter therefore depends on if a model needs to be laterally dynamic or not, and thus if it has to overcome the grid size-dependent incision. Therefore, the difference in slope factor that is used in dynamic, erosional or depositional systems in previous model studies is also explained by the research objective, next to flow conditions and the choice in sediment transport predictor. In models of a dynamic environment this is always the case, and that is why the literature study in Chapter 5 revealed that many models of these environments used high slope parameters. In case of erosional models, in some studies bank erosion was calibrated and therefore slope effects were increased, while the majority of the models presumably only focused on the network characteristics and therefore saw no need to increase slope effect. The default slope parameter was used in all depositional models in the literature review, most likely since morphology already looks rather realistic and increasing the slope effect would quickly lead to a diffuse morphology, even though channels on the delta incise and often show unnatural bends.

6.5 Recommendations for further research

Results from this thesis demonstrate the necessity for further research into the balance between incision and transverse sediment transport, since current morphodynamic models predict unrealistically high channel incision which is masked by increased downslope sediment transport up to two orders of magnitude too high. Future research should focus on:

1. *Slope effects on suspended sediment transport.* In morphodynamics models, the bed slope effect does not act on the suspend load, which causes more extreme incision with increasing sediment mobility and decreasing sediment size, resulting in static large-scale morphology with e.g long and thin bars and unrealistically sharp bends with up to 90 degree angles (Edmonds and Slingerland, 2009; Caldwell and Edmonds, 2014; Van der Vegt et al., 2016)(Chapter 5). However, the experimental results in this thesis suggest that slope effects still act on the suspended load, but in lesser extent and independent of

sediment mobility. Furthermore, several studies commented on the uncertainty of how slope effects act on suspended sediment and how the vertical distribution in the water column affects this (Talmon et al., 1995; Schuttelaars and De Swart, 1999; Walstra et al., 2007). Other studies suggest that horizontal eddy diffusivity is the main process that redistributes suspended sediment in numerical models (Hibma et al., 2003; Van Der Wegen and Roelvink, 2008), and this is the reason why the model of (Dam et al., 2016) showed realistic bed slopes even though all sediment was assumed to be transported in suspension. However, this could also be contributed to numerical diffusion instead of physical processes. Therefore, it is advised to further study the role of slope effects and diffusion of suspended sediment transport by modelling and experiments.

2. *Grid size dependent incision.* With the default transverse slope parameter, the flow seems to prefer flowing through as few grid cells as possible, resulting in extreme incision of channels that are only one grid cell wide. This implies strong resolution and numerical diffusion effects. In current model studies this grid size-dependent incision is counteracted by increasing the slope parameter. As showed in this thesis, the transverse slope parameter that is needed to balance this extreme incision depends on the sediment transport predictor and environment, and can result in differences up to two orders of magnitude in the transverse sediment transport rate. When this issue is solved, large-morphology is expected to become less dependent on choices by the modeller, and will show more realistic sediment transport vectors.
3. *Implementing and testing improved transverse bed slope relations.* The non-linear and grain size-dependent relation of the transverse slope effect with the power function of sediment mobility that was found in the experiments is expected to have a significant effect on modelled local bed slopes, channel and bar dimensions, and consequently on channel patterns (Chapter 2). The experimental results suggest a different behavior between systems with fine and coarse sediment. Furthermore, a change in sediment mobility has a larger effect at lower mobilities, compared with relatively high mobilities were the slope effect is constant with increasing sediment mobility. This is therefore especially important in areas with low sediment mobility where a significant difference in sediment mobility over time or space occurs, e.g. near channel banks and shoal margins. How exactly a nonlinear bed slope relation changes local morphology remains to be studied by modelling. Additionally, experiments with a sediment mixture showed limited effect of vertical sorting by bedforms on lateral sorting on transverse slopes, which justifies the use of the active layer when modelling lateral sorting over a longer time period (Chapter 4). However, before lateral sorting can be described accurately, a more physics based predictor needs to be implemented to calculate the deflection of the available grain size fractions in the active layer as a function of transverse slope (Sloff and Mosselman, 2012), which could be based on the new bend sorting model described in this thesis.
4. *Quantifying dune characteristics and their influence on slope effects.* Dunes in coarse grained sediment had a significant effect on the transverse bed slope effect, since their presence resulted in steeper average transverse slopes (Chapter 2). These steeper transverse slopes showed a relation with grain size-dependent lee side angle, since steep lee side angles result in permanent flow separation (e.g. Best, 2005; Lefebvre and Winter, 2016) and it

was assumed that this enhances secondary flow in the dune troughs (Chapter 3). However, still some questions remain. Firstly, it is unknown how grain size sets the lee side angle. Possible explanations could relate to saltation lengths, angularity of the grains, or the sediment porosity. To study the influence of saltation more detailed experiments are needed, while the influence of porosity could for example be studied by adding fines to the coarse sediment that fill up the pores and therefore results in less hyporheic flow (Blois et al., 2014). Secondly, dunes in experiments are relatively large compared to the water depth (up to $\frac{1}{2}$ of the water depth) and compared to dunes in natural rivers (Talmon et al., 1995), and additionally recent work has observed that dunes with lee sides less than 15 degrees (low angle dunes) are common in natural large rivers (e.g. Roden, 1998; Kostaschuk and Villard, 1996). These differences in height and possible lee side angles implies the relative influence by bedforms on the flow and sediment transport in natural rivers could also be significantly lower than in experiments, since the possible lack of flow separation in low angle dunes may not be creating the same enhancement of bend flow as in the experiments. However, it is unclear if lee side angles are also generally lower in bends as these field observations were done in straight reaches. An interesting study would be to compare the effect of bends on natural dune morphology similar to the current analysis. Furthermore, describing relations for dune characteristics and their effect on sediment transport in bends could help the parametrization of friction in morphodynamic models. Finally, the orientation of a bedform crest is expected to influence flow patterns (e.g. Dietrich and Smith, 1984; Kisling-Moller, 1993; Hasbo, 1995), but showed no relation with secondary flow, transverse slope or bedform morphology in the experiments, but instead seemed to depend on interactions between bedforms within the experiment. Previous literature describes the interaction between bedforms and how dune three-dimensionality depends on the morphology of the dune upstream (e.g. Parsons et al., 2005; Reesink et al., 2018), and it would be interesting to likewise study the development and interaction of dunes in bends.

5. *Linking local sediment transport vectors to local flow velocities.* The experimental trend in slope effect with sediment mobility still showed a significant amount of scatter that could not be explained by averaged values for flow conditions, transverse slope and bedform characteristics. Although the new dataset on transverse bed slopes is a major advance in identifying important sediment transport processes compared to previous scarce datasets, the ultimate aim should be to describe the local deviation of the transport vector, instead of cross-sectionally averaged values. However, in that case detailed local flow velocities and sediment transport measurements are needed. Future studies could therefore focus on methods to track individual grains on slopes and characterize local flow conditions. This can for example be used to quantify the effect of local slopes caused by bedforms, and the difference between the angle of deflection of rolling and saltating grains. However, another uncertainty is how deflection of individual grains is related to avalanching of multiple grains all at once, which depends on static and dynamic friction. For lower slopes static and dynamic friction are assumed to be constant (Sekine and Parker, 1992; Parker et al., 2003), but for higher transverse slopes the dynamic friction

changes and thus depends on the magnitude of the slope. However, how it changes is still under debate (Parker et al., 2003).

6. *Applying the bend sorting model in existing analytical models.* The relatively simple bend sorting model that was developed in Chapter 4 can be used in any model that already predicts transverse slope and flow conditions, such as analytical models that predict bifurcation dynamics based on upstream transverse slope (Bolla Pittaluga et al., 2003; Kleinhans et al., 2008), and models that predict grain size distribution along lateral accretion surfaces in a point bar (van de Lageweg et al., 2014). The bend sorting model predicts lateral sorting along the transverse slope at the bend apex, but this pattern can have a large influence on morphology by different trajectories of the different grain sizes through the bend and towards bends downstream (Parker and Andrews, 1985). The current bend sorting model could therefore be a starting point to predict spatial distribution along the bend, and thereby improve predictions of sediment transport, bed level elevations and point bar connectivity models by predicting the dimensions and spatial distribution of stratigraphic units (Willis and Tang, 2010).
7. *Modelling bend flow in a rotating annular flume.* The rotating annular flume that is used in all experimental studies in this thesis has proven to be effective to determine the balance between transverse sediment transport and bend flow, since it allows control of the secondary flow intensity separate from the main flow and therefore is able to simulate varying bend radii. However, flow velocities could only be measured at one location near a flat bed and Vectrino measurements showed a significant amount of scatter. Therefore, an analytical model was developed to determine the right trend in near bed flow velocities with changing lid and floor rotation (Appendix A). This analytical model predicts one characteristic value of transverse and streamwise flow velocity for each experiment, while in reality flow patterns are complex and 3D, especially near the ratio of lid and floor rotation that results in minimal secondary flow intensity (Booij, 1994; Booij, 2003). As a result, low secondary flow intensities were underpredicted by the analytical flow model (Fig. 2.3), and this model also deviated for experiments with no floor rotation. Therefore, although the analytical model provides a good estimation of characteristic flow velocities to compare to flume average values, if more detailed flow characteristics are needed in future experiment in the rotating annular flume, flow patterns should be modelled with a CFD model with various lid to floor rotation ratios. Furthermore, this model can then also be used to study the effect of bedform dimensions on the flow patterns.

6.6 Implications for calibration practices of large-scale morphodynamic models

The results in this thesis show that the local balance between channel incision and downslope sediment transport has a large effect on sediment transport, bar and channel dynamics, and consequently large-scale morphology. Therefore, modelled morphology heavily depends on the combination of sediment transport predictor and slope parametrization. Pending further investigations into sediment transport parameterizations and numerical effects, the choice of sediment transport predictor and slope parametrization in future studies should depend on

the environment that is modelled and the research objective, instead of arbitrary choices. The recommendations described below are therefore not a solution, but a way to limit unintended artifacts until the real problems are solved.

As showed in previous sections, the sediment transport predictor determines the tendency to incise and therefore the increase in transverse slope parameter that is needed to counteract this incision in order to get a dynamic system. The slope parametrization determines local direction of sediment transport and thereby the magnitude of downslope sediment transport. The method of Ikeda (1984) increases the total sediment transport by calculating an additional transverse transport vector, while the method of Koch and Flokstra (1981) only causes a larger rotation of the transport vector. When incision is high, increasing the slope parameter with the method of Ikeda (1984) is therefore most effective, since by increasing the slope parameter more sediment will become available for counteracting incision. The method of Koch and Flokstra (1981) is less effective, since by only rotating the vector the amount of sediment that is available to balance incision is limited to the streamwise sediment transport rate.

This difference between slope parameterizations in direction and magnitude of the transport vector significantly influences the development of morphology across scales. The larger magnitude of the total transport vector in models with the slope predictor of Ikeda (1984) results in wider and shallower channels. The larger rotation of the transport vector in models with the slope predictor of Koch and Flokstra (1981) results in a different distribution of sediment over bifurcates and a shorter adaptation length to changes in flow conditions, influencing bifurcation dynamics and bar dimensions. Since the methods of Koch and Flokstra (1981) and Ikeda (1984) distribute sediment differently, this also modifies channel curvature and therefore the orientation of channels at bends and bifurcations. This orientation affects locations of bank erosion, migration rate, and chute cutoff processes (Van Dijk et al., 2014). On the larger scale, this alters the timescale of morphological adaptation and the frequency of avulsion (Kleinhans and van den Berg, 2011), and therefore has a large influence on the development of channel patterns.

Practically, this means that the choice of sediment transport predictor and slope parametrization in morphodynamic model studies depends on if the objective is related to sediment transport processes or to channel and bar patterns (Fig. 6.4). Furthermore, morphodynamic models can be used for different purposes, for example as a tool to study the effect of initial and boundary conditions on behavior of large-scale idealized systems, or for management decisions about e.g. navigation and engineering. In case of the former, the predictor of Engelund-Hansen will lead to more realistically shaped bars and channel networks in systems were lateral dynamics are essential, since it needs much lower slope effects to counteract the severe incision than Van Rijn. However, sediment transport rates are too high which overdampens perturbations. Therefore, if the objective is to have realistic sediment transport rates and morphological adaptation, the predictor of Van Rijn works better. Furthermore, since this predictor makes a distinction between bed load and suspended load, it is the only option in environments were suspended sediment is essential, for example in tidal environments with waves, varying flow directions, or mud. In depositional environments where lateral dynamics are initially less important, the use of the predictor of Engelund-Hansen is

difficult due to the diffusive nature of this predictor. This predictor should only be used if the channels that eventually form have to be dynamic.

The choice of slope parametrization depends on the sediment transport predictor. In models with Engelund-Hansen, the best option is in general the method of Koch and Flokstra (1981), since this resulted in the most realistically shaped bars and braiding index (Fig. 5.9) (Struiksma et al., 1985; Crosato and Mosselman, 2009). The slope parameterization of Ikeda (1984) will lead to even more subdued morphology, since the increase in sediment transport with increasing slope parameter will further overdampen perturbations. In models with Van Rijn on the other hand, it is advisable to use the method of Ikeda (1984), since this is often the only way to counteract the higher incision rate. However, it should be noted that any model with slope parameters higher than $\alpha_I = 5$ in case of the method of Ikeda (1984) or lower than $\alpha_K = 0.5$ for the method of Koch and Flokstra (1981) for certain do not produce realistic sediment transport rates and direction, according to the range in experimental results (Fig. 6.1).

In case models are designed to represent existing morphology for e.g. decision making or case studies, the effect of slope parametrization might seem less obvious due to often smaller or constrained model domains and shorter run time. However, results still critically depend on the choice of slope predictor in combination with the sediment transport predictor, since this determines local direction and magnitude of sediment transport. When the model is calibrated on bed slopes or the shape of morphological features, different slope parametrizations will lead to a different magnitude and direction of the transport vector on the same slope (Fig. 5.10), and therefore leads to different local channel dynamics, such as bank erosion rates and location of erosion and deposition. This difference will increase over time, as local bed slopes begin to deviate. This means that when a model is calibrated on mor-

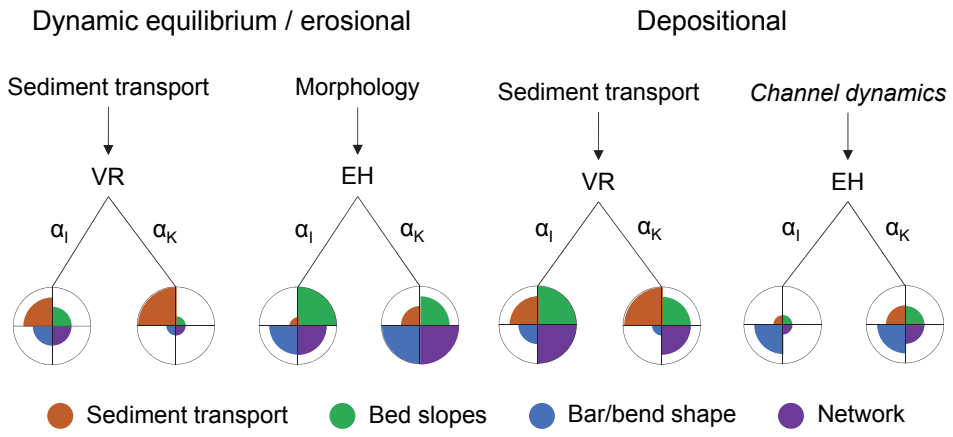

Figure 6.4: Adaptation of Figure 5.12. Relative performance for each combination of transport predictor and slope method in models of either environments where bank erosion is necessary, or depositional environments. Relative performance is divided in four categories, such that the choice of predictors can be made depending on the research objective.

phology but used to make an estimate of time scales of erosion or sediment migration, these estimates will depend on the choice of slope parametrization. This is for example the case in models of existing estuaries that are used for dredging and dumping strategies, like the model of the Western Scheldt in Chapter 5. When the objective is to determine time scales of erosion or sediment migration, it is better to calibrate the model on for example migration rates of channels instead of bed levels. On the other hand, when models are calibrated to sediment transport time scales, morphology and bed slopes will differ between different methods. These are for example models that focus on the migration rate of dumped sediment, the sediment distribution at bifurcations, or the rate of bank erosion. Therefore, when models are calibrated by increasing downslope sediment transport, either sediment transport magnitude or bed slopes match to measured data, while both is not possible.

Appendix A

Analytical estimation of near-bed flow velocities in the rotating annular flume

The rotating annular flume that is used in all experimental studies in this thesis has proven to be effective to determine the balance between transverse sediment transport and bend flow, since it allows control of the secondary flow intensity separate from the main flow and therefore is able to simulate varying bend radii. Chapter 2 describes how near-bed streamwise and normal flow velocities were determined with an analytical model that was calibrated with flow velocity measurements. Here, we describe the derivation of this analytical model that is a function of the rotation rates of flume lid and floor

The analytical flow model is based on the assumption that shear stresses and centrifugal forces caused by lid and floor rotation, which drive the flow in the annular flume, are balanced by frictional forces of the lid and the walls of the flume. The trend in streamwise flow velocity is based on the model of Booij (1994), who found a reasonable agreement with flow velocity measurements in the same annular flume, but with a smooth bed without sediment. He assumed that shear stresses should cancel around the axis of rotation and therefore used the average value of the absolute tangential velocity (U) of the lid (l) and floor (f) at the center of the flume, multiplied with the ratio in surface area of the lid and flume. This ratio accounts for the larger surface area of the floor and sidewalls that apply shear to the water, and therefore have a larger influence on the average flow velocity than the lid. For the dimensions of the flume in this study, this ratio would be 0.78. However, in the current model this ratio is represented by a factor A_{s1} and is calibrated on measured data to account for unknown effects of three dimensional flow patterns on the non-linearity of the velocity profile. Furthermore, due to the sediment bed, in the current experiments the floor has a higher friction coefficient than during the measurements of Booij (1994), and therefore only a fraction of the floor velocity is transferred to the flow. This fraction is indicated with a second calibration parameter A_{s2}, which is absent in the model of Booij (1994). The resulting approximation for the streamwise flow velocity is:

$$u_s = A_{s1} \frac{U_l + A_{s2}|U_f|}{2} \tag{A.1}$$

In this flume, the best fit of the analytical flow velocity model on measured flow velocities was obtained with calibration parameters $A_{s1} = 0.65$ and $A_{s2} = 0.5$ (Chapter 2). An A_{s1} of 0.65 is thus similar to the 0.78 obtained by Booij (1994), but lower because of higher bed friction.

The trend in normal flow velocity is determined using a model of a cross-section of the flume. The centrifugal force generated by the lid forces water towards the outer bend, which creates a pressure difference that drives the secondary flow and creates an inward-directed bed shear stress. Counter-rotation of the floor adds an outward-directed centrifugal force on the flow low in the water column, which decreases the pressure difference over the water

column at the outer bend, and thereby decreases the secondary flow and the inward-directed bed shear stress. Therefore, the net-centrifugal force (F_c) is determined by the difference between these two centrifugal forces. We assume that the lid rotation influences the top half of the water column ($H/2$) and the floor rotation affects the bottom half:

$$F_c = \rho \frac{H}{2} W \frac{U_l^2}{r} - \rho \frac{H}{2} W \frac{U_f^2}{r} \tag{A.2}$$

This force is balanced by friction exerted along the lid, side walls and sediment bed:

$$\rho \frac{H}{2} W \frac{U_l^2 - U_f^2}{r} = \tau'_w + \tau'_b + \tau'_l \tag{A.3}$$

where τ' = shear stress per unit of downstream length $[N/m]$ exerted on the walls (w), bed (b) and lid (l) respectively.

We consider a cross-section of unit length where the friction depends on a measure of both the magnitude of the streamwise flow velocity and the normal flow velocity. Shear stress for any boundary section i is therefore defined as:

$$\tau'_i = \rho c_i L_i u_n u_s \tag{A.4}$$

where L = that part of the hydraulic radius on which the shear stress component is exerted $[m]$ and c_i = friction coefficient. As a simple estimate of the characteristic streamwise flow velocity, the average of the lid and floor angular velocity was used as described by Equation A.1. After inserting the definitions of the shear stress and the streamwise flow velocity into Equation A.3, u_n can be isolated:

$$u_n = \frac{HW}{r(c_w(W+H) + c_b W)} \frac{U_l^2 - U_f^2}{(U_l + |U_f|)} \tag{A.5}$$

where:

$$\frac{U_l^2 - U_f^2}{(U_l + |U_f|)} = \frac{(U_l - |U_f|)(U_l + |U_f|)}{(U_l + |U_f|)} = U_l - |U_f| \tag{A.6}$$

The friction coefficient for the rough surface of the bed (c_b) is defined as:

$$c_b = \frac{8}{\left[5.75 log\left(\frac{12 r_h}{k_s}\right)\right]^2} \tag{A.7}$$

where r_h = hydraulic radius $[m]$ and k_s = Nikuradse roughness height $[m]$. For the flow measurements we assumed $k_s = 2.5D$. For both the smooth lid and glass walls, smooth wall friction is assumed:

$$c_w = \frac{8}{[5.75 log(\frac{12 r_h u_*}{3.3\nu})]^2} \tag{A.8}$$

where u_* = shear velocity $[m/s]$ and ν = viscosity $[m^2/s]$.

Finally, this results in:

$$u_n = \frac{A_{n1} HW(U_l - A_{n2}|U_f|)}{r(c_w(W+H) + c_b W)} \tag{A.9}$$

where A_{n1} and A_{n2} are calibration factors, accounting for non-linearity of the velocity profile and the relatively larger influence of floor rotation on the average flow velocity due to a larger cross-sectional surface, respectively. In this study, the best fit with flow velocity measurements was obtained with $A_{n1} = 0.025$ and $A_{n2} = 2.5$. When the ratio of lid to floor rotation is equal to A_{n2}, secondary flow is minimal and an infinite straight river section can be simulated. The ratio of 2.5 found in this study is higher than the 1.8 found by Booij (1994) due to the added roughness of the sediment bed.

Appendix B

Sediment transport and slope effect in Delft3D

In this thesis the problems that arise with bed slope effects in morphodynamic models is illustrated with Delft3D. In this section it is explained how the transverse bed slope effect is implemented in Delft3D, and how the two main paramterizations can be compared. However, to understand the implementation of the bed slope effect and how it interacts with the sediment transport predictor, we first explain the calculation of streamwise sediment transport. In this thesis, the focus is on the difference between the Van Rijn and Engelund-Hansen sediment transport predictor and their influence on the balance of incision and downslope sediment transport. Furthermore, in Chapter 5 the results were briefly compared with a general sediment transport predictor, where the non-linearity of sediment transport and the addition of a critical shear stress can be specified by the user. Henceforth, we refer to the predictor of Van Rijn as VR, and to the predictor of Engelund-Hansen as EH.

VR makes a distinction between bed load and suspended load transport, by imposing a reference height, below which sediment transport is treated as bed load and everything above this height is treated as suspended load. Gravity only acts on the bed load, which is calculated as follows:

$$q_b = 0.5\rho_s d_{50} D_*^{-0.3} \left(\frac{\tau}{\rho}\right)^{0.5} \frac{\tau - \tau_{cr}}{\tau_{cr}} \tag{B.1}$$

where q_b = bed load sediment transport rate per meter width $[m^2/s]$, ρ_s = sediment density $[kg/m^3]$, ρ_w = water density $[kg/m^3]$, D_{50} = median grain size $[m]$, D_* = dimensionless particle size, τ = shear stress $[N/m^2]$, ρ = density $[kg/m^3]$, τ_{cr} = critical shear stress based on the Shields criterion $[N/m^2]$. As a result, the sediment transport rate is related to flow velocity to the power of 3, which determines the non-linearity of the sediment transport predictor. However, since this predictor also includes a critical flow velocity, the relation between flow velocity and sediment transport will be more non-linear near the beginning of motion.

EH is a total load predictor (q_t), and unlike VR, it does not include a critical velocity or critical shear stress:

$$q_t = \frac{0.005\alpha u^5}{\sqrt{g}C^3 \frac{\rho_s - \rho_w}{\rho_w} D_{50}} \tag{B.2}$$

where α = a calibration coefficient in the order of 1. Here, the sediment transport rate is related to flow velocity to the power of 5.

The general sediment transport predictor in Delft3D is based on the predictor of Meyer-Peter MuellerMeyer-Peter and Müller, 1948:

$$q_t = \alpha D_{50} \sqrt{\frac{\rho_s - \rho_w}{\rho_w} g D_{50}} \theta^b (\theta - \theta_c)^c \tag{B.3}$$

where b and c are user defined parameters, which determine the non-linearity of the sediment transport predictor and the addition of a critical sediment mobility. The sediment mobility

θ, a dimensionless form of the bed shear stress, reads:

$$\theta = \frac{u^2}{C^2 \frac{\rho_s - \rho_w}{\rho_w} D_{50}} \tag{B.4}$$

When the magnitude of the bed load or total load sediment transport is calculated parallel to the flow velocity, the direction and magnitude of the transport vector is adjusted for bed slopes. For transverse slopes, the two commonly used parameterizations are the predictor of Koch and Flokstra (KF)Koch and Flokstra, 1981 (ISlope = 3) and Ikeda (IK)Ikeda, 1984 (ISlope = 2). The main difference between both options is in the calculation of the transport vector (Fig. 5.1). For KF the direction of sediment transport is corrected for transverse gradients by rotating the transport vector based on the user-defined factors α_K and β_K:

$$tan(\psi) = \frac{1}{\alpha_K \theta^{\beta_K}} \frac{\partial z_b}{\partial y} \tag{B.5}$$

For IK an additional transport vector is calculated perpendicular to the flow direction, based on the input parameter α_I:

$$q_n = q_s \alpha_I \sqrt{\frac{\theta_c}{\theta}} \frac{\partial z_b}{\partial y} \tag{B.6}$$

where q = sediment transport load $[m^2/s]$ in the streamwise (s) or transverse (n) direction, and $\frac{\partial z_b}{\partial y}$ = transverse slope $[m/m]$.

As a result, the IK method increases the direction and total magnitude of sediment transport when a transverse slope is present, while for KF only the direction is changed. Another difference is that the IK method uses a critical shear stress, which is absent in the KF method. The default value of α_I in Delft3D is set to 1.5, while the parameter α_K is not defined in the model, but should be 1.5 according to Koch and FlokstraKoch and Flokstra, 1981. The method of calculating the sediment transport vector in both slope options therefore has major implications for calibrating models with the transverse slope parameter. By increasing the α_I in the IK method by a factor of ten for example, the amount of downslope sediment transport is also increased by a factor of ten, which increases the total sediment transport significantly (Fig. 5.1). With the KF method sediment transport is not increased, but here, decreasing the α_K to values reported in literature could easily result in more downslope sediment transport than streamwise sediment transport.

It is possible to compare the effect on resulting morphology of using different slope predictors by requiring either the magnitude or the direction of transverse sediment transport to be equal. When assuming an equal magnitude, the method of KF needs to be corrected for a given slope and sediment mobility. Using Equation B.5 and Equation B.6 with a β_K of 0.5 it follows that:

$$\alpha_I = \left(\alpha_K \sqrt{\theta_c + \frac{\theta_c}{\alpha_K^2 \theta} \left(\frac{dz}{dy} \right)^2} \right)^{-1} \tag{B.7}$$

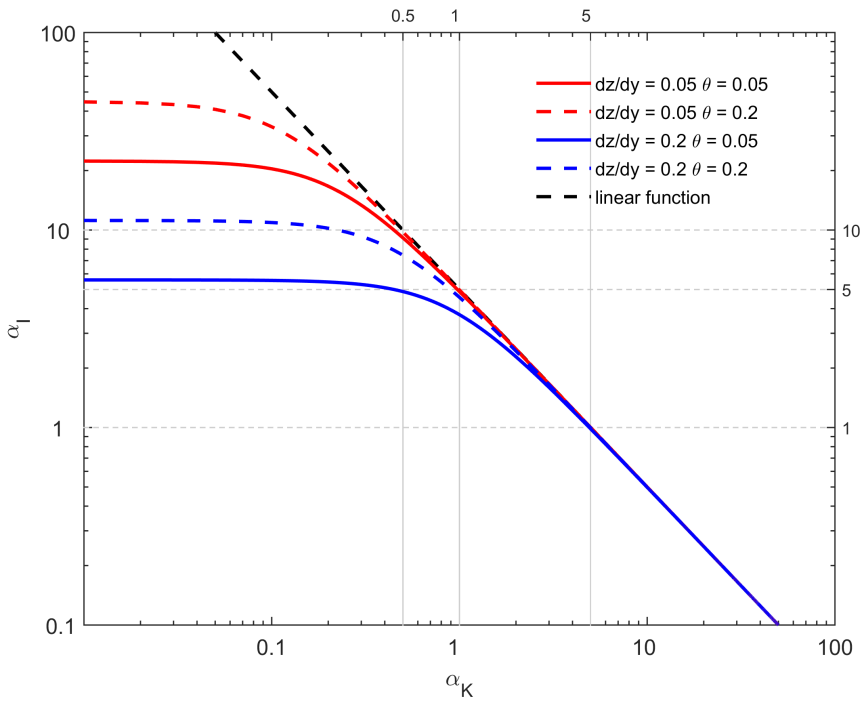

Figure B.1: Relation between α_I and α_K, the input parameters of the two main options to calculate sediment transport on transverse bed slopes in the morphodynamic model Delft3D, when assuming equal downslope sediment transport (Eq B.7). Colored lines indicate combinations of transverse slope and sediment mobility, with a critical sediment mobility of 0.04. Gray lines indicate values for the α_I and α_K used in the delta model (Fig. 5.4).

The resulting relation between α_I and α_K is plotted in Fig. B.1 for four combinations of transverse slope and sediment mobility. When assuming equal direction of sediment transport, it follows that:

$$\alpha_I = \left(\alpha_K \sqrt{\theta_c}\right)^{-1} \tag{B.8}$$

which is shown as the linear solution in Figure B.1.

Appendix C

Theoretical balance between incision and transverse sediment transport

To help identify the cause of the overdeepening of channels in numerical models, we compare the balance between incision and transverse sediment transport in a straight river channel in Delft3D with an analytical model of a channel cross-section with the same characteristics (Chapter 5). The analytical model consists of three grid cells in cross-section, with an initial bed level difference between the middle cell and the surrounding cells, representing a disturbance that either decays or grows by incising further (Fig. C.1). The aim of this model is to find the equilibrium width-to-depth ratio at which incision is equal to transverse sediment transport, and how this ratio depends on flow conditions, sediment transport processes, and size of the disturbance.

The model first calculates upstream flow characteristics and corresponding sediment transport rate based on the input parameters, which are a constant Chezy coefficient for friction (C), channel slope (S), grain size (D_{50}), the non-linearity of the sediment transport predictor (k), and a height difference (dh). We assume a constant specific discharge such that the

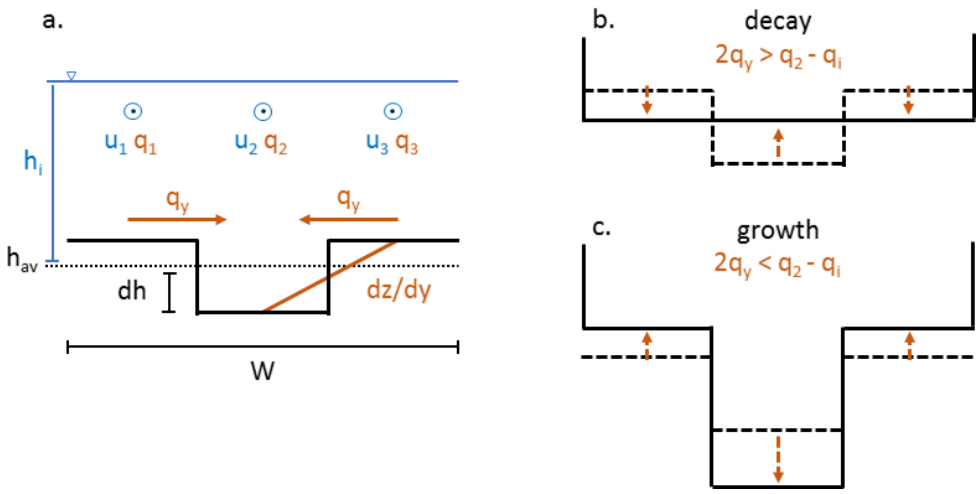

Figure C.1: Concept of the analytical model. The cross-section is three grid cells wide with a bed level difference between the middle grid cell and the surrounding cells as an initial perturbation. The numerical channel is also based on this concept. a) Definition of the flow velocity and transport vectors, channel width (W), initial channel depth (h_i), bed level difference (dh), and transverse slope (dz/dy). b) The perturbation decays when transverse sediment transport is larger than the difference between incoming and outgoing sediment transport. The middle grid cell will accrete, while the surrounding cells will erode till the average bed level. c) The perturbation grows when transverse sediment transport is smaller than the difference between incoming and outgoing sediment transport. The middle grid cell will incise further, while the surrounding cells will accrete.

relation between channel width and discharge Q $[m^3/s]$ is linear:

$$Q = aW \tag{C.1}$$

The upstream flow velocity (u_i) and water depth (h_i) are calculated by iteration, using the following equations for flow velocity:

$$u_i = C\sqrt{h_i S} \tag{C.2}$$

$$u_i = \frac{a}{h_i} \tag{C.3}$$

The upstream sediment transport rate (q_i) is based on the same general sediment transport predictor as in Delft3D:

$$q_i = \alpha D_{50} \sqrt{\frac{\rho_s - \rho_w}{\rho_w} g D_{50}} \theta_i^{\frac{k}{2}} \tag{C.4}$$

Then, flow characteristics and sediment transport fluxes are calculated for the cross-section under consideration, based on the height difference between the middle grid cell (h_2) and the outer two grid cells (h_1, h_3) (Fig. C.1a). It is assumed that the average water depth at the cross-section is equal to the initial water depth, which leads to:

$$h_1 = h_3 = h_i - 0.5dh \tag{C.5}$$

$$h_2 = h_i + dh \tag{C.6}$$

The sediment transport rate for each cell is calculated with Equations 2.5, C.2 and C.4, but with the specific water depths. The sediment transport rate towards the middle cell as a result of the transverse slope (q_n) is based on the method of IkedaIkeda, 1984:

$$q_n = q_1 \frac{\beta}{\sqrt{\theta}} \frac{1.5dh}{\frac{W}{3}} \tag{C.7}$$

where β = transverse slope parameter, which is based on α_I from Equation 2.7. The transverse slope is defined as the height difference between two cells divided by the width of one grid cell, which is the same method as in Delft3D.

A balance between incision and downslope sediment transport is assumed when the difference between the upstream sediment transport and the sediment transport rate for the middle grid cell is equal to the total downslope sediment transport:

$$2q_n = q_2 - q_i \tag{C.8}$$

When the transverse sediment flux is larger, there is sedimentation and the perturbation will likely decay (Fig. C.1b), while when the transverse sediment flux is smaller, the grid cell is incised and the perturbation will grow (Fig. C.1c). Using Equations 2.5, C.2 and C.4 it follows that:

$$W_{eq} = \frac{h_1^{k/2}}{h_2^{k/2} - h_i^{k/2}} \frac{9\beta dh}{\sqrt{\theta}} \tag{C.9}$$

where W_{eq} = width of the channel when incision is equal to the transverse sediment transport. The equilibrium width-to-depth ratio is now a function of the size of the disturbance, sediment mobility and the non-linearity of sediment transport. All other parameters influence this equilibrium by changing the sediment mobility. In further analyses we first assume a constant channel slope of 0.5 mm/m, a Chezy coefficient of 40 $\sqrt{m}/s$, a ratio between channel width and discharge of 12.5, and a grain size of 0.5 mm.

With increasing sediment mobility, the equilibrium width-to-depth ratio decreases exponentially (Fig. C.2), which means that at higher sediment mobility a channel is more likely to incise. A higher non-linearity of the transport predictor causes a higher sediment transport rate, and therefore results in more incision and a lower equilibrium width-to-depth ratio at any sediment mobility. Increasing the transverse slope parameter has the opposite effect, since more sediment is transported downslope which counteracts incision. Increasing the depth of the initial perturbation also decreases the equilibrium width (Fig. C.2), since deeper channels attract more flow and therefore need more downslope sediment transport to counteract this. However, this influence is less than changing the bed slope effect or the non-linearity.

To be able to show the effects of height of the perturbation and the other parameters that influence sediment mobility, the width-to-depth ratio is multiplied by the square root of the sediment mobility divided by the slope parameter, which is the ratio that describes the slopes of the graphs in Figure C.2. We call the resulting parameter the channelization factor, since it describes the balance between the tendency to enhance perturbations determined by the width-to-depth ratio, and the bed slope effect that counteracts incision. This balance thereby controls the formation of channels. As a result, Figure C.3a shows how models with varying slope effect and sediment mobility collapse when plotting this factor against height of the perturbation. Again, a higher non-linearity of sediment transport results in a growth of the perturbation at lower width-to-depth ratios. Higher Chezy values, and thus lower friction, also results in a growth of the perturbation at lower width-to-depth ratios when increasing the depth of the perturbation, but less dramatically. However, negative perturbations, i.e. when the middle grid cell is higher than the surrounding cells, need higher width-to-depth ratios for the perturbation to grow. Increasing the channel slope or decreasing the ratio between discharge and channel width shows the same trend.

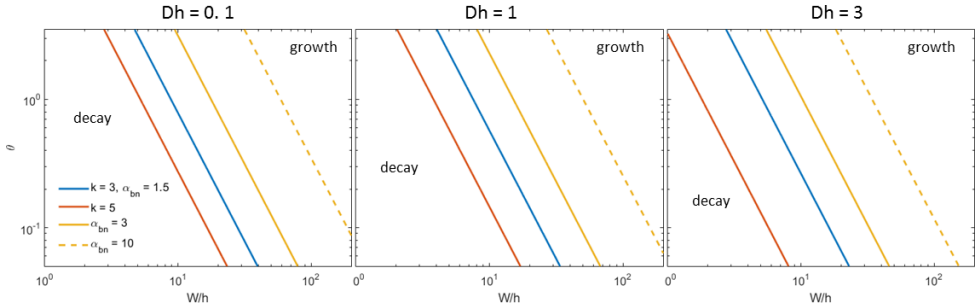

Figure C.2: The trend in equilibrium width-to-depth ratios with increasing sediment mobility, for three different depths of the initial perturbation (*dh*), resulting from the analytical model. Colors indicate the non-linearity of sediment transport (k). Solid lines indicate default slope effect (α_I = 1.5), dashed lines indicate an increased slope effect (α_I = 10). Width-to-depth ratios to the left of these lines will result in a decay of the initial perturbation, while ratios towards the right will result in a growth.

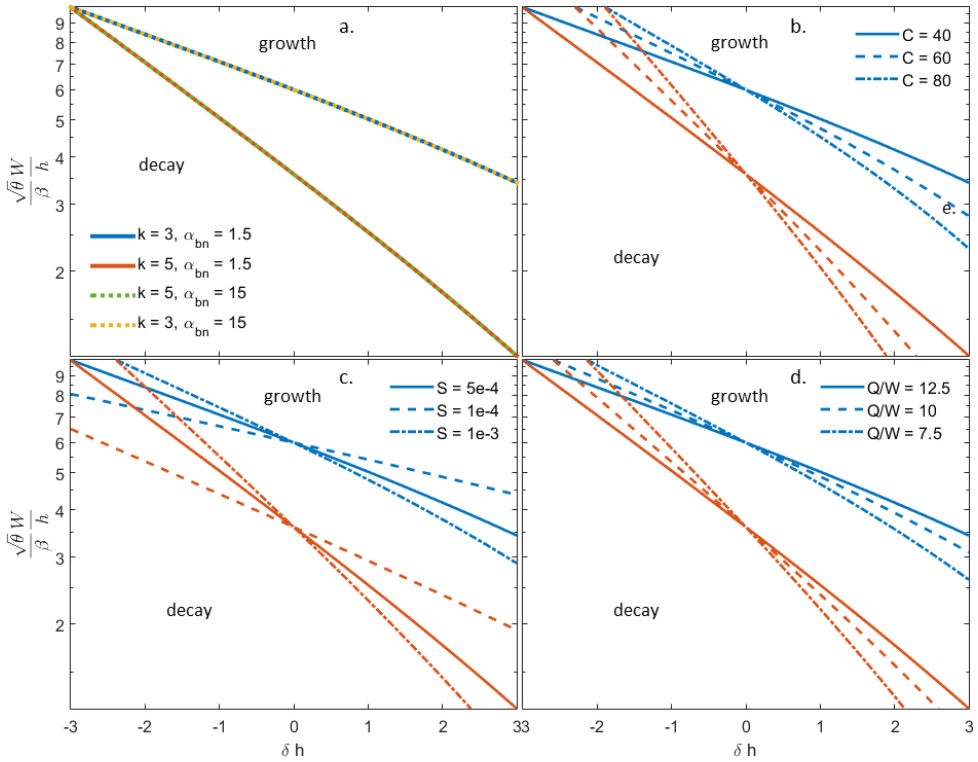

Figure C.3: Channelization factor resulting from the analytical model, plotted against the depth of the initial perturbation. Width-to-depth ratios lower than these lines will result in a decay of the initial perturbation, while higher ratios will result in a growth.

Appendix D

Slope effect in previous morphodynamic model studies

Table D.1 shows the results of the literature study described in Chapter 5. For each study, the morphodynamic model and the magnitude of the slope factor that is used is indicated, and whether this study mentions or discusses the effect on morphology of the slope parameter (yes = 1, no = 0). The environment that is modelled can be erosional (1), depending on a large-scale balance between erosion and deposition (2), or depositional (3). Models are included in this literature study when they either have an upstream river boundary (1), a river boundary as well as a downstream tidal boundary (2), or only a tidal boundary (3). Lastly, it is noted whether the model considers suspension (1) or treats all sediment transport as bedload (0).

Table D.1: Results of the literature study described in Chapter 5.

paper	model	slope effect	mention? (1/0)	discuss? (1/0)	environment e/b/d (1/2/3)	boundary r,r+t,t (1/2/3)	suspension? (1/0)
Yuill et al. (2016a)	Delft3D	1,5	0	0	1	1	1
Asahi et al. (2013)	Nays2D	1,5	0	0	1	1	0
Van Der Wegen and Roelvink (2008)	Delft3D	1,5	1	1	1	2	0
Tran et al. (2012)	Delft3D	1,5	0	0	1	3	1
Tuan et al. (2008)	MOGEC	2	1	0	1	1	1
Dissanayake et al. (2009)	Delft3D	5	1	1	1	3	0
Marciano et al. (2005)	Delft3D	5	1	0	1	3	0
Zhou et al. (2014)	Delft3D	1,5	1	1	1	3	0
Schuurman et al. (2013)	Delft3D	15	1	1	2	1	0
Oorschot et al. (2016)	Delft3D	15	1	0	2	1	0
Caldwell and Edmonds (2014)	Delft3D	1,5	1	0	3	1	1
Matsubara and Howard (2014)	Delft3D	4,4	1	0	1	1	1
Schuurman and Kleinhans (2015)	Delft3D	7	1	0	2	1	0
Stecca et al. (2017)	Delft3D	1,43	1	0	1	1	0
Williams et al. (2016)	Delft3D	1,5	1	1	1	1	0
Edmonds and Slingerland (2008)	Delft3D	1,5	1	1	3	1	1
Schuurman et al. (2016)	Delft3D/ Nays2D	6	1	0	2	1	0
Jiménez-Robles et al. (2016)	Delft3D	1,5	0	0	3	1	1
Nicholas et al. (2013)	Delft3D	25	1	1	2	1	1
Xie et al. (2009)	Delft3D	1,5	0	0	1	1	1
van der Wegen and Roelvink (2012)	Delft3D	10	1	1	2	2	0
Nnafie et al. (2018)	Delft3D	2	1	0	1	2	0
Leonardi et al. (2013)	Delft3D	1,5	1	1	3	2	1
Van der Wegen and Jaffe (2014)	Delft3D	100	1	0	2	2	1
van Dijk et al. (2018)	Delft3D	30	1	0	2	2	1

Nienhuis et al. (2016)	Delft3D	1,5	0	0	3	1	1
Kleinhans et al. (2010)	Delft3D	1,5	0	0	3	1	1
Edmonds and Slingerland (2007)	Delft3D	1,5	1	0	3	1	1
Van Dijk et al. (2014)	Delft3D	7	1	1	1	1	0
Schuurman et al. (2018)	Delft3D	25	1	1	2	1	0
Van Maren et al. (2009)	Delft3D	-	0	0	2	1	1
Vargas-Luna et al. (2018)	Delft3D	-	0	0	2	1	0
Liedermann et al. (2018)	iSed	-	0	0	2	1	1
Martínez-Fernández et al. (2018)	Delft3D	-	0	0	2	1	0
Mariotti et al. (2013)	Delft3D	-	0	0	3	1	1
Canestrelli et al. (2014)	Delft3D	-	0	0	3	1	1
Yuill et al. (2016b)	Delft3D	-	0	0	3	1	1
Rousseau et al. (2017)	Telemac	-	0	0	1	1	0
Norman et al. (2017)	Nays2D	-	0	0	1	1	1
French (2010)	Telemac	-	0	0	2	2	1
French (2003)	Telemac	-	0	0	2	2	1
Son and Hsu (2011)	Delft3D	-	0	0	1	2	1
Xie et al. (2017)	Delft3D	-	0	0	2	2	1
Van Der Wegen et al. (2011)	Delft3D	-	0	0	2	2	1
Ralston and Geyer (2017)	ROMS +CSTMS	-	0	0	3	2	1
Ganju et al. (2009)	ROMS +CSTMS	-	0	0	2	2	1
Luan et al. (2017)	Delft3D	-	0	0	2	2	1
Davies and Robins (2017)	Telemac	-	0	0	2	2	1
Hibma et al. (2004)	Delft3D	-	0	0	2	2	1
Guo et al. (2015)	Delft3D	-	0	0	2	2	0
Mariotti and Canestrelli (2017)	Delft3D	-	0	0	1	3	1
Schwarz et al. (2014)	Delft3D	-	0	0	1	3	1
Horstman et al. (2015)	Delft3D	-	0	0	1	3	1

Dissanayake et al. (2012)	Delft3D	-	0	0	1	3	1
Hu et al. (2018)	Delft3D	-	0	0	1	3	1
Rossi et al. (2016)	Delft3D	1,5	0	0	3	1	1
Hajek and Edmonds (2014)	Delft3D	1,5	0	0	3	1	1
Geleynse et al. (2010)	Delft3D	1,5	0	0	3	1	0
Van de Lageweg and Feldman (2018)	Delft3D	1,5	0	0	3	2	0
Hibma et al. (2003)	Delft3D	1	1	0	2	2	0
Lotsari et al. (2014)	TUFLOW	2	1	0	2	1	1
Braat et al. (2017)	Delft3D	25	1	1	2	2	0
Van der Vegt et al. (2016)	Delft3D	1,5	0	0	3	1	1
Edmonds and Slingerland (2009)	Delft3D	1,5	0	0	3	1	1
Temmerman et al. (2007)	Delft3D	1,5	0	0	1	3	1
Ridderinkhof et al. (2014)	Delft3D	20	1	0	1	3	1
Van Leeuwen et al. (2003)	Delft3D	1,5	0	0	1	3	0
Sanyal (2017)	Delft3D	1,5	0	0	1	1	0

Appendix E

Experimental data: uniform sediment

Table E.1: Median grain size (D_{50}), angular velocity (ω) of the lid (l) and floor (f), transverse slope (dz/dy), average flow velocity (u) in streamwise (s) and normal (n) direction, sediment mobility (θ), characteristic dune height (Δ), length (λ), and lee side angle (°) of all 269 morphodynamic experiments in the rotating annular flume with uniform sediment ($\rho_s = 2650\ kg/m^3$).

exp.	D_{50} [mm]	ω_l [rad/s]	ω_f [rad/s]	dz/dy [m/m]	u_s [m/s]	u_n [m/s]	θ [-]	Δ [m]	λ [m]	lee [°]
1	0,17	0,598	0,000	0,411	0,360	0,063	0,128	0,060	1,330	18,6
2	0,17	0,503	0,000	0,330	0,302	0,052	0,090	0,008	0,360	6,3
3	0,17	0,503	-0,628	-0,425	0,491	-0,119	0,238	0,169	2,150	26,1
4	0,17	0,503	-0,314	-0,476	0,397	-0,031	0,155	0,013	0,770	36,5
5	0,17	0,503	-0,209	-0,094	0,365	-0,002	0,132	0,006	0,000	6,4
6	0,17	0,503	-0,157	0,019	0,349	0,012	0,120	0,007	0,310	7,0
7	0,17	0,503	-0,126	0,102	0,340	0,020	0,114	0,005	0,380	7,4
8	0,17	0,503	0,209	0,217	0,239	0,100	0,056	0,003	0,000	5,0
9	0,17	0,503	0,126	0,168	0,264	0,082	0,069	0,005	0,340	4,9
10	0,17	0,393	0,000	0,308	0,236	0,040	0,055	0,007	0,320	9,8
11	0,17	0,314	0,000	0,088	0,189	0,031	0,035	0,005	0,315	9,4
12	0,17	0,314	-0,314	-0,455	0,283	-0,050	0,079	0,025	0,855	32,1
13	0,17	0,314	-0,209	-0,274	0,252	-0,022	0,063	0,007	0,320	9,6
14	0,17	0,314	-0,126	0,009	0,227	0,000	0,051	0,005	0,000	8,3
15	0,17	0,251	0,000	0,000	0,151	0,024	0,023	0,000	0,000	1,1
16	0,17	1,795	0,000	0,409	1,079	0,207	1,150	0,005	2,210	36,9
17	0,17	1,795	-0,628	0,083	1,268	0,026	1,587	0,001	0,000	1,3
18	0,17	1,795	-0,314	0,306	1,174	0,118	1,360	0,001	0,000	10,5
19	0,17	1,795	-0,209	0,369	1,142	0,148	1,288	0,002	0,000	2,9
20	0,17	1,795	-0,157	0,365	1,127	0,163	1,252	0,003	2,370	11,0
21	0,17	1,795	-0,126	0,367	1,117	0,171	1,231	0,002	2,360	13,8
22	0,17	1,795	0,628	0,402	0,890	0,375	0,782	0,076	0,885	20,0
23	0,17	0,209	-0,126	0,006	0,164	-0,010	0,026	0,002	0,000	4,6
24	0,17	1,396	0,000	0,411	0,840	0,158	0,695	0,058	2,830	15,3
25	0,17	1,142	0,000	0,369	0,687	0,127	0,466	0,136	1,840	29,0
26	0,17	1,142	-0,628	-0,124	0,876	-0,049	0,757	0,001	0,000	4,1
27	0,17	1,142	-0,314	0,217	0,781	0,040	0,602	0,003	2,840	5,4
28	0,17	1,142	-0,209	0,279	0,750	0,070	0,555	0,068	2,190	12,3
29	0,17	1,142	-0,157	0,333	0,734	0,084	0,532	0,024	2,360	7,7
30	0,17	1,142	-0,126	0,335	0,725	0,093	0,518	0,046	1,870	17,8
31	0,17	1,142	0,628	0,449	0,498	0,281	0,245	0,038	0,470	20,8
32	0,17	1,142	0,314	0,438	0,592	0,209	0,346	0,084	0,595	28,3
33	0,17	1,142	0,209	0,533	0,624	0,182	0,384	0,146	1,360	28,6
34	0,17	1,142	0,157	0,470	0,640	0,169	0,404	0,049	1,630	36,4

35	0,17	1,142	0,126	0,532	0,649	0,160	0,416	0,087	2,250	16,2
36	0,17	0,898	0,000	0,352	0,540	0,098	0,287	0,117	2,030	21,6
37	0,17	0,739	0,000	0,345	0,444	0,079	0,195	0,007	1,430	9,4
38	0,17	0,739	-0,628	-0,303	0,633	-0,094	0,396	0,021	5,900	15,5
39	0,17	0,739	-0,314	-0,110	0,539	-0,005	0,287	0,004	0,000	8,2
40	0,17	0,739	-0,209	0,227	0,507	0,024	0,254	0,054	2,295	13,4
41	0,17	0,739	-0,157	0,271	0,492	0,038	0,239	0,097	2,340	17,7
42	0,17	0,739	-0,126	0,325	0,482	0,046	0,229	0,023	2,270	33,7
43	0,17	0,739	0,209	0,517	0,381	0,131	0,144	0,020	0,720	26,6
44	0,17	0,739	0,157	0,483	0,397	0,119	0,156	0,029	0,850	35,3
45	0,17	0,739	0,126	0,472	0,407	0,111	0,163	0,039	0,840	24,0
46	0,26	0,503	0,000	0,273	0,302	0,048	0,066	0,007	0,280	9,4
47	0,26	0,503	-0,209	-0,236	0,365	-0,002	0,096	0,009	0,000	13,5
48	0,26	0,503	-0,157	-0,010	0,349	0,011	0,088	0,006	0,000	6,7
49	0,26	0,503	-0,126	0,033	0,340	0,019	0,083	0,005	0,340	5,7
50	0,26	0,503	0,126	0,257	0,264	0,077	0,050	0,008	0,230	23,0
51	0,26	0,393	0,000	0,096	0,236	0,037	0,040	0,004	0,000	5,9
52	0,26	0,393	-0,209	-0,353	0,299	-0,013	0,065	0,012	0,280	11,1
53	0,26	0,393	-0,126	0,011	0,274	0,008	0,054	0,005	0,000	6,9
54	0,26	0,314	0,000	0,042	0,189	0,029	0,026	0,003	0,000	8,6
55	0,26	1,795	-0,628	0,108	1,268	0,024	1,161	0,001	0,000	1,4
56	0,26	1,795	-0,314	0,278	1,174	0,109	0,994	0,026	2,425	8,7
57	0,26	1,795	-0,209	0,236	1,142	0,137	0,942	NaN	3,935	NaN
58	0,26	1,142	0,000	NaN	0,687	0,118	0,340	0,127	1,660	25,4
59	0,26	1,142	-0,314	-0,279	0,781	0,038	0,440	0,197	2,310	30,4
60	0,26	1,142	-0,209	0,189	0,750	0,065	0,406	0,074	2,110	14,0
61	0,26	1,142	-0,157	0,298	0,734	0,078	0,389	0,089	1,950	17,0
62	0,26	1,142	-0,126	0,352	0,725	0,086	0,379	0,101	2,020	19,9
63	0,26	1,142	0,314	0,379	0,592	0,194	0,253	0,084	0,705	24,5
64	0,26	1,142	0,157	0,437	0,640	0,157	0,295	0,116	0,690	36,3
65	0,26	0,898	0,000	0,430	0,540	0,091	0,210	0,096	1,400	22,5
66	0,26	0,739	0,000	0,289	0,444	0,074	0,143	NaN	1,490	NaN
67	0,26	0,739	-0,314	-0,414	0,539	-0,005	0,210	0,040	0,705	12,7
68	0,26	0,739	-0,209	0,059	0,507	0,022	0,186	0,018	0,910	8,7
69	0,26	0,739	-0,157	0,142	0,492	0,035	0,174	0,054	1,290	16,7
70	0,26	0,739	-0,126	0,203	0,482	0,043	0,168	0,028	2,110	15,3
71	0,26	0,739	0,157	0,404	0,397	0,111	0,114	0,016	0,490	25,5
72	0,26	0,739	0,126	0,396	0,407	0,103	0,119	0,014	0,360	13,4
73	0,26	0,661	0,000	0,400	0,398	0,065	0,114	0,031	1,100	22,0
74	0,37	0,598	0,000	0,305	0,360	0,055	0,072	0,018	0,625	21,0
75	0,37	0,503	0,000	0,259	0,302	0,045	0,051	0,006	0,350	7,3
76	0,37	0,503	-0,314	-0,367	0,397	-0,027	0,088	0,084	1,100	23,0
77	0,37	0,503	-0,209	-0,123	0,365	-0,002	0,075	0,010	0,300	8,6
78	0,37	0,503	-0,157	-0,007	0,349	0,010	0,068	0,005	0,270	7,0
79	0,37	0,503	-0,126	0,037	0,340	0,017	0,065	0,006	0,340	7,6
80	0,37	0,503	0,209	0,106	0,239	0,088	0,032	0,003	0,210	5,0
81	0,37	0,503	0,157	0,356	0,255	0,078	0,036	0,007	0,220	10,8

82	0,37	0,503	0,126	0,252	0,264	0,072	0,039	0,006	0,240	9,3
83	0,37	0,393	0,000	0,169	0,236	0,035	0,031	0,006	0,260	9,4
84	0,37	0,393	-0,314	-0,393	0,331	-0,037	0,061	0,057	0,650	20,5
85	0,37	0,393	-0,209	-0,243	0,299	-0,012	0,050	0,009	0,305	10,1
86	0,37	0,393	-0,157	-0,045	0,283	0,000	0,045	0,005	0,220	7,1
87	0,37	0,393	-0,126	-0,045	0,274	0,007	0,042	0,006	0,225	8,6
88	0,37	0,314	0,000	0,063	0,189	0,027	0,020	0,005	0,235	9,3
89	0,37	0,314	-0,126	0,004	0,227	0,000	0,029	0,004	0,000	5,6
90	0,37	1,795	-0,628	0,112	1,268	0,023	0,899	0,000	0,000	1,2
91	0,37	1,795	-0,314	0,249	1,174	0,101	0,771	0,078	2,480	16,6
92	0,37	1,795	-0,209	0,199	1,142	0,127	0,730	0,076	2,700	17,1
93	0,37	1,795	-0,157	0,277	1,127	0,140	0,710	0,158	2,035	16,2
94	0,37	1,795	-0,126	0,338	1,117	0,148	0,698	0,096	2,020	17,7
95	0,37	1,795	0,628	0,303	0,890	0,325	0,443	0,099	0,630	25,4
96	0,37	1,142	-0,628	-0,281	0,876	-0,043	0,429	NaN	0,000	NaN
97	0,37	1,142	-0,314	-0,016	0,781	0,035	0,341	0,069	2,200	16,0
98	0,37	1,142	-0,209	0,244	0,750	0,060	0,314	0,113	2,155	17,5
99	0,37	1,142	-0,157	0,285	0,734	0,073	0,301	0,108	2,420	17,5
100	0,37	1,142	-0,126	0,298	0,725	0,080	0,294	0,141	2,360	20,8
101	0,37	1,142	0,209	0,352	0,624	0,158	0,218	0,139	0,790	26,8
102	0,37	1,142	0,157	0,386	0,640	0,146	0,229	0,153	0,850	26,0
103	0,37	1,142	0,126	0,447	0,649	0,139	0,236	0,154	0,875	26,3
104	0,37	0,898	0,000	0,385	0,540	0,085	0,163	0,115	1,060	26,4
105	0,37	0,739	0,000	0,372	0,444	0,069	0,110	0,041	1,300	21,1
106	0,37	0,739	-0,314	-0,464	0,539	-0,004	0,162	0,063	1,010	22,7
107	0,37	0,739	-0,209	0,094	0,507	0,021	0,144	0,061	0,830	19,3
108	0,37	0,739	-0,157	0,201	0,492	0,033	0,135	0,031	0,910	12,7
109	0,37	0,739	-0,126	0,252	0,482	0,040	0,130	0,046	1,510	15,2
110	0,37	0,739	0,157	0,423	0,397	0,104	0,088	0,023	0,450	14,6
111	0,37	0,739	0,126	0,422	0,407	0,097	0,092	0,022	0,530	16,8
112	0,37	0,661	0,000	0,371	0,398	0,061	0,088	0,033	0,980	25,9
113	1,00	0,598	0,000	0,373	0,360	0,044	0,036	0,017	1,270	27,0
114	1,00	0,598	-0,314	-0,343	0,454	-0,014	0,058	NaN	0,770	NaN
115	1,00	0,598	-0,209	0,056	0,423	0,006	0,050	0,016	0,850	3,9
116	1,00	0,598	-0,157	0,170	0,407	0,015	0,046	0,008	0,700	8,0
117	1,00	0,598	-0,126	0,173	0,398	0,021	0,044	0,018	0,810	6,4
118	1,00	0,598	0,126	0,172	0,322	0,066	0,029	0,021	0,920	10,4
119	1,00	0,546	0,000	0,253	0,329	0,040	0,030	0,017	1,645	12,0
120	1,00	0,503	0,000	0,153	0,302	0,036	0,026	NaN	0,860	NaN
121	1,00	0,503	-0,314	-0,367	0,397	-0,021	0,044	0,059	0,705	15,6
122	1,00	0,503	-0,209	0,033	0,365	-0,002	0,037	0,007	0,925	2,7
123	1,00	0,503	-0,157	0,217	0,349	0,008	0,034	0,006	1,480	8,2
124	1,00	0,503	-0,126	0,215	0,340	0,014	0,032	0,008	2,395	5,4
125	1,00	0,503	0,126	0,000	0,264	0,058	0,020	NaN	0,000	NaN
126	1,00	0,465	0,000	0,043	0,280	0,034	0,022	0,005	0,500	2,2
127	1,00	0,465	-0,126	0,190	0,318	0,011	0,028	0,016	1,680	20,1
128	1,00	1,795	0,000	0,455	1,079	0,140	0,327	0,090	1,180	17,9

129	1,00	1,795	-0,419	-0,245	1,205	0,059	0,408	0,135	1,140	12,8
130	1,00	1,795	-0,314	0,153	1,174	0,079	0,387	0,048	1,870	12,9
131	1,00	1,795	-0,251	0,152	1,155	0,092	0,374	0,037	1,245	9,0
132	1,00	1,396	0,000	0,388	0,840	0,108	0,198	0,057	0,850	16,3
133	1,00	1,396	-0,628	-0,384	1,028	-0,014	0,297	NaN	0,695	NaN
134	1,00	1,396	-0,419	-0,348	0,965	0,027	0,262	NaN	0,780	NaN
135	1,00	1,396	-0,314	-0,051	0,934	0,048	0,245	0,060	0,710	11,0
136	1,00	1,396	-0,209	0,132	0,902	0,068	0,229	0,044	0,590	15,8
137	1,00	1,396	-0,157	0,169	0,887	0,078	0,221	0,030	0,730	6,5
138	1,00	1,396	-0,126	0,244	0,877	0,084	0,216	0,030	0,720	17,2
139	1,00	1,396	0,157	0,451	0,792	0,137	0,176	NaN	0,630	NaN
140	1,00	1,396	0,126	0,394	0,802	0,131	0,180	NaN	0,670	NaN
141	1,00	1,142	0,000	0,354	0,687	0,087	0,132	0,027	0,905	14,1
142	1,00	1,142	-0,628	-0,436	0,876	-0,033	0,215	0,088	0,645	30,9
143	1,00	1,142	-0,314	-0,108	0,781	0,028	0,171	0,054	0,550	15,0
144	1,00	1,142	-0,251	0,014	0,762	0,040	0,163	0,023	0,550	5,5
145	1,00	1,142	-0,209	0,087	0,750	0,048	0,158	0,030	0,555	10,3
146	1,00	1,142	-0,157	0,179	0,734	0,058	0,151	0,047	0,670	9,6
147	1,00	1,142	-0,126	0,197	0,725	0,063	0,147	0,032	0,630	11,8
148	1,00	1,142	0,628	0,192	0,498	0,197	0,070	0,025	0,410	12,0
149	1,00	1,142	0,314	0,297	0,592	0,144	0,099	0,032	0,365	11,2
150	1,00	1,142	0,209	0,295	0,624	0,125	0,109	0,032	0,340	14,6
151	1,00	1,142	0,157	0,312	0,640	0,116	0,115	0,024	0,460	21,1
152	1,00	1,142	0,126	0,335	0,649	0,110	0,118	0,027	0,515	25,2
153	1,00	0,967	0,000	0,307	0,581	0,073	0,095	0,044	0,750	14,4
154	1,00	0,967	-0,314	-0,252	0,676	0,014	0,128	0,042	0,560	12,3
155	1,00	0,967	-0,251	0,022	0,657	0,026	0,121	0,038	0,590	7,4
156	1,00	0,967	-0,209	0,082	0,644	0,034	0,116	0,019	0,630	7,1
157	1,00	0,967	-0,157	0,142	0,628	0,044	0,111	0,022	0,570	7,0
158	1,00	0,967	-0,126	0,178	0,619	0,050	0,108	0,025	0,590	13,0
159	1,00	0,967	0,314	0,308	0,487	0,129	0,067	0,047	0,480	23,8
160	1,00	0,967	0,209	0,265	0,518	0,111	0,075	0,034	0,370	15,6
161	1,00	0,967	0,157	0,257	0,534	0,101	0,080	0,031	0,360	18,7
162	1,00	0,967	0,126	0,281	0,543	0,096	0,083	0,024	0,340	16,3
163	1,00	0,838	0,000	0,263	0,504	0,063	0,071	0,031	0,750	14,1
164	1,00	0,739	0,000	0,285	0,444	0,055	0,055	0,025	1,380	13,3
165	1,00	0,739	-0,628	-0,376	0,633	-0,064	0,113	0,070	0,595	27,1
166	1,00	0,739	-0,251	-0,014	0,520	0,008	0,076	0,026	0,505	5,8
167	1,00	0,739	-0,209	0,051	0,507	0,016	0,072	0,015	0,480	4,4
168	1,00	0,739	-0,157	0,124	0,492	0,026	0,068	0,016	0,600	9,2
169	1,00	0,739	-0,126	0,153	0,482	0,032	0,065	0,020	0,605	7,6
170	1,00	0,739	0,157	0,148	0,397	0,083	0,044	0,058	0,815	15,2
171	1,00	0,739	0,126	0,169	0,407	0,077	0,046	0,032	0,770	22,1
172	1,00	0,661	0,000	0,483	0,398	0,049	0,044	0,075	1,335	14,7
173	2,00	0,628	0,000	0,000	0,378	0,038	0,026	NaN	NaN	NaN
174	2,00	0,546	0,000	0,000	0,329	0,032	0,019	NaN	NaN	NaN
175	2,00	1,795	0,000	0,324	1,079	0,113	0,209	0,152	1,580	21,5

176	2,00	1,795	-0,628	-0,411	1,268	0,014	0,288	0,056	0,855	28,4
177	2,00	1,795	-0,314	0,185	1,174	0,064	0,247	0,035	0,990	12,2
178	2,00	1,795	-0,209	0,282	1,142	0,080	0,234	0,070	1,190	18,3
179	2,00	1,795	-0,157	0,329	1,127	0,088	0,227	0,098	1,485	20,5
180	2,00	1,795	-0,126	0,363	1,117	0,093	0,224	0,090	1,420	21,2
181	2,00	1,795	0,628	0,281	0,890	0,208	0,142	0,040	0,450	16,8
182	2,00	1,795	0,314	0,412	0,985	0,161	0,174	0,035	0,550	20,1
183	2,00	1,795	0,209	0,393	1,016	0,145	0,185	0,103	0,880	24,0
184	2,00	1,795	0,126	0,380	1,042	0,132	0,194	0,111	1,075	24,7
185	2,00	1,396	0,000	0,406	0,840	0,087	0,126	0,110	1,510	24,9
186	2,00	1,396	-0,628	-0,488	1,028	-0,011	0,189	0,061	0,720	23,5
187	2,00	1,396	-0,314	0,119	0,934	0,038	0,156	0,025	0,635	11,8
188	2,00	1,396	-0,209	0,245	0,902	0,055	0,146	0,038	0,890	16,6
189	2,00	1,396	-0,157	0,282	0,887	0,063	0,141	0,050	0,920	16,5
190	2,00	1,396	-0,126	0,337	0,877	0,068	0,138	0,052	1,135	21,1
191	2,00	1,142	0,000	0,370	0,687	0,070	0,085	0,078	1,270	22,1
192	2,00	1,142	-0,628	-0,455	0,876	-0,027	0,137	0,021	0,485	39,1
193	2,00	1,142	-0,314	0,106	0,781	0,022	0,109	0,025	0,765	10,9
194	2,00	1,142	-0,209	0,221	0,750	0,038	0,101	0,025	0,760	14,7
195	2,00	1,142	-0,157	0,284	0,734	0,046	0,097	0,038	0,985	12,8
196	2,00	1,142	-0,126	0,308	0,725	0,051	0,094	0,079	1,050	17,9
197	2,00	1,142	0,314	0,343	0,592	0,117	0,063	0,046	0,970	16,0
198	2,00	1,142	0,209	0,308	0,624	0,102	0,070	0,075	0,855	20,0
199	2,00	1,142	0,157	0,401	0,640	0,094	0,073	0,048	0,640	17,3
200	2,00	1,142	0,126	0,395	0,649	0,089	0,075	0,043	0,780	21,9
201	2,00	0,811	0,000	0,212	0,487	0,049	0,043	0,015	1,505	5,9
202	2,00	0,898	0,000	0,340	0,540	0,055	0,052	0,039	1,275	17,3
203	2,00	0,898	-0,314	0,052	0,634	0,007	0,072	0,025	0,795	11,6
204	2,00	0,898	-0,209	0,231	0,603	0,023	0,065	0,035	0,940	12,8
205	2,00	0,898	-0,157	0,308	0,587	0,031	0,062	0,066	1,320	17,9
206	2,00	0,898	-0,126	0,299	0,577	0,036	0,060	0,041	1,825	16,2
207	2,00	0,898	0,209	0,198	0,477	0,085	0,041	0,014	0,550	10,6
208	2,00	0,898	0,157	0,261	0,492	0,078	0,043	0,023	1,215	16,8
209	2,00	0,898	0,126	0,294	0,502	0,073	0,045	0,019	1,570	12,7
210	2,00	0,739	0,000	0,119	0,444	0,045	0,035	0,003	0,000	2,6
211	2,00	0,739	-0,314	0,092	0,539	-0,003	0,052	0,026	1,185	9,1
212	2,00	0,739	-0,209	0,201	0,507	0,013	0,046	0,014	2,225	8,5
213	2,00	0,739	-0,157	0,225	0,492	0,021	0,043	0,100	2,215	19,7
214	2,00	0,739	-0,126	0,222	0,482	0,026	0,042	0,103	2,470	21,2
215	2,00	0,739	0,126	0,000	0,407	0,063	0,030	NaN	NaN	NaN
216	4,00	1,964	0,419	0,397	1,055	0,144	0,132	0,036	1,090	18,2
217	4,00	1,795	0,000	0,458	1,079	0,086	0,138	0,085	1,300	20,0
218	4,00	1,795	-0,628	-0,460	1,268	0,011	0,190	0,078	1,100	13,5
219	4,00	1,795	-0,519	-0,009	1,235	0,024	0,180	0,014	1,140	6,2
220	4,00	1,795	-0,499	0,043	1,229	0,026	0,179	0,025	1,210	4,0
221	4,00	1,795	-0,314	0,245	1,174	0,049	0,163	0,010	1,510	4,2
222	4,00	1,795	-0,200	0,379	1,140	0,062	0,154	0,015	2,200	15,1

223	4,00	1,795	-0,157	0,462	1,127	0,067	0,150	0,018	1,595	15,9
224	4,00	1,795	-0,126	0,325	1,117	0,071	0,148	0,111	2,180	14,7
225	4,00	1,676	0,419	-0,060	0,881	0,129	0,092	0,057	1,170	14,1
226	4,00	1,396	0,000	0,202	0,840	0,066	0,083	0,028	1,615	12,5
227	4,00	1,396	-0,628	-0,439	1,028	-0,008	0,125	0,134	1,700	9,5
228	4,00	1,396	-0,419	0,165	0,965	0,017	0,110	0,005	1,295	8,4
229	4,00	1,396	-0,314	0,265	0,934	0,029	0,103	0,006	1,400	3,6
230	4,00	1,396	-0,209	0,317	0,902	0,042	0,096	0,006	2,215	11,1
231	4,00	1,396	-0,157	0,341	0,887	0,048	0,093	0,009	1,450	13,6
232	4,00	1,396	-0,121	0,415	0,876	0,052	0,091	0,011	1,575	16,6
233	4,00	1,396	0,286	0,016	0,754	0,099	0,067	0,009	0,860	9,5
234	4,00	1,396	0,190	0,012	0,782	0,089	0,072	0,022	0,920	6,6
235	4,00	1,396	0,143	0,092	0,797	0,083	0,075	0,033	0,900	21,2
236	4,00	1,396	0,114	0,041	0,805	0,080	0,077	0,066	0,870	13,6
237	4,00	1,571	0,000	0,332	0,944	0,075	0,105	0,030	1,480	22,4
238	4,00	1,571	-0,628	-0,316	1,133	0,000	0,152	0,060	1,550	9,6
239	4,00	1,571	-0,419	0,194	1,070	0,025	0,135	0,008	1,295	13,4
240	4,00	1,571	-0,314	0,343	1,039	0,038	0,128	0,010	1,775	14,8
241	4,00	1,571	-0,209	0,360	1,007	0,050	0,120	0,011	1,965	17,4
242	4,00	1,571	-0,157	0,415	0,992	0,056	0,116	0,010	1,700	19,2
243	4,00	1,571	-0,126	0,489	0,982	0,060	0,114	0,015	1,970	14,4
244	4,00	1,571	0,628	0,000	0,756	0,147	0,068	NaN	NaN	NaN
245	4,00	1,571	0,419	-0,009	0,819	0,124	0,079	0,031	0,910	9,8
246	4,00	1,571	0,314	0,035	0,850	0,112	0,085	0,105	1,155	17,7
247	4,00	1,571	0,209	0,182	0,881	0,099	0,092	0,056	1,065	12,4
248	4,00	1,571	0,157	0,280	0,897	0,093	0,095	0,092	0,810	17,6
249	4,00	1,571	0,126	0,360	0,907	0,090	0,097	0,104	1,350	16,4
250	4,00	1,142	0,000	-0,004	0,687	0,054	0,056	0,011	1,015	6,9
251	4,00	1,142	-0,628	-0,408	0,876	-0,021	0,091	0,031	1,470	5,5
252	4,00	1,142	-0,314	0,069	0,781	0,017	0,072	0,004	0,000	5,9
253	4,00	1,142	-0,190	0,066	0,744	0,032	0,065	0,006	0,705	6,4
254	4,00	1,142	-0,143	0,069	0,730	0,037	0,063	0,009	1,515	6,8
255	4,00	1,142	-0,114	0,007	0,721	0,041	0,062	0,007	0,880	18,8
256	4,00	1,257	0,000	0,016	0,756	0,059	0,068	0,072	0,820	10,1
257	4,00	1,257	-0,628	-0,303	0,944	-0,015	0,105	0,007	1,560	4,9
258	4,00	1,257	-0,314	0,168	0,850	0,022	0,085	0,006	1,100	3,3
259	4,00	1,257	-0,209	0,197	0,819	0,035	0,079	0,008	0,940	4,2
260	4,00	1,257	-0,143	0,115	0,798	0,043	0,075	0,012	2,130	7,5
261	4,00	1,257	-0,126	0,119	0,793	0,045	0,074	0,011	1,690	5,5
262	4,00	1,257	0,628	0,000	0,567	0,130	0,038	NaN	NaN	NaN
263	4,00	1,257	0,314	0,000	0,661	0,096	0,052	NaN	NaN	NaN
264	4,00	1,257	0,209	0,019	0,693	0,084	0,057	0,008	0,880	7,0
265	4,00	1,257	0,143	0,019	0,713	0,076	0,060	0,008	0,815	4,2
266	4,00	1,257	0,126	-0,008	0,718	0,074	0,061	0,014	0,830	7,9
267	4,00	1,047	0,000	0,000	0,630	0,049	0,047	NaN	NaN	NaN
268	4,00	1,047	-0,209	-0,003	0,693	0,025	0,057	0,005	0,595	4,2

269	4,00	1,047	-0,157	0,024	0,677	0,031	0,054	0,004	0,000	5,8

Table E.2: Median grain size (D_{50}), angular velocity (ω) of the lid (l) and floor (f), transverse slope (dz/dy), average flow velocity (u) in streamwise (s) and normal (n) direction, sediment mobility (θ), characteristic dune height (Δ), length (λ), and lee side angle (°) of all morphodynamic experiments with low-density sediment (ρ_s = 1300 kg/m^3)

exp.	D_{50} [mm]	ω_l [rad/s]	ω_f [rad/s]	dz/dy [m/m]	u_s [m/s]	u_n [m/s]	θ [-]	Δ [m]	λ [m]	lee [°]
1	1.55	0.598	0.000	0.526	0.360	0.039	0.148	0.106	1.365	27.1
2	1.55	0.503	0.000	0.520	0.302	0.033	0.105	0.072	1.225	26.7
3	1.55	0.503	-0.157	-0.401	0.349	0.007	0.140	0.063	1.105	20.8
4	1.55	0.503	-0.126	0.126	0.340	0.012	0.133	0.032	0.610	14.1
5	1.55	0.503	-0.088	0.291	0.329	0.018	0.124	0.030	0.965	15.4
6	1.55	0.425	-0.065	0.323	0.275	0.017	0.087	0.043	1.630	18.5
7	1.55	0.422	-0.051	0.391	0.269	0.019	0.083	0.032	1.450	14.7
8	1.55	0.422	-0.128	-0.377	0.292	0.007	0.098	0.061	1.160	22.3
9	1.55	0.422	-0.106	0.129	0.285	0.010	0.093	0.033	0.800	16.3
10	1.55	0.393	0.000	0.525	0.236	0.025	0.064	0.106	1.440	25.3
11	1.55	0.359	0.000	0.512	0.216	0.023	0.053	0.083	1.370	25.6
12	1.55	0.353	-0.126	-0.350	0.250	0.003	0.072	0.050	1.420	19.7
13	1.55	0.353	-0.088	0.241	0.239	0.009	0.065	0.034	0.855	13.9
14	1.55	0.340	0.000	0.447	0.204	0.021	0.048	0.103	1.535	35.8
15	1.55	0.290	-0.084	0.234	0.199	0.005	0.046	0.040	0.980	14.6
16	1.55	0.286	0.000	0.355	0.172	0.018	0.034	0.077	1.485	20.3
17	1.55	0.251	0.000	0.185	0.151	0.016	0.026	0.003	0.855	3.5
18	1.55	0.739	0.000	0.406	0.444	0.049	0.227	0.162	1.445	25.2
19	1.55	0.739	-0.251	-0.318	0.520	0.007	0.310	0.121	1.270	20.5
20	1.55	0.739	-0.209	-0.357	0.507	0.014	0.295	0.113	1.110	21.0
21	1.55	0.739	-0.157	0.239	0.492	0.023	0.277	0.079	1.020	13.5
22	1.55	0.739	-0.126	0.258	0.482	0.028	0.267	0.039	1.330	12.7
23	1.55	0.739	-0.094	0.390	0.473	0.034	0.256	0.146	3.030	19.5

Appendix F

Experimental data: sorting experiments

Table F.1: Angular velocity (ω) of the lid (l) and floor (f), transverse slope (dz/dy), average flow velocity (u) in streamwise (s) and normal (n) direction, sediment mobility (θ), characteristic dune height (Δ) and length (λ) of the sorting experiments described in Chapter 4. When morphodynamic equilibrium was reached, 13 of the 28 experiments were sampled (y = sampled, n = not sampled).

exp.	sampled	ω_l	ω_f	dz/dy	u_s	u_n	θ	Δ	λ
	y/n	[rad/s]	[rad/s]	[m/m]	[m/s]	[m/s]	[-]	[m]	[m]
1	y	0.610	-0.124	0.254	0.404	0.026	0.069	0.082	2.010
2	y	0.610	-0.121	0.224	0.403	0.026	0.069	0.090	2.120
3	y	0.561	-0.150	0.146	0.382	0.016	0.062	0.053	1.530
4	n	0.528	-0.207	-0.265	0.380	0.001	0.061	0.117	1.540
5	y	0.528	-0.171	0.048	0.369	0.009	0.058	0.032	1.150
6	y	0.571	0.000	0.265	0.343	0.048	0.050	0.100	1.160
7	n	0.505	0.000	0.253	0.304	0.042	0.039	0.066	1.030
8	n	0.503	0.000	0.219	0.302	0.042	0.039	0.089	1.745
9	y	0.495	-0.180	0.078	0.351	0.004	0.052	0.030	1.270
10	y	0.487	-0.165	0.148	0.343	0.006	0.050	0.034	1.115
11	n	0.524	-0.190	-0.167	0.372	0.004	0.058	0.085	1.660
12	y	0.480	-0.085	0.255	0.314	0.022	0.042	0.079	0.800
13	n	0.465	-0.314	0.291	0.374	-0.028	0.633	0.051	1.195
14	y	0.483	-0.140	0.227	0.333	0.011	0.047	0.056	2.360
15	y	0.413	-0.159	0.007	0.296	0.001	0.037	0.034	2.460
16	n	0.405	0.000	0.223	0.244	0.033	0.025	0.015	1.370
17	y	0.405	-0.127	0.176	0.282	0.007	0.034	0.049	2.210
18	n	0.405	-0.105	0.235	0.275	0.012	0.032	0.043	2.145
19	n	0.374	-0.131	0.146	0.264	0.004	0.030	0.013	1.260
20	n	0.370	-0.140	0.191	0.264	0.002	0.029	0.024	1.600
21	n	1.142	0.000	0.331	0.687	0.101	0.199	0.144	1.690
22	n	0.911	-0.028	0.375	0.556	0.073	0.131	0.127	1.000
23	n	0.816	-0.025	0.384	0.498	0.065	0.105	0.137	1.055
24	y	0.806	-0.030	0.347	0.493	0.063	0.103	0.135	1.700
25	n	0.762	-0.209	-0.293	0.521	0.021	0.115	0.076	1.380
26	n	0.668	-0.217	-0.291	0.467	0.011	0.092	0.137	1.705
27	y	0.661	-0.181	0.038	0.452	0.018	0.086	0.060	1.200
28	n	0.661	-0.180	-0.017	0.452	0.018	0.086	0.050	1.110

Table F.2: Initial sediment mixture

sieve diameters $[mm]$	fractions retained
5.6	0.00e+00
2.8	1.98e-03
2	2.42e-02
1.7	8.06e-02
1.4	6.01e-02
1.18	5.47e-02
1	6.27e-02
0.85	9.22e-02
0.71	1.73e-01
0.6	1.91e-01
0.5	1.20e-01
0.425	4.18e-02
0.355	2.31e-02
0.3	3.82e-02
0.25	2.52e-02
0.212	8.49e-03
0.18	2.19e-03
0.15	2.35e-04
0.125	3.57e-05
0.106	2.36e-07
0.09	1.65e-06
0.075	0.00e+00
0.063	0.00e+00
0.053	0.00e+00

Table F.3: Example of a sieved bulk sample. This sample was taken at the end of experiment 2. The five columns represent the five locations along the cross-section at which the samples were taken.

sample location	inner bend r1 (-0.43)	r2 (-0.22)	centerline r3 (0)	r4 (0.22)	outer bend r5 (0.43)
sieve diameters [mm]	fractions retained				
5.6	0.00e+00	0.00e+00	0.00e+00	0.00e+00	0.00e+00
2.8	5.58e-04	1.57e-03	2.80e-03	7.54e-03	1.12e-02
2	9.91e-03	1.92e-02	3.43e-02	8.05e-02	1.09e-01
1.7	4.22e-02	6.71e-02	1.10e-01	2.48e-01	2.70e-01
1.4	3.59e-02	4.43e-02	7.77e-02	1.58e-01	1.47e-01
1.18	3.17e-02	4.53e-02	5.78e-02	8.68e-02	1.04e-01
1	5.07e-02	4.16e-02	7.98e-02	9.28e-02	5.27e-02
0.85	6.04e-02	9.78e-02	9.26e-02	7.12e-02	8.93e-02
0.71	1.41e-01	1.59e-01	1.91e-01	1.06e-01	7.78e-02
0.6	2.21e-01	2.16e-01	1.77e-01	8.08e-02	6.65e-02
0.5	1.74e-01	1.44e-01	9.65e-02	3.80e-02	3.68e-02
0.425	7.05e-02	5.16e-02	3.14e-02	1.16e-02	1.14e-02
0.355	3.45e-02	3.15e-02	1.14e-02	4.34e-03	6.08e-03
0.3	7.17e-02	4.02e-02	2.19e-02	7.40e-03	8.31e-03
0.25	3.76e-02	3.13e-02	1.01e-02	4.35e-03	7.25e-03
0.212	1.46e-02	7.75e-03	3.89e-03	1.83e-03	1.95e-03
0.18	2.85e-03	1.97e-03	8.46e-04	3.58e-04	5.43e-04
0.15	1.67e-04	1.66e-04	8.46e-05	4.94e-05	4.07e-05
0.125	1.40e-05	0.00e+00	8.46e-05	7.41e-05	0.00e+00
0.106	0.00e+00	0.00e+00	0.00e+00	0.00e+00	0.00e+00
0.09	0.00e+00	0.00e+00	0.00e+00	0.00e+00	0.00e+00
0.075	0.00e+00	0.00e+00	0.00e+00	0.00e+00	0.00e+00
0.063	0.00e+00	0.00e+00	0.00e+00	0.00e+00	0.00e+00
0.053	0.00e+00	0.00e+00	0.00e+00	0.00e+00	0.00e+00

References

Allen, J. (1968). The diffusion of grains in the lee of ripples, dunes, and sand deltas. *Journal of Sedimentary Research* 38.2, pp. 621–633.

Allen, J. and J. Collinson (1974). The superimposition and classification of dunes formed by unidirectional aqueous flows. *Sedimentary Geology* 12.3, pp. 169–178.

Armanini, A., G. Di Silvio, and S. Albanis (1989). A one-dimensional model for the transport of a sediment mixture in non-equilibrium conditions [Un modèle filaire en régime non permanent du transport de sediments de granulométrie etendue]. *Journal of Hydraulic Research* 27.3. cited By 1, pp. 455–462. DOI:10.1080/00221688909499177.

Asahi, K., Y. Shimizu, J. Nelson, and G. Parker (2013). Numerical simulation of river meandering with self-evolving banks. *Journal of Geophysical Research: Earth Surface* 118.September, pp. 2208–2229. DOI:10.1002/JGRF.20150.

Ashley, G. M. (1990). Classification of large-scale subaqueous bedforms: a new look at an old problem-SEPM bedforms and bedding structures. *Journal of Sedimentary Research* 60.1.

Ashworth, P. J. and R. I. Ferguson (1989). Size-selective entrainment of bed load in gravel bed streams. *Water Resources Research* 25.4, pp. 627–634.

Ashworth, P. J., J. L. Best, J. E. Roden, C. S. Bristow, and G. J. Klaassen (2000). Morphological evolution and dynamics of a large, sand braid-bar, Jamuna River, Bangladesh. *Sedimentology* 47.3, pp. 533–555.

Baar, A. W., J. de Smit, W. S. Uijttewaal, and M. G. Kleinhans (2018). Sediment transport of fine sand to fine gravel on transverse bed slopes in rotating annular flume experiments. *Water Resources Research* 54.1, pp. 19–45.

Bagnold, R. (1977). Bed load transport by natural rivers. *Water resources research* 13.2, pp. 303–312.

Bennett, S. J., J. S. Bridge, and J. L. Best (1998). Fluid and sediment dynamics of upper stage plane beds. *Journal of Geophysical Research* 103, pp. 1239–1274.

Bennett, S. and J. Best (1995). Mean flow and turbulence structure over fixed, two-dimensional dunes: Implications for sediment transport and bedform stability. *Sedimentology* 42.3, pp. 491–513.

Best, J. (2005). The fluid dynamics of river dunes: A review and some future research directions. *Journal of Geophysical Research: Earth Surface* 110.F4.

Best, J. and R. Kostaschuk (2002). An experimental study of turbulent flow over a low-angle dune. *Journal of Geophysical Research: Oceans* 107.C9.

Blanckaert, K. and H. J. de Vriend (2003). Nonlinear modeling of mean flow redistribution in curved open channels. *Water Resources Research* 39.12.

Blois, G., J. L. Best, G. H. Sambrook Smith, and R. J. Hardy (2014). Effect of bed permeability and hyporheic flow on turbulent flow over bed forms. *Geophysical Research Letters* 41.18, pp. 6435–6442.

Blom, A. and G. Parker (2004). Vertical sorting and the morphodynamics of bed form–dominated rivers: A modeling framework. *Journal of Geophysical Research: Earth Surface* 109.F2.

Blom, A., J. S. Ribberink, and G. Parker (2008). Vertical sorting and the morphodynamics of bed form-dominated rivers: A sorting evolution model. *Journal of Geophysical Research: Earth Surface* 113.1, pp. 1–15. DOI:10.1029/2006JF000618.

Blondeaux, P. and G. Vittori (2016). A model to predict the migration of sand waves in shallow tidal seas. *Continental Shelf Research* 112, pp. 31–45. DOI:10.1016/J.CSR.2015.11.011.

Bolla Pittaluga, M., R. Repetto, and M. Tubino (2003). Correction to "Channel bifurcation in braided rivers: Equilibrium configurations and stability". *Water Resources Research* 39.3, pp. 1–13. DOI:10.1029/2003WR002754.

Bolla Pittaluga, M., G. Coco, and M. G. Kleinhans (2015). A unified framework for stability of channel bifurcations in gravel and sand fluvial systems. *Geophysical Research Letters* 42.18, pp. 7521–7536. DOI:10.1002/2015GL065175.

Booij, R (1994). Measurements of the flow field in a rotating annular flume. *Communications on Hydraulic and Geotechnical Engineering*.

Booij, R. (2003). Measurements and large eddy simulations of the flows in some curved flumes. *Journal of Turbulence* 4.March 2015, pp. 37–41. DOI:10.1088/1468-5248/4/1/008.

Braat, L., T. v. Kessel, J. R. Leuven, and M. G. Kleinhans (2017). Effects of mud supply on large-scale estuary morphology and development over centuries to millennia. *Earth Surface Dynamics* 5.4, pp. 617–652.

Bridge, J. S. (1992). A revised model for water flow, sediment transport, bed topography and grain size in natural river bends. *Water Resources Research* 28.4, pp. 999–1013.

Bridge, J. S. (2003). *Rivers and Floodplains*. Oxford:Blackwell.

Bridge, J. S. and J. L. Best (1988). Flow, sediment transport and bedform dynamics over the transition from dunes to upper-stage plane beds: Implications for the formation of planar laminae. *Sedimentology* 35.5, pp. 753–763.

Bridge, J. S. and J. Jarvis (1976). Flow and sedimentary processes in the meandering river South Esk, Glen Clova, Scotland. *Earth surface processes* 1.4, pp. 303–336.

Bridge, J. and J. Jarvis (1982). The dynamics of a river bend: a study in flow and sedimentary processes. *Sedimentology* 29.4, pp. 499–541.

Brown, S. et al. (2014). Shifting perspectives on coastal impacts and adaptation. *Nature Climate Change* 4.9, p. 752.

Caldwell, R. L. and D. A. Edmonds (2014). Journal of Geophysical Research : Earth Surface. *Journal of Geophysical Research: Earth Surface* 119, pp. 961–982. DOI:10.1002/2013JF002965.RECEIVED.

Canestrelli, A., W. Nardin, D. Edmonds, S. Fagherazzi, and R. Slingerland (2014). Importance of frictional effects and jet instability on the morphodynamics of river mouth bars and levees. *Journal of Geophysical Research: Oceans* 119.1, pp. 509–522.

Carling, P. A. (1999). Subaqueous gravel dunes. *Journal of Sedimentary Research* 69.3, pp. 534–545.

Carrigy, M. A. (1970). Experiments on the angles of repose of granular materials 1. *Sedimentology* 14.3-4, pp. 147–158.

Chavarrías, V., G. Stecca, and A. Blom (2018). Ill-posedness in modeling mixed sediment river morphodynamics. *Advances in Water Resources* 114, pp. 219–235.

Cisneros, J., J. Best, and T. Van Dijk (In prep). The shape of dunes in the World's big rivers. *Nature Geoscience*.

Crosato, A. and E. Mosselman (2009). Simple physics-based predictor for the number of river bars and the transition between meandering and braiding. *Water Resources Research* 45.3, pp. 1–14. DOI:10.1029/2008WR007242.

Dam, G, M Van der Wegen, R. Labeur, and D Roelvink (2016). Modeling centuries of estuarine morphodynamics in the Western Scheldt estuary. *Geophysical Research Letters* 43.8, pp. 3839–3847.

Dam, G. and A. J. Bliek (2013). Using a sand–mud model to hindcast the morphology near Waarde, the Netherlands. In: *Proceedings of the Institution of Civil Engineers-Maritime Engineering*. Vol. 166. Thomas Telford Ltd, pp. 63–75.

Dastgheib, A and J. Roelvink (2010). Effect of different sediment mixtures on the long-term morphological simulation of tidal basins. *River, Coastal and Estuarine Morphodynamics: RCEM 2009*, pp. 913–918.

Davies, A. and P. Robins (2017). Residual flow, bedforms and sediment transport in a tidal channel modelled with variable bed roughness. *Geomorphology* 295, pp. 855–872.

Dietrich, W. E. and J. D. Smith (1984). Bed Load Transport in a River Meander. *Water Resources Research* 20.10, pp. 1355–1380. DOI:10.1029/WR020I010P01355.

Dietrich, W. E. and P. Whiting (1989). Boundary shear stress and sediment transport in river meanders of sand and gravel. *River meandering* 12, pp. 1–50.

Dinehart, R. L. (1992). Evolution of coarse gravel bed forms: Field measurements at flood stage. *Water Resources Research* 28.10, pp. 2667–2689.

Dissanayake, D., J. Roelvink, and M Van der Wegen (2009). Modelled channel patterns in a schematized tidal inlet. *Coastal Engineering* 56.11-12, pp. 1069–1083.

Dissanayake, D., A. Wurpts, M. Miani, H. Knaack, H. Niemeyer, and J. Roelvink (2012). Modelling morphodynamic response of a tidal basin to an anthropogenic effect: Ley Bay, East Frisian Wadden Sea - applying tidal forcing only and different sediment fractions. *Coastal Engineering* 67. cited By 12, pp. 14–28. DOI:10.1016/J.COASTALENG.2012.04.001.

Edmonds, D. and R. Slingerland (2007). Mechanics of river mouth bar formation: Implications for the morphodynamics of delta distributary networks. *Journal of Geophysical Research: Earth Surface* 112.F2.

Edmonds, D. and R. Slingerland (2008). Stability of delta distributary networks and their bifurcations. *Water Resources Research* 44.9.

Edmonds, D. A. and R. L. Slingerland (2009). Significant effect of sediment cohesion on delta morphology. *Nature Geoscience* 3.2, pp. 105–109. DOI:10.1038/NGEO730.

Einstein, H. A. et al. (1950). *The bed-load function for sediment transportation in open channel flows*. Vol. 1026.

Engelund, F. (1974). Flow and bed topography in channel bends. *Jounal of the Hydraulics Division* 100.11, pp. 1631–1647.

Engelund, F. (1975). Instability of flow in a curved alluvial channel. *Journal of Fluid Mechanics* 72.1, p. 145. DOI:10.1017/S002211207500300X.

Engelund, F. and E. Hansen (1967). A monograph on sediment transport in alluvial streams. *Technical University of Denmark ostervoldgade 10, Copenhagen K.*

Fernandez Luque, R and R Van Beek (1976). Erosion and transport of bed-load sediment. *Journal of hydraulic research* 14.2, pp. 127–144.

Francalanci, S. and L. Solari (2008). Bed-Load Transport Equation on Arbitrarily Sloping Beds. *Journal of Hydraulic Engineering* 134.January, pp. 110–115. DOI:10.1061/(ASCE)0733-9429(2008)134:1(110).

Francalanci, S., L. Solari, and M. Toffolon (2009). Local high-slope effects on sediment transport and fluvial bed form dynamics. *Water Resources Research* 45.5, pp. 1–15. DOI:10.1029/2008WR007290.

French, J. (2003). Airborne LiDAR in support of geomorphological and hydraulic modelling. *Earth Surface Processes and Landforms: The Journal of the British Geomorphological Research Group* 28.3, pp. 321–335.

French, J. (2010). Critical perspectives on the evaluation and optimization of complex numerical models of estuary hydrodynamics and sediment dynamics. *Earth Surface Processes and Landforms: The Journal of the British Geomorphological Research Group* 35.2, pp. 174–189.

Frings, R. M. (2008). Downstream fining in large sand-bed rivers. *Earth-Science Reviews* 87.1-2, pp. 39–60. DOI:10.1016/J.EARSCIREV.2007.10.001.

Ganju, N. K., D. H. Schoellhamer, and B. E. Jaffe (2009). Hindcasting of decadal-timescale estuarine bathymetric change with a tidal-timescale model. *Journal of Geophysical Research: Earth Surface* 114.F4.

Geleynse, N., J. E. A. Storms, D. R. Walstra, H. R. A. Jagers, Z. B. Wang, and M. J. F. Stive (2010). Controls on river delta formation: insights from numerical modelling. *Earth and Planetary Science Letters* 302, pp. 217–226. DOI:10.1016/J.EPSL.2010.12.013.

Grasmeijer, B., G. Dam, and M. Taal (2013). *Actualisatierapport Delft3D Schelde-estuarium (in Dutch)*. Tech. rep. International Marine & Dredging Consultants.

Grenfell, M. C. (2012). Chute Channels in Large , Sand-Bed Meandering Rivers Chute Channels in Large , Sand-Bed Meandering Rivers. PhD thesis. University of Exeter.

Gruijters, S. H.L. L., J. Schokker, and J. G. Veldkamp (2004). *Kartering moeilijk erodeerbare lagen in het Schelde estuarium (in Dutch)*. rapport NITG 03213B1208. TNO.

Guijters, S., J. Veldkamp, J Gunnink, and J. Bosch (2001). De lithologische en sedimentologische opbouw van de ondergrond van de Pannerdensche Kop. *TNONITG report NITG*, pp. 01–166.

Guo, L., M. van der Wegen, D. Roelvink, and Q. He (2015). Exploration of the impact of seasonal river discharge variations on long-term estuarine morphodynamic behavior. *Coastal Engineering* 95. cited By 9, pp. 105–116. DOI:10.1016/J.COASTALENG.2014.10.006.

Guy, H. P., D. B. Simons, and E. V. Richardson (1966). *Summary of alluvial channel data from flume experiments, 1956-61*. US Government Printing Office.

Hajek, E. A. and D. Edmonds (2014). Is river avulsion style controlled by floodplain morphodynamics?. *Geology* 42.3, pp. 199–202.

Hasbo, P. B. (1995). Flow and sediment transport over oblique bed forms. *Series paper/Institute of hydrodynamics and hydraulic engineering (Lyngby)*.

Hasegawa, K. (1981). Bank-erosion discharge based on a non-equilibrium theory. In: *Proc. JSCE, Tokyo*, pp. 37–50.

Hey, R. (1991). Distribution and sedimentary characteristics of bedload transport in gravel-bed rivers. In: *Proceedings of the International Grain Sorting Seminar*. Vol. 1, pp. 371–398.

Hibma, A, H. De Vriend, and M. Stive (2003). Numerical modelling of shoal pattern formation in well-mixed elongated estuaries. *Estuarine, Coastal and Shelf Science* 57.5-6, pp. 981–991.

Hibma, A., M. Stive, and Z. Wang (2004). Estuarine morphodynamics. *Coastal Engineering* 51.8-9. cited By 42, pp. 765–778. DOI:10.1016/J.COASTALENG.2004.07.008.

Hickin, E. J. (1974). The development of meanders in natural river-channels. *American Journal of Science* 274.4, pp. 414–442.

Hoey, T. B. and R. Ferguson (1994). Numerical simulation of downstream fining by selective transport in gravel bed rivers: Model development and illustration. *Water Resources Research* 30.7, pp. 2251–2260. DOI:10.1029/94WR00556.

Horstman, E., C. Dohmen-Janssen, T. Bouma, and S. Hulscher (2015). Tidal-scale flow routing and sedimentation in mangrove forests: Combining field data and numerical modelling. *Geomorphology* 228. cited By 13, pp. 244–262. DOI:10.1016/J.GEOMORPH.2014.08.011.

Hu, K., Q. Chen, H. Wang, E. Hartig, and P. Orton (2018). Numerical modeling of salt marsh morphological change induced by Hurricane Sandy. *Coastal Engineering* 132. cited By 1, pp. 63–81. DOI:10.1016/J.COASTALENG.2017.11.001.

Hulscher, S. J. (1996). Tidal-induced large-scale regular bed form patterns in a three-dimensional shallow water model. *Journal of Geophysical Research: Oceans* 101.C9, pp. 20727–20744.

Ikeda, B. S., M Asce, M. Yamasaka, A. M. Asce, and M. Chiyoda (1987). Bed Topography and Sorting in Bends. *Journal of Hydraulic Engineering* 113.2, pp. 190–204.

Ikeda, S. (1984). Lateral bed-load transport on side slopes - closure. *Journal of Hydraulic Engineering* 110.2, pp. 200–203.

Ikeda, S. (1989). Sediment transport and sorting at bends. *Water Resources Monograph* 12, pp. 103–125. DOI:10.1029/WM012P0103.

Ikeda, S. and T. Nishimura (1986). Flow and Bed Profile in Meandering Sand Silt Rivers. *Journal of Hydraulic Engineering* 112.7, pp. 562–579. DOI:10.1061/(ASCE)0733-9429(1986)112:7(562).

Jiménez-Robles, A., M Ortega-Sánchez, and M. Losada (2016). Effects of basin bottom slope on jet hydrodynamics and river mouth bar formation. *Journal of Geophysical Research: Earth Surface* 121.6, pp. 1110–1133.

Johannesson, H. and G. Parker (1989). Linear theory of river meanders. *River meandering* 12, pp. 181–213.

Julien, P. Y. and G. J. Klaassen (1995). Sand-dune geometry of large rivers during floods. *Journal of Hydraulic Engineering* 121.9, pp. 657–663.

Kisling-Moller, J (1993). Bedform migration and related sediment transport in a meander bend. *Alluvial Sedimentation (Special Publication 17 of the IAS)* 66, p. 51.

Kleinhans, M. G., H. R. A. Jagers, E. Mosselman, and C. J. Sloff (2008). Bifurcation dynamics and avulsion duration in meandering rivers by one-dimensional and three-dimensional models. *Water Resources Research* 44.8, pp. 1–31. DOI:10.1029/2007WR005912.

Kleinhans, M. G. (2001). The key role of fluvial dunes in transport and deposition of sand–gravel mixtures, a preliminary note. *Sedimentary Geology* 143.1-2, pp. 7–13.

Kleinhans, M. G. (2005). Grain-size sorting on grainflows at the lee side of deltas. *Sedimentology* 52.2, pp. 291–311. DOI:10.1111/j.1365-3091.2005.00698.x.

Kleinhans, M. G. (2010). Sorting out river channel patterns. *Progress in Physical Geography* 34.3, pp. 287–326. DOI:10.1177/0309133310365300.

Kleinhans, M. G. and L. C. van Rijn (2002). Stochastic prediction of sediment transport in sand-gravel bed rivers. *Journal of hydraulic engineering* 128.4, pp. 412–425.

Kleinhans, M. G. and J. H. van den Berg (2011). River channel and bar patterns explained and predicted by an empirical and a physics-based method. *Earth Surface Processes and Landforms* 36.6, pp. 721–738. DOI:10.1002/esp.2090.

Kleinhans, M. G., H. J. Weerts, and K. M. Cohen (2010). Avulsion in action: reconstruction and modelling sedimentation pace and upstream flood water levels following a Medieval tidal-river diversion catastrophe (Biesbosch, The Netherlands, 1421–1750 AD). *Geomorphology* 118.1-2, pp. 65–79.

Kleinhans, M. G., J. R.F. W. Leuven, L. Braat, and A. W. Baar (2017). Scour holes and ripples occur below the hydraulic smooth to rough transition of movable beds. *Sedimentology* 64.5, pp. 1381–1401. DOI:10.1111/sed.12358.

Kleinhans, M., A. Wilbers, and W. Ten Brinke (2007). Opposite hysteresis of sand and gravel transport upstream and downstream of a bifurcation during a flood in the River Rhine, the Netherlands. *Netherlands Journal of Geosciences/Geologie en Mijnbouw* 86.3.

Kleinhans, M., H Markies, S. De Vet, F. Postema, et al. (2011). Static and dynamic angles of repose in loose granular materials under reduced gravity. *Journal of Geophysical Research: Planets* 116.E11.

Koch, F. and C. Flokstra (1981). Bed level computations for curved alluvial channels. In: *19th International association for hydraulic research congress*.

Kostaschuk, R. and P. Villard (1996). Flow and sediment transport over large subaqueous dunes: Fraser River, Canada. *Sedimentology* 43.5, pp. 849–863.

Kwoll, E, J. Venditti, R. Bradley, and C. Winter (2017). Observations of Coherent Flow Structures Over Subaqueous High-and Low-Angle Dunes. *Journal of Geophysical Research: Earth Surface* 122.11, pp. 2244–2268.

Leeder, M. (1980). On the stability of lower stage plane beds and the absence of current ripples in coarse sands. *Journal of the Geological Society* 137.4, pp. 423–429.

Lefebvre, A. and C. Winter (2016). Predicting bed form roughness: the influence of lee side angle. *Geo-Marine Letters* 36.2, pp. 121–133.

Leonardi, N., A. Canestrelli, T. Sun, and S. Fagherazzi (2013). Effect of tides on mouth bar morphology and hydrodynamics. *Journal of Geophysical Research: Oceans* 118.9, pp. 4169–4183.

Leopold, L. B. (1960). *Flow resistance in sinuous or irregular channels*. US Government Printing Office.

Leuven, J. R.F. W., M. G. Kleinhans, S. A. H. Weisscher, and M. V. D. Vegt (2016). Tidal sand bar dimensions and shapes in estuaries. *Earth Science Reviews* 161, pp. 204–223. DOI:10.1016/j.earscirev.2016.08.004.

Liedermann, M., P. Gmeiner, A. Kreisler, M. Tritthart, and H. Habersack (2018). Insights into bedload transport processes of a large regulated gravel-bed river. *Earth Surface Processes and Landforms* 43.2, pp. 514–523.

Lotsari, E., D. Wainwright, G. D. Corner, P. Alho, and J. Käyhkö (2014). Surveyed and modelled one-year morphodynamics in the braided lower Tana River. *Hydrological Processes* 2716.April 2013, pp. 2685–2716. DOI:10.1002/hyp.9750.

Luan, H., P. Ding, Z. Wang, and J. Ge (2017). Process-based morphodynamic modeling of the Yangtze Estuary at a decadal timescale: Controls on estuarine evolution and future trends. *Geomorphology* 290. cited By 10, pp. 347–364. DOI:10.1016/J.GEOMORPH.2017.04.016.

Marciano, R., Z. B. Wang, A. Hibma, H. J. D. Vriend, and A. Defina (2005). Modeling of channel patterns in short tidal basins. *Journal of Geophysical Research* 110, pp. 1–13. DOI:10.1029/2003JF000092.

Mariotti, G. and A. Canestrelli (2017). Long-term morphodynamics of muddy backbarrier basins: Fill in or empty out?. *Water Resources Research* 53.8. cited By 3, pp. 7029–7054. DOI:10.1002/2017WR020461.

Mariotti, G, F Falcini, N Geleynse, M Guala, T Sun, and S Fagherazzi (2013). Sediment eddy diffusivity in meandering turbulent jets: Implications for levee formation at river mouths. *Journal of Geophysical Research: Earth Surface* 118.3, pp. 1908–1920.

Martínez-Fernández, V., M. Van Oorschot, J. De Smit, M. González del Tánago, and A. D. Buijse (2018). Modelling feedbacks between geomorphological and riparian vegetation responses under climate change in a Mediterranean context. *Earth Surface Processes and Landforms*.

Matsubara, Y. and A. D. Howard (2014). Modeling planform evolution of a mud-dominated meandering river: Quinn River, Nevada, USA. *Earth Surface Processes and Landforms* 39.10, pp. 1365–1377.

Maximova, T., S. Ides, T. De Mulder, and F. Mostaert (2009a). *LTV O & M thema Veiligheid - Deelproject 1: Verbetering hydrodynamisch NeVla model ten behoeve van scenario-analyse (in Dutch)*. WL rapporten 756_05. Antwerp, Belgium: Flanders Hydraulics Research & Deltares.

Maximova, T., S. Ides, J. Vanlede, T. De Mulder, and F. Mostaert (2009b). *Verbetering 2D randvoorwaardenmodel. Deelrapport 3: kalibratie bovenlopen (in Dutch)*. WL rapporten 753_09. Antwerp, Belgium: Flanders Hydraulics Research.

Maximova, T., S. Ides, T. De Mulder, and F. Mostaert (2009c). *Verbetering randvoorwaardenmodel. Deelrapport 4: Extra aanpassingen Zeeschelde (in Dutch)*. WL rapporten 753_09. Antwerp, Belgium: Flanders Hydraulics Research.

McLean, S., J. Nelson, and S. Wolfe (1994). Turbulence structure over two-dimensional bed forms: Implications for sediment transport. *Journal of Geophysical Research: Oceans* 99.C6, pp. 12729–12747.

Meyer-Peter, E. and R Müller (1948). Formulas for bed-load transport. In: *IAHSR 2nd meeting, Stockholm, appendix 2*. IAHR.

Mosselman, E, A Sieben, K Sloff, and A Wolters (1999). Effect of spatial grain size variations on two-dimensional river bed morphology. In: *Proceedings of River, Coastal and Estuarine Morphodynamics, Genova*. Vol. 1, pp. 499–507.

Motamedi, A., H. Afzalimehr, J. Gallichand, and E. F. N. Abadi (2012). Lee angle effects in near bed turbulence: An experimental study on low and sharp angle dunes. *International Journal of Hydraulic Engineering* 1.6, pp. 68–74.

Motamedi, A., H. Afzalimehr, G. Zenz, and M. Galoie (2014). Rans simulations of flow over dunes with low lee and sharp lee angles. In: *Advances in Hydroinformatics*. Springer, pp. 525–533.

Nanson, R. A. (2010). Flow fields in tightly curving meander bends of low width-depth ratio. *Earth Surface Processes and Landforms: The Journal of the British Geomorphological Research Group* 35.2, pp. 119–135.

Naqshband, S., J. S. Ribberink, and S. J. Hulscher (2014). Using both free surface effect and sediment transport mode parameters in defining the morphology of river dunes and their evolution to upper stage plane beds. *Journal of Hydraulic Engineering* 140.6, p. 06014010.

Nelson, J. M. and J. D. Smith (1989). Mechanics of flow over ripples and dunes. *Journal of Geophysical Research: Oceans* 94.C6, pp. 8146–8162.

Nicholas, A. P. (2013). Modelling the continuum of river channel patterns. *Earth Surface Processes and Landforms* 1196.June, pp. 1187–1196. DOI:10.1002/ESP.3431.

Nicholas, A., P. Ashworth, G. Sambrook Smith, and S. Sandbach (2013). Numerical simulation of bar and island morphodynamics in anabranching megarivers. *Journal of Geophysical Research: Earth Surface* 118.4, pp. 2019–2044.

Nienhuis, J. H., A. D. Ashton, W. Nardin, S. Fagherazzi, and L. Giosan (2016). Alongshore sediment bypassing as a control on river mouth morphodynamics. *Journal of Geophysical Research: Earth Surface* 121.4, pp. 664–683.

Nnafie, A, T Van Oyen, B De Maerschalck, Y Plancke, T Verwaest, and F. Mostaert (2016). *Modeling effects of geometry, initial bathymetry and sediment availability on the morphodynamic evolution of the Scheldt mouth area. Version 4.0. WL Rapporten,* 14_094. Tech. rep. Flanders Hydraulics Research: Antwerp, Belgium.

Nnafie, A, T Van Oyen, B De Maerschalck, M van der Vegt, and M. v. d. Wegen (2018). Estuarine channel evolution in response to closure of secondary basins: An observational and morphodynamic modeling study of the Western Scheldt Estuary. *Journal of Geophysical Research: Earth Surface* 123.1, pp. 167–186.

Norman, L. M., J. B. Sankey, D. Dean, J. Caster, S. DeLong, W. DeLong, and J. D. Pelletier (2017). Quantifying geomorphic change at ephemeral stream restoration sites using a coupled-model approach. *Geomorphology* 283, pp. 1–16.

Odgaard, A. J. (1981). transverse bed slope in alluvial channel bends. *Journal of the Hydraulics Division, Proceedings of the American Society of Civil Engineers* 107, pp. 1577–1594.

Oorschot, M. v., M. Kleinhans, G. Geerling, and H. Middelkoop (2016). Distinct patterns of interaction between vegetation and morphodynamics. *Earth Surface Processes and Landforms* 41.6, pp. 791–808.

Parker, G. and E. D. Andrews (1985). Sorting of Bed Load Sediment by Flow in Meander Bends. *Water Resources Research* 21.9, pp. 1361–1373. DOI:10.1029/WR021I009P01361.

Parker, G., C. Paola, and S. Leclair (2000). Probabilistic Exner sediment continuity equation for mixtures with no active layer. *Journal of Hydraulic Engineering* 126.11, pp. 818–826.

Parker, G., G. Seminara, and L. Solari (2003). Bed load at low Shields stress on arbitrarily sloping beds: Alternative entrainment formulation. *Water Resources Research* 39.7, pp. 1–11. DOI:10.1029/2001WR001253.

Parker, G. (1979). Hydraulic geometry of active gravel rivers. *Journal of the Hydraulic Division, American Society of Civil Engineers* 105.9, pp. 1185–1201.

Parsons, D., J. Best, O Orfeo, R. Hardy, R Kostaschuk, and S. Lane (2005). Morphology and flow fields of three-dimensional dunes, Rio Paraná, Argentina: Results from simultaneous multibeam echo sounding and acoustic Doppler current profiling. *Journal of Geophysical Research: Earth Surface* 110.F4.

Powell, D. M. (1998). Patterns and processes of sediment sorting in gravel-bed rivers. *Progress in Physical Geography* 22.1, pp. 1–32.

Ralston, D. and W. Geyer (2017). Sediment Transport Time Scales and Trapping Efficiency in a Tidal River. *Journal of Geophysical Research: Earth Surface* 122.11. cited By 1, pp. 2042–2063. DOI:10.1002/2017JF004337.

Raudkivi, A. J. and H.-H. Witte (1990). Development of bed features. *Journal of Hydraulic Engineering* 116.9, pp. 1063–1079.

Reesink, A., D. Parsons, P. Ashworth, J. Best, R. Hardy, B. Murphy, S. McLelland, and C Unsworth (2018). The adaptation of dunes to changes in river flow. *Earth-Science Reviews*.

Reesink, A. J. H. and J. Bridge (2007). Influence of superimposed bedforms and flow unsteadiness on formation of cross strata in dunes and unit bars. *Sedimentary Geology* 202.1-2, pp. 281–296.

Ribberink, J. S. (1987). Mathematical modelling of one-dimensional morphological changes in rivers with non-uniform sediment. *Faculty of Civil Engineering* Docteral.

Ridderinkhof, W., H. E. de Swart, M. van der Vegt, and P. Hoekstra (2014). Influence of the back-barrier basin length on the geometry of ebb-tidal deltas. *Ocean dynamics* 64.9, pp. 1333–1348.

Roden, J. E. (1998). The sedimentology and dynamics of mega-dunes, Jamuna River, Bangladesh. PhD thesis. University of Leeds.

Rossi, V. M., W. Kim, J. L. López, D. Edmonds, N. Geleynse, C. Olariu, R. J. Steel, M. Hiatt, and P. Passalacqua (2016). Impact of tidal currents on delta-channel deepening , stratigraphic architecture , and sediment bypass beyond the shoreline. *Geology* 44.11, pp. 927–930. DOI:10.1130/G38334.1.

Rousseau, Y. Y., M. J. Van de Wiel, and P. M. Biron (2017). Simulating bank erosion over an extended natural sinuous river reach using a universal slope stability algorithm coupled with a morphodynamic model. *Geomorphology* 295, pp. 690–704.

Ruessink, B. G., Y. Kuriyama, A. J.H. M. Reniers, J. A. Roelvink, and D. J. R. Walstra (2007). Modeling cross-shore sandbar behavior on the timescale of weeks. *Journal of Geophysical Research: Earth Surface* 112.3, pp. 1–15. DOI:10.1029/2006JF000730.

Sanyal, J. (2017). Predicting possible effects of dams on downstream river bed changes of a Himalayan river with morphodynamic modelling. *Quaternary International* 453, pp. 48–62.

Schramkowski, G. P., H. M. Schuttelaars, and H. E. De Swart (2002). The effect of geometry and bottom friction on local bed forms in a tidal embayment. *Continental Shelf Research* 22.11-13, pp. 1821–1833. DOI:10.1016/S0278-4343(02)00040-7.

Schrijvershof, R. and J. Vroom (2016). *Effecten van realistische (extreme) stortstrategieën in de Westerschelde (in Dutch)*. Tech. rep. Deltares.

Schuttelaars, H. and H. De Swart (1999). Initial formation of channels and shoals in a short tidal embayment. *Journal of fluid mechanics* 386, pp. 15–42.

Schuurman, F, Y Shimizu, T Iwasaki, and M. Kleinhans (2016). Dynamic meandering in response to upstream perturbations and floodplain formation. *Geomorphology* 253, pp. 94–109.

Schuurman, F. (2015). Bar and channel evolution in meandering and braiding rivers using physics-based modeling. PhD thesis. Utrecht University.

Schuurman, F. and M. G. Kleinhans (2015). Bar dynamics and bifurcation evolution in a modelled braided sand-bed river. *Earth surface processes and landforms* 40.10, pp. 1318–1333.

Schuurman, F., W. a. Marra, and M. G. Kleinhans (2013). Physics-based modeling of large braided sand-bed rivers: Bar pattern formation, dynamics, and sensitivity. *Journal of Geophysical Research: Earth Surface* 118.4, pp. 2509–2527. DOI:10.1002/2013JF002896.

Schuurman, F., W. Ta, S. Post, M. Sokolewicz, M. Busnelli, and M. Kleinhans (2018). Response of braiding channel morphodynamics to peak discharge changes in the Upper Yellow River. *Earth Surface Processes and Landforms*.

Schwarz, C., Q. Ye, D. Van Der Wal, L. Zhang, T. Bouma, T. Ysebaert, and P. Herman (2014). Impacts of salt marsh plants on tidal channel initiation and inheritance. *Journal of Geophysical Research: Earth Surface* 119.2. cited By 15, pp. 385–400. DOI:10.1002/2013JF002900.

Sekine, M. and G. Parker (1992). Bed-load transport on transverse slope. *Journal of Hydraulic Engineering* 118.4, pp. 513–535.

Seminara, G and M Turbino (2001). Sand bars in tidal channels. Part 1. Free bars. *Journal of fluid mechanincs* 440.2001, pp. 49–74.

Seminara, G., L. Solari, and G. Parker (2002). Bed load at low Shields stress on arbitrary sloping beds: Failure of the Bagnold hypothesis. *Water Resources Research* 38.11, pp. 31–1–31–16.

Sieben, J. and A. M. Talmon (2011). Bed-load transport in obliquely dune-covered riverbeds. *Journal of Hydraulic Research* 493.November 2012, pp. 317–324. DOI:10.1080/00221686.2011.566252.

Sloff, K. and E. Mosselman (Dec. 2007). Implications of Bed-Schematization in Morphological Models with Graded Sediment. *AGU Fall Meeting Abstracts*.

Sloff, K. and E. Mosselman (2012). Bifurcation modelling in a meandering gravel-sand bed river. *Earth Surface Processes and Landforms* 37.14, pp. 1556–1566. DOI:10.1002/ESP.3305.

Smajgl, A., T. Toan, D. Nhan, J Ward, N. Trung, L. Tri, V. Tri, and P. Vu (2015). Responding to rising sea levels in the Mekong Delta. *Nature Climate Change* 5.2, p. 167.

Smith, J. D. and S. McLean (1977). Boundary layer adjustments to bottom topography and suspended sediment. In: *Elsevier Oceanography Series*. Vol. 19. Elsevier, pp. 123–151.

Son, M. and T.-J. Hsu (2011). The effects of flocculation and bed erodibility on modeling cohesive sediment resuspension. *Journal of Geophysical Research: Oceans* 116.C3.

Soulsby, R., R. Whitehouse, et al. (1997). Threshold of sediment motion in coastal environments. In: *Pacific Coasts and Ports' 97: Proceedings of the 13th Australasian Coastal and Ocean Engineering Conference and the 6th Australasian Port and Harbour Conference; Volume 1*. Centre for Advanced Engineering, University of Canterbury, p. 145.

Southard, J. B. and L. A. Boguchwal (1990). Bed configuration in steady unidirectional water flows; Part 2, Synthesis of flume data. *Journal of Sedimentary Research* 60.5, pp. 658–679.

Stecca, G, R Measures, and D. Hicks (2017). A framework for the analysis of noncohesive bank erosion algorithms in morphodynamic modeling. *Water Resources Research* 53.8, pp. 6663–6686.

Struiksma, N., K. W. Olesen, C. Flokstra, and H. J. De Vriend (1985). Bed deformation in curved alluvial channels. *Journal of Hydraulic Research* 23.1, pp. 57–79. DOI:10.1080/00221688509499377.

Talmon, A. M. and J. Wiesemann (2006). Influence of Grain Size on the Direction of Bed- Load Transport on Transverse Sloping Beds. *Proceedings Third International Conference on Scour and Erosion*, pp. 632–639.

Talmon, A., N. Struiksma, and M. Van Mierlo (1995). Laboratory measurements of the direction of sediment transport on transverse alluvial-bed slopes. *Journal of Hydraulic Research* 33.4, pp. 495–517. DOI:10.1080/00221689509498657.

Temmerman, S, T. Bouma, J Van de Koppel, D Van der Wal, M. De Vries, and P. Herman (2007). Vegetation causes channel erosion in a tidal landscape. *Geology* 35.7, pp. 631–634.

Ten Brinke, W., A. Wilbers, and C Wesseling (1999). Dune Growth, Decay and Migration Rates during a Large-Magnitude Flood at a Sand and Mixed Sand–Gravel Bed in the Dutch Rhine River System. *Fluvial sedimentology VI*, pp. 15–32.

Thomas, R. G., D. G. Smith, J. M. Wood, J. Visser, E. A. Calverley-Range, and E. H. Koster (1987). Inclined heterolithic stratification—terminology, description, interpretation and significance. *Sedimentary Geology* 53.1-2, pp. 123–179.

Tran, T.-t., J. V. D. Kreeke, M. J. F. Stive, and D.-j. R. Walstra (2012). Cross-sectional stability of tidal inlets : A comparison between numerical and empirical approaches. *Coastal Engineering* 60, pp. 21–29. DOI:10.1016/J.COASTALENG.2011.08.005.

Tuan, T. Q., M. J. Stive, H. J. Verhagen, and P. J. Visser (2008). Process-based modeling of the overflow-induced growth of erosional channels. *Coastal Engineering* 55.6, pp. 468–483.

Van Bendegom, L. (1947). Enige beschouwingen over riviermofologie en rivierverbetering. *De Ingenieur* 59.4, pp. 1–11.

Van Dijk, W., M. Hiatt, J. van der Werf, and M. G. Kleinhans (2018). Effect of perturbations by shoal margin collapses on the morphodynamics of a sandy estuary. *Earth Surface Processes and Landforms*.

Van Rijn, L. C. (1984). Sediment transport, part III: bed forms and alluvial roughness. *Journal of hydraulic engineering* 110.12, pp. 1733–1754.

Van Rijn, L. C. (1993). *Principles of Sediment Transport in Rivers, Estuaries and Coastal Seas*. Aqua Publications.

Van de Lageweg, W. I., W. M. van Dijk, A. W. Baar, J. Rutten, and M. G. Kleinhans (2014). Bank pull or bar push: What drives scroll-bar formation in meandering rivers?. *Geology* 42.4, pp. 319–322. DOI:10.1130/G35192.1.

Van de Lageweg, W. I. and H. Feldman (2018). Process-based modelling of morphodynamics and bar architecture in confined basins with fluvial and tidal currents. *Marine Geology* 398.January, pp. 35–47. DOI:10.1016/J.MARGEO.2018.01.002.

Van den Berg, J. and A Van Gelder (1993). A new bedform stability diagram, with emphasis on the transition of ripples to plane bed in flows over fine sand and silt. In: *Alluvial Sedimentation, Special Publication*. Vol. 17. International Association of Sedimentologists, pp. 11–21.

Van der Wegen, M. and B. Jaffe (2014). Processes governing decadal-scale depositional narrowing of the major tidal channel in San Pablo Bay, California, USA. *Journal of Geophysical Research: Earth Surface* 119.5. cited By 8, pp. 1136–1154. DOI:10.1002/2013JF002824.

Van der Wegen, M. and J. A. Roelvink (2012). Reproduction of estuarine bathymetry by means of a process-based model: Western Scheldt case study, the Netherlands. *Geomorphology* 179, pp. 152–167. DOI:10.1016/J.GEOMORPH.2012.08.007.

Van der Vegt, H, J. E. A. Storms, D. J. R. Walstra, and N. C. Howes (2016). Can bed load transport drive varying depositional behaviour in river delta environments ?. *Sedimentary Geology* 345, pp. 19–32. DOI:10.1016/J.SEDGEO.2016.08.009.

Van Der Wegen, M. and J. A. Roelvink (2008). Long-term morphodynamic evolution of a tidal embayment using a two-dimensional, process-based model. *Journal of Geophysical Research: Oceans* 113.3, pp. 1–23. DOI:10.1029/2006JC003983.

Van Der Wegen, M., A. Dastgheib, B. E. Jaffe, and D. Roelvink (2011). Bed composition generation for morphodynamic modeling: Case study of San Pablo Bay in California, USA. *Ocean Dynamics* 61.2-3, pp. 173–186. DOI:10.1007/S10236-010-0314-2.

Van Dijk, W. M., M. Hiatt, J. J. Van der Werf, and M. G. Kleinhans (subm). Effect of perturbations by shoal margin collapses on the morphodynamics of a sandy estuary. *Journal of Geophysical Research – Earth Surface*.

Van Dijk, W. M., F. Schuurman, W. I. Van de Lageweg, and M. G. Kleinhans (2014). Bifurcation instability and chute cutoff development in meandering gravel-bed rivers. *Geomorphology* 213, pp. 277–291.

Van Leeuwen, S., M Van der Vegt, and H. De Swart (2003). Morphodynamics of ebb-tidal deltas: a model approach. *Estuarine, Coastal and Shelf Science* 57.5-6, pp. 899–907.

Van Maren, D., J. Winterwerp, B. Wu, and J. Zhou (2009). Modelling hyperconcentrated flow in the Yellow River. *Earth Surface Processes and Landforms* 34.4, pp. 596–612.

Van Rijn, L., D. Walstra, and M. v. Ormondt (2004). Description of TRANSPOR2004 and Implementation in Delft3D-ONLINE. *Z3748*.

Van Rijn, L. C. (1984a). Sediment pick-up functions. *Journal of Hydraulic engineering* 110.10, pp. 1494–1502.

Van Rijn, L. C. (1984b). Sediment transport, part I: bed load transport. *Journal of hydraulic engineering* 110.10, pp. 1431–1456.

Vanoni, V. A. and L.-S. Hwang (1967). Bed forms and friction in streams. *Journal of the Hydraulics Division*.

Vargas-Luna, A., A. Crosato, N. Anders, A. J. Hoitink, S. D. Keesstra, and W. S. Uijttewaal (2018). Morphodynamic effects of riparian vegetation growth after stream restoration. *Earth Surface Processes and Landforms*.

Venditti, J. G., M. Church, and S. J. Bennett (2005). On the transition between 2D and 3D dunes. *Sedimentology* 52.6, pp. 1343–1359.

Vroom, J., P. L. M. De Vet, and J. J. Van der Werf (2015). *Validatie waterbeweging Delft3D NeVla model Westerscheldemonding (in Dutch)*. Tech. rep. Deltares.

Walstra, D. J. R., L. C. Van Rijn, M Van Ormondt, C Bri?re, and a. M. Talmon (2007). The effects of bed slope and wave skewness on sediment transport and morphology. *6th International Symposium on Coastal Engineering and Science of Coastal Sediment Processes*, pp. –. DOI:10.1061/40926(239)11.

Wiesemann, J.-U., P. Mewis, and U. C. E. Zanke (2006). Downslope Transport (Transverse Sediment Transport). *Third Chinese-German Joint Symposium in COastal and Ocean Engineering*.

Wilcock, P. R. and J. C. Crowe (2003). Surface-based transport model for mixed-size sediment. *Journal of Hydraulic Engineering* 129.2, pp. 120–128.

Williams, R., R Measures, D. Hicks, and J Brasington (2016). Assessment of a numerical model to reproduce event-scale erosion and deposition distributions in a braided river. *Water resources research* 52.8, pp. 6621–6642.

Willis, B. J. and H. Tang (2010). Three-Dimensional Connectivity of Point-Bar Deposits. *Journal of Sedimentary Research* 80.5, pp. 440–454. DOI:10.2110/JSR.2010.046.

Xie, D., Z. Wang, S. Gao, and H. De Vriend (2009). Modeling the tidal channel morphodynamics in a macro-tidal embayment, Hangzhou Bay, China. *Continental Shelf Research* 29.15, pp. 1757–1767.

Xie, D., S. Gao, Z. B. Wang, C. Pan, X. Wu, and Q. Wang (2017). Morphodynamic modeling of a large inside sandbar and its dextral morphology in a convergent estuary: Qiantang Estuary, China. *Journal of Geophysical Research: Earth Surface* 122.8, pp. 1553–1572.

Yang, S.-H., I.-T. Im, K.-N. Hwang, Y.-S. Cho, and H.-R. Ryu (2015). A numerical study on optimal rotation ratio and bottom shear stress in the counter-rotation mode of an annular flume. *Journal of Hydro-environment Research* 9.4, pp. 473 –481. DOI:HTTP://DX.DOI.ORG/10.1016/J.JHER.2015.02.002.

Yen, C. and K. Lee (1995). Bed Topography and Sediment Sorting in Channel Bend with Unsteady Flow. *Journal of Hydraulic Engineering* 121.August, pp. 591–599.

Yuill, B. T., A. Gaweesh, M. A. Allison, and E. A. Meselhe (2016a). Morphodynamic evolution of a lower Mississippi River channel bar after sand mining. *Earth Surface Processes and Landforms* 41.4, pp. 526–542.

Yuill, B. T., A. K. Khadka, J. Pereira, M. A. Allison, and E. A. Meselhe (2016b). Morphodynamics of the erosional phase of crevasse-splay evolution and implications for river sediment diversion function. *Geomorphology* 259, pp. 12–29.

Zhou, Z., M. Olabarrieta, L. Stefanon, A. D'Alpaos, L. Carniello, and G. Coco (2014). A comparative study of physical and numerical modeling of tidal network ontogeny. *Journal of Geophysical Research: Earth Surface* 119.4, pp. 892–912.

Acknowledgements

Looking back at the beginning of my PhD research, I thought that I would study sediment transport in experiments for 4 years, and if I was lucky, also in models. I had no idea that PhD research is so much more than working on a project. I learned a lot about doing research and about myself, and I was able to make this progress due to the people that I worked with. I would like to thank everyone that helped me along the way and that made it a lot of fun! Here, I would like to thank some of you in particular.

Maarten, ik ben je erg dankbaar voor alle kansen die je mij hebt gegeven en vooral voor de manier waarop je me hebt begeleid. Je bent altijd enthousiast en zoekt naar creatieve oplossingen waar anderen problemen zien. Vooral onze vele discussies hebben me gemotiveerd om het meeste uit mijn onderzoek te halen. Je daagde me altijd uit om mijn grenzen te verleggen, maar door jouw rotsvaste vertrouwen voelde het nooit alsof het mis kon gaan.

I was lucky to be part of a close research group, which made work so much fun and easier at times. Thanks to all the people that were part of it over the years: Lisanne, Jasper, Wout, Muriel, Marcio, Ivar, Will, Sanja, Harm-Jan, Jana, Steven and others. We had fun during dinners and drinks, and I especially have fond memories of going on fieldwork and to conferences together. It was very valuable to have a positive environment to practice presentations, test new ideas and ask for help on anything. Lisanne en Jasper, we zijn samen begonnen en dat voelde gelijk goed, het was fijn om samen met jullie uit te vinden hoe we zo'n PhD moesten aanpakken en om ervaringen te kunnen uitwisselen. Lisanne, wat ben ik blij dat we goede vriendinnen zijn geworden. Het betekent heel veel voor me dat je er altijd voor me bent en ik voel me helemaal thuis bij jou en Bas. Muriel, it feels like we have always been friends. Thank you for all the talks over coffees and croissants! Marcio, it was great to be able to talk to someone with the same cycling obsession, and I will miss our discussions over coffee and your humor. I hope we will continue our cycling bets and I promise to send you chocolate in the rare occasion that you will win. Wout, heel erg bedankt voor al je hulp en adviezen! Mijn project was een onderdeel van het Vici project *Turning the tide*. Ik wil graag de gebruikerscommissie van de Vici bedanken voor de discussies en enthousiasme voor mijn project.

Marjolein, we zijn al vriendinnen sinds dag 1 van onze studie en hebben daarna eigenlijk altijd hetzelfde gedaan. Ik heb ontzettend veel gehad aan jouw vriendschap als constante factor gedurende al die jaren! We hebben samen veel meegemaakt en het zal raar zijn om niet meer op dezelfde plek te werken (of bij dezelfde dagopvang te zitten). Ik ben blij dat je mijn paranimf bent. Wimala, jouw steun en aanmoedigingen waren onmisbaar. Ik vind het heel fijn dat je altijd enthousiast bent om wat leuks te doen, van bioscoopuitjes tot logeerpartijtjes. Eveline, wat vond ik het fijn om je als kantoorgenootje te hebben! Jouw praktische aanpak van je PhD was een inspiratie en de vanzelfsprekendheid waarmee je me helpt met zaken die jij natuurlijk al lang uitgezocht hebt is heel fijn. Maar het allerbelangrijkste: we hadden het altijd gezellig samen, we hebben veel afgekletst tijdens thee/koffie pauzes en etentjes. Ik wil ook graag de rest van het departement bedanken voor alle gezellige koffie- en lunchpauzes,

goede discussies en gesprekken die juist nergens over gaan, maar vooral ook voor de oprechte interesse. De goede werksfeer is heel belangrijk voor mij geweest, ik voelde me altijd thuis op het departement door de mensen die er werken.

Tijdens mijn PhD heb ik veel tijd doorgebracht in het lab van de TU Delft om alle experimenten uit te voeren die in dit proefschrift beschreven staan. Ik wil Wim en de technische staf hartelijk bedanken voor het meedenken en de vele hulp. De carrousel was niet de meest simpele experimentele opstelling en alles wat kapot kon, is wel eens kapot gegaan. Sander, de experimenten zouden niet mogelijk zijn geweest zonder je geduld en oplossingen voor al mijn gekke wensen ("kan er ook een computer op de ronddraaiende deksel?"). I always felt very welcome in Delft, and I would like to thank everyone working at the lab for adopting me as part of the group. Victor and Andres, thank you for the great times when sharing an office.

Jaco en Steven, bedankt voor jullie hulp met de experimenten en de gezelligheid in het lab. Jullie harde werk is een mooi onderdeel van mijn proefschrift geworden! Jaco en Niels, wat was het fijn dat jullie altijd kwamen helpen met zand verwisselen, vooral de vanzelfsprekendheid vond ik bijzonder.

Julia, we met at our first international conference when we were both inexperienced and slightly nervous. It was immediately clear that we had the same interests and way of thinking, which eventually resulted in writing a paper together. Especially staying at your place and working enthusiastically and efficiently on our project was an unforgettable experience. I am happy that we became friends, and that I can always call you for advice or just to talk!

Ik wil mijn familie en vrienden heel erg bedanken voor alle interesse in mijn onderzoek. Carien, Marleen, Rebecca en Saskia, bedankt voor de vele etentjes, uitjes en vakanties, viool-lessen, peptalks etc. Het is ontzettend fijn dat jullie er altijd voor me zijn. Tantemam Petra, bedankt dat je er altijd bent voor een luisterend oor en goede adviezen. Opa en oma, wat had ik graag gewild dat jullie dit nog hadden kunnen meemaken. Mede door jullie heb ik altijd het beste uit mezelf willen halen, en jullie liefde en trots helpt me nog steeds als ik me onzeker voel.

Marjolein, woorden kunnen niet beschrijven hoeveel je voor mij betekent. Wat is het fijn om iemand te hebben die mij altijd begrijpt, zonder dat ik het hoef uit te leggen. Zonder jou ben ik nergens. Lieve pap en mam, bedankt voor jullie steun en liefde. Door jullie was het logisch om door te studeren en jullie hebben mij altijd gestimuleerd om te doen wat goed voelt. Ik ben heel erg dankbaar voor alles wat jullie voor mij doen. Jullie vinden dat heel vanzelfsprekend, maar ik vind het heel bijzonder.

About the author

Anne Baar was born on 18 November 1989 in Hilversum. In 2008, she started her bachelor in Earth Sciences at Utrecht University, and graduated in 2011. She conducted experiments for her bachelor thesis on the formation of tidal channels in a tilting flume, which served as a pilot study for the Vici grant that funded her PhD research. In 2011, Anne continued at Utrecht University with a master in Physical Geography, focusing on river and coastal dynamics. Within her masters she gained more research experience by conducting experiments on a multitude of sediment transport processes. For her master thesis, she focused on the formation of scroll bars in experimental meandering rivers. Additionally, she gained modelling experience during an internship at Deltares by developing a Delft3D morphodynamic model of the West Bay sediment diversion at the Lower Mississippi River. She received her MSc degree in 2014 (cum laude). After graduating, Anne worked as a junior researcher at Utrecht University for 6 months, writing a literature review and research proposal on the dynamics of nature friendly river banks in groyne fields along the IJssel and Nederrijn-Lek rivers. In December 2014, she started as a PhD researcher at the department of Physical Geography at Utrecht University, working on transverse bed slope effects on sediment transport in experiments and morphodynamic models. Anne contributed to teaching and supervision of master students in thesis writing, fieldwork and multiple courses during her PhD. She actively participated in science outreach, by developing lessons for elementary schools on inquiry-based learning about rivers, and by assisting with several elementary outreach projects.

List of Publications

Journal articles

Baar, A.W., De Smit, J.C., Uijttewaal, S.J., and Kleinhans, M.G. (2018). Sediment transport of fine sand to fine gravel on transverse bed slopes in rotating annular flume experiments. *Water Resources Research*, 54(1), 19-45.

Baar, A.W., Weisscher, S.A.H., and Kleinhans, M.G (conditionally accepted). Interaction between lateral sorting in river bends and vertical sorting in dunes. *Sedimentology*.

Baar, A.W., and Cisneros, J. (under review). Influence of grain size-dependent bedform morphology on flow and downslope sediment transport in river bends. *Journal of Geophysical Research: Earth Surface*.

Baar, A.W., Boechat Albernaz, M, Van Dijk, W.M., and Kleinhans, M.G. Slip-sliding away: critical dependence of morphodynamic models of fluvial and tidal systems on empirical downslope sediment transport.

Lokhorst, I.R., Braat, L., Leuven, J.F.W., Baar, A. W., Van Oorschot, M., Selakovic, S. Kleinhans, M.G. (2018). Morphological effects of vegetation on the fluvial-tidal transition in Holocene estuaries. *Earth Surface Dynamics*, 29.

Kleinhans, M. G., Leuven, J.R.F.W., Braat, L., and Baar, A. W. (2017). Scour holes and ripples occur below the hydraulic smooth to rough transition of movable beds. *Sedimentology*, 64(5), 1381-1401.

Van de Lageweg, W. I., van Dijk, W. M., Baar, A. W., Rutten, J., and Kleinhans, M. G. (2014). Bank pull or bar push: What drives scroll-bar formation in meandering rivers?. *Geology*, 42(4), 319-322.

Marra, W. A., Braat, L., Baar, A. W., and Kleinhans, M. G. (2014). Valley formation by groundwater seepage, pressurized groundwater outbursts and crater-lake overflow in flume experiments with implications for Mars. *Icarus*, 232, 97-117.

Kleinhans, M. G., Van der Vegt, M., Terwisscha van Scheltinga, R., Baar, A. W., and Markies, H. (2012). Turning the tide: experimental creation of tidal channel networks and ebb deltas. *Netherlands Journal of Geosciences-Geologie en Mijnbouw*, 91(3), 311.

Other publications

Baar, A.W., and Sprong, M. (2017). TOOLS Lesbrief onderzoekend leren over stromingen. Publicatie: Wetenschapsknooppunt, Universiteit Utrecht.
English: TOOLS: instructions for teachers on inquiry-based learning about rivers. Publication: Science Hub, Utrecht University.

Baar, A.W., Stouthamer, E., and M.G. Kleinhans (2014). Oeverstabiliteit Rivieren Oost Nederland. Opzet van een conceptueel model en aanzet tot projectmonitoring (39p). Rijkswaterstaat Waterdienst.
English: Bank stability of rivers in the Eastern Netherlands. A conceptual model to initiate project monitoring (39 pages).

Van Wessel, T., Kleinhans, M.G., van Keulen, H., and Baar, A.W. (2014). Wetenschapper in de klas: Wetenschappelijk onderzoek en technologie vertalen naar onderzoekend en ontwerpend leren in het basisonderwijs (72p). Publicatie: Centrum voor Onderwijs en Leren, Wetenschapsknooppunt, Universiteit Utrecht.
English: Science in the classroom: how to translate scientific research and technology to inquiry-based learning on elementary schools (72 pages). Publication: Centre for Teaching and Learning, Utrecht University.

Selected conference abstracts

Baar, A.W., Boechat Albernaz, M., Van Dijk, W.M., and Kleinhans, M.G. (2018). Impact of transverse bed slope effects on large-scale morphology. *Oral presentation at the AGU fall meeting, Washington, USA, 10-14 December 2018.*

Baar, A.W., Boechat Albernaz, M., Van Dijk, W.M., and Kleinhans, M.G. (2018). Slip-sliding away: modelled morphology in fluvial and tidal systems depends on downslope sediment transport. *Invited speaker at the Delft3D user days, Delft, The Netherlands, 14 November 2018.*

Baar, A.W., Boechat Albernaz, M., Van Dijk, W.M., and Kleinhans, M.G. (2018). Local bed slope effect on sediment transport determines large-scale morphology in all numerical models. *Oral presentation at River Flow, Lyon, France, 5-8 September 2018.*

Baar, A.W., Boechat Albernaz, M., Van Dijk, W.M., and Kleinhans, M.G. (2018). The influence of transverse slope effects on large scale morphology in morphodynamic models. *Oral presentation at the EGU General Assembly, Vienna, Austria, 8-13 April 2018.*

Baar, A.W., Boechat Albernaz, M., Van Dijk, W.M., and Kleinhans, M.G. (2018). Transverse slope effects in large-scale morphodynamic models. *Oral presentation at the annual meeting of the Netherlands Centre for River studies, Delft, The Netherlands, 8-9 February 2018.*

Baar, A.W., Kleinhans, M.G., Uijttewaal, W.S.J., and Hardy, R.J. (2017). Modelling secondary flow patterns in a rotating annular flume. *Oral presentation at the 4th International Symposium of Shallow Flows, Eindhoven, The Netherlands, 26-28 June 2017.*

Baar, A.W., Kleinhans, M.G., Weisscher, S.A.H., Sloff, C.J., and Uijttewaal, W.S.J. (2017). Sediment transport processes on transverse bed slopes in rotating annular flume experiments. *Oral presentation at the annual meeting of the Netherlands Centre for River studies, Wageningen, The Netherlands, 2-3 February 2017.*

Baar, A.W., Kleinhans, M.G., De Smit, J.C., and Uijttewaal, W.S.J. (2016). Effect of bedforms on the transverse bed slope effect. *Oral presentation at the 5th conference on Marine and River Dune Dynamics, Bangor, UK, 4-6 April 2016.*